Multiplexing Techniques in Quantitative Proteomics to Study Disease

by

Adam Richard Evans

Bachelor of Science, Thiel College, 2009

Submitted to the Graduate Faculty of

The Kenneth P. Dietrich School of Arts and Sciences in partial fulfillment

of the requirements for the degree of

Doctor of Philosophy

University of Pittsburgh

2014

UNIVERSITY OF PITTSBURGH

The Kenneth P. Dietrich School of Arts and Sciences

This dissertation was presented

by

Adam Richard Evans

It was defended on

December 1st, 2014

and approved by

Dr. Renã A. S. Robinson, Assistant Professor, Department of Chemistry

Dr. Adrian Michael, Professor, Department of Chemistry

Dr. Steve Weber, Professor, Department of Chemistry

Dr. Bruce A. Freeman, Professor, Department of Pharmacology and Chemical Biology

Dissertation Advisor: Dr. Renã A. S. Robinson, Assistant Professor, Department of Chemistry

Committee Chair: Dr. Renã A. S. Robinson

Multiplexing Techniques in Quantitative Proteomics to Study Disease

Adam Richard Evans, Ph.D.

University of Pittsburgh, 2014

Proteomics is the large scale study of a set of proteins from a biological species to understand protein expression, post translation modifications, and protein-protein interactions. Mass spectrometry (MS)-based proteomics allows large scale protein identification and quantitation in the same experiment. Quantitative proteomics reports abundance changes between multiple protein samples, which principally reflect a biological process or disease state. Relative quantitation can be achieved using stable isotope chemical labeling of proteins or peptides using MS or tandem mass spectrometry (MS/MS). Sample throughput is limited by the chemical tag and technique. MS-based protein quantitation employs methods which generate a mass shift in MS to compare abundance changes between two to three samples. An example of precursor quantitation is described using acetylation to study the spleen proteome of mice treated with Adriamycin. Isobaric tags, such as tandem mass tags (TMT), achieve relative quantitation of up to ten samples in MS/MS. In order to analyze additional biological samples beyond ten, multiple experiments must be performed separately, which leads to increased instrument time, higher cost, and variation due to additional preparation steps, sample handling, and MS injections.

Herein, novel methods which enhance multiplexing in quantitative proteomics beyond the current limitations are presented. Enhanced multiplexing is achieved by combining precursor MS labeling with isobaric tags, which is termed "combined precursor isotopic labeling and isobaric tagging" (cPILOT). Initially, cPILOT is used to identify and quantify 3-nitrotyrosine (3NT) containing proteins. The biological significance and proteomic techniques employed to study 3NT are reviewed. cPILOT is expanded to a global strategy by coupling low pH dimethylation with TMT. Global cPILOT was applied

to study the liver proteome of an Alzheimer's disease mouse model, which revealed alterations in metabolism. Finally, the versatility of cPILOT is demonstrated by incorporating N,N-dimethyl Leucine isobaric tags. Overall, the work presented throughout the dissertation highlights novel strategies to enhance multiplexing in quantitative proteomics which are applied to study various diseases.

TABLE OF CONTENTS

LIST OF TABLES

LIST OF FIGURES

ACKNOWLEDGMENTS

1.0. INTRODUCTION

1.1. PROTEOMICS

Proteomics is the study and characterization of expressed proteins from biological fluids, tissue homogenates, cell lysates, and dried blood spots [1, 2]. Proteomics provides key information about protein abundance, post-translational modifications (PTM), protein-protein interactions, and differences in expression [3, 4]. Clinically, proteomics is applied to discover potential drug targets and identify disease biomarkers [5]. Traditional analysis of proteins employs two-dimensional polyacrylamide gel electrophoresis (2D-PAGE) [6]. Proteins migrate through a gel based on mobility in the first dimension followed by isoelectric point separation in the second dimension. Separated proteins are detected using fluorescence [7], chemiluminescence [8], and Coomassie blue or silver staining [9], however only protein abundance information is obtained with these methods. Primary antibodies can be coupled with 2D-PAGE for targeted protein identification, but this method is low throughput and impractical for large scale proteomic studies [6]. Gel-based proteomics offer several advantages in robustness, reproducibility, and straight-forward analysis of whole proteins, but limitations include the missed detection of hydrophobic and low abundant proteins (< 1-10 ng), low resolution, and a limited dynamic range. Mass spectrometry (MS) provides in-depth protein identification, quantitation and sequencing information and has become a principal tool in proteomics [10]. 2D-PAGE can be coupled with MS, where proteins are separated through gels, excised, then analyzed using MS [6, 11].

Advances in proteomics are driven by the continuous developments in analytical techniques and MS instrumentation. It is estimated that over 100,000 unique protein sequences, isoforms, and post-translation modifications are encoded by the human genome, resulting in protein concentrations spanning several orders of magnitude [12]. MS-based proteomics and tandem mass spectrometry (MS/MS) provides the ability to detect thousands of proteins in a single experiment. Multiple separation techniques are frequently coupled with MS to enhance proteome coverage, which includes liquid chromatography (LC) and capillary electrophoresis (CE) [13, 14]. Additionally, mass spectrometers routinely used in

1

proteomics offer high resolution, high mass accuracy and fast MS/MS scan rates, allowing for high throughput protein identification. For example, the most advanced MS instrumentation can identify approximately 90% of the yeast proteome in one hour of LC-MS/MS analysis time [15] and over 10,000 proteins in *C. elegans* [16]. While these numbers are impressive and were not possible with past technology, there is no standard experiment in proteomics and results vary depending on project goals and experimental conditions. Choices in sample preparation, chromatographic separation, instrumentation, MS/MS fragmentation, data collection, and data processing must be considered when designing a proteomics experiment. The following sections in **Chapter 1** discuss options available for key experimental parameters used in proteomics. Emphasis is placed on techniques employed throughout this dissertation.

1.1.1. *Post-Translation Modifications*

Post-translation modifications (PTM) result from the covalent attachment of a chemical species to amino acid functional groups. Proteins expressed in nature are rarely pure, but instead exist in various combinations of isoforms and PTMs. Mapping protein PTM sites is critical to understand biological processes. Approximately 300 PTMs are known in eukaryote proteins [17], however the most common PTMs studied in proteomics are phosphorylation [18], cysteine oxidation [19] and nitrosylation [20], acetylation [21], glycosylation [22], and ubiquitination [23]. PTMs are involved in cellular signaling, communication, and regulation of biological processes. For example, protein phosphorylation can occur as O-phosphorylation on Ser, Thr, and Tyr residues and N- phosphorylation on Arg, Lys, and His residues [18]. Biologically, phosphorylation is a PTM controlled by protein kinases and phosphatase enzymes to regulate metabolism, proliferation, cell differentiation and cell survival [24]. MS and MS/MS are powerful tools in protein characterization to provide further insight to relationships between function and PTM location [25].

Redox proteomics involves the study and characterization of PTMs caused by reactive oxygen species (ROS) and reactive nitrogen species (RNS) under conditions of oxidative stress [26]. Examples

2

of ROS and RNS include the superoxide anion (O_2^-), hydrogen peroxide (H_2O_2), hydroxide (OH^-), and peroxynitrite ($ONOO^-$). Due to the high reactivity of ROS and RNS, these species cause oxidative damage by creating unnatural modifications on protein sites, which can alter function and biological pathways [27, 28]. Oxidative damage includes the formation of protein carbonyls [29, 30] and nitration [31, 32] and is observed Alzheimer's and Parkinson's diseases, cardiovascular diseases, diabetes, and aging [33]. **Chapter 3** reviews the proteomic techniques and analytical challenges in studying 3-nitrotyrosine and **Chapter 4** presents a novel proteomics method to selectively identify and quantify protein nitration.

1.1.2. Shotgun Proteomics

MS-based proteomics can be performed on intact proteins (top-down) or peptides resulting from enzymatic digestion of proteins (bottom-up). Top-down methods provide PTM and protein isoform characterization, however limitations exist due to difficulties in reproducible protein ionization, fragmentation, and separation techniques [34]. Bottom-up ("shotgun") proteomics performs liquid chromatography tandem mass spectrometry (LC-MS/MS) analysis on peptides, which exhibit more efficient ionization, gas phase fragmentation, and versatility in quantitative experiments compared to top-down methods [12]. The general procedure for bottom-up proteomics is illustrated in Figure 1.1. Proteins are extracted from cell cultures or tissue homogenates and digested into peptides using a protease. Trypsin is the most common protease, which cleaves proteins at lysine or arginine residues [35], however other proteases such as LysC and chymotrypsin can be used if alternative cleavage sites are required [36]. Proteins are digested into a pool of peptides and separated using a chromatographic technique in order to collect MS spectra free of background interfering species. LC [6], capillary electrophoresis (CE) [37] and isoelectric focusing [38] can be used to separate peptide mixtures in one or more dimensions to increase identification in large scale experiments. For example, **Chapter 6** presents a 2D-separation of liver protein digests using strong cation exchange (SCX) coupled with RPLC [7]. Peptides are separated according to charge state on a Polysulfethyl A column to collect multiple fractions
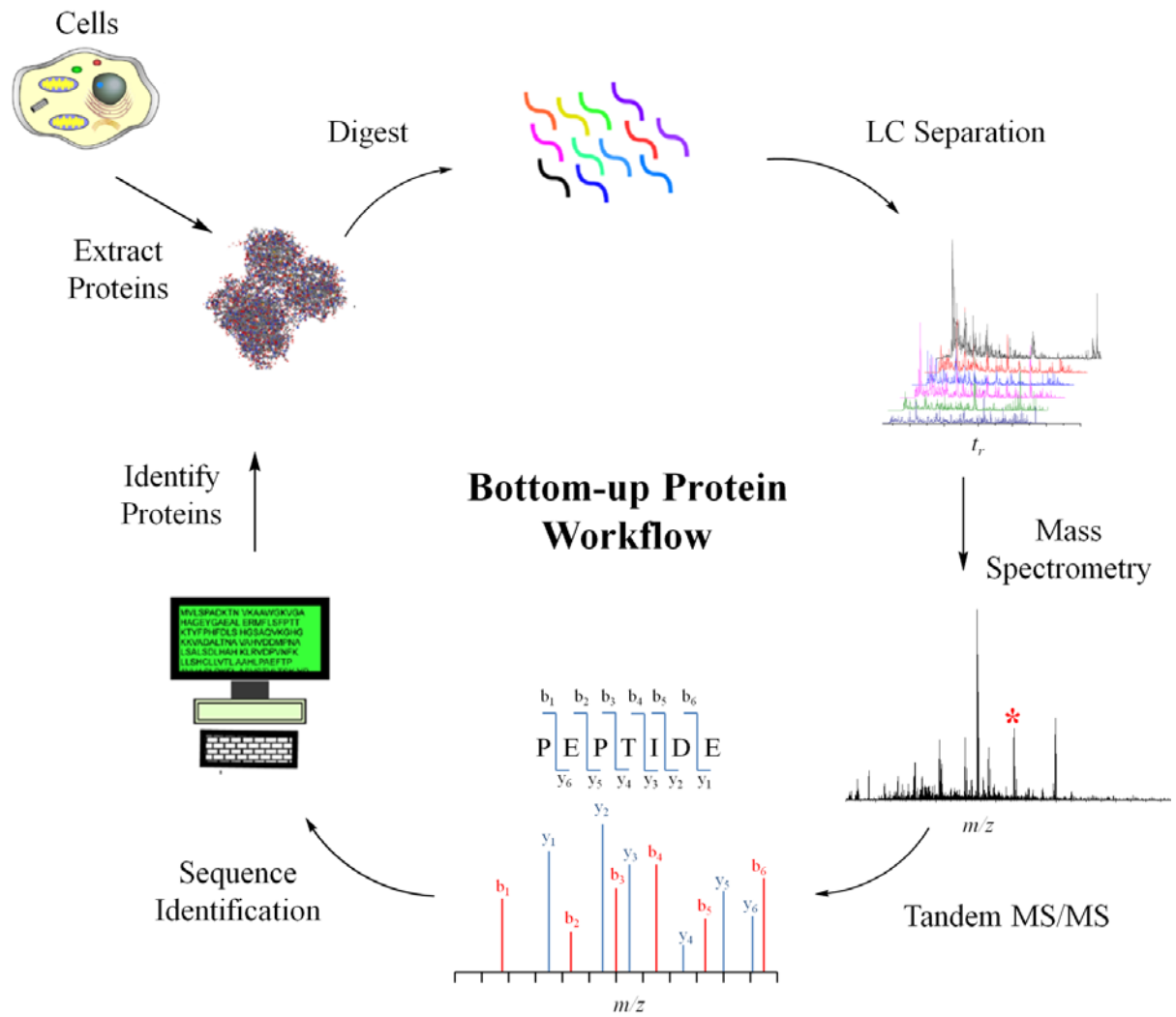
Figure 1.1. Procedure for bottom-up proteomics.

of equal concentration. Elution is performed by increasing a KCl salt gradient. Each fraction is collected, desalted, and subject to reversed phase liquid chromatography (RPLC), which exploits the differences in peptide hydrophobicity for separation. Eluted peptides are ionized and introduced into MS, where ions are separated according to their mass to charge ratios (m/z) and abundances recorded by a detector. Tandem mass spectrometry (MS/MS) is routinely incorporated in MS-based proteomics to provide sequence information, which is discussed in **Section 1.1.4.** Database search algorithms, such as SEQUEST (**Section 1.1.5**) [39], match experimental and theoretical MS/MS spectra to identify peptide sequences. This strategy is used throughout the dissertation to identify proteins. Quantitation can be built into the bottom-up proteomics procedure and will be discussed in **Section 1.2.**

1.1.3. MS Instrumentation in Proteomics

Eluted peptides from RPLC separations must be ionized prior to MS and MS/MS analysis. Electrospray ionization (ESI) [40] and matrix assisted laser desorption ionization (MALDI) [41] are two popular ionization sources in shotgun proteomics due to their ability to ionize large molecules at atmospheric pressure. In ESI (used throughout the dissertation), LC eluted peptides form charged droplets resulting from an applied potential and travel towards the MS inlet. Solvent evaporates from the droplet, which increases the charge density until a coulombic explosion creates smaller droplets and ions. ESI typically results in peptide ions of multiple charge states and couples well with mass analyzers with a limited m/z range. Recently, other ionization techniques have emerged in proteomics and include desorption ESI (DESI) [42], laserspray ionization (LSI) [43], and solvent assisted inlet ionization (SAII) [44], which results in enhanced sensitivity while generating ESI-like ions.

New developments in mass spectrometry have driven the progress in proteomics in recent years. Quadrupoles, ion traps, time of flight, and high resolution mass spectrometers [45], such as the Orbitrap [46] and FT-ion cyclotron resonance (FTICR), [47] have been employed in proteomic analysis [10]. Hybrid mass spectrometers utilize multiple mass analyzers in one instrument, which provide the most potential in proteomics due to their versatility and multi-dimensional analysis. Orbitrap-ion trap hybrid

instruments couple high resolution (> 100,000) and high mass accuracy (< 2ppm) with fast, sensitive MS/MS scans creating an instrument suited for large scale discovery-based proteomics. The principal instrument used throughout this dissertation is the LTQ-Orbirtap Velos shown in Figure 1.2 [48]. High resolution MS scans are performed in the Orbitrap to detect intact peptides. Scan rates occur at approximately 700 ms per scan (R = 60,000), which can impact the duty cycle of LC-MS/MS experiments. However, simultaneous MS/MS scans are performed in the dual ion trap, which performs four to five MS/MS scans during the high resolution Orbitrap analysis. Additional MS/MS scan events can be performed resulting in an enhanced identification, but with a longer duty cycle. Together, this creates an efficient method capable of collecting tens of thousands of peptide fragmentation spectra in a single LC-MS/MS experiment.

When work for this dissertation began, the LTQ-Orbitrap Velos was the state-of-the-art mass spectrometer in proteomics. Orbitrap hybrids have rapidly evolved in the last five years with the release of the Orbitrap-Elite [49] and the Q-Exactive [50]. Additionally, Orbitrap resolution has reached up to R = 1,000,000 using reduced mass analyzer dimensions and enhanced Fourier transform algorithms [51]. The current-state-of-the-art is the Orbitrap Fusion, which is a tribred mass spectrometer containing a high resolution Orbitrap, a quadrupole mass analyzer, and a dual ion trap capable of performing 20 MS/MS scan events per second [52]. Emphasis with each new hybrid model is placed on increasing the scan speeds so that more spectra are collected in real time resulting in enhanced protein identification. While newer Orbitrap instrumentation is impressive, the Orbitrap Velos is capable of identifying thousands of unique proteins in an experiment.

1.1.4. Peptide Fragmentation

Large scale proteomic experiments typically operate using data dependent acquisition (DDA) [53], which results in isolation and MS/MS fragmentation of the most intense ions detected in MS. Peptides cleave at specific sites along the backbone into a series of a/x, b/y, and c/z type ions shown in Figure 1.3. Different fragmentation techniques can affect the appearance of peptide MS/MS spectra [54].
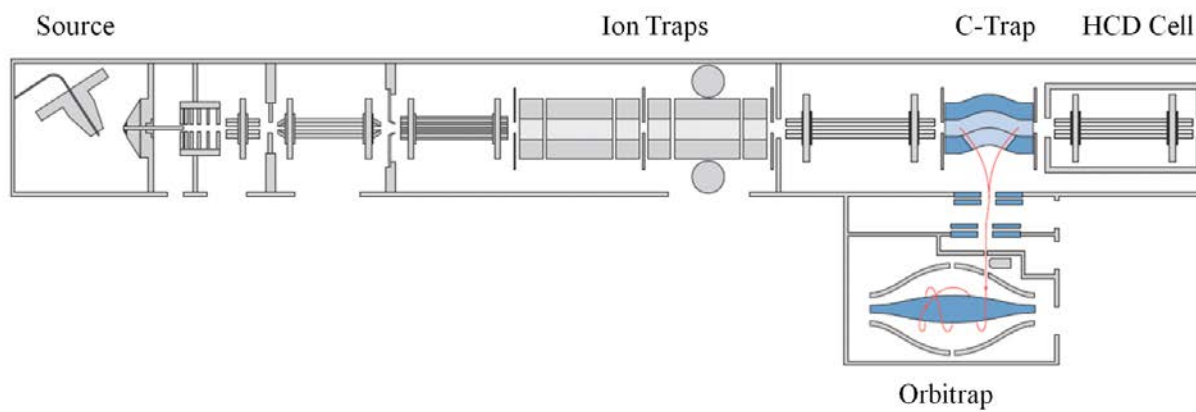
Figure 1.2. Schematic of the LTQ-Orbitrap Velos [52] (Thermo Scientific).
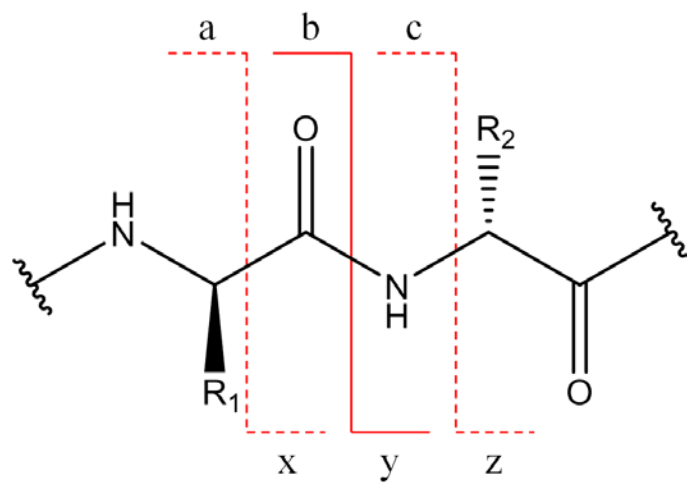
Figure 1.3. Peptide fragmentation in MS/MS showing cleavage sites for a/x, b/y, and c/z ion pairs.

Collision induced dissociation (CID) occurs in the ion trap of the LTQ-Orbitrap Velos. Selected ions of interest are isolated and exposed to an RF excitation to increase the kinetic energy. Excited ions collide with helium gas causing fragmentation favored between the amide bond of peptides resulting in b-type and y-type ions. CID-MS/MS is the principal fragmentation technique used throughout the dissertation to generate MS/MS spectra due to its robustness, reproducibility and fragmentation efficiency. One disadvantage of CID in ion traps is a low mass cutoff of approximately one-third of the selected m/z in MS/MS spectra (due to the RF increase required for excitation) [55]. In order to detect low m/z ions in MS/MS, higher energy collisional dissociation (HCD) is employed where ions are fragmented in an octopole HCD collision cell (Figure 1.2) and detected using the Orbitrap [48, 56]. Ions are isolated in the linear ion trap and transferred to the HCD cell, where a DC offset is applied in the presence of nitrogen gas to cause fragmentation. Quantitative proteomic experiments using isobaric tags **(Section 1.2)** require HCD fragmentation to detect ions from 100-150 m/z for quantitation. HCD also provides reproducible and efficient fragmentation, however peptide coverage (i.e. b- and y-type ions) is impaired. As a result, MS experiments use a combination of CID- and HCD-MS/MS scan events during data collection for peptide identification and quantitation, respectively [57].

1.1.5. Database Searching and Protein Identification

Proteomic data files can contain > 50,000 total MS and MS/MS spectra from a single LC separation. Database search algorithms and data processing software tools have been developed to streamline spectral interpretation in large scale studies. Data files (.RAW) are searched with algorithms such as SEQUEST [39, 58] to generate a list of detected peptides and proteins in a shotgun proteomic experiment. First, a FASTA file is uploaded from an online protein database such as Uniprot or SwissProt, which contain a list of protein sequences and accession numbers for a given species [59]. SEQUEST performs *in silico* digestion of the protein database matching the user's experimental criteria, which results in a list of theoretical peptides and corresponding MS/MS spectra. Experimental and theoretical MS/MS spectra are compared, matched, and scored to identify peptide sequences [60, 61]. A

single SEQUEST search result contains a mix of correctly identified peptides and false positive identifications. Misidentified peptides are filtered by searching the RAW data against a decoy database to measure the frequency of peptide identifications due to random matching [62]. False discovery rates (FDR) for peptide identification are set to 0.05 and 0.01 for 95% and 99% confidence, respectively. SEQUEST is built into the software package Proteome Discoverer (PD, Thermo Scientfic), which assists in processing data for protein identification and quantitation.

1.2. MS-BASED QUANTITATIVE PROTEOMICS

Quantitative proteomics provides significant insight to disease states or other experimental conditions [63, 64]. Complex protein digests result in a pool of peptides with varying chemical and physical properties that differ in charge state, hydrophobicity, amino acid sequence, and PTMs [12, 65, 66]. As a result, relative quantitation is employed by comparing the abundance changes between peptides originating from separate samples. Relative quantitation can be performed using label free approaches or chemical tagging. Label free quantitation uses spectral counting or comparisons of peptide peak area between multiple samples and has been extensively reviewed [67-69]. Quantitation is also achieved by modifying peptide functional groups with stable isotope chemical tags, which is divided into two groups: precursor isotopic labels and isobaric tags. For purposes of this dissertation, only isotope chemical tagging techniques will be highlighted.

1.2.1. Precursor Isotopic Labeling

Precursor isotopic labeling achieves relative quantitation between multiple samples in MS. Peptides or proteins are modified with the same chemical label, however one tag incorporates heavy atoms within the structure creating a "light" and "heavy" tag. When samples are pooled and analyzed using LC-MS/MS, light and heavy peptide pairs co-elute to create an *m/z* shift in MS corresponding to the mass difference between the chemical tags. Relative quantitation compares the peak areas between each peptide pair. Table 1.1 shows common precursor isotopic labeling techniques. Metabolic labeling

10

Table 1.1. Common Stable Isotope Tags for Relative Quantitation

Tag	Multiplex	Reactive Site	MS Order	Mass Shift (Da)	Reporter Ions (m/z)
SILAC[a]	3	Arg, Lys	MS	0, +6, +8, +10	n/a
SILAM[b]	2	All AA	MS	> 10	n/a
Acetylation	2	N-term, Lys	MS	0, +3	n/a
Dimethylation	5	N-term, Lys	MS	0, +2, +4, +6, +8	n/a
ICAT[c]	2	Cys	MS	0, +8	n/a
ICPL[d]	2	Lys	MS	0, +6	n/a
Oxygen 18	2	C-term	MS	0, +2, +4	n/a
iTRAQ[e]	8	N-term, Lys	MS/MS	n/a	113-119, 121
TMT[f]	6	N-term, Lys	MS/MS	n/a	126-131
DiLeu[g]	8	N-term, Lys	MS/MS	n/a	114-119, 121-122
DIART[h]	6	N-term, Lys	MS/MS	n/a	114-119

[a]Stable isotopic labeling of amino acids in cell cultures

[b]Stable isotopic labeling of amino acids in mammals

[c]Isotope coded affinity tags

[d]Isotope coded protein labels

[e]Isobaric tags for relative and absolute quantitation

[f]Tandem mass tags

[g]Dimethyl leucine tags

[h]Deuterium isobaric anime reactive tags

incorporates stable isotopes at the earliest point in sample preparation [65]. For example, stable isotopic labeling of amino acids in cell cultures (SILAC) [70] employs a cell medium rich in heavy arginine or lysine, which incorporates heavy amino acids on the protein primary structure during expression. Since the chemical labeling occurs at the earliest point in the experiment, variation is minimal [64], however SILAC techniques are limited to cell cultures. Metabolic labeling can be achieved *in vivo* by feeding animals fortified heavy lysine food pellets [71, 72], however this technique is highly expensive, requires multiple animal generations to achieve >95% labeling efficiency, and is not compatible with all species.

Alternatively, precursor isotopic labeling can employ chemical tags, which target reactive amino acid functional groups. Common precursor chemical tagging techniques (Table 1.1) include acetylation [73], dimethylation [74, 75], isotope-coded affinity tags [76], isotope-coded protein labels [77], and C-terminal oxygen 18 labeling [9, 78]. Precursor quantitation provides versatility, modifies large peptide quantities, and provides a dynamic range approximately three orders of magnitude [12, 79, 80]. Multiplexing is limited to two or three samples per experiment due to increasing MS spectra complexity as quantitation channels are added. Dimethylation can achieve multiplexing up to five samples with mass shifts of +2 Da per precursor channel [81], however significant peptide overlap is observed at peptide charge states of +3 or higher. Precursor labeling strategies used in the dissertation are acetylation **(Chapters 2,4)** and dimethylation **(Chapters 5, 6, and 7)**.

1.2.2. Isobaric Tags

Isobaric tags are an alternative chemical labeling approach in quantitative proteomics and are capable of analyzing up to 10 samples in a single experiment using MS/MS. Tandem mass tags (TMT) [11], the isobaric tag for relative and absolute quantitation (iTRAQ) [13], deuterium isobaric amine-reactive tags (DiART) [82] and dimethyl leucine tags (DiLeu) [83] are available for multiplexed protein quantitation. Figure 1.4 illustrates the TMT 6-plex isobaric reagents used throughout the dissertation in **Chapters 4-6**. Isobaric tags consist of three regions: a reporter ion group, a mass balance group, and a reactive site that targets a peptide functional group such as amines. Heavy isotopes
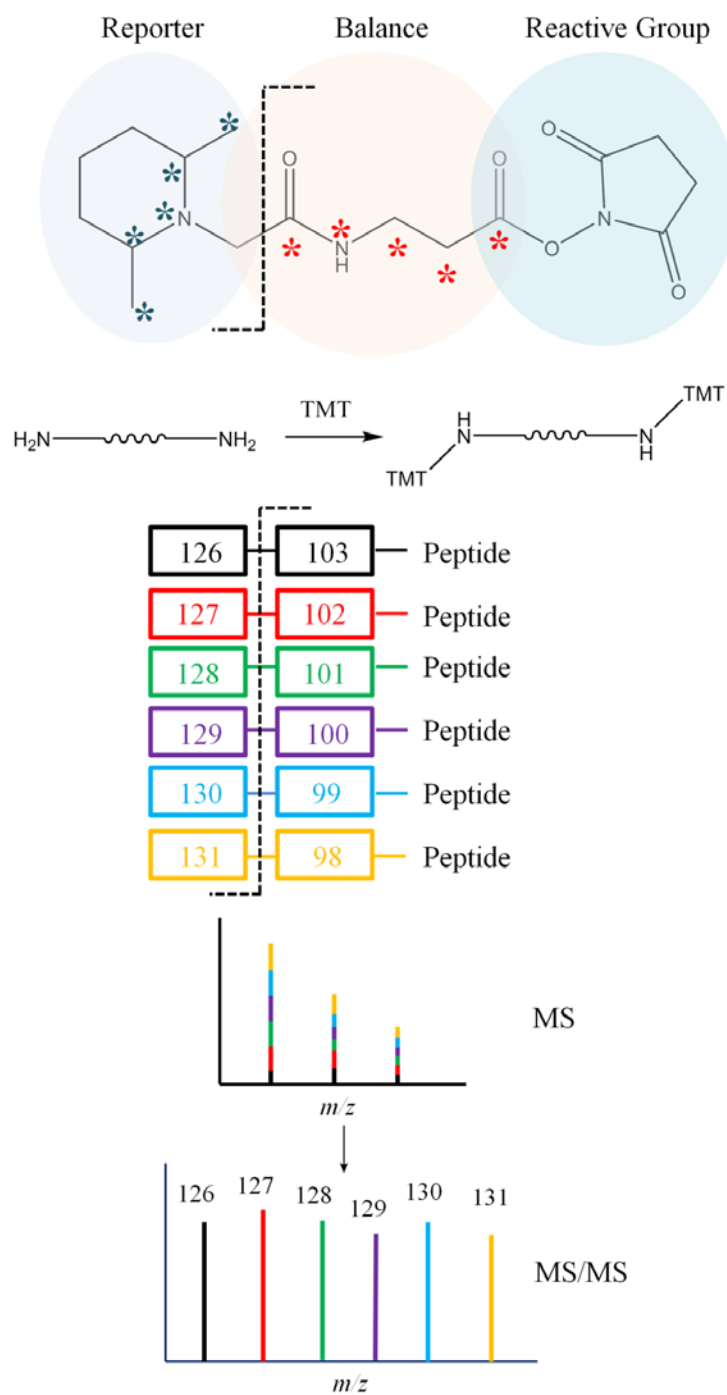
Figure 1.4. Chemical structure for 6-plex tandem mass tags (TMT) showing reporter ion, mass balance, and peptide reactive groups. Samples are pooled for LC-MS analysis resulting in a single peak in MS. Isolation and fragmentation generates six reporter ion signals in MS/MS corresponding to the mass of each reporter ion.

13

(^{13}C, ^{15}N) are incorporated into the reporter ion and mass balance regions of the tag to retain the same mass (Figure 1.4). For TMT tags, reporter ions span from *m/z* 126 through 131, while the respective balance group ranges from *m/z* 103 through 98. When samples are modified with different TMT reagents and pooled for LC-MS/MS analysis, peptide sequences have similar retention times, ionization, and precursor mass resulting in a single peak in the MS spectrum. However, upon isolation and MS/MS fragmentation of the peptide ion, the TMT tag cleaves between the mass balance and reporter ion group resulting in six unique signals corresponding to the mass of the reporter ions (*m/z* 126-131 for TMT tags). Relative quantitation is achieved by comparing reporter ion signals in MS/MS. Isobaric tags provide the advantage of performing multiplexed experiments without creating additional precursor MS complexity since all peptides have the same mass. TMT tags can multiplex up to 10 samples using isotopologues, which take advantage of the difference in mass shift caused by ^{15}N and ^{13}C [84, 85]. These tags require high resolution Orbitrap scans of at least R = 35,000 to obtain accurate quantitation and separate all 10 reporter ions. While this dissertation primarily uses the TMT 6-plex tag, the methods can easily incorporate TMT 10-plex tags since the reaction chemistry is identical.

Quantitation using isobaric tags is accurate and linear up to two orders of magnitude with 10-30% relative standard deviation (RSD) depending on the fold change ratios [66]. Limitations to isobaric quantitation include ratio compression due to the isolation and fragmentation of background peptides [86, 87]. In quantitative proteomic experiments, it is expected that a majority of proteins are equimolar in which only a small percentage of detected proteins yield a significant change. Co-isolation and co-fragmentation occurs when a background ion is detected within the isolation window of the peptide of interest. Since the background ion is also likely modified with an isobaric tag due to the global nature, MS/MS spectra contains the combined reporter ion signal originating from all fragmented precursor ions. This results in inaccurate quantitation using isobaric tags and underestimates the true value [88]. Charge state reduction in the gas phase [89], analysis of TMT clusters in MS/MS [90], ion mobility [91, 92], DDA optimization [93], and isobaric isotopologues [17] have solved this issue to provide accurate quantitation. However, these techniques require additional MS hardware or specialized data processing

software scripts. Ting and Gygi presented a higher order MS data collection method by HCD fragmentation to generate reporter ion spectra (MS^3) [94]. This technique can be easily implemented using the LTQ Orbitrap Velos and is employed in **Chapters 5 and 6** to perform protein quantitation using isobaric tags.

1.2.3. Multiplexing

Current relative quantitation techniques can multiplex up to ten samples in a single experiment. While an impressive number, this does not meet the demands in clinical laboratories [5, 95]. Figure 1.5 outlines the challenges in performing large scale proteomic experiments which exceed an N of ten. Multiple samples must be prepared and analyzed separately, which extends instrumental analysis time, increases cost, and increases variation due to additional preparation steps, instrument injections, and sample handling (i.e. pipetting errors) [95]. Optimization in protein buffers, digestion procedures, and instrumental parameters (i.e. Orbitrap overfill, extended gradients, longer columns, etc.) have helped achieve ~20% RSD across 24 samples [96] and 60 samples [97]. The tradeoffs include highly exhaustive sample preparation procedures and individual injections of each sample creating an instrument analysis experiment lasting over 20 days. Novel enhanced multiplexing techniques can create higher sample throughput, reduce variation, and analyze large N simultaneously in one LC-MS/MS injection.

Two strategies have been developed to enhance multiplexing. The first is presented in Figure 1.6, which develops methods that combine precursor labeling techniques with isobaric tags. This dissertation presents combined precursor isotopic labeling and isobaric tagging (cPILOT) to enhance multiplexing of protein nitration [98, 99] (**Chapter 4**) and global quantitative proteomics [100, 101] (**Chapters 5 and 6**). Using cPILOT, peptides are modified with a precursor labeling reagent creating light and heavy peaks solely to generate a mass shift in MS. Light and heavy peptides are further modified with isobaric tags targeting a different functional group. HCD-MS/MS or MS^3 fragmentation of both light and heavy peptides results in two unique reporter ion spectra, thus quantifying additional samples simultaneously. Other multiplexing techniques using a similar approach include the combination of SILAC and TMT tags

15
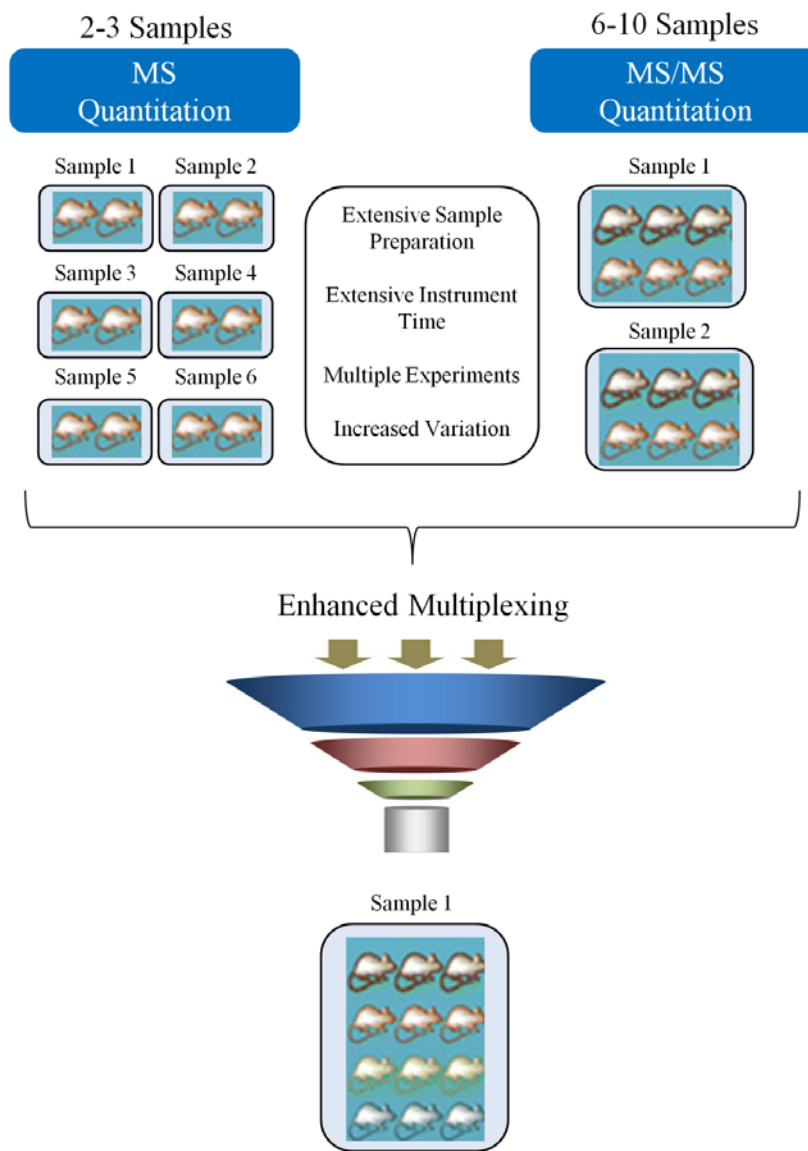
Figure 1.5.   Illustration showing the need for enhanced multiplexing in quantitative proteomics.   Precursor MS quantitation multiplexes two to three samples in a single experiment while isobaric tagging can analyze up to six samples at once using TMT tags. Enhanced multiplexing expands sample throughput.
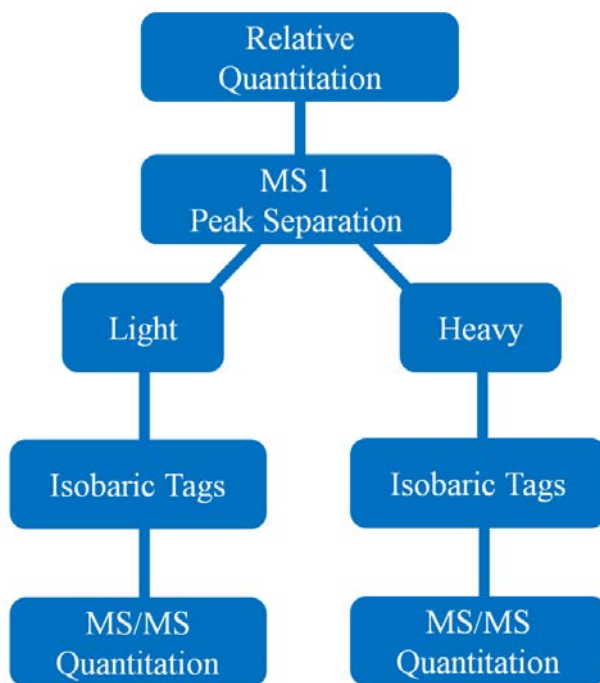
Figure 1.6. Strategy for combined precursor isotopic labeling and isobaric tagging.

[102] and the synthesis of novel TMT tags [103]. An alternative strategy to enhance multiplexing takes advantage of isotopologues that expands 6-plex TMT isobaric tags to 8-plex [104] and 10-plex [85]. NeuCode labeling can multiplex 12 samples in precursor MS, but requires ultra-high resolution Orbitrap mass analyzers (R = 480k) to distinguish 6 mDa mass shifts for relative quantitation at higher m/z ratios [105]. Recently, TMT tags were combined with iTRAQ in a single experiment since both sets of tags result in unique m/z reporter ions offering further potential in multiplexing [106]. **Chapters 4**-**7** discuss the development of various cPILOT strategies to expand multiplexing in quantitative proteomics.

1.3. OVERVIEW OF DISSERTATION

This dissertation focuses on the method development of novel multiplexing strategies in quantitative proteomics to study disease. First, an acetylation precursor labeling technique is applied in **Chapter 2** to study the effects of an anti-cancer drug, Adriamycin, on the spleen proteome to uncover changes in the immune system of healthy mice. **Chapter 3** reviews proteomic techniques to quantify 3-nitrotyrosine (3NT). **Chapter 4** introduces combined precursor isotopic labeling and isobaric tagging (cPILOT), which selectively quantifies 3NT peptides and enhances multiplexing in protein quantitation. **Chapter 5** extends cPILOT from a PTM selective approach to a global approach and also experiments with alternative data collection techniques to acquire more efficient multiplexed data in real time. Twelve-plex global cPILOT is analytically characterized in **Chapter 6** and applied to study the effects of Alzheimer's disease in the liver of a mouse model. **Chapter 7** demonstrates the versatility of cPILOT by incorporating N,N-dimethyl leucine tags to provide a more cost effective cPILOT method. Finally, **Chapter 8** summarizes the dissertation and presents the future outlook, goals, and current challenges in multiplexing. **Chapters 2-6** are primarily written from published papers or submitted manuscripts.

2.0. GLOBAL EFFECTS OF ADRIAMYCIN TREATMENT ON MOUSE SPLENIC PROTEIN LEVELS*

2.1. INTRODUCTION

Adriamycin [(ADR), also known as doxorubicin] is an anthracycline drug used to treat hemopoietic and a wide range of solid tumors in lung, breast, ovarian, prostate, and bladder cancers, amongst others [108, 109]. Although the mechanisms of ADR drug action in non-cancerous tissues are not completely understood, there are two widely supported phenomena. The first primary action involves the intercalation of DNA and inhibition of topoisomerase II enzymatic activity, which results in the termination of DNA replication and transcription [110, 111]. Clinically, ADR is very effective as an anticancer treatment, however some patients can suffer from major side effects such as cardiomyopathy and heart failure [112], dizziness, lack of concentration, and cognitive deficits characterized as "chemobrain" [113, 114]. In other cases, patients develop a resistance to ADR and treatment fails [115].

The second primary action of ADR involves the generation of toxic free radical species such as the superoxide anion. The structure of ADR contains a quinone, which is converted to a semi-quinone through a one electron reduction. In the presence of oxygen, the semi-quinone is converted back to the quinone resulting in the formation of reactive oxygen species causing oxidative stress [116], which become detrimental to nontargeted cells, in addition to cancerous cells [117]. Oxidative stress can result in protein oxidation, DNA damage, and lipid peroxidation which disrupt cellular functions. Several reports have demonstrated that ADR leads to elevated oxidative stress in plasma [118], brain [119], heart [120], cardiomyocytes [121], liver [122], testes [123], and kidney [124]. The cytotoxicity of ADR also

causes alterations to apoptotic pathways, lipid membrane structure and function [125], Ca^{2+} homeostasis [126], and cellular arrest and differentiation [127].

Proteomic methods have been employed to study the effects of ADR treatment in different cell lines and tissues, including brain [119, 128, 129], plasma [130], heart [131], MCF-7 human breast cancer cells [132], hepatoma cells [133], Jurkat T cells [134], Raji cells [135], and thymus [136]. Proteomic studies of ADR-resistant cells lines [137] have been performed on K562/ADM cells [138, 139], K562/ADR cells [140], DLKP cell lines [141], and MCF-7/ADR cells [142-144]. It has been shown that cellular populations in spleen tissue undergo substantial changes after ADR treatment, which may have global effects on immunity in ADR-treated patients [145]. To-date no quantitative proteomics studies of spleen tissue from ADR-treated mice has been reported. Herein is the first report that has examined the effects of ADR treatment on protein expression in spleen. The proteomics method employs global internal standard technology (GIST), which is a post-digestion precursor isotopic labeling approach (**Chapter 1**) [73]. Nanoflow reversed phase liquid chromatography (RPLC)-tandem MS (MS/MS) was used to detect relative changes in splenic protein expression in control and ADR-treated mice.

2.2. EXPERIMENTAL

2.2.1. Animal Housing and Treatment

Approximately three month old male B6C3 mice were housed at the University of Kentucky Central Animal Facility with 12 hour light/12 hour dark cycle. Animals were fed standard Purina rodent chow *ad libitum*. The animal protocol was approved by the University of Kentucky Animal Care and Use Committee. Animals used in these studies were the same as those previously reported [136]. Mice were divided into two groups and injected with either saline (hereafter referred to as control mice) or adriamycin (25mg/kg body weight; hereafter referred to as ADR-treated mice). Spleen tissue was harvested 72 hours post injection from saline-perfused mice. For these studies, an N = 5 was used for each treatment group.

2.2.2. Spleen Homogenization

Spleen tissues were homogenized in an ice-cold phosphate buffer saline (PBS) solution containing 8 M urea with 100 passes of a Wheaton homogenizer. Homogenate solution was collected, sonicated, and centrifuged at 13000 RPM for 10 minutes (4 °C). Supernatants were collected and protein concentrations determined using the BCA assay according to the manufacturer's instructions (Pierce Thermo; Rockford, IL). Samples were stored at -80 °C until further use.

2.2.3. Protein Digestion

For individual samples, 100 μg of spleen protein was spiked with 1 μg of bovine β-lactoglobulin (Sigma Aldrich; St. Louis, MO) and subject to tryptic digestion as follows. 0.25 M dithiothreitol (Thermo Fisher; Pittsburgh, PA) was added in a 1:40 protein:reagent molar excess and incubated at 37 °C for two hours. 0.25 M iodoacetamine (Acros Organics; Morris Plains, NJ) was added in a 1:80 protein:reagent molar excess and incubated at 0 °C for two hours in the dark followed by the addition of 0.25 M L-cysteine in a 1:40 protein:reagent molar excess at room temperature for 30 minutes. Tris buffer solution (0.2 M Tris, 10 mM $CaCl_2$, pH 8.0) was added to reduce the urea concentration to 2 M. TPCK-treated trypsin from bovine pancreas (Sigma Aldrich) was added to each sample in a 2% w:w enzyme:protein ratio and incubated at 37 °C for 24 hours. Samples were flash-frozen with liquid nitrogen and cleaned using Waters Oasis HLB C18 cartridges.

2.2.4. Synthesis of N-acetoxy-H_3-succinimide and N-acetoxy-$^2H_3$-succinimide

The procedure for synthesis of N-acetoxy-H_3-succinimide and N-acetoxy-$^2H_3$-succinimide is described elsewhere [146]. Briefly, 1.9478 g of N-hydroxysuccinimide (NHS, Sigma Aldrich) was added to 4.8 mL of >99% acetic anhydride (Sigma Aldrich) or 1.9451 g of NHS was added to 4.4 mL of 99% atom $^2H_6$-acetic anhydride (Sigma Aldrich). Both reactions occurred at room temperature for 15 hours under nitrogen. White crystals products were collected, washed thoroughly with hexane, and dried under vacuum. Product purity was confirmed with NMR analysis (>95% purity).

21

2.2.5. Isotopic Labeling of Peptides

Stock solutions (0.25 M) of N-acetoxy-H$_3$-succinimide and N-acetoxy-^{2}H$_3$-succinimide were prepared in 50 mM phosphate buffer (pH = 7.5). Tryptic peptide samples (1 mg·mL^{-1}) were reconstituted in 50 mM phosphate buffer and reacted with 100 molar excess of the N-acetoxy-H$_3$-succinimide (light) and N-acetoxy-^{2}H$_3$-succinimide (heavy) for control and ADR-treated mice, respectively. Reactions occurred at room temperature for 5 hours under constant stirring. Control and ADR-treated samples were pooled and treated with excess 0.25 M hydroxylamine hydrochloride (Sigma Aldrich) and adjusted to pH 10. After 20 minutes at room temperature the samples were adjusted to pH 7 and were cleaned, dried, and stored at -80°C.

2.2.6. LC-MS/MS

Isotopically labeled peptide samples were reconstituted in formic acid solution (0.1% in water) to a concentration of 0.5 µg·µL^{-1} and injected onto a trapping column (2 cm × 100 µm i.d.) packed with 200 Å C$_{18}$ material (Michrom Bioresources Inc.; Auburn, Ca) using an autosampler on a nanoflow Eksigent 2D LC system.   Buffers A and B were composed of water:acetonitrile (97:3) and acetonitrile, respectively, each with 0.1% formic acid. Samples were washed with buffer A and eluted onto an analytical column (13.2 cm × 75 µm i.d.) packed with 100 Å C$_{18}$ material (Michrom Bioresources Inc.). Gradient elution was performed as follows (%A/%B): 90:10 for 2 minutes, ramp to 85:15 over 4 minutes, hold for 4 minutes, ramp to 70:30 over 120 minutes, ramp to 40:60 over 30 minutes, ramp to 20:80 over five minutes, hold for 10 minutes followed by column re-equilibration. Eluted peptides were detected on an LTQ-Orbitrap Velos MS using data-dependent acquisition with the following parameters: full FT parent scan at 60,000 resolution over the *m/z* range of 300-1800, positive ion mode, the top 6 most intense ions were selected for CID fragmentation (35% collision energy, 10 ms activation time, 5000 minimum ion count threshold) and mass analyzed using the LTQ. Each pooled isotopically labeled sample (N = 5) was analyzed with three technical LC-MS/MS replicates.

2.2.7. Database Searching and Analysis

.RAW files were searched against the mouse International Protein Index (IPI) database (56957 total sequences on 4/26/2010) using the SEQUEST algorithm embedded in Proteome Discoverer 1.2 software (Thermo). The FASTA sequence for bovine β-Lactoglobulin (National Center for Biotechnology Information Accession Number: gi4388846) was manually added to the database. Search parameters included: precursor mass tolerance of 15 ppm, fragmentation tolerance of 1.0 Da, dynamic modifications of light and heavy acetyl groups on lysine residues and the N-terminus and oxidation of methionine, and a static modification of carbamidomethyl on cysteine. All files were searched against a decoy database with false discovery rates set at $p<0.05$ and $p<0.01$ so that only medium and high confidence peptides, respectively, were used for further analysis. Proteome Discoverer 1.2 provided peak intensity and area information for light and heavy labeled peptides and protein ratio calculations.

2.2.8. Statistics for Differentially-Expressed Proteins

The search results were treated as follows in order to generate a confident and conservative list of differentially-expressed proteins. After calculation of protein ratios, the protein list was filtered to include only proteins that were detected in a minimum of any six LC-MS/MS analyses. One-way ANOVA ($p <$ 0.05) was carried out in Origin 8.0 to assess statistical differences in the ADR/control (CTR) ratios across biological (N = 5) and technical (N=3) replicates for each protein. Proteins were considered differentially-expressed if the following two criteria were met: 1) a calculated F score < the tabulated F score ($\alpha = 0.05$) and, 2) a ADR/CTR or CTR/ADR ratio > 1.5.

2.2.9. Western Blot Verification

Protein samples (50 μg) were denatured in an appropriate sample buffer and electrophoretically separated on a Criterion TGX gel (Biorad Laboratories; Hercules, CA) at 250 V. Protein from the gel was transferred onto a nitrocellulose membrane paper using a Fast-Transfer Blot System (Biorad). Blots were washed three times in Wash blot. BSA blocking solution was added to the membrane and incubated on a

rocker for one hour. A 1:1000 dilution of rabbit polyclonal anti-annexin A2 primary antibody (Sigma Aldrich) and 1:2000 dilution of rabbit polyclonal anti-actin primary antibody (Sigma Aldrich) was added and incubated at 4 °C overnight. The blot was rinsed and incubated with a 1:8000 dilution of anti-rabbit IgG alkaline phosphatase secondary antibody (Sigma Aldrich) for one hour on a rocker. The blot was rinsed and colorometrically developed as described above for protein carbonyls. The dried blot was scanned using a Canon scanner, saved as a .TIFF file, and densitometry analyses carried out with Scion Image Software.

2.3. RESULTS

2.3.1. Effects of ADR Treatment on Spleen Tissue

In order to better understand the effects that ADR treatment has on spleen tissue we initially began by measuring spleen weights. The ADR-treated mice used in these studies exhibited an ~11% decrease in body weight and an ~68% decrease in thymus weight [136]. Additionally, this work reports an ~66% loss in spleen weight of ADR-treated mice relative to controls (Table 2.1). Because lower body weight and thymus size are correlated with lower numbers of lymphocytes [136], we hypothesize that there is also a lower number of splenic lymphocytes based on smaller spleen sizes in ADR-treated mice.

2.3.2. GIST Proteomics Workflow

The quantitative proteomics workflow, shown in Figure 2.1, was used to determine differences in protein expression after ADR treatment as follows. Protein samples extracted from homogenized spleen tissue of control and ADR-treated mice were spiked with an internal protein standard (i.e., bovine β-lactoglobulin) prior to trypsin digestion. Tryptic peptide samples from control and ADR-treated mice were isotopically labeled with either a light or heavy GIST reagent, respectively, and pooled in a 1:1 ratio. Isotopically labeled peptide mixtures (N = 5 for biological replicates) were analyzed with triplicate nanoflow LC-MS/MS experiments using a LTQ-Orbitrap Velos MS. Identified proteins were filtered (as discussed above) in order to generate a list of differentially-expressed proteins.

Table 2.1. Masses of Spleen Tissues Collected from Control and ADR-treated Mice.

Animal	Control (g)	ADR (g)
1	0.0814	0.0297
2	0.0909	0.0346
3	0.0859	0.0378
4	0.115	0.0269
5	0.0840	0.0278
Ave. ± SD	.0914 ± .0135	.0314 ± .0047
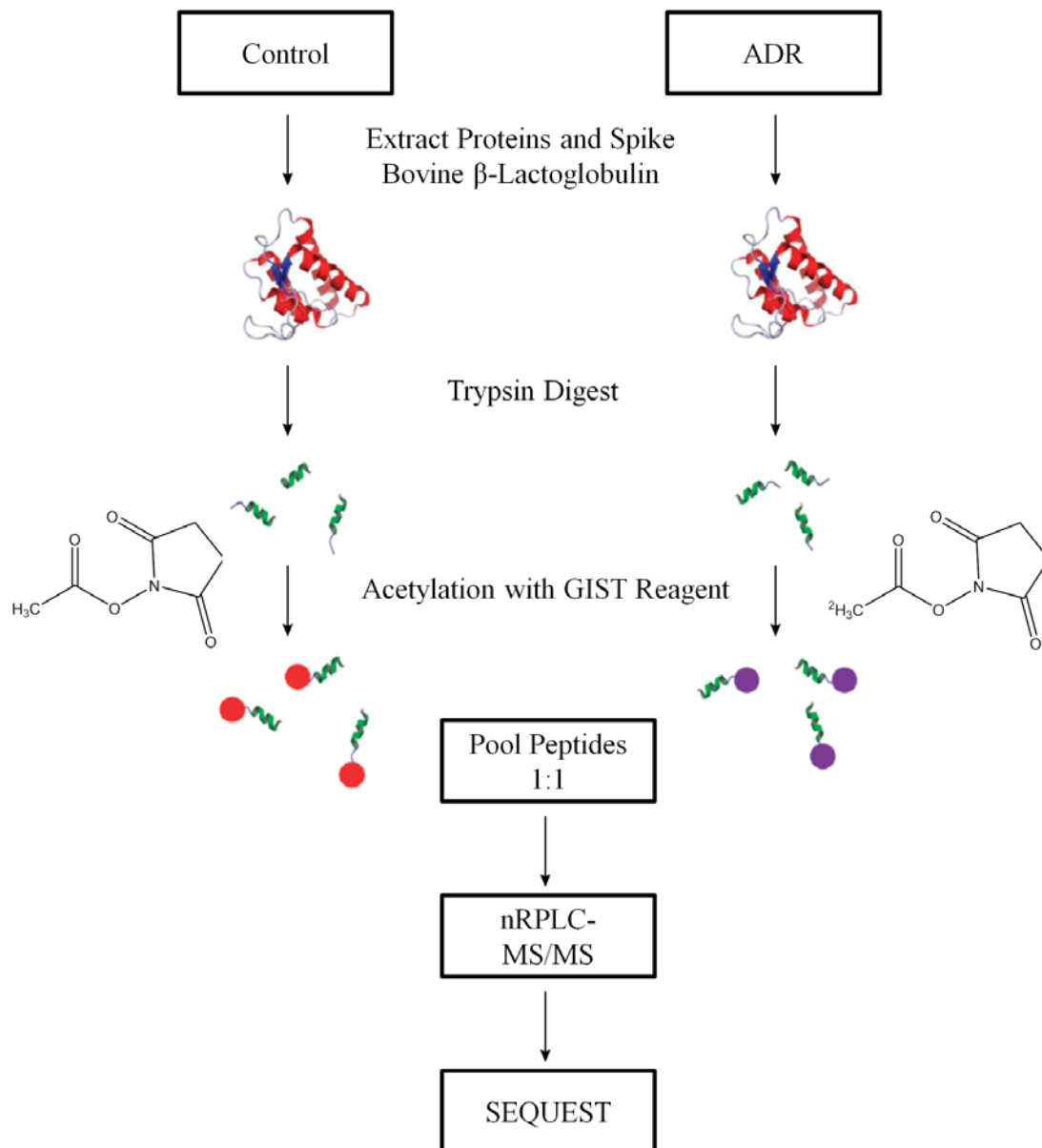
Figure 2.1. Schematic of the proteomics workflow showing internal standard spiking, GIST labeling, and nanoflow RPLC-MS/MS to determine differentially-expressed proteins in the spleen proteome of ADR-treated mice.

2.3.3. Internal Standard Normalization

Figure 2.2a shows an example parent mass spectrum obtained for a doubly-charged peptide pair at *m/z* 509.289 and 512.308 that eluted from the column at t_r = 80.8 minutes. The observed mass shift of 6 Da between the light and heavy labeled peptide peaks indicates that the peptide contains the addition of two acetylations to the peptide sequence. The CID-MS/MS spectrum for the light labeled peptide is shown in Figure 2.2b displaying a consecutive series of b- and y-type fragment ions. The CID-MS/MS spectrum for the heavy labeled peptide is similar (data not shown). This peptide pair has been assigned as the [(Acetyl)LIVQTMK(Acetyl)+2H]$^{2+}$ peptide of β-lactoglobulin. The ratio of heavy/light labeled peptides for the internal standard should be unity as 1 µg of β-lactoglobulin was spiked into protein extracts of both control and ADR-treated spleen samples. The measured ratio for heavy/light labeled peaks shown in Figure 2a is 1.0 based on peak areas, which agree with the expected values. The ratio values for other tryptic peptides of β-lactoglobulin are similar and an average protein ratio value of 0.98±0.10 is observed across all 15 injected samples. β-lactoglobuin ratio values within each technical replicate were used to normalize ratio values of mouse splenic proteins.

As previously discussed, isotopically labeled peptide mixtures were subject to triplicate LC-MS/MS analyses. Figure 2.3 shows a bar graph of the total number of proteins identified in each individual analysis. The average number of proteins detected in a single injection is 189± 29. The total number of proteins identified increases with each new sample injection such that, after accounting for redundant entries, we identified a total of 388 unique proteins across the 15 injections. This accounts for a total of 70,033 spectral peptide counts.

2.3.4. Differentially-Expressed Proteins in ADR-Treated Mice

Using a conservative set of criteria (see section 2.2.8), 59 proteins were assessed as differentially-expressed in ADR-treated mice (Table 2.2). These proteins are involved in processes such as cell signaling, protein translation, defense response, metabolism, Ca^{2+} binding and apoptosis, and structural
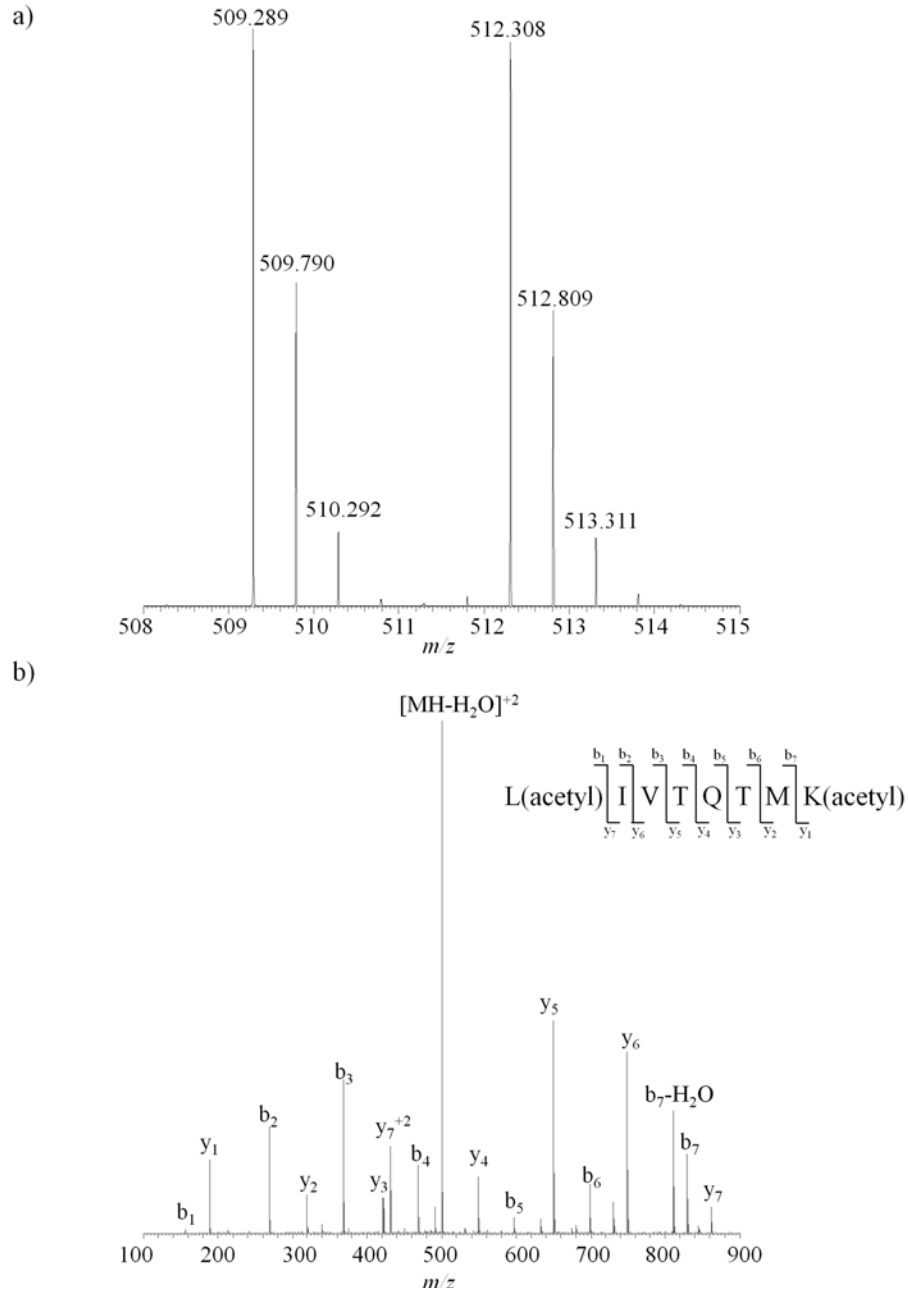
Figure 2.2. Example mass spectra a) of a peak pair [L(acetyl)IVTQTMK(acetyl)+2H]$^{2+}$ that eluted at t_r 80.8 minutes with *m/z* 509.289 and 512.308 for the light and heavy labeled peaks, respectively, and b) of the CID generated fragments obtained upon isolation of the light labeled peak at *m/z* 509.289. The peptide assigned belongs to β-lactoglobulin
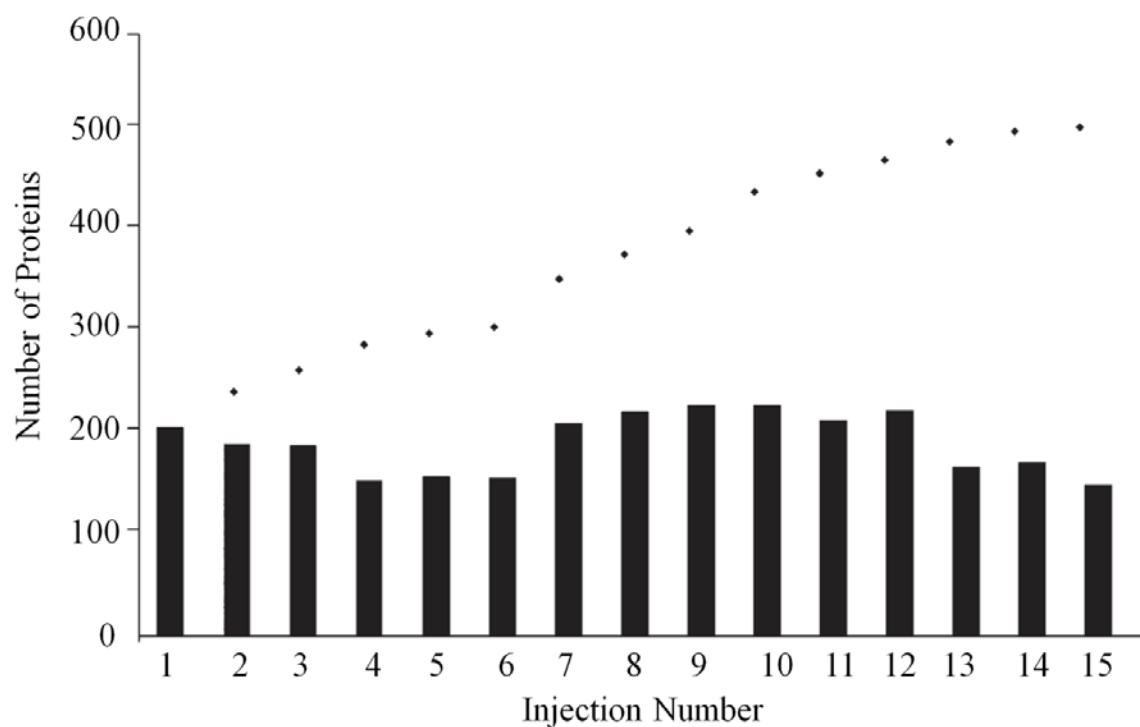
Figure 2.3. Bar graph of the total number of proteins identified in individual LC-MS/MS analyses and the total number of newly assigned proteins identified with each consecutive experiment (diamonds). The values shown include redundant protein assignments that arise due to isoforms.

Table 2.2. List of Differentially-Expressed Proteins in Adriamycin-Treated Mice.

Accession[a]	Protein Name	ADR/CTR $\pm$ SE[b]	Injection Number[c]	Function
Upregulated				
00130589.8	Superoxide dismutase [Cu-Zn]	1.5 ± .3	14	antioxidant
00317309.5	Annexin A5	2.0 ± .3	15	Ca+2 binding / apoptosis
00885292.1*	Annexin A2	2.5 ± .4	11	Ca2+ binding
00761696.2	Calmodulin	3.5 ± 2.1	6	Ca2+ binding / apoptosis
00123639.1	Calreticulin	1.9 ± .7	11	Ca2+ binding/chaperone
00319992.1	78 kDa glucose-regulated protein	1.6 ± .3	12	Ca2+ chaperone
00128484.1	Hemopexin	18 ± 7.6	6	immune response
00323624.3	Complement C3	5.5 ± 1.3	10	immune response
00406302.2*	Alpha-1-antitrypsin 1-1	2.3 ± .4	11	immune response
00118413.2*	Thrombospondin 1	1.8 ± .4	10	immune response
00131830.1	Serine protease inhibitor A3K	3.8 ± 1.2	6	metabolism
00831033.1	Phospholipase D4	3.1 ± 1.2	6	metabolism
00928204.1*	Sulfated glycoprotein 1 preproprotein	3.1 ± .7	11	metabolism
00466919.7	6-phosphogluconate dehydrogenase, decarboxylating	2.8 ± 1.8	12	metabolism
00221402.7	Fructose-bisphosphate aldolase A	2.5 ± 1.5	13	metabolism
00649586.1*	Nucleoside diphosphate kinase	1.8 ± .6	8	metabolism
00111218.1	Aldehyde dehydrogenase, mitochondrial	1.6 ± .1	11	metabolism
00135686.2	Peptidyl-prolyl cis-trans isomerase B	6.2 ± 3.1	8	signaling
00894769.1	Parkinson disease (Autosomal recessive, early onset) 7	1.7 ± .7	10	signaling
00118899.1	Alpha-actinin-4	3.3 ± 1.3	15	structure
00380436.1	Alpha-actinin-1	2.2 ± .6	15	structure

Table 2.2. (continued)

Accession[a]	Protein Name	ADR/CTR ± SE[b]	Injection Number[c]	Function
00114375.2	Dihydropyrimidinase-related protein 2	2.3 ± .3	10	structure
00874728.1	Isoform 2 of tropomyosin beta chain	5.9 ± 2.5	9	structure
00421223.3	Tropomyosin alpha-4 chain	3.6 ± 1.0	14	structure
00405227.3	Vinculin	3.2 ± .5	15	structure
00830701.1	37 kDa protein	3.0 ± .6	6	structure
00348094.4	Tubulin, beta 1	2.1 ± .7	6	structure
00131376*	Spectrin beta chain, erythrocyte	1.9 ± .7	7	structure
00465786.3	Talin-1	1.9 ± .2	15	structure
00227299.6	Vimentin	1.8 ± .2	15	structure
00130102.4	Desmin	2.4 ± .3	11	structure
00226515.5	Transgelin	2.3 ± .3	11	structure
00125778.4	Transgelin-2	1.9 ± .3	14	structure
00664643.2*	Filamin, alpha	1.8 ± .2	15	structure
00226073.2*	Heterogeneous nuclear ribonucleoprotein F	1.6 ± .7	6	translation
00109044.8*	Myosin	3.1 ± 1.5	11	transport
00938530.1	Myosin-11 isoform 1	1.6 ± .3	14	transport
00123181.4	Myosin-9	1.6 ± .2	15	transport

Table 2.2. (continued)

Accession[a]	Protein Name	ADR/CTR ± SE[b]	Injection Number[c]	Function
Downregulated				
00320217.9	T-complex protein 1 subunit beta	.64 ± .06	9	chaperone
00755843.1*	SET translocation	.50 ± .11	6	chaperone
00136906.1	Macrophage-capping protein	.43 ± .10	9	immune response/structure
00112719.1	Delta-aminolevulinic acid dehydratase	.44 ± .19	9	metabolism
00420363.2	Probable ATP-dependent RNA helicase DDX5	.50 ± .09	7	metabolism
00665513.3	Putative uncharacterized protein Gm6636	.49 ± .19	6	metabolism
007544464.1*	GTPase IMAP family member 4	.58 ± .33	6	metabolism
00223757.4	Aldose reductase	.52 ± .16	6	metabolism
00113996.7	Flavin reductase	.37 ± .17	7	redox
001127358.1	SH3 domain-binding glutamic acid-rich-like protein 3	.65 ± .11	7	redox

32

Table 2.2. (*continued*)

Accession[a]	Protein Name	ADR/CTR $\pm$ SE[b]	Injection Number[c]	Function
00462291.5	High mobility group protein B2	.26 ± .05	6	signaling
00656269.1	14-3-3 protein theta	.66 ± .17	8	signaling
00330063.6*	F-actin-capping protein subunit alpha	.65 ± .09	6	structure
00317794.5	Nucleolin	.39 ± .06	8	transcription
00230133.5	Histone H1.5	.41 ± .05	10	transcription
00282848.1	Histone H3.2	.66 ± .08	10	transcription
00124287.1	Polyadenylate-binding protein 1	.59 ± .10	6	translation
00123604.4	40S ribosomal protein SA	.62 ± .32	7	translation
00134599.1	40S ribosomal protein S3	.25 ± .08	8	translation
00322562.5	40S ribosomal protein S14	.62 ± .13	6	translation
00817004.1	Heterogeneous nuclear ribonucleoprotein A1	.53 ± .11	6	translation

*Indicates a protein sequence that was returned in the search results with redundant identifications due to protein isoforms that could not be distinguished based on peptides observed

[a]Accession numbers reported are taken from the International Protein Index mouse database

[b]Values represent the average ADR/CTR value ± standard error, whereby 6<N<15 (see Experimental of details) depending on the number of biological and technical replicates in which the protein (peptides) were observed

[c]Total count of proteins identifications across all experiments (injections). 6<N<15

stability. In total, 37 proteins are upregulated (ADR/CTR > 1.5) and 21 proteins are downregulated (CTR/ADR > 1.5). Most of the upregulated proteins and all of the down-regulated proteins change by a factor of 1.5-4.0. Four upregulated proteins (i.e., complement C3 protein, tropomyosin 2, peptidyl-*cis/trans*-isomerase, and hemopexin) were expressed by a factor of >4 in spleen tissue as a result of ADR treatment.

2.3.5. *MS/MS and Western Blot Analysis of Annexin A2*

Figure 2.4a shows an example MS/MS spectrum for a doubly-charged peptide pair at *m/z* 792.934 and 794.445. The isotopically labeled peaks have a ADR/CTR ratio of 2.0, indicating the upregulation of this species in ADR-treated mice. The MS/MS spectrum in Figure 2.4b shows fragment ions that correspond to the peptide sequence $[(Acetyl)GVDEVTIVNILTNR+2H]^{2+}$ that belongs to the protein, annexin A2. Annexin A2 has an average ADR/CTR ratio of 2.5 ± 0.4 as measured across 11 injections (Table 2.2). Western validation was carried out in order to confirm protein changes measured with our proteomics workflow for annexin A2. Figure 2.5 shows an example Western blot obtained for control and ADR-treated splenic proteins for annexin A2 and actin (loading control). A 50% increase in annexin A2 levels is observed in ADR-treated mice supporting upregulation of this protein, which is consistent with proteomics results (Figure 2.5).

2.4. DISCUSSION

This work reports the first investigation of the effects of ADR treatment on splenic protein levels in mice. The spleen is involved in innate and adaptive immunity and helps to regulate immune homeostasis [147]. The spleen consists of lymphocytes such as T-cells, B-cells, and macrophages with functions that include blood filtering, iron recycling, pathogen response, and immune induction, activation, and proliferation [147]. These functions are critical for normal conditions and even more so in diseased states, such as cancer. The smaller spleen weight measured in this work (Table 2.1) is consistent with other reports of reduced body weight and spleen size in ADR-treated mice [136, 148-150] and

Figure 2.4. Example mass spectra a) of a peak pair [(Acetyl)GVDEVTIVNILNR+2H]$^{2+}$ that eluted at t_r 117.5 minutes with *m/z* 792.934 and 794.445 for the light and heavy labeled peaks, respectively, and b) of the CID generated fragments obtained upon isolation of the light labeled peak at *m/z* 792.934. The peptide belongs to the annexin A2 protein.
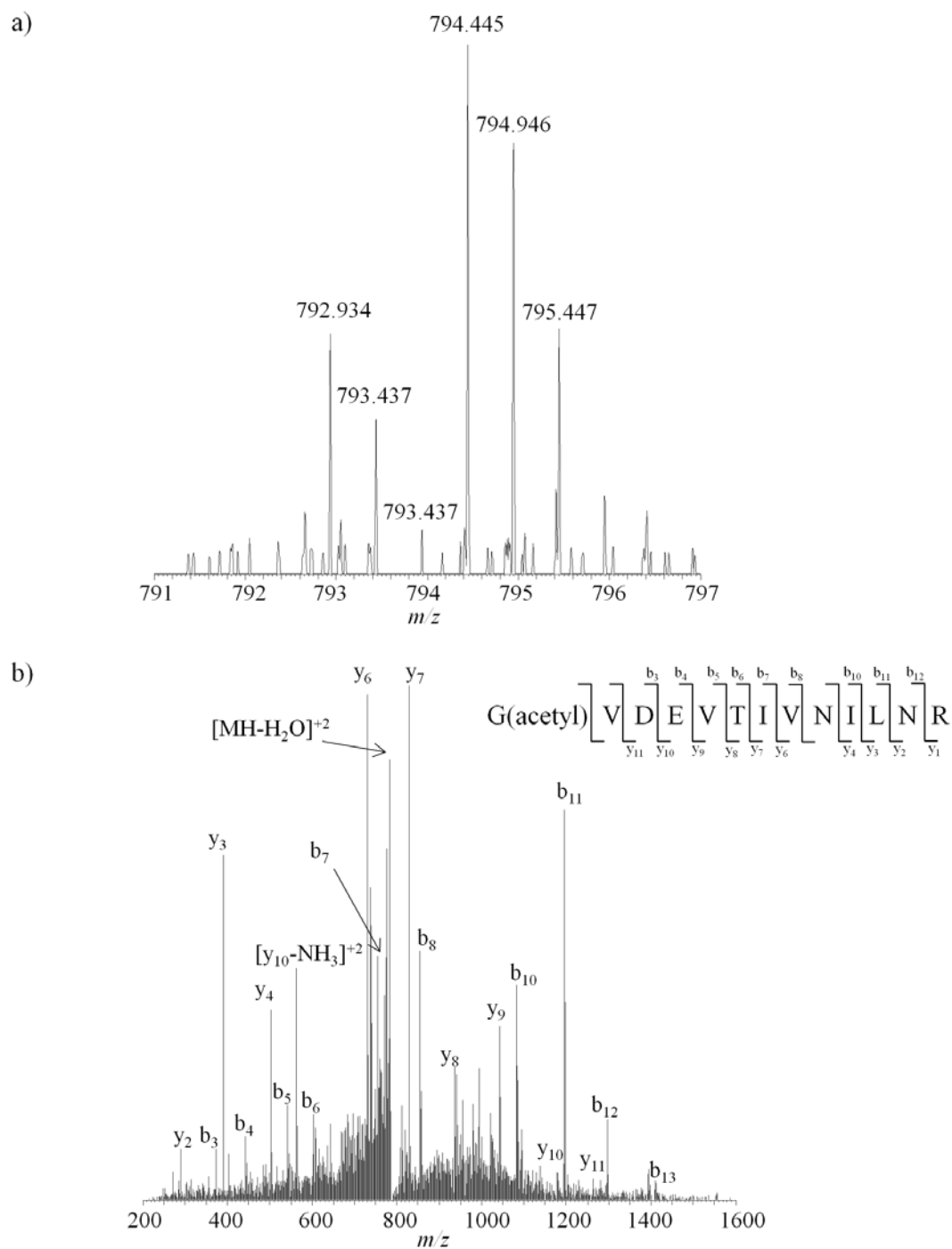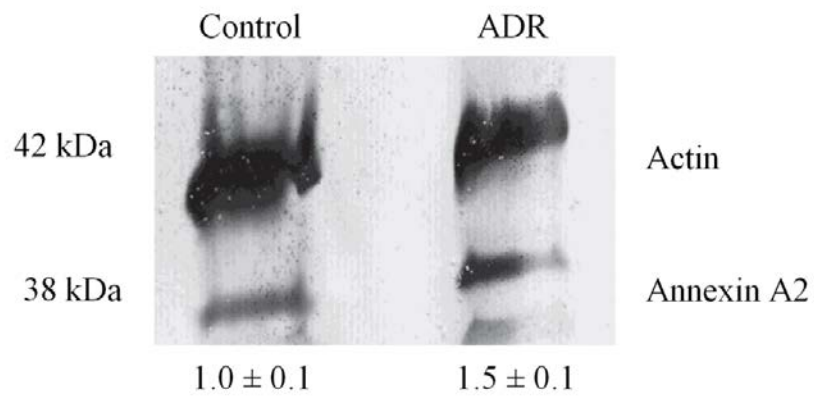
Figure 2.5. Example Western blot image of annexin A2 and actin (loading control) protein expression. The percent annexin A2 in control and ADR-treated mice obtained after normalization of annexin A2 levels to actin levels are listed underneath the image, N = 3.

supports the notion that altered cell differentiation [127] as well as decreased lymphocyte proliferation [148, 151] persist with ADR treatment. Reduced spleen size is also reflective of lower numbers of lymphocytes, which occurs with aging [152] and could result in a weakened immune response in ADR-treated patients.

Following acute ADR treatment in mice, 59 splenic proteins were differentially-expressed (Table 2.2). Figure 2.6 shows a graphical illustration of the major pathways affected by ADR treatment, which we discuss below. These proteins are involved in a number of biological processes such as Ca^{2+} binding and apoptosis, DNA transcription and repair, cellular signaling, redox maintenance, metabolism, immune/defense response, and structural maintenance.

2.4.1. Ca^{2+} Binding/Apoptosis Proteins

Proteins involved in Ca^{2+}-binding, apoptosis, and chaperone activity were upregulated in ADR-treated mice. Annexins 2 and 5 belong to a class of Ca^{2+}-dependent membrane binding proteins. Annexin binds to both free Ca^{2+} and the phospholipids of the membrane structure [153] and may be a key moderator of apoptosis. Annexin A2 has been reported as upregulated in ADR resistant cells [138, 154] suggesting its importance for chemoresistance. Annexin A5 has been found to inhibit apoptosis of phagocytes [155]. Upregulation of annexin A5 in ADR-treated mice is consistent with upregulation in the thymus [136], ADR-treated HepG2 cells [133], and in MCF-7/ADR resistant cells [143, 156].

Calreticulin, is a Ca^{2+}-binding chaperone protein that is localized to the endoplasmic reticulum. Although calreticulin has a number of biological functions its primary roles involve modulation of Ca^{2+} homeostasis and molecular chaperone activity. Upregulation of calreticulin can lead to elevated levels of free Ca^{2+} that is housed in intracellular stores [157]. Additionally this protein is localized to the cell surface and is critical for initiating immune response [158]. In ADR-treated cells calreticulin migrates from the ER and localizes to the surface of pre-apoptotic and cancerous cells, which will undergo clearance by lymphocytes [159]. Calmodulin is another Ca^{2+}-binding protein, which is involved in Ca^{2+} homeostasis, cellular growth, proliferation, and transport processes and has been implicated in

37
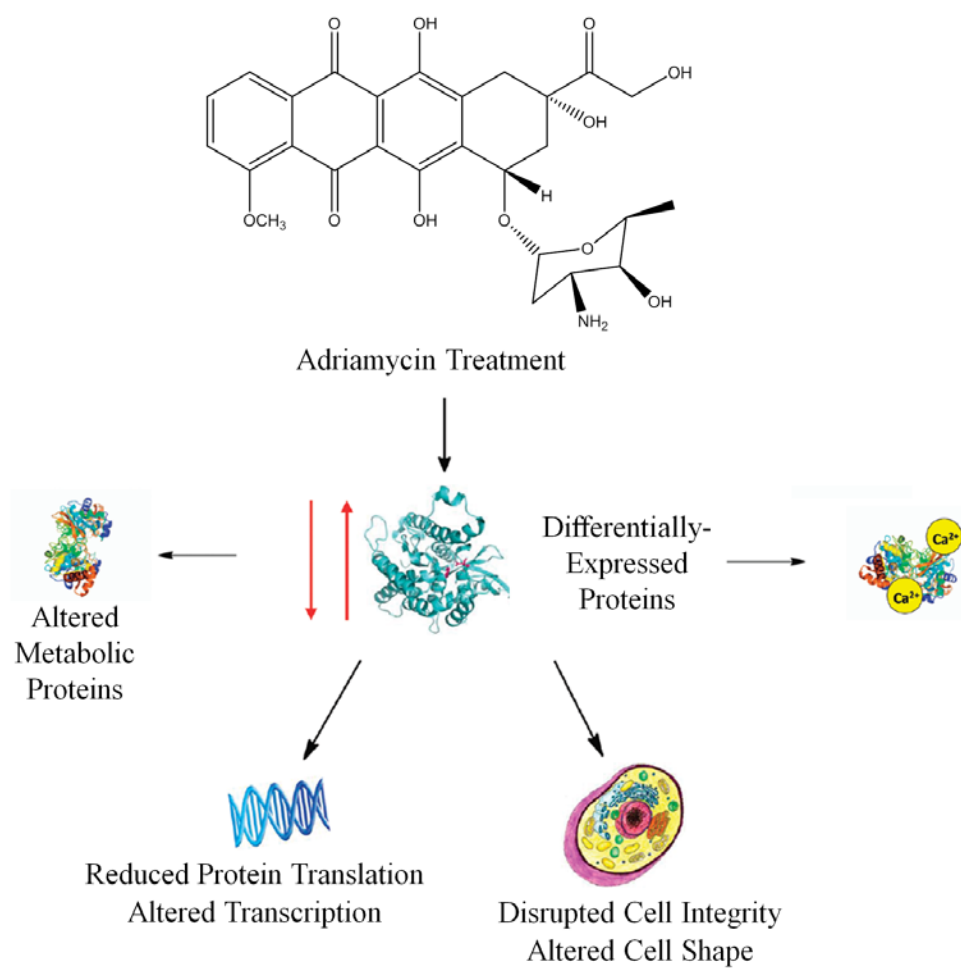
Figure 2.6. Illustrative depiction of differentially-expressed splenic proteins (pathways) that are affected from ADR-treatment.

chemoresistance of cancer therapies [160]. Ca^{2+} ion flux is important in modulating cell death in the immune system [161], thus overexpression of Ca^{2+}-binding proteins observed in ADR-treated mice could alter free Ca^{2+} levels and lead to irreversible cell injury and death.

2.4.2. Transcription and Translation

Several transcriptional and translational-related proteins were downregulated in ADR-treated mice. Histone proteins oligomerize to form the nucleosome, which is the core component of chromatin, and help to recruit proteins to DNA. Nucleolin is a histone chaperone protein that is found on the surface of cancerous cells [162]. Downregulation of nucleolin and histones H1.5 and H3.2 may be directly related with ADR's mechanistic action of DNA intercalation and inhibition of topoisomerase II, which results in disrupted transcription. Other histone proteins have been reported as upregulated in human Jurkat T-cells treated with ADR [134]. It is not clear why there are differences in histone expression between these studies but it may be because transcription is affected by ADR treatment.

The 40S ribosomal proteins SA, S3, and S14 were downregulated in ADR-treated mice, which is consistent with studies in ADR-treated Jurkat T-cells [134]. Heterogeneous nuclear ribonucleoproteins (HNRP) in this work differed in expression levels. For example, HNRP A1 is downregulated, whereas HNRP F is upregulated (Table 2.2) in ADR-treated mice. In Raji cells treated with ADR, HNRP C1/C2 was downregulated, whereas in ADR resistant cells HNRP D is upregulated [138]. Polyadenylate-binding protein 1, another protein involved in protein translation, is downregulated in these studies. Overall, it appears that ADR treatment reduces protein translational activity which may be related with oxidative damage and altered transcription.

2.4.3. Cytoskeletal/Structural Proteins

Proteins involved in integrity of the cytoskeleton or other structures represent the largest group of differentially-expressed proteins in ADR-treated mice. Cytoskeletal proteins have been implicated as potential targets for chemotherapeutic treatments in cancer [163]. Cytoskeletal and structural related

proteins in these studies were all found to be upregulated, with the exception of F-acting-capping protein, which is downregulated in ADR-treated mice. Upregulation of filamin, tropomyosin, spectrin, and tubulin is consistent with studies in ADR-treated HepG2 cells [133]. Vimentin is upregulated in these studies and in ADR-treated human Jurkat T cells [134] but has also been reported as downregulated in ADR-treated Raji cells [135].

Tubulin proteins are the base unit of microtubules in the cell, which are needed for cellular transport and structural integrity. Both α- and β-tubulin were upregulated in the thymus of ADR-treated mice [136], which is consistent with these results. However, β-tubulin has also been observed to be downregulated following ADR treatment [133]. α-actinin is a ubiquitously expressed cytoskeletal protein that is comprised of an actin-binding domain, a calmodulin-like domain, and a calponin-homology domain [164]. Actinin belongs to a family of F-actin cross linking proteins that also includes spectrin. α-actinin-1 and -4 are found in nonmuscle tissues and are necessary for T-cell migration and activation [164].

The proteins described above as well as transgelin, transgelin-2, and dihydropyrimidinase-related protein 2 detected in these studies, each has a key role for normal maintenance of the cytoskeletal structure. Upregulation of cytoskeletal proteins following ADR treatment could occur due to a compensatory mechanism to maintain structural stability. In addition to detrimental effects caused by cancerous cells, chemotherapeutic compounds (e.g., ADR) have been suggested to be a major cause of disruption of cytoskeletal proteins [165]. Consequences of disrupted cytoskeletal integrity include alterations to cell shape, growth, and transport which may lead to cell destruction and failure.

2.4.4. Chaperone/Immune and Defense Response/Antioxidant

Differential regulation of proteins involved in cellular defense processes indicates that cells are under attack or there is cellular dyshomeostasis, particularly in these studies as a result of ADR treatment. Glucose-regulated 78 kDa (GRP78) protein belongs to the class of heat shock 70 proteins, which serve as

molecular chaperones. GRP78 is endoplasmic reticulum resident and involved in misfolded protein response. Other functions of GRP78 include Ca^{2+} homeostasis, apopotosis, and cellular signaling related with cancer cell proliferation and survival [166]. GRP78 overexpression is associated with a number of cancers and may be indicative of cellular stress or favorable survival outcomes due to the removal of cancerous cells [166]. Upregulation of GRP78 in these studies may suggest that ADR treatment provides cells with additional defenses against misfolded proteins that are likely to occur in cancer patients. Downregulation of T-complex protein 1-a cytosolic chaperone protein[167] suggests that there is an imbalance in the overall cellular chaperone machinery in the presence of ADR.

Immune response proteins: complement C3, α-1-antitrypsin 1-1, and thrombospondin 1 were upregulated in ADR-treated mice. Thrombospondin 1 inhibits tumor cell progression and angiogenesis and has been investigated as a potential target for cancer therapy [168]. Due to the multifunctional roles of thrombospondin 1, it is possible that upregulation of this protein following ADR treatment results in reduced tumor growth in normal and cancerous cells. Complement C3 is directly involved in the complement system that is a part of the innate immune response. α-1 antitrypsin 1, a proteinase inhibitor, is also involved in immune response by protecting cells in inflammatory conditions. Hemopexin, is a scavenger of free heme that is used to transport molecular oxygen. It belongs to the acute-phase proteins, which can be activated in the immune system under inflammatory conditions and is sometimes localized to the surface of macrophages in spleen for receptor binding [169]. ADR treatment, based on upregulation of these splenic proteins, may help to increase immune response by initiating compensatory inflammation mechanisms.

Superoxide dismutase (SOD) is an endogenous antioxidant defense enzyme that eliminates superoxide anion through catalyzing the dismutation of superoxide anion to oxygen and hydrogen peroxide. Manganese SOD has been heavily implicated in cancer [170], however we detected upregulation of Cu-Zn SOD (or SOD1) in ADR-treated mice. St. Clair *et al.* demonstrated that an overexpression of SOD2 in heart tissue helps protect the heart from oxidative damage and ADR

cardiotoxicity [171]. Due to the antioxidant nature of SOD, upregulation of this enzyme may be in result to the free radicals generated from ADR redox recycling and thus serves to protect cells from oxidative damage.

2.4.5. Metabolism

Metabolic proteins in these studies had varying expression in response to ADR treatment (Table 2.2). Serine protease inhibitor A3K, isoform 2 of phospholipase D4, sulfated glycoprotein 1 preprotein, 6 –phosphogluconate dehydrogenase, fructose-bisphosphate aldolase A, nucleoside diphosphate kinase, and aldehyde dehydrogenase were upregulated in ADR-treated mice, whereas δ-aminolevulinic acid dehydratase, probable ATP-dependent RNA helicase DDX5, GTPase IMAP family member 4, aldose reductase, and flavin reductase were downregulated. Alterations to metabolic proteins were also observed in thymus from ADR-treated mice [136]. Alterations to metabolism in peripheral immune organs (i.e., spleen, and thymus) can be compared with reports describing changes to myocardial energy metabolism [172]. Differential-expression of metabolic splenic proteins shows that ADR treatment has downstream effects in glycolysis, glucogenesis, and other metabolic pathways. For example, aldose reductase, which converts glucose to fructose during impaired glycolysis, also functions to reduce toxicity of lipid peroxidation products, such as 4-hydroxy-trans-nonenal. Downregulation of this particular enzyme may be detrimental to spleen in ADR-treated mice. Normal energy production is critical to help cells have a better defense response against cellular toxicity and cancer and to maintain normal cellular homeostasis.

2.4.6. Redox/Cellular Signaling/Transport

The redox system in the cell is crucial to maintaining a balance between reactive oxygen species and antioxidants, which keeps cells free from oxidative stress and damage. Redox processes are altered following ADR treatment in cancer cells [137]. Splenic proteins involved in cellular signaling and transport processes were differentially-expressed in ADR-treated mice (Table 2.2) and have been implicated in other proteomic studies investigating effects of ADR treatment [128, 133-135]. Peptidyl-

prolyl cis-trans isomerase B belongs to the family of PPIase enzymes that isomerize proline residues in target proteins and assist in protein folding. This particular PPIase is upregulated in spleen whereas Pin 1 is downregulated in the brains of ADR-treated mice [128]. Myosin proteins (i.e., Myosin, Myosin-11, Myosin-9) are ATP-dependent proteins which regulate actin-based cell motility and were detected as upregulated in these studies. Myosin-9 and Myosin-11 were downregulated in mitochondrial Raji cells after ADR treatment [135]. The differences observed in expression of myosin, Pin1, and 14-3-3 may be tissue specific. Upregulation of these proteins following ADR treatment could be related to upregulation of cytoskeletal proteins, which would be necessary for maintenance of cellular structure and hence cellular transport.

2.5. CONCLUSIONS

ADR treatment is reported to have detrimental effects on a number of tissues in animal models and in cell cultures. Downstream effects of ADR-treatment on mouse spleen tissue include reduced spleen size and alterations to the global splenic proteome for proteins involved in cellular processes such as cytoskeletal structural integrity, Ca^{2+} binding, immune response and others. It is possible that ADR treatment through alterations to protein expression leads to weakened immunity. Insights gained from these studies will be useful for understanding toxic mechanisms of ADR treatment, which is necessary to minimize drug side effects and improve quality of life in cancer patients undergoing ADR treatment. In this work, we perform differential analysis of ADR-treated mice using the precursor quantitation technique global internal standard technology. Control and ADR-treated mice were treated with light and heavy acetyl groups, respectively creating a mass shift of 3 Da. While effective at providing accurate quantitation and determination of differentially-expressed proteins, five samples were prepared and analyzed individually.

3.0. PROTEOMICS QUANTIFICATION OF PROTEIN NITRATION*

3.1. INTRODUCTION

Protein nitration is a post-translational modification (PTM) that can occur under oxidative stress (**Section 1.1.1**) [33]. Nitration is mediated by an increased concentration of reactive oxygen and nitrogen species (ROS and RNS, respectively) such as $O_2^{\cdot-}$, $ONOO^-$, and $NO_2^{\cdot}$. An overabundance of cellular RNS levels can result in the formation of 3-nitrotyrosine (3NT) and 3NT-modified proteins [173]. Protein nitration may result in altered enzymatic activity [174, 175], reduced cellular signaling, disruption of phosphorylation pathways [176], and protein degradation [177]. In addition, this PTM has been linked to various diseases such as cancer, cardiovascular disease [178], arthritis [179], and neurodegenerative disorders such as Alzheimer's (AD) disease [180] and Parkinson disease (PD) [181, 182].

Elevated protein nitration has been observed in the brains of AD patients and is correlated with disease hallmarks such as amyloid-β peptide levels, senile plaque deposition, and neurofibrillary tangles (composed of tau proteins) as well as physiological symptoms such as memory loss, decreased motor and language skills, and other behavioral changes [26]. Furthermore, protein nitration is linked to AD disease progression and is detected in mild cognitive impairment (MCI), early AD, and advanced stages of AD [183-186]. The primary effects of protein nitration in AD are manifested in energy metabolism. For example, glyceraldehyde 3-phosphate dehydrogenase and α-enolase, proteins involved in the glycolytic pathway are nitrated [180, 187] leading to reduced enzymatic function [188] potentially limiting ATP production [189]. Nitration of tau proteins has been observed in MCI and may influence the early onset of AD [190]. Other pathways such as cytoskeletal integrity [191], pH buffering [192], mitochondrial

dysfunction [193], and lipid abnormalities [194] are also affected by protein nitration in AD and indicate the importance of this PTM for disease pathogenesis [190].

Other neurodegenerative disorders such as PD [195], Down's syndrome [196], Huntington's disease [197], and amyotrophic lateral sclerosis [198, 199] are also affected by protein nitration [33, 200]. Similarly, elevated levels of nitration are observed in cardiomyopathy, cardiovascular disease, atherosclerosis [201-205], arthritis [206], diabetes [207], cancer [208], and aging [209, 210]. It can be inferred from the range of disorders affected by this PTM that the immune system is a major target of RNS. Increased NO production by nitric oxide synthases has been suggested to be linked to tissue injury [211]. Evidence of oxidative damage has been observed in lymphatic vessels of aged rats [212], CD8+ prostatic tumor-infiltrating lymphocytes[213], and T-cell receptors [214] ultimately weakening immune system response. Since protein nitration, specifically 3NT PTMs, are heavily implicated in disease it is worthwhile to review the state of current technology available to characterize this PTM in biological tissues. Herein, an overview of 3NT chemical properties and proteomics methods which allow the enrichment, characterization, and particularly the quantification of 3NT-modified proteins will be discussed.

The formation of 3NT occurs due to a series of chemical reactions involving ROS and RNS. Figure 3.1 outlines the most commonly encountered intracellular mechanism. A free radical oxidizes tyrosine to form a tyrosyl radical. The structure is stabilized by resonance moving the radical to the *ortho* carbon of the phenol ring [215]. Simultaneously occurring, endogenous nitrogen monoxide radicals (NO·) react with superoxide anion ($O_2^{·-}$) to produce peroxynitrite (ONOO⁻), a conjugate base of the peroxynitrous acid, which has a pKa close to physiological pH 7.0 [216]. In the presence of carbon dioxide, ONOO⁻ reacts to form nitrocarbonate anions [217]. The nitrocarbonate anion undergoes homolytic cleavage to form a highly reactive nitrite radical, which undergoes a combination reaction with the tyrosyl radical resulting in 3NT. Nitration has also been observed in other aromatic residues such as tryptophan and phenylalanine [218] through similar reaction mechanisms [219].
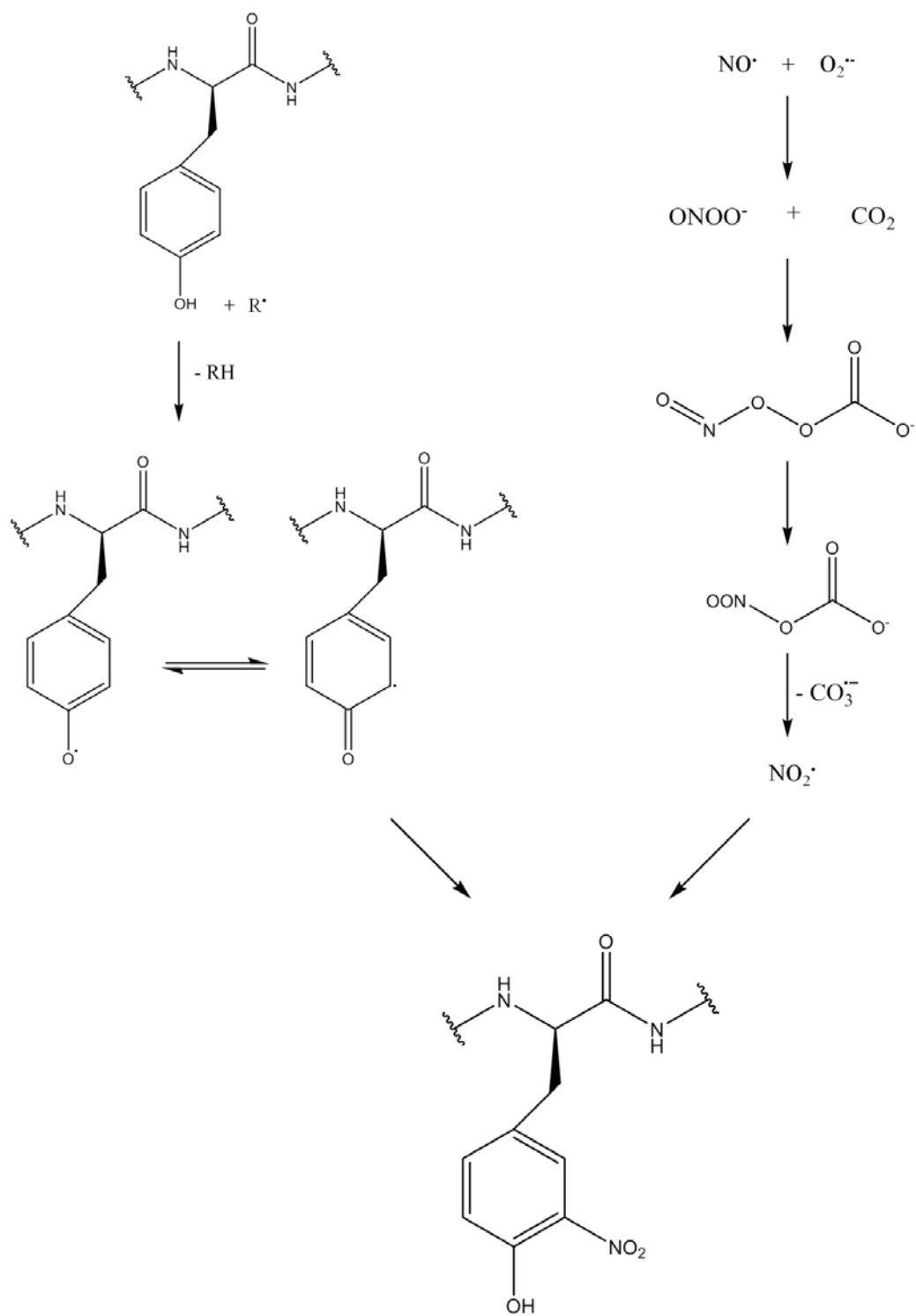
Figure 3.1. Chemical reactions describing the formation of 3-nitrotyrosine.

Aside from oxidative stress mechanisms, signaling pathways may rely on 3NT [218, 220]. Evidence of protein denitration in biological tissues has been observed suggesting that 3NT may be initiated and controlled by ROS and RNS leading to redox signaling in cellular processes [221]. Though tyrosine nitration is considered to be a stable PTM, and therefore a suitable marker for oxidative damage, there has been increasing evidence of a redox signaling pathway involving protein nitration. 3NT has been shown to interfere with kinase and phosphatase enzymes, which may have a regulatory effect on tyrosine phosphorylation pathways [217]. In addition, Mn superoxide dismutase has reduced function due to 3NT formation [222]. It has also been suggested that denitration may be selective to specific substrates. This has been observed in Histone H1.2 and calmodulin as specific targets for protein denitration [223]. Further research is currently underway in order to better understand the physiological importance of a reversible nitration signaling system [224].

The addition of the nitro group to the tyrosine ring alters chemical properties of the amino acid. The most notable change is the decreased pKa of the phenol group from 10.1 to 7.2 [225] or 6.8 [226]. This is a result of the nitro group on the phenol ring drawing electron density, which makes the phenol proton more labile and tyrosine more acidic. The lower pKa increases the amount of deprotonated nitrotyrosine molecules relative to tyrosine, which in addition to steric effects, can prevent phosphorylation events altering cellular signaling processes[218]. Spectroscopic measurements can be used to monitor the shift in pKa. For example, under acidic conditions the phenolic group of 3NT is protonated allowing hydrogen bonding with an oxygen atom of the nitro group, which can be observed in the 360 nm UV region. However, basic conditions which lead to deprotonation of the hydroxyl group and elimination of this hydrogen bonding shift the absorbance to 430 nm [218]. It should be noted that the absorbance changes of 3NT can allow monitoring of sample preparation procedures.

3.2. PROTEOMICS

Better insight to the effects of 3NT can be realized through the analysis of 3NT-modified proteins. Proteomic analysis of 3NT can be classified as redox proteomics, which focus on oxidative

modifications. It is noteworthy that redox proteomic technologies have also been developed for the detection of oxidized thiols [227], carbonylation [228], lipid peroxidation [229], and nitration amongst others. Specialized proteomic approaches for the detection of low abundant PTMs have been developed [230]. **Chapter 1** introduced techniques and strategies used in bottom-up proteomic experiments for protein identification and quantitation, which can also be applied to study 3NT presented below.

3.2.1. Enrichment

In vivo nitration of tyrosine residues are such that only five nitrated sites are detected per 10,000 tyrosine residues in inflammation conditions [217]. Because 3NT is a low abundance PTM, issues with ion suppression and false-positive identification arise. A conservative set of guidelines have been proposed to increase confidence in the identification of 3NT-modified proteins as follows: accurate peptide charge state and mass, detection of the 3NT immonium ion fragment peak (m/z 181.1), validation of 3NT peptide chromatographic retention (in comparison to unmodified peptide), and limitation of unassigned fragment peaks [231]. These guidelines can be adopted by any laboratory. In the context of biological tissues it can be challenging to identify 3NT-modified proteins, which has led to the development of enrichment strategies [232]. The earliest enrichment approaches included the use of an insoluble-antibody column specific to nitrated proteins [233] and immunoprecipitation [234]. Generally, enrichment of 3NT-modified proteins can be performed through the use of antibodies (e.g., anti-3NT) or alternatives such as chemical tags that target the nitro group.

Chemical tags rely on increasing the reactivity of 3NT through reduction reactions that generate 3-aminotyrosine (3AT) at the peptide level. This can be achieved with reducing reagents such as sodium dithionite and dithiothreitol (DTT) in the presence of heme as shown in Figure 3.2. A chemical tagging approach targeting 3AT offers the advantage of being gel-free and antibody-free. The significant pKa difference between the aromatic amine (~4.7) and other primary amines on a peptide chain (~8-10) allow for selective addition of chemical tags to 3AT. A plethora of these tags have been applied targeting 3AT
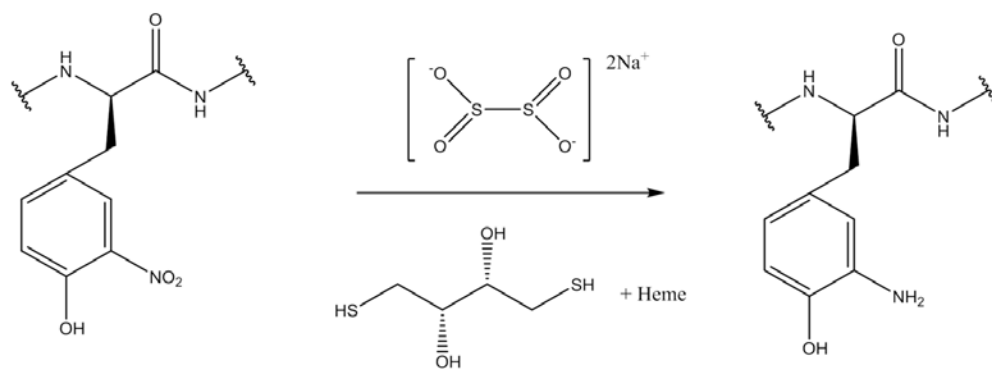
Figure 3.2. Reactions demonstrating the reduction of 3-nitrotyrosine to 3-aminotyrosine using sodium dithionite or dithiothreitol in the presence of heme.

including biotin/avidin interactions [235-237], nickel affinity chromatography [173], sulfhydryl enrichment [238], and fluorinated carbon tags [239]. Signature fragment ions that locate the site of 3NT-modifications can be generated with the use of dansyl chloride tags on the 3AT residue [240]. Fluorogenic derivatization of 3AT peptides with 1-(4(aminomethyl)phenylsulfonyl)pyrrolidine-3,4-diol allows enrichment with boronate affinity chromatography and quantification with fluorescence spectroscopy [241]. A summary of enrichment protocols for 3NT enrichment methods is presented [232].

An alternative enrichment method for 3NT-modified proteins, which is based on diagonal chromatographic separations, was recently reported [242, 243]. Combined fractional diagonal chromatography (COFRADIC) is a technique that recognizes the differences in hydrophilicity of 3NT- and 3AT-modified peptides in reversed phase chromatography. Peptide samples are subject to a one-dimensional reversed phase separation in which several off-line fractions are collected. Each fraction is subsequently reduced so that the 3NT residues are converted to 3AT residues. Direct LC analysis of the 3AT-peptide samples results in a shift in retention time due to the hydrophilic nature of the peptides relative to the original LC analysis of the 3NT-peptides. COFRADIC is designed to be a targeted analysis of 3NT modifications by focusing only on peptides which shift in retention time. As this is not a direct enrichment method, it does provide a straightforward means of identifying nitrated proteins in complex mixtures. A major observation from the application of COFRADIC to Jurkat cell lines was the detection of sulfated 3NT residues which arise due to a side reaction that occurs with the use of sodium dithionite during the reduction step. Thus, database search parameters should include sulfation as an additional dynamic modification of nitrated tyrosine residues.

3.3. QUANTITATIVE PROTEOMICS

3.3.1. Antibodies and Gel Electrophoresis-Based Methods

Enzyme-linked immunosorbent assay (ELISA) is a traditional method to quantify nitrated proteins using anti-3NT antibodies [244]. ELISA assays have been applied to quantitate 3NT in human plasma [245, 246], brain of traumatic injury patients [247], plasma from diabetic patients [248], and

plasma from smokers with chronic obstructive pulmonary disease [249]. Quantitation of protein bound 3NT has also been reported using ELISA analysis of human serum plasma [250] and can achieve a detection limit of 20 nmol/L [251]. Challenges occur with ELISA quantification due to the limited availability of highly specific antibodies [252] potentially resulting in underestimation of nitration levels. Additionally, the nature (e.g., monoclonal, polyclonal) and source (e.g., vendor) of the antibody and location of the 3NT modification can influence the recognition of 3NT-modified proteins [253]. Limitations with antibodies are not specific to 3NT or 3NT-based ELISA methods as will be discussed below.

Redox proteomics approaches for high throughput 3NT detection were initiated through gel electrophoresis-based measurements [254]. Figure 3.3 gives an overview of the gel-based approach. Two-dimensional (2D) gel electrophoresis separates proteins in the first dimension separation according to relative mobility (and hence MW) and by protein isoelectric point in the second dimension. For comparative analyses, individual 2D gels are prepared for control and experimental samples. Detection of protein spots can be achieved with fluorescence [7], chemiluminescence [255], or colorimetric assays such as Coomassie blue and silver staining [9]. At this stage, only information about the total protein abundance is obtained.

For targeted analysis of 3NT-modified proteins, the proteins in the gel are transferred to a nitrocellulose or PVDF membrane such that the 2D blot can be probed with an anti-3NT antibody [256] and scanned with an image reader. In this Western analysis, only protein bands which contain 3NT should appear on the blot and be indicative of the relative concentration of the 3NT-modified protein. Normalization is used to compare the 3NT signal from the blot to the total protein signal on the 2D gel prior to comparisons between the control and experimental samples. The Western blot image serves to locate the nitrated proteins and provide quantification, however does not provide identification of the protein spot. Thus, the Western blot and 2D gel must be aligned, and the protein spots of interest are excised, digested, and analyzed with MS. Examples of the application of this gel-based Western analysis

51
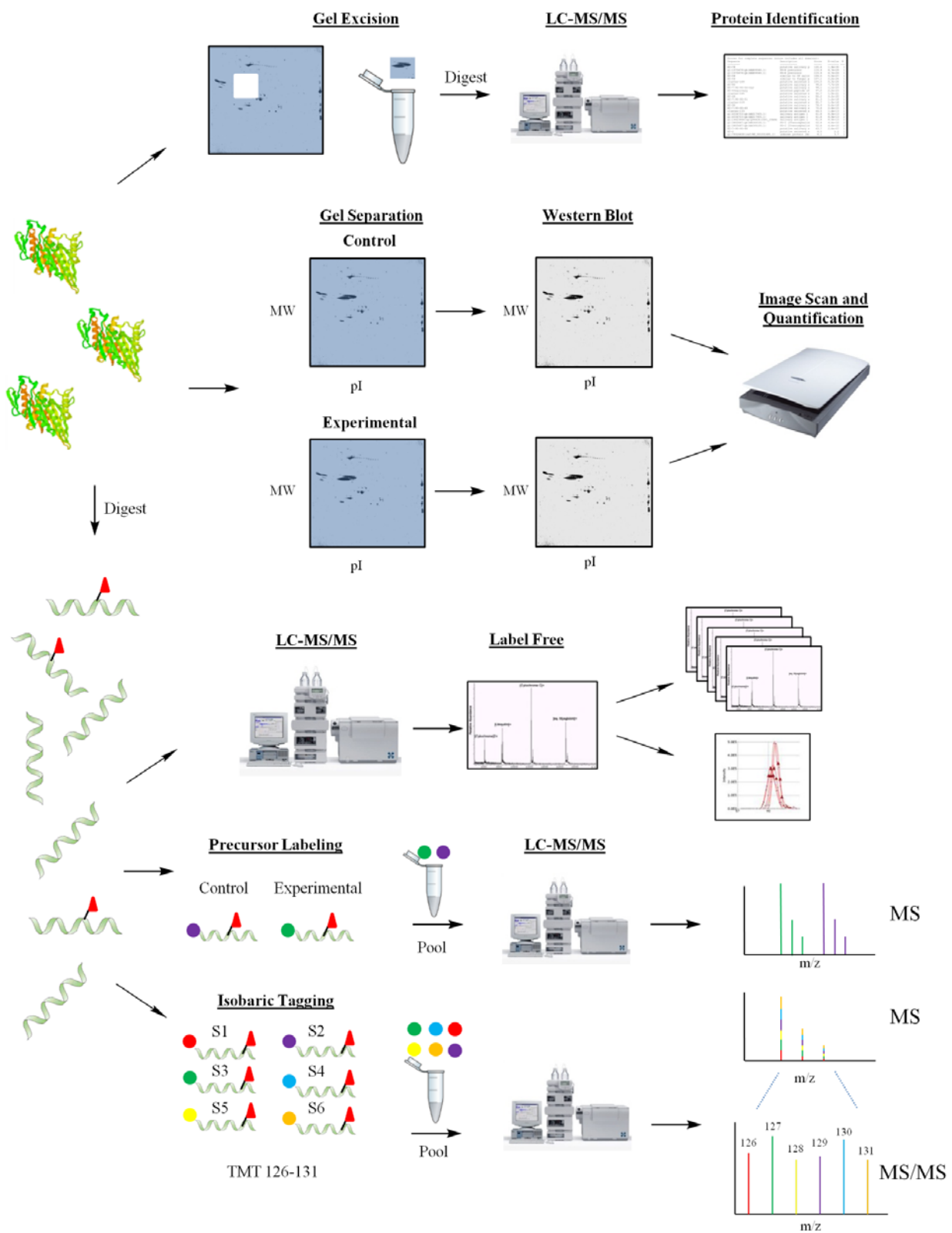
Figure 3.3. Schematic of general workflows for quantitative proteomic studies of nitrated proteins. Note that 3NT sites are identified by triangles.

include studies of undernourished rats [257], nitration levels of manganese superoxide dismutase in liver [222], and cystic fibrosis in lung [258].

Gel-based approaches are very attractive because they are robust, allow detection of thousands of protein spots, and can be targeted for specific PTMs such as 3NT. However, there are some challenges with this approach, which require further development. For example, sample preparation steps which incorporate DTT can cause reduction of 3NT-modified proteins (to 3AT) in the presence of heme found in many biological samples [259]. This contributes to underestimation of nitrated protein levels. Site-specific information about the location of the 3NT modification can only be obtained through MS detection of the excised spot [253], however MS analysis of peptides often miss the nitrated peptides. In addition, protein solubility of 3NT-modified proteins in gel-based buffers may not be complete providing limited abundance or no abundance information [253, 260]. Finally, antibody specificity as noted above and high background signals from antibodies in the blots can mask low level nitrated proteins [261].

3.3.2. Label-Free Methods

Label-free methods of quantification in proteomics, as implied, do not use chemical tags. Quantification is achieved through protein abundance index [68], MS/MS spectral counts [262] or extracted ion intensity (based on peak heights or areas) [65, 263] after LC-MS/MS analyses as shown in Figure 3.3. These methods are advantageous because they are simple, inexpensive, and require minimal sample preparation in comparison to chemical tagging approaches. Additionally, it is possible to analyze an unlimited number of samples with label-free methods. However, with each additional sample the overall throughput of the approach is lessened thus making multiplexing approaches attractive.

The native reference peptide method is capable of quantifying 3NT by comparing the peak area of nitrated peptides to a selected peptide present in the mixture [264]. Ideal characteristics concerning the choice of the reference peptide have been previously described [265]. Briefly, the peptide must be inherent in the digest mixture, contain no potentially modifiable residues, have high digestion efficiency, and have similar chromatographic retention times and detector responses to the 3NT peptide of interest.

53

Overall these characteristics result in an internal peptide standard that is inherent in the original digest. Native reference peptides selected from in vitro nitrated albumin resulted in a 10% relative standard deviation and femtomole detection limit of nitrated peptides [265].

Stable isotope dilution, which relies on spiking known concentrations of heavy isotope 3NT into a hydrolyzed protein sample (i.e., a mixture of free amino acids), can provide absolute quantitative information. Selected ion monitoring (SIM) of heavy isotope peaks using a triple quadrupole MS produce detection limits of 3NT as low as five pg in reported nitration studies of human urine [266]. While this method gives insight to the global levels of 3NT in the mixture it lacks site- and protein-specific detail, which is important for complete characterization of 3NT-modified proteins.

Nitrated peptides upon gas-phase fragmentation result in a peak at m/z 181.1 which is the immonium ion of nitrotyrosine [195]. Selected (SRM) or multiple reaction monitoring (MRM) allows selective detection of fragments from nitrated peptides by scanning the Q3 of a triple quadrupole MS in a collision induced dissociation experiment. Peak areas from the signature fragments are compared to that from reference peptides and are indicative of the relative concentrations of the 3NT-modified peptides and hence proteins. Using MRM, levels of 3NT-modified peptides from α-synuclein have been characterized in PD [195]. SRM analyses have also revealed eleven 3NT sites in human hemoglobin obtained from cigarette smokers suggesting that *in vivo* $ONOO^-$ levels are higher in smokers [267].

3.3.3. Precursor Labeling

Complementary or alternative MS-based methods to gel-based approaches have been developed in the last two decades and are attractive due to multiplexing capabilities [1]. Sample multiplexing with bottom-up proteomic methods can be achieved with precursor or isobaric tags at the MS [67] and MS/MS spectral levels. **Chapter 1** reviewed precursor quantitation strategies in bottom-up proteomics. To briefly highlight, 3NT-modified proteins can be digested to peptides (e.g., 3NT modified and unmodified) using trypsin. Primary amine groups found in lysine, N-termini, or 3AT residues can be manipulated to incorporate chemical groups using acetylation [268] or dimethylation [74] that can contain stable isotopes

54

(e.g., ^{2}H and ^{13}C). Depending on the nature of the chemical tag and heavy isotope incorporation, a total of two to three samples can be pooled and simultaneously measured in the LC-MS/MS experiment. As illustrated in Figure 3.3, the peptide peaks from light and heavy labeled samples elute from the LC column simultaneously and are detected in the mass spectrometer. This assumes that electrospray ionization of the peptides is similar and will not influence the final signal measured. Therefore the peaks are shifted in mass by the number of heavy isotopes incorporated into the tag and the intensities or areas of the peptide peaks can be used for relative quantification.

Due to the reactivity of both primary amine groups in peptides and reduced 3NT to 3AT groups, it becomes necessary to block primary amine chemistry on peptides in order to track the location of modified residues. Generally, precursor labeling uses the following major steps to make quantitative tagging selective for 3NT sites: 1) digest proteins to peptides, 2) block primary amines with acetyl (or other) groups, 3) reduce 3NT to 3AT, and 4) derivatize 3AT with a light or heavy isotope chemical tag. Figure 3.4a highlights the incorporation of a light or heavy (e.g., ^{2}H$_3$) 1-(6-methylnicotinoyloxy) succinimide reagent to 3AT residues [269]. The structure of this reagent contains a pyridine ring with a methyl group in the *para* position that has hydrogen atoms which can be exchanged for deuterium. A mass shift of 3 Da would result for every peptide containing a 3NT modification. Additionally, since peptides are capped with either a light or heavy acetyl group at Step 2, a global shift of 3 Da per acetyl group is observed for all peptides and an additional 3 Da is observed per 3NT modification. Interestingly, the use of this nicotinoyloxy based reagent results in higher ionization efficiencies for peptides generated with matrix assisted laser desorption ionization (MALDI) and prevents photodecomposition with the laser [269, 270].

Derivatization of 3AT can also be performed using light or heavy (-^{2}H$_5$) phenylisothiocyanate depicted in Figure 3.4b [271]. The structure of the tag contains heavy atoms which are incorporated in the phenyl ring generating a mass shift of 5 Da and a reactive thiocyanate group to selectively target 3AT. The mechanism involves an intermolecular cyclization between the sulfur atom of thiourea and the

a) 1-(6-methylnicotinoyloxy) succinimide
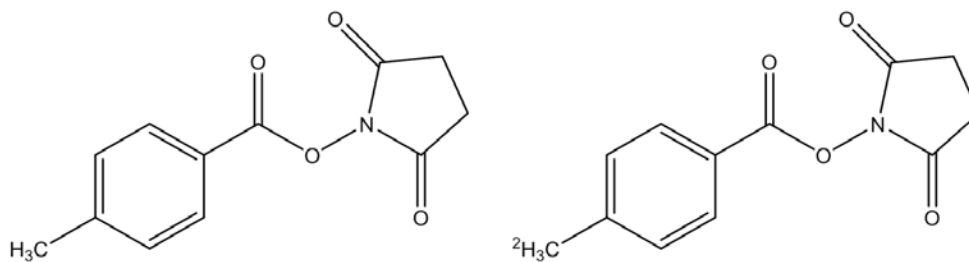
b) Phenylisothiocyanate
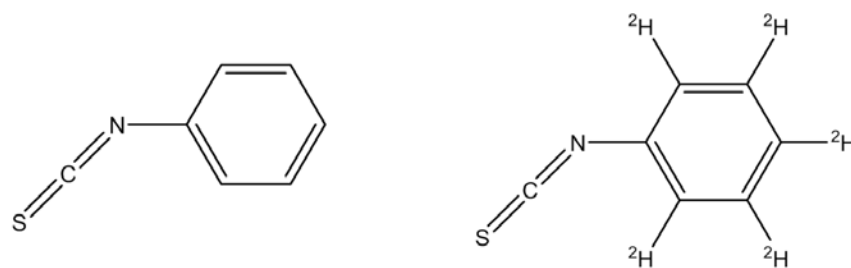
Figure 3.4. Example precursor quantification tags: a) 1-(6-methylnicotinoyloxy) succinimide and b) phenylisothiocyanate which incorporate mass shifts of 3 and 5 Da, respectively.

hydroxyl group of tyrosine, which is the first reported transformation in aqueous media using photocatalysis. Due to the addition of deuterium atoms, the hydrophilic shift which can occur due to kinetic isotope effects [272] was evaluated and its effects are negligible. For quantification purposes, this tag demonstrates precursor quantification capabilities and the potential use of signature fragments (m/z 116 and 121 for light and heavy tags, respectively) in SRM or MRM experiments. The presence of the signature fragment peaks also confirms 3NT-modification sites as the fragments are unique to the phenylisothiocyanate tag.

3.3.4. Isobaric Tags

A secondary approach to multiplexing techniques is the use of commercially available isobaric tags (Figure 3.3). The most commonly used isobaric tags are tandem mass tags (TMT) [273] and the isobaric tag for relative and absolute quantification (iTRAQ) [274], which can multiplex six or eight samples, respectively. To briefly summarize **Chapter 1**, isobaric tags incorporate heavy isotopes of ^{13}C, ^{15}N, and ^{18}O such that the overall mass of the tags are similar, however, upon gas-phase fragmentation specific low m/z reporter ions (e.g., 126-131 for TMT) are generated. The reporter ion signals can be related to the relative abundances of the peptides from which they were cleaved. Because relative quantification occurs in MS/MS spectra, increased precursor MS complexity is avoided. Advantages and disadvantages of isobaric tagging methods are reviewed [88], as well as improvements to instrumental analysis to obtain accurate reporter ion ratios [89, 94]. These methods should be included for future quantitation experiments using isobaric tags including the analysis of 3NT-modified proteins.

Few reports of isobaric tagging applications for 3NT modifications are reported. Quantification of nitrated peptides with isobaric tags was first demonstrated by Chiappetta *et. al.* using mixtures of nitrated bovine serum albumin (BSA) and bovine milk proteins [275]. After acetylation, 3AT BSA peptides were tagged with iTRAQ reagents and analyzed with precursor ion scanning using a triple quadrupole MS. The presence of iTRAQ fragment immonium ions at m/z 292.1 proved advantageous for confirming modification sites of low abundant nitrated peptides. Additionally, this approach does not

require time consuming sample fractionation steps and provided accurate reporter ion quantification. **Chapter 4** introduces the novel quantitative approach termed "Combined Precursor Isotopic Labeling and Isobaric Tagging (cPILOT)", which selectively quantifys nitrated peptides and expands the quantification capacity of isobaric tags to either 12 or 16 for TMT and iTRAQ, respectively [98].

3.4. CONCLUSIONS AND FUTURE OUTLOOK

Obtaining quantitative information for 3NT allows a better understanding of the role this PTM plays in biological systems. 3NT has been linked to neurodegenerative disorders, cancer, and cardiovascular disease and has been shown to impact protein function and potentially redox cellular signaling pathways. With the advent of proteomics for PTM investigation, there have been a number of reports focusing on qualitative information of 3NT-modified proteins obtained through targeted analyses or enrichment methods. There are fewer reports that address quantification of 3NT-modified proteins in complex mixtures. Perhaps this is partially attributable to the low abundance of this PTM in biological samples, which leads to the need for highly selective and sensitive analytical techniques. As a result, enrichment approaches, which rely on antibodies or other chemical tagging strategies, must continue to be developed to allow targeted analyses of nitrated proteins in complex biological samples. A number of these methods currently exist, however limitations in antibody selection including nonspecific binding have prevented their widespread ability to identify large numbers of nitrated proteins. Gel-based redox proteomics methods offer targeted identification and relative quantification of nitrated proteins using 2D Western Analysis, but also have similar issues that arise from antibody use such as high background signals and nonspecific binding of non-nitrated proteins. Furthermore, peptide loss during excision and digestion processes often limits the MS detection of nitrated peptides preventing 3NT site-specific information.

Currently, most of the approaches available have yet to provide large-scale identification and quantification of nitrated proteins in biological samples since a large percentage of total peptides detected

in these experiments contain no site of nitration. This is notably a result of the challenges associated with the low abundance of this modification, sample loss during lengthy derivatization steps using chemical tags, and the complexity of samples of interest. Guidelines that help to strengthen the confidence in identification of nitrated peptides and proteins from MS data should also be adapted by many of these groups. Due to the importance of 3NT in numerous diseases, this research area will continue to be of great interest such that improved proteomics methods are desirable.

4.0 ENHANCED SAMPLE MMULTIPLEXING FOR NITROTYROSINE-MODIFIED PROTEINS USING COMBINED PRECURSOR ISOTOPIC LABELING AND ISOBARIC TAGGING *

4.1. INTRODUCTION

Chapter 3 introduces the biological significance and previous proteomic techniques to quantitate 3NT. Briefly, gel electrophoresis with Western blot detection is commonly used to identify and quantify 3NT proteins, however relies on mass spectrometry (MS) for sequence identification. Matrix-assisted laser desorption ionization (MALDI)-MS [276, 277], electrospray ionization (ESI) tandem mass spectrometry (MS/MS) [278, 279], and liquid chromatography (LC) coupled with MS/MS have also been employed to identify nitrated residues in tryptic peptides [264, 280, 281]. Precursor [269] [282] and isobaric tagging [275] methods have been employed to quantify 3NT. The isobaric tag for relative and absolute quantitation (iTRAQ) was used to tag 3AT peptides after the blocking of N-termini and lysine residues with an acetyl group. In this approach, no enrichment is carried out however, 3NT-modified peptides are easily identified by performing precursor ion scanning for specific iTRAQ containing ions. Although it was only partially demonstrated, this approach can quantify up to a total of eight samples using the iTRAQ 8-plex reagent kit.

Chapter 4 presents an approach that increases the multiplexing capability of quantitative proteomics to assess differences in the relative abundances of 3NT-modified proteins. Through combined precursor isotopic labeling and isobaric tagging (cPILOT), we have developed a novel strategy that uses commercially available tandem mass tags (TMT) and iTRAQ reagents in order to increase the number of

samples that can be compared in a single analysis to 12 and 16, respectively. Additionally, the presence

of reporter ions in the mass spectra can be used to identify nitrated peptides and help to eliminate false

positive identifications that can arise from shotgun proteomics experiments [283]. cPILOT builds upon

currently used quantitative proteomics strategies presented in **Chapter 1** [73, 275]. Herein, proof-of-

principle cPILOT experiments are presented using simple mixtures of *in vitro* nitrated bovine serum

albumin (BSA) and mouse splenic protein digests, which are analyzed using nanoflow LC-MS/MS

coupled with an LTQ-Orbitrap Velos MS.

4.2. EXPERIMENTAL

4.2.1. *In Vitro Nitration of BSA*

One milligram of BSA (Sigma Aldrich; St. Louis, MO) was dissolved in 500 μL of phosphate

buffer saline (PBS) and a 50 μL aliquot of ~40 mM $ONOO^-$ (Millipore; Billerica, MA) was added to the

solution. The sample was incubated at room temperature for 30 minutes under constant stirring (hereafter

referred to as 3NT-BSA). The reaction was quenched by flash freezing in liquid nitrogen. A control BSA

sample was treated in the same manner with the exception of the addition of $ONOO^-$ to the buffer

solution. Samples were stored at -80 °C until further use.

4.2.2. *Spleen Homogenization*

Mouse spleen tissue was homogenized in an ice-cold phosphate buffer saline (PBS) solution

containing 8 M urea with 100 passes of a Wheaton homogenizer. Homogenate solution was collected,

sonicated, and centrifuged at 13000 RPM for 10 minutes (4 °C). Supernatants were collected and protein

concentrations determined using the BCA assay according to the manufacturer's instructions (Pierce

Thermo; Rockford, IL). Samples were stored at -80 °C until further use.

4.2.3. Immunochemical Measurement of 3NT-BSA Level

Control and 3NT-BSA samples (5 µL) were incubated at room temperature for 20 min with 5 µL of SDS (12% v/v) and 10 µL of Laemmli buffer [0.125 M Tryzma base, pH 6.8, SDS (4% v/v), and glycerol (20% v/v)]. Samples (250 ng) were blotted onto a nitrocellulose membrane and blocked with BSA (3% w/v) in a PBS solution containing 0.04% (v/v) Tween-20, and 0.10 M NaCl (hereafter referred to as Wash blot). A 1:2000 dilution of rabbit polyclonal anti-3NT primary antibody (Sigma-Aldrich) was added and the blot incubated for 3 hours on a rocker. The blot was rinsed for 5 min in Wash Blot three times and subsequently incubated with a 1:8000 dilution of anti-rabbit IgG alkaline phosphatase secondary antibody (Sigma-Aldrich) in Wash blot for 1 h at room temperature on a rocker. The membrane was washed as described above and developed using a solution of 0.2 mM nitrotetrazolium blue chloride and 0.4 mM 5-bromo-4-chloro-3-indolyl phosphate dipotassium in an alkaline phosphatase buffer (0.1 M Tris, 0.1 M NaCl, 5 mM MgCl2; pH 9.5). The dried blot was scanned on a Canon scanner and saved as a .TIF image.

4.2.4. BSA Trypsin Digestion

Desired amounts of samples were subject to trypsin digestion as follows. 0.25 M DTT (Thermo Fisher; Pittsburgh, PA) was added in a 1:40 protein:reagent mole excess and incubated at 37°C for 2 hours. 0.25 M iodoacetamide (Acros Organics; Morris Plains, NJ) was added in a 1:80 protein:reagent mole excess at 0°C for two hours in the dark followed by the addition of 1:40 protein:reagent mole excess L-cysteine at room temperature for 30 minutes. Tris buffer (0.2M tris, 10mM CaCl$_2$, pH 8.0) was added to the mixture until final volume was four times the original volume. TPCK-treated trypsin (Sigma Aldrich) was added to each sample at 2% w:w enzyme:protein and incubated at 37°C for 24 hours. Samples were flash frozen with liquid nitrogen and stored at -80 °C until further use.

4.2.5. Synthesis of N-acetoxy-H$_3$-succinimide and N-acetoxy-^{2}H$_3$-succinimide

The procedure for synthesis of N-acetoxy-H$_3$-succinimide and N-acetoxy-^{2}H$_3$-succinimide is described elsewhere[73, 146]. Briefly, 1.9478 g of N-hydroxysuccinimide (NHS, Sigma Aldrich) was added to 4.8mL of >99% acetic anhydride (Sigma Aldrich) or 1.9451 g of NHS was added to 4.4 mL of 99% ^{2}H$_6$-acetic anhydride (Sigma Aldrich). Reactions occurred at room temperature under nitrogen with constant stir for 15 hours. White crystals were collected, washed thoroughly with hexane, and allowed to dry under vacuum. Product yield was 1.9909 g and 1.5085 g for N-acetoxy-H$_3$-succinimide and N-acetoxy-^{2}H$_3$-succinimide, respectively. Nuclear magnetic resonance (NMR) analysis confirmed the formation of the appropriate succinimide ester (>95% purity).

4.2.6. 3NT Reduction and Isobaric Tagging of Peptides

For experiments using the TMT^0 reagent, 50 μg of the light and heavy labeled 3AT-BSA peptides were pooled into a single mixture. To this sample (100 μg), one vial of TMT^0 dissolved in anhydrous acetonitrile, was added directly to the sample according to manufacturer's instructions (Thermo Scientific). Reactions incubated at room temperature under constant stirring for one hour. Excess hydroxylamine hydrochloride (Sigma Aldrich) was used to quench the reaction. For experiments using the TMT 6-plex reagents (hereafter referred to as TMT^6), light and heavy labeled 3AT-BSA peptide samples were split into six mixtures each. Samples were reacted with the appropriate TMT^6 reagent according to manufacturer's instructions. Next, portions of the light and heavy labeled TMT^6 derivatized samples were mixed into a new sample tube to generate the desired mass ratios for reporter ions (discussed below). Overall, the total mass of light and heavy labeled peptides was equal after pooling. For experiments using the iTRAQ 8-plex reagents (hereafter referred to as iTRAQ^8), light and heavy labeled peptide samples (100 μg) were each split into two equal aliquots. The appropriate iTRAQ^8 reagent was dissolved in 70 μL of ethanol and directly added to the light or heavy labeled peptide samples. Reactions incubated at room temperature under constant stirring for one hour. Light and heavy

labeled peptide samples were then pooled into a single mixture to generate the desired iTRAQ[8] reagent ratios (discussed below). Finally, samples were cleaned using Waters Oasis HLB C_{18} cartridges and dried using a speedy-vac.

4.2.7. LC-MS/MS

Samples were reconstituted in a water solution with 0.1% formic acid (1 µg·µL^{-1}) and separated on a nanoflow Eksigent 2D LC system. Buffer A was composed of 97:3 H_2O:Acetonitrile (ACN) with 0.1% formic acid. Buffer B was composed of ACN with 0.1% formic acid. Samples were injected onto a trapping column (100 µm i.d. × 2 cm) packed with 200 Å C_{18} material (Michrom Bioresources Inc.; Auburn, CA) using an autosampler. After a short wash, samples were eluted to a pulled-tip analytical column (75 µm i.d. × 13.2 cm) packed with 100 Å C_{18} material (Michrom Bioresources Inc.). Gradient elution was performed as follows (% buffer A:% buffer B): 90:10 for 10 minutes, ramp to 70:30 over 90 minutes, ramp to 40:60 over 30 minutes, ramp to 20:80 over 5 minutes, hold for 10 minutes, followed by column equilibration. Eluted peptides were ionized using the nanospray source (~1.7 kV) of an LTQ-Orbitrap Velos MS. The MS was operated using data-dependent acquisition with the following parameters: full FT parent scans at 60,000 resolution over the m/z range 300-1600, top seven most intense ions were selected for CID (isolation width 3 m/z, 35% normalized collision energy) and HCD (10 ms activation time, isolation width 3 m/z, 45% normalized collision energy). CID- and HCD-MS/MS spectra were recorded in the LTQ and Orbitrap (7500 resolution), respectively.

4.2.8. Database Searching and Data Analysis

RAW data files were searched against the BSA sequence (Swiss Prot Entry: P02769) or mouse International Protein Index Database with SEQUEST in Proteome Discoverer 1.2 (Thermo Scientific). Database searching parameters include: precursor mass tolerance of 15 ppm, fragment mass tolerance of 1.0 Da, static modification of carbamidomethylation to cysteine, dynamic modifications of light and

heavy acetyl groups at the N-terminus and lysine residues, methionine oxidation, and special modification for TMT or iTRAQ derivatized 3AT residues. Masses for these modifications were 239.163 Da (TMT^0), 244.174 Da (TMT^6), and 319.216 Da ($iTRAQ^8$). False discovery rates of $p<0.05$ and $p<0.01$ were set using decoy database searching such that only medium and high confidence peptides, respectively, were used for analyses. Intensity and area information for light and heavy labeled peptides were provided in the software output (.msf file). Manual calculation of relative reporter ion peak intensity (or peak area) ratios was performed due to limitations in the software output for this cPILOT strategy.

4.3. RESULTS AND DISCUSSION

4.3.1. *Combined Precursor Isotopic Labeling and Isobaric Tagging (cPILOT)*

Herein we present the novel approach cPILOT, which combines isotopic labeling with isobaric tagging strategies such as TMT and iTRAQ in order to extend the number of 3NT-modified samples that can be multiplexed in a single experiment to 12 and 16, respectively. The strategy consists of three primary steps as shown in Figure 4.1: acetylation of primary amine groups, reduction of 3NT groups to 3AT, and isobaric tagging (using TMT or iTRAQ) of 3AT groups. Nitrated tryptic peptides are initially reacted with N-acetoxy-H_3-succinimide ester or isotopically labeled N-acetoxy-$^2H_3$-succinimide ester in order to acetylate primary amine groups (i.e., N-termini and lysine residues) with an isotopically light (-H_3) or heavy (-$^2H_3$) label, respectively. The second step involves the use of sodium dithionite to reduce 3NT to 3AT. The third major step uses commercially available TMT reagents (Figure 4.1) or the iTRAQ reagent to react with 3AT according to manufacturer's instructions. Finally, the derivatized samples are mixed in a 1:1 light:heavy ratio and analyzed by LC-MS/MS. We reduce sample loss of low abundance 3NT-modified peptides by performing a single clean-up step, which occurs after isobaric tagging.
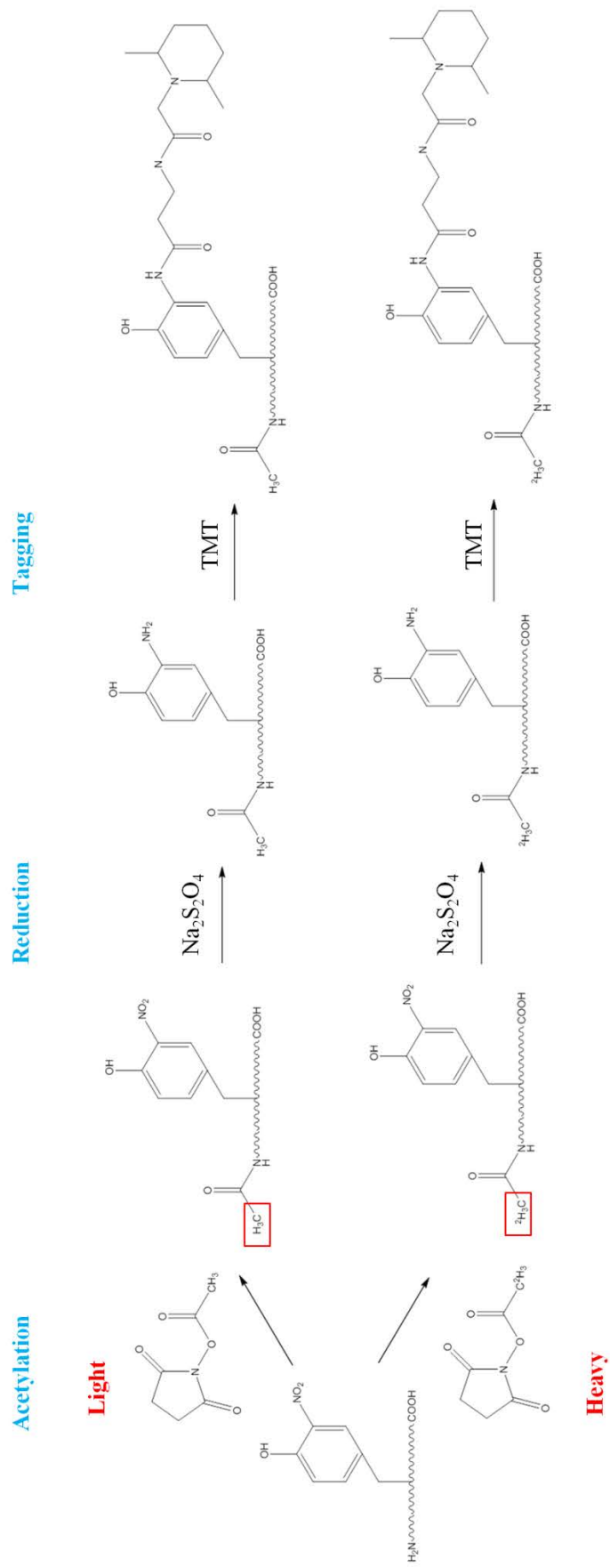
Figure 4.1. Schematic representation of the chemical derivatization steps performed in the cPILOT strategy.

4.3.2. Validation of In Vitro Nitration and Isotopic Acetylation of BSA

  Immunochemistry and LC-MS/MS experiments were initially performed in order to confirm nitration and acetylation of BSA. BSA 3NT-modification sites have been well-characterized using various enrichment methods [173, 242, 275, 284-286]. In total, BSA has 21 Tyr residues (Swiss Prot Entry: P02769) that could potentially be nitrated. Figure 4.2a shows an immunoblot with a dark band corresponding to the 3NT-BSA sample. Under similar reaction conditions, without the presence of ONOO$^-$, BSA control samples showed no immunoreactivity verifying the generation of *in vitro* nitrated BSA. Validation of the first step of cPILOT was tested by tryptically digesting and acetylating (light label) 3NT-BSA followed by LC-MS/MS analysis on an LTQ-Orbitrap Velos MS. Nitrated peptides should be shifted in mass according to the number of added acetyl (42.011 Da) and nitro (44.985) groups. Figure 4.2b shows an example MS/MS spectrum obtained upon fragmentation of a peak with a precursor *m/z* 783.897. Based on the *b-* and *y*-type fragment ions detected in the CID MS/MS analysis, the peptide has been assigned as [L(Acetyl)GEY(NO$_2$)GFQNALIVR+2H]$^{2+}$. The acetylation of the N-terminus was observed in this spectrum as well the y_9/y_{10} and b_3/b_4 singly charged fragment ions locating the position of nitration to Tyr424. The Δm of 208 Da corresponds to the mass shift of a nitrated tyrosine residue. Overall in these experiments, we observed nitration of 15 Tyr residues in which MS/MS spectra were manually validated. The location of the 3NT-modification sites are as follows: Tyr54, Tyr108, Tyr161, Tyr163, Tyr171, Tyr173, Tyr179, Tyr180, Tyr355, Tyr357, Tyr364, Tyr376, Tyr424, Tyr475, and Tyr520.
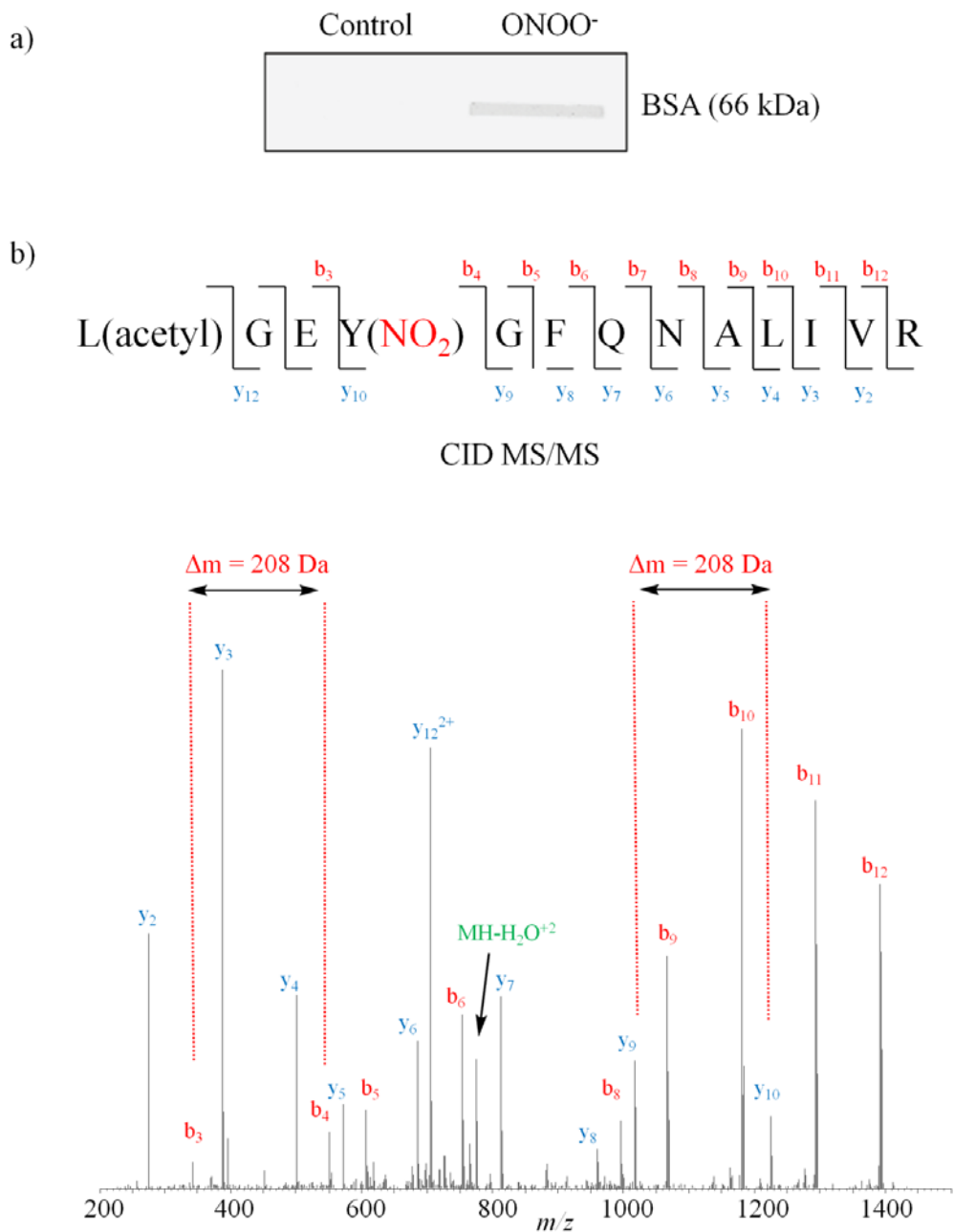
Figure 4.2. Validation of *in vitro* nitration. a) Immunochemical blot of BSA incubated with buffer (control) and ONOO⁻ after probing with primary anti-3NT antibody. b) Example MS/MS spectrum obtained for a doubly-charged peak at t_r 101.47 min with *m/z* 783.897 that has been assigned as $[L(Acetyl)GEY(NO_2)GFQNALIVR+2H]^{2+}$. The corresponding CID generated b- and y-type fragment ions are labeled in the spectrum.

4.3.3. 3AT-BSA Isotopic Labeling & TMT^0

Having validated the presence of nitration and acetylation, 3NT-BSA samples were reduced to 3AT-BSA, split into two equal aliquots, and isotopically labeled with either a light or heavy acetyl group. Acetylated 3AT-BSA samples were derivatized with the TMT^0 reagent that generates reporter ion *m/z* 126 and pooled in a 1:1 ratio light:heavy mixture. Figure 4.3a shows an example pair of doubly-charged peaks at *m/z* 913.402 and 916.421 that have a total mass shift of 6 Da. This mass shift indicates the presence of two acetylations to the peptide. Upon independent CID-MS/MS of the light and heavy precursor peaks (Figure 4.3b), this pair has been identified as the peptide [E(Acetyl)Y(NH-TMT^0)EATLEEccAK(Acetyl)+2H]$^{2+}$. This tryptic peptide has been modified with both N-terminal and Lys acetyl groups, carbamidomethyl groups to Cys, and the addition of the TMT^0 reagent to Tyr376. Confirmation of the TMT derivatization can be determined by the presence of the reporter ion *m/z* 126.13 in the HCD spectra (low *m/z* range shown) for both the light and heavy labeled precursor ions (Figure 4.3c).

It should be noted that fragmentation of acetylated tryptic peptides generates an immonium ion at *m/z* 143.12, which upon loss of NH_3 produces a fragment peak at *m/z* 126.09 [287]. This immonium ion - NH_3 fragment can be detected in the HCD-MS/MS spectrum of the light precursor peak, however at R = 7500 it is resolved from the TMT^0 reporter ion *m/z* 126.13 in the Orbitrap MS. For lower resolution MS, it will be difficult to discern the contribution of relative peak intensity that is derived from acetylated immonium ions -NH_3 and TMT reporter ions. This is not the case for the heavy precursor ions, in which the immonium ion -NH_3 is shifted by 3 Da. For example, in the HCD-MS/MS spectrum shown in the upper right of Figure 4.3c, the immonium ion -NH_3 occurs at *m/z* 129.11. For TMT^6 reagents, in which reporter ions are generated at *m/z* 126-131, lower resolution MS will not be able to distinguish immonium ion vs. reporter ion signal generated at *m/z* 126 and 129. Therefore, these reporters would have to be avoided in low resolution instruments especially for analysis of more complex mixtures in which the relative abundances across samples would not be known *a priori*. Another approach is to use iTRAQ
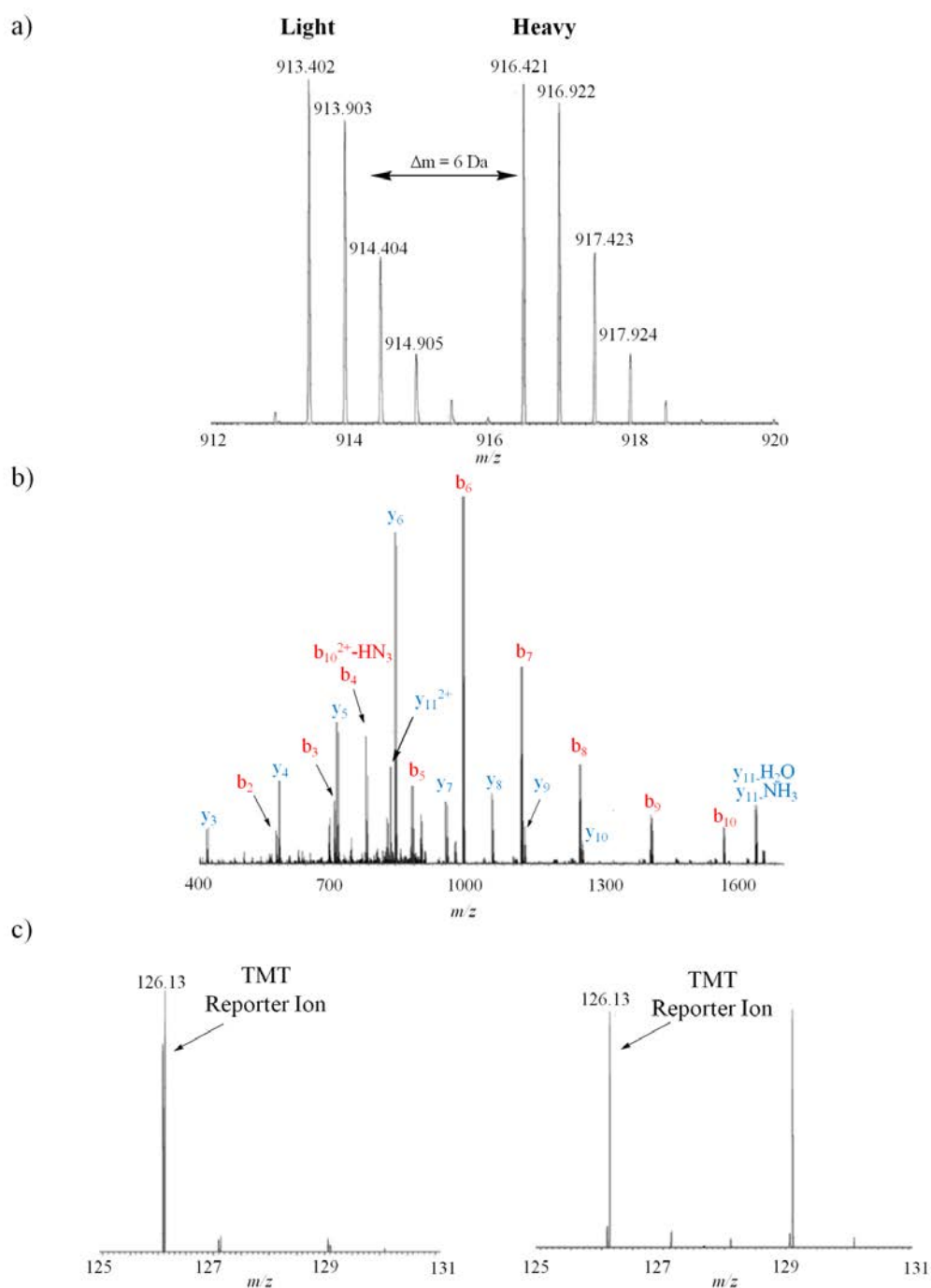
Figure 4.3. Demonstration of chemical derivatization using TMT^0 reagents. a) Integrated parent mass spectrum at t_r 54.00-54.45 minutes across the m/z range 912-920 in which a doubly-charged isotopic pair is observed at m/z 913.402 and 916.421 for the light and heavy labeled peptide, respectively. b) An overlay of the MS/MS spectra obtained after CID of the light and heavy labeled peaks shown in a). It should be noted that each peptide peak was isolated individually. The MS/MS spectra from the light and the heavy labeled peptides have been superimposed in this spectrum. The b- and y-type fragment ions (as labeled in the plot) have led to the peptide assignment of [E(Acetyl)Y(NH-TMT^0)EATLEEccAK(Acetyl)+2H]$^{2+}$. The lowercase letter "c" in the peptide sequence corresponds to carbamidomethylated cysteine. c) Zoomed-in low m/z region of the HCD spectra shown in light (left) and heavy (right) labeled peptide peaks, respectively.

70

reagents in which reporter ions occur at lower *m/z* values (i.e., 113-121); this approach is presented below.

4.3.4. *Twelve Sample Multiplexing with TMT^6 Reagents*

Isobaric tagging strategies have an inherent cost, which is augmented with the desired sample multiplexing capability for an experiment. This makes analyses expensive for projects involving a large N, use of technical and/or biological replicates, and experimental validation (e.g., forward and reverse tagging). Herein, we demonstrate how cPILOT can be employed in order to maximize the cost of isobaric tagging strategies for a single experiment that involves the identification of nitrated peptides. Figure 4.4a shows a precursor ion MS spectrum obtained for a pair of peaks in 3AT-BSA whereby light and heavy acetylated peptides were derivatized with the TMT^6 reagents (reporter ions *m/z* 126-131). The particular peptide pair shown at *m/z* 488.282 and 489.792 has been assigned to [A(Acetyl)W(NH-TMT^6)SVAR+2H]$^{2+}$. The corresponding mass shift of 3 Da confirms the presence of only one acetyl group which has been detected on the N-terminus. Additionally, this peptide contains a Trp residue that was nitrated *in vitro* as validated by the mass shift corresponding to the TMT^6 reagent in CID- and HCD-MS/MS spectra (data not shown).

In order to assess the ability of this approach to measure quantitative differences across multiple samples, we prepared a 3NT-BSA sample and split into twelve equal aliquots whereby six aliquots were acetylated with the light label and an additional six aliquots were acetylated with the heavy label. Each sample was then derivatized with a particular TMT^6 reagent and samples were pooled to generate the following mass ratios. For aliquots containing 3AT light acetylation and TMT^6 tagged peptides, the six aliquots were mixed in a 1:50:10:1:2:0.5 ratio corresponding to reporter ions *m/z* 126:127:128:129:130:131. The six aliquots containing 3AT heavy acetylation and TMT^6 tagged peptides were mixed in a 1:0.5:2:1:10:50 ratio corresponding to reporter ions *m/z* 126:127:128:129:130:131. Overall, the total mass ratios of the derivatized light labeled:heavy labeled tryptic peptides was 1:1. This is reflected in the precursor peaks measured in the parent MS (Figure 4.4a). Figures 4.4b and 4.4c show
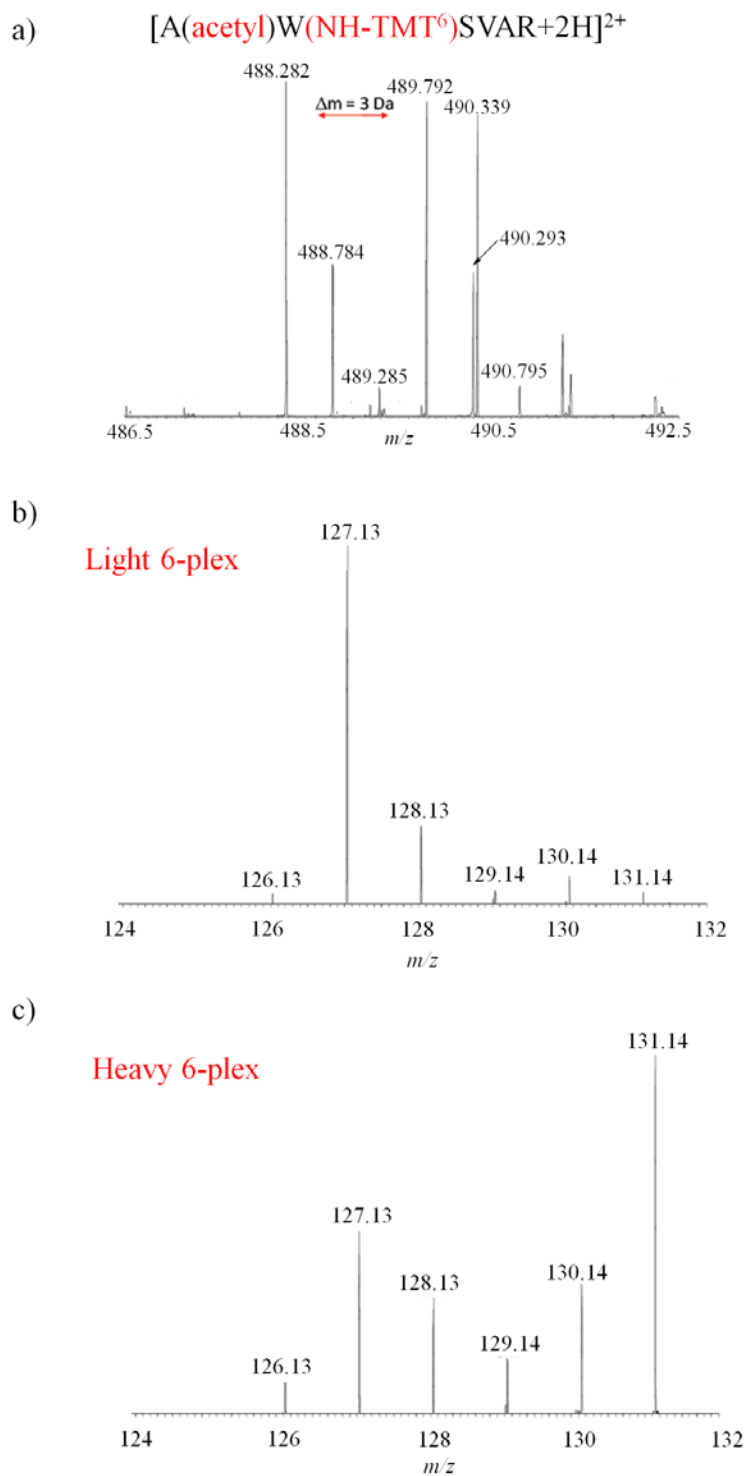
Figure 4.4. Multiplexing of twelve independent samples using TMT[6] reagents. a) Integrated parent mass spectrum at t_r 32.65-33.99 minutes of the doubly-charged isotopic pair observed at *m/z* 488.282 and 489.792 for the light and heavy labeled peptide, respectively, that has been assigned as [A(Acetyl)W(NH-TMT[6])SVAR+2H]$^{2+}$. b) A zoomed-in low *m/z* region of the HCD-MS/MS spectra obtained upon isolation and fragmentation of the light labeled peak shown in a). c) A zoomed-in low *m/z* region of the HCD-MS/MS spectra obtained upon isolation and fragmentation of the heavy labeled peak shown in a).

the presence of each of the TMT[6] reagents for the light and heavy labeled precursor ions, respectively. The observed relative abundance ratios for the light precursor peak (Figure 4.4b) according to peak areas are 1.0:38:8.5:1.2:2.9:1.2 and the ratios for the heavy precursor peak (Figure 4.4c) are 1.0:5.6:3.6:1.7:4.0:11. The correlation in measured versus expected reporter ion ratios is linear for both the light (R^2=0.9991) and heavy (R^2=0.7956) precursor ions. However, the measured reporter ion ratios are compressed in some cases and overestimated in others deviating from expected reporter ion ratios from sample preparation. While some error in quantitation can be related to errors during sample preparation, upon closer inspection of the precursor and CID-MS/MS and HCD-MS/MS spectra, we attribute the inaccuracy in measured reporter ion ratios to overlap of the isotopically labeled precursor ions that occurs during isolation in the LTQ. The [A(Acetyl)W(NH-TMT[6])SVAR+2H]$^{2+}$ peptide shown in Figure 4.4 is doubly charged and contains a single label; thus precursor ions are shifted in mass by 1.5 *m/z*. The isolation window used in these studies was 3.0 *m/z* (±1.5 *m/z*). Therefore, it is highly possible that ions from the heavy labeled precursor *m/z* were isolated with the light labeled precursor *m/z* and vice versa. Isolation of both precursor ions in one MS scan event would cause an overlap in the ion signal for each of the reporter ions and hence inaccuracies in the measured relative abundances. This is consistent with the compressed and overestimated reporter ion ratios that were detected in the [A(Acetyl)W(NH-TMT[6])SVAR+2H]$^{2+}$ and other peptides detected in this dataset. Similar issues with underestimation of reporter ion abundance ratios have been previously discussed [288, 289]. Solutions to reduce quantitation errors might involve the use of proton transfer reactions to charge reduce precursor ions [89, 290] or the use of different isotopically labeled reagents (e.g., dimethylation) that will increase the mass shift between light and heavy labeled precursors in the parent mass scan [94]. Overall, this is the first demonstration of a quantitative proteomics approach that couples precursor isotopic labeling with isobaric tagging to enhance sample multiplexing capabilities for 3NT-modified peptides. Roughly speaking, the relative abundances for the cPILOT 12-plex study presented above are reflective of the expected abundances based on sample pooling for most of the reporter ions. The ability to distinguish immonium ions is indicated in these spectra (Figures 4.4b and 4.4c) by the two resolved peaks at *m/z* 126.09 and

129.10 in both HCD-MS/MS spectra. Based on experimental design, cPILOT offers inter- and intra-sample quantification. For example, cPILOT could be employed to control (light) vs. diseased (heavy) samples whereby information regarding the relative change in abundance across multiple N could be assessed at the level of precursor ion signal (i.e., average of all control or disease biological replicates) and intra-sample variation can be assessed at the level of reporter ion signal.

4.3.5. 3AT-BSA Isotopic Labeling & iTRAQ

Figure 4.5 shows the extension of cPILOT to iTRAQ multiplex reagents. The doubly charged peptide pair at m/z 949.380 and 952.399 shifted in mass by 6 Da (Figure 4.5a) has been assigned to [E(Acetyl)TY(NH-iTRAQ[8])GDmADccEK(Acetyl)+2H]$^{2+}$. The number of observed acetyl groups agrees with labeling of the N-terminus and a Lys residue, carbamidomethylation of Cys, and tagging of Tyr108 with the iTRAQ[8] reagent that produces reporter ion m/z 113. Addition of the iTRAQ[8] reagent to the Tyr108 is also confirmed by the presence of the reporter ion m/z 113 in the HCD-MS/MS spectra of both the light and heavy labeled precursor ions (Figures 4.5b and 4.5c, respectively). This peptide also contains an oxidized Met residue in which oxidation could have occurred during the *in vitro* nitration reaction. Due to the lower m/z range (i.e., 113-121) of iTRAQ reporter ions there is no overlap with the acetylated immonium ion-NH$_3$ that occurs at m/z 126.

4.3.6. Multiplexing with iTRAQ Reagents

We designed another proof-of-principle experiment to assess whether or not overlap in reporter ion abundances occurs during precursor ion isolation. Non-overlapping reporter ion m/z values for isotopically labeled peptides were purposefully selected for this experiment. Briefly, two aliquots of light labeled 3AT-BSA were derivatized with iTRAQ[8] reagents that produce reporter ions m/z 113 and 115 and mixed in a 1:1 ratio. Two equal aliquots of heavy labeled 3AT-BSA were derivatized with iTRAQ[8] reagents that produce reporter ions m/z 117 and 118 and mixed in a 1:4 ratio. Light and heavy labeled samples (1:1 ratio) were combined into a single mixture for analysis. Figure 4.6 shows the low m/z
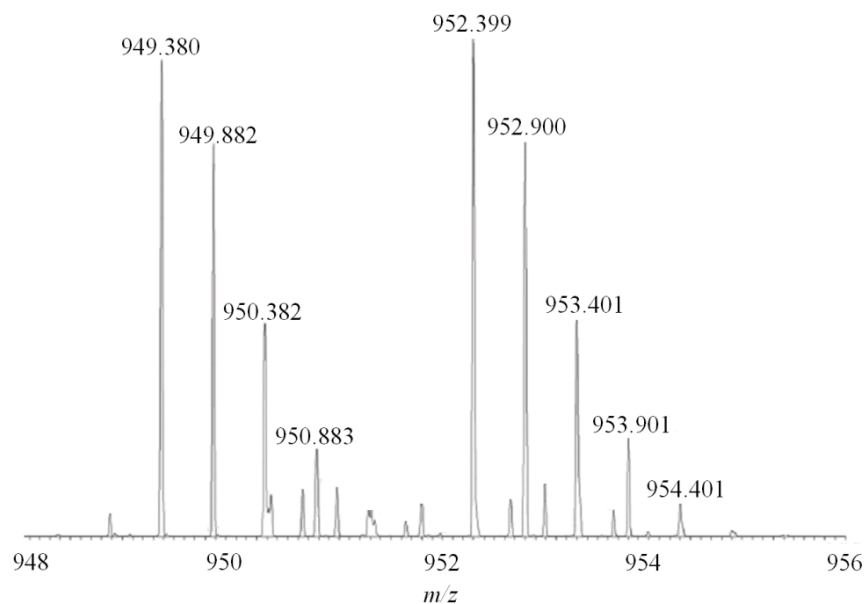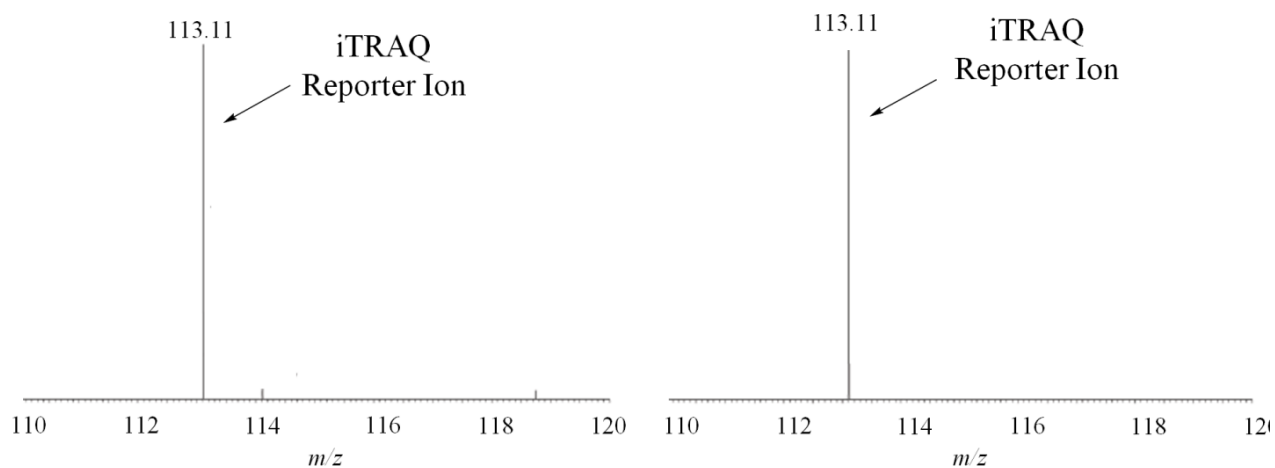
Figure 4.5. Demonstration of chemical derivatization using a single iTRAQ^8 reagent (i.e., reporter ion m/z 113). a) Integrated parent mass spectrum at t_r 44.93-47.83 minutes in which a doubly-charged isotopic pair is observed at m/z 949.380 and 952.399 for the light and heavy labeled peptide, respectively, that has been assigned as [E(Acetyl)TY(NH-iTRAQ^8)GDmADccEK(Acetyl)+2H]$^{2+}$. The lowercase "m" and "c" correspond to methionine oxidation and cysteine carbamidomethylation, respectively. b) and c) Zoomed-in low m/z region of the HCD-MS/MS spectra obtained for the light and heavy labeled peptide peaks shown in a), respectively.

75

Reporter ion m/z	Peak intensity	Peak area
113	3.58E03	1.37E04
115	3.20E03	1.16E04

Reporter ion m/z	Peak intensity	Peak area
117	8.41E02	3.08E03
118	3.37E03	1.27E04
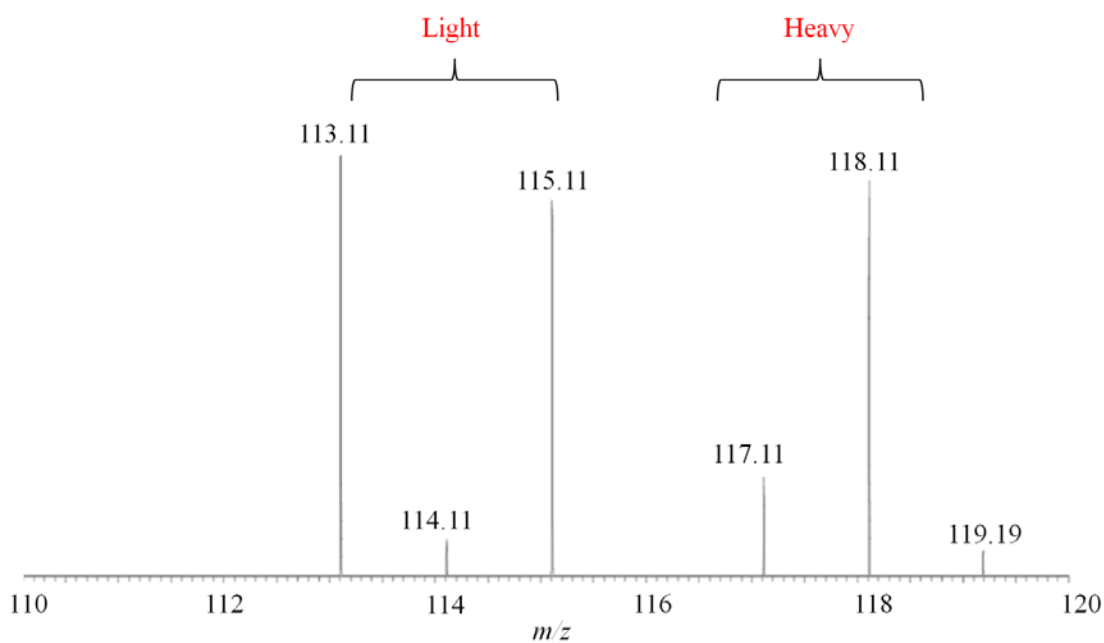
Figure 4.6. Quantitative demonstration of four multiplexed samples using iTRAQ[8] reagents. A zoomed-in low *m/z* region of the HCD MS/MS spectra obtained upon isolation and fragmentation of the light labeled peak at t_r 67.48 minutes and *m/z* 548.983 that has been assigned as [H(Acetyl)PEY(NH-iTRAQ[8])AVSVLLR+3H]$^{3+}$. The observed reporter ion peak intensities and peak areas are displayed in the tables (top).

region of the HCD-MS/MS spectra generated upon isolation and fragmentation of the light labeled precursor peak at *m/z* 548.983. Based on CID- and HCD-MS/MS spectra (data not shown) this peak has been assigned as [H(Acetyl)PEY(NH-iTRAQ[8])AVSVLLR+3H][3+]. The issue of overlapping precursor ion isolation for the isotopically labeled pairs is better demonstrated in this data than could be delineated with the data presented in Figure 4.4. Theoretically, the HCD-MS/MS spectrum (Figure 4.6) should only contain the reporter ions at *m/z* 113 and 115 since it was generated upon isolation and fragmentation of the light labeled precursor peak. However, there is signal observed from the heavy labeled precursor ion peak as the reporter ions at *m/z* 117 and 118 are also present in the spectrum. Detection of the heavy labeled reporter ion peaks confirms that overlap in precursor ion isolation is occurring in the LTQ and is consistent with the inaccurate abundances measured in the 12-plex experiments (Figures 4.4b and 4.4c).

Figure 4.6 only displays the HCD-MS/MS spectrum obtained for the light labeled precursor peak, however accurate reporter ion abundances for both isotopically labeled peaks are observed. The expected reporter ion ratios for the light labeled peak are 1:1 for *m/z* 113:115 and for the heavy labeled peak are 1:4 for *m/z* 117:118. For the light labeled precursor peak, the measured reporter ion abundances based on peak intensity are 1:1.1 for *m/z* 113:115. The heavy labeled precursor peak measured reporter ion abundances are 1:4.0 for *m/z* 117:118. Similar ratio values are obtained using peak areas as opposed to peak intensities for abundance calculations (see table in Figure 4.6). These data provide evidence to support that cPILOT allows differences in relative protein abundances to be measured across multiple samples. Furthermore, cPILOT can increase the multiplexing capability of iTRAQ[8] (*m/z* 113-121) to the analysis of 16 samples in a single experiment. We also note that the presence of reporter ion tags in the HCD spectra can be used as a selection criterion to filter for 3NT-modified peptides during data analysis. In order to demonstrate the potential capability of this approach to detect nitrated peptides in complex mixtures, the cPILOT workflow was carried out on tryptic peptides from mouse splenic proteins. Based on the aforementioned issues, only a four-plex experiment was designed which allowed us to track the occurrence of precursor ion overlap and evaluate the reporter ion quantitation. The peptide mixture was split into four individual aliquots, acetylated with either light or heavy labels, derivatized with iTRAQ[8]

reagents, and mixed in a 1:1 ratio for *m/z* 113, 114 and 1:1 ratio for *m/z* 115 and 116, respectively. Figure 4.7a shows a precursor mass spectrum for a doubly-charged precursor peak pair at *m/z* 810.972 (light) and 812.481 (heavy) that is shifted by 3 Da. This pair has been assigned as the [A(Acetyl)PGISY(NH-iTRAQ^8)QRLVR+2H]$^{2+}$ peptide belonging to phosphoinositide 3-kinase regulatory subunit 5 protein (IPI00400180.1). From the HCD-MS/MS spectra obtained from the light and heavy labeled precursors, it is evident that this peptide was nitrated as indicated by the presence of the four reporter ions. Additionally, the observed peak intensity ratios for reporter ions are similar to the expected values. It is still apparent from the MS/MS spectra that there is overlap in the precursor isolation indicated by the presence of the reporter ions at *m/z* 115 and 116 in the HCD spectra (Figure 4.7b) taken upon isolation of the light precursor peak and the presence of *m/z* 113 and 114 in the HCD spectra taken upon isolation of the heavy precursor peak (Figure 4.7b). Under ideal conditions, only reporter ions at 113 and 114 *m/z* should be present in HCD spectra from the light labeled precursor (similarly 115 and 116 *m/z* should be observed for the heavy precursor). Overall, we identified 371 peptides, which correspond to 96 mouse splenic proteins. Five proteins (five peptides and twelve spectral counts) were identified with nitrated residues: phosphoinositide 3-kinase regulatory subunit 5 protein [A(Acetyl)PGISY(NH-iTRAQ^8)QRLVR], nebulin [D(Acetyl)Y(NH-iTRAQ^8)DLREDAISIK(Acetyl)], Ep300 protein [K(Acetyl)VEGDM(Ox)Y(NH-iTRAQ^8)ESANNR], Isoform 1 of Bullous pemphigoid antigen 1 [S(Acetyl)IDELNSAWDSLNK(Acetyl)AW(NH-iTRAQ^8)K(Acetyl)], and Npas3 protein [V(Acetyl)ERY(NH-iTRAQ^8)VESEADLR]. We note that a low percentage (i.e., 1.6%) of nitrated peptides was identified with modifications on Tyr or Trp residues. Additional enrichment steps (i.e., immunoprecipitation of 3NT-modified peptides prior to cPILOT) will be necessary in order to identify large numbers of nitrated peptides in complex mixtures.

Caveats to obtaining accurate quantitative information with cPILOT relies on minimal to no overlap in the precursor ion isolation for isotopically labeled peaks, efficient chemical reactions, and minimal errors during sample preparation. The N-acetoxy-^{2}H$_3$-succinimide reagent used to isotopically label tryptic peptides in these studies can be substituted with other reagents that will increase the mass

a) [A(acetyl)PGISY(NH-iTRAQ⁸)QRLVR+2H]²⁺
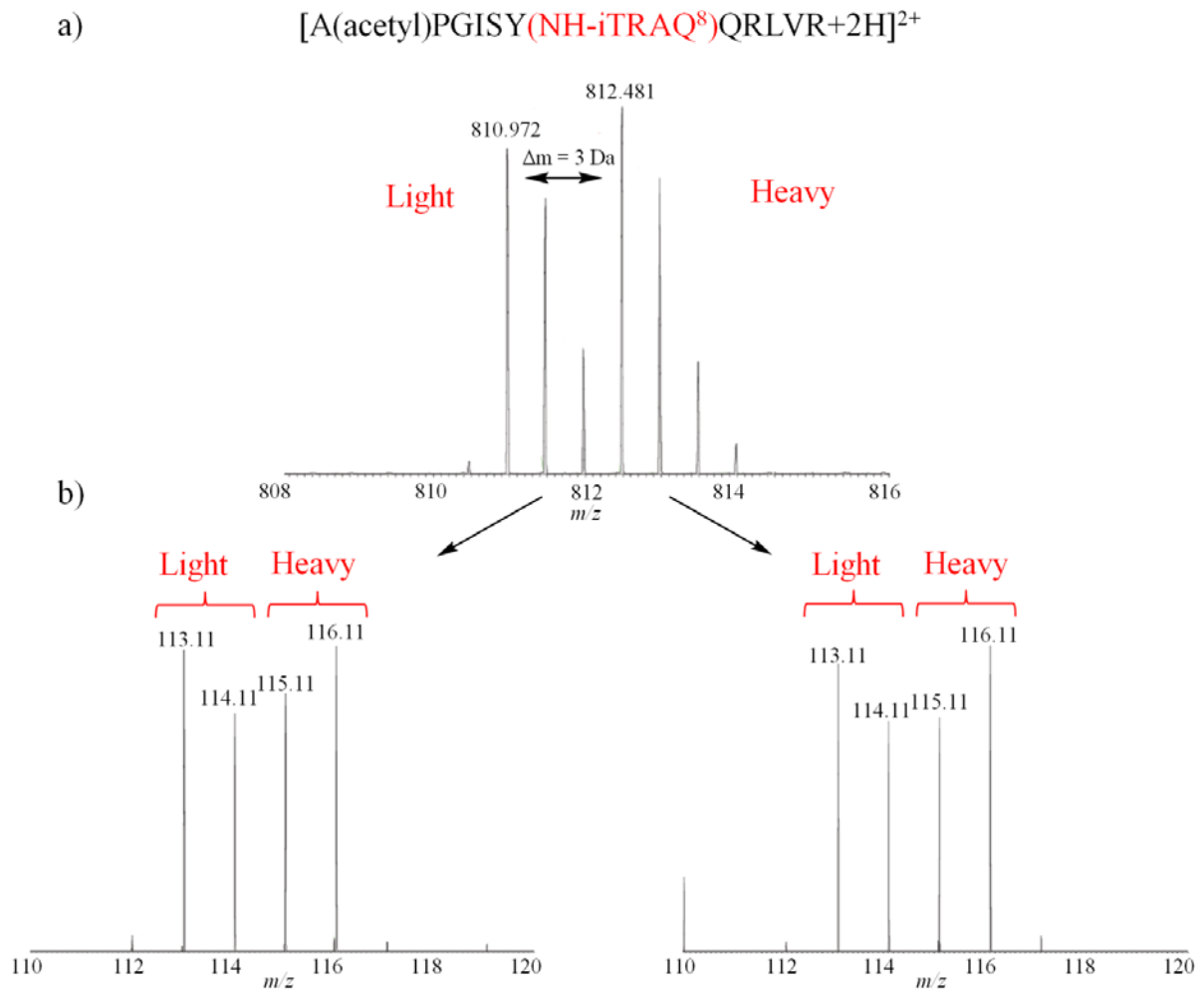
Figure 4.7. Application of cPILOT to mouse spleen tissue using iTRAQ^8 reagents in a four-plex experiment. a) Parent mass spectrum at t_r 105.03 minutes of the doubly-charged isotopic pair observed at *m/z* 810.972 and 812.481 for the light and heavy labeled peptide, respectively, [A(Acetyl)PGISY(NH-iTRAQ^8)QRLVR+2H]$^{2+}$ of the phosphoinositide 3-kinase regulatory subunit 5 protein (IPI00400180.1) protein from spleen tissue. b) A zoomed-in low *m/z* region of the HCD-MS/MS spectra obtained upon isolation and fragmentation of the light (left) and heavy (right) labeled peaks shown in a).

shift between light and heavy labeled peptides, thus eliminating compression and overestimation of reporter ion abundance ratios. **Section 4.3.7** and **Chapters 5 and 6** explore alternative precursor isotopic labeling reagents to improve these issues. Errors associated with sample loss were minimized during these experiments by performing "one-pot" reactions and using a single sample clean-up step prior to LC-MS/MS analysis. Finally, for application of cPILOT to complex peptide mixtures in which protein abundances are not known *a priori* it is necessary to have efficient chemical reactions in order to reduce complexity in data analysis and interpretation. The isotopic labeling and commercial TMT and iTRAQ reactions have efficiencies reported to be greater than 98% [74, 218, 291, 292]. Our results are consistent with these reported efficiencies.

4.3.7. Improved cPILOT Quantitative Accuracy using $^{13}C_2$, $^2H_3$-Acetylation*

(*De Gruyter Proteomics Quantification of Protein Nitration, Walter De Gruyter GmbH Berlin Boston, 2013. Copyright and all rights reserved. Material from this publication has been used with the permission of Walter De Gruyter GmbH.) [99]

To directly address the issue of precursor ion overlap, acetylation reagents which generate higher mass shifts in the precursor MS spectra have been employed as shown in Figure 4.8. The cPILOT workflow was modified by exchanging the GIST reagent with direct addition of light ($C_4H_6O_3$) and heavy ($^{13}C_4{}^2H_6O_3$) acetic anhydride for acetylation of protein digests. Nitrated BSA peptides after acetylation exhibit a mass shift of 5 Da between light and heavy ($^{13}C_2,{}^2H_3$-acetyl) precursor peaks. Due to the enhanced *m/z* shift, there should be no overlap in MS ion selection between light and heavy precursors. Improvements in quantification are observed using this approach. For example, the light and heavy MS/MS spectra generated for the doubly-charged peptide (Acetyl)NY(NH-TMT^6)QEAK(Acetyl), show a 1.0:4.5 and 3.7:1.0 reporter ion ratio for m/z 130:131, respectively. Due to the accuracy of the ratios (which should be 1:4 and 4:1 for light and heavy, respectively), this demonstrates the applicability of increasing precursor mass shifts for reducing ion overlap while yet improving quantification. Also, the

80

a)

b)

$[N(\text{Acetyl})Y(\text{NH-TMT}^6)\text{QEAK}(\text{Acetyl})+2H]^{2+}$

Theoretical Ratio **1:4**   Theoretical Ratio **4:1**

Light   Heavy
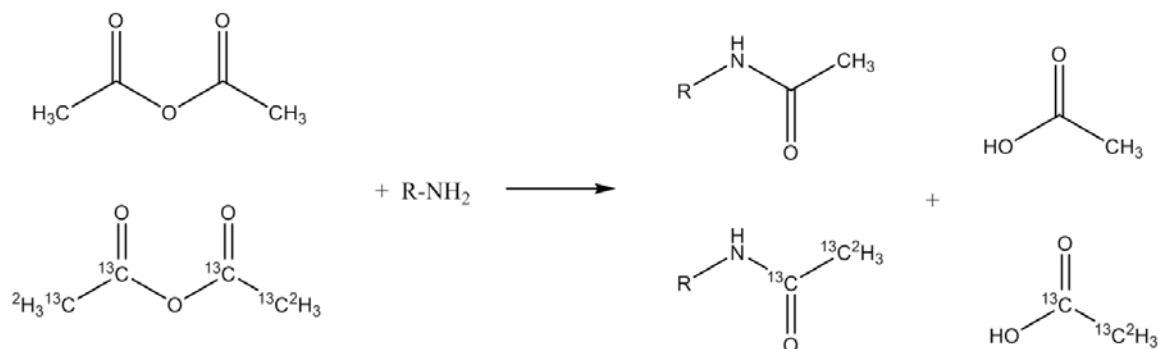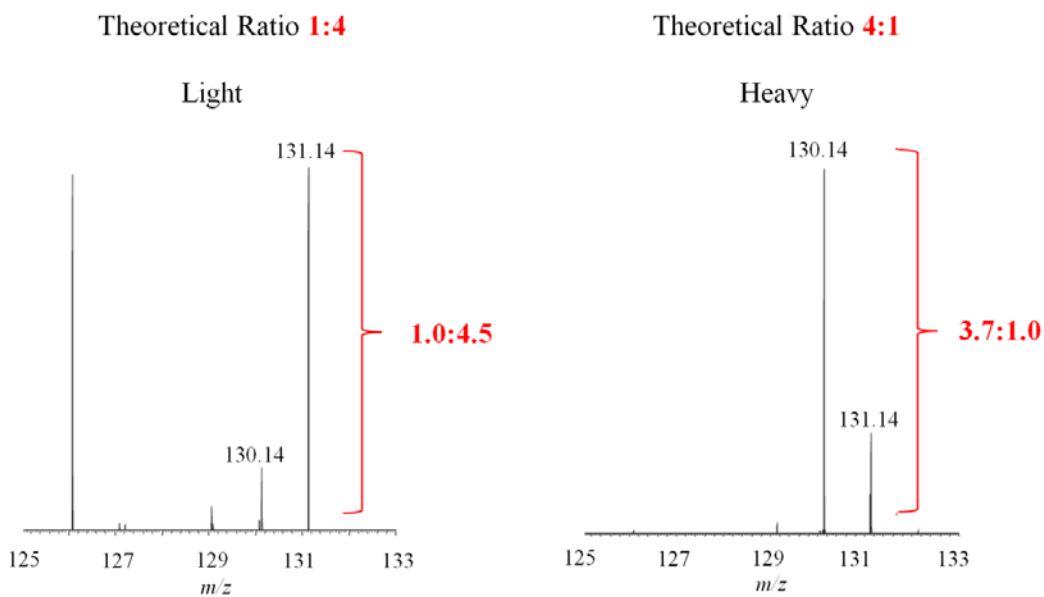
Figure 4.8. Chemical reaction of peptide primary amines with acetic anhydride (top). Example HCD MS/MS spectra (zoom-in of lower m/z region) of BSA peptide whereby light (-COCH$_3$, bottom left) and heavy (-^{13}CO^{13}C^{2}H$_3$, bottom right) peptide mixtures were tagged with TMT reagents that generate reporter ions at m/z 130 and 131. Theoretical ratios should be 1:4 and 4:1 (m/z 130:131) for light and heavy peptides, respectively.

use of Lys C protease as opposed to trypsin results in all Lysine terminated peptides ensuring at least two sites of acetylation (and thus a mass shift of 10 Da).

4.4. CONCLUSIONS

This work reports on the first quantitative proteomics approach that combines precursor ion isolation with isobaric tagging strategies such as TMT and iTRAQ for the analysis of 3NT-modified proteins. cPILOT extends sample multiplexing capabilities to 12 and 16 samples with commercial TMT[6] and iTRAQ[8] reagents, respectively, and provides the identification of nitrated peptides through detection of reporter ions in HCD MS/MS spectra. Despite the observed limitations with the reagents used for this cPILOT strategy, accurate quantitative information could be obtained with appropriate precursor tagging reagents and/or improvements to experimental design. The incorporation of a 5 Da acetylation mass shift and the use of LysC protease are an important steps to achieve accurate quantitation using cPILOT. Since 3NT modifications are low-abundance, we also note that this approach can be combined with prior enrichment procedures for nitrated peptides such as immunoprecipitation or with selected ion monitoring experiments to search for reporter ions. Primary advantages with cPILOT include the ability to use reporter ion tags to identify nitrated peptides, reduction of cost associated with purchasing commercial isobaric tag kits, and increasing the number of samples analyzed in a single experiment. The ability to increase multiplexing of proteomics experiments is an attractive area for many researchers that are examining expression differences in a large number of biological samples. **Chapters 5 and 6** extend cPILOT to a global quantitative proteomic approach to enhance multiplexing, which can be applied to protein samples of any origin.

5.0. GLOBAL COMBINED PRECURSOR ISOTOPIC LABELING AND ISOBARIC TAGGING (cPILOT) APPROACH WITH SELECTIVE MS³ ACQUISITION*

(*Global Combined Precursor Isotopic Labeling and Isobaric Tagging (cPILOT) Approach with Selective MS3 Acquisition. Evans, A. R.; Robinson, R. A. S. Proteomics. 13. Copyright © 2013. Permission granted by John Wiley and Sons. 2014.)

5.1. INTRODUCTION

Enhanced multiplexing techniques were presented in **Chapter 1**, which include SILAC combined with TMT [102], Neucode tags [105], and the synthesis of novel TMT reagents [103]. However, these approaches are limited to cell cultures, ultra-high resolution mass analyzers (R > 480k), or require tags not commercially available. **Chapter 4** reported a strategy for combining precursor isotopic labeling and isobaric tagging, termed "*cPILOT*", which increases the multiplexing of isobaric tagging to 12 and 16 samples for TMT and iTRAQ, respectively [98]. This approach however, is exclusive to the detection of nitrated peptides. Herein, **Chapter 5** presents a novel global cPILOT method, which can be applied to protein samples from any origin (e.g., cell cultures, tissues, biological fluids, etc.) using common commercially available reagents. This new approach relies on the use of low pH dimethylation to chemically tag peptide N-termini [293], leaving lysine residues accessible for TMT tagging. The key to this workflow for future multiplexing experiments is the use of light $[-(CH_3)_2]$ and heavy $[-(^{13}C^2H_3)_2]$ dimethyl tags for precursor labeling of up to 12 or 16 samples that will be subsequently tagged with TMT six-plex or iTRAQ eight-plex reagents, respectively. Global cPILOT is a technique, which can be applied to any laboratory interested in enhanced multiplexing.

The second aspect of global cPILOT includes a novel strategy which increases detection of reporter ions at the MS³ level. Several methods have been presented, which clean up precursor

interferences [86, 87] and thus improve reporter ion quantitation, such as gas-phase purification with electron transfer dissociation [89], HCD-MS[3] [94], and the analysis of fragment ions other than the traditional reporter ions (i.e., TMT clusters) [90]. It has been previously suggested that HCD-MS[3] data collection using gas phase fractionation significantly increases the number of MS[3] reporter ion spectra from trypsin digests [294]. This method is limited because it generates MS[3] spectra that do not contain reporter ions due to the selection of y-ions from arginine-terminated peptides, which lack a TMT tag. To overcome this limitation and increase the number of HCD-MS[3] spectra with reporter ions accessible for quantitation, we developed a selective MS[3] data acquisition method that uses y_1 (*m/z 371.2*) collisional induced dissociation (CID) fragments arising from C-terminal lysine-TMT peptides.

5.2. EXPERIMENTAL

In order to demonstrate the global nature of this new cPILOT workflow, peptide mixtures from wild-type mice (14 months old, C57BL/6J) brain homogenates were prepared. Mice were purchased from Jackson Laboratory and housed in the Division of Laboratory Animal Resources at the University of Pittsburgh. All animal protocols were approved by the Institutional Animal Care and Use Committee at the University of Pittsburgh. Brains were homogenized in phosphate buffer saline (PBS) with 8M urea, centrifuged at 13000 rpm, and the protein concentration of the supernatant was determined by BCA assay (Pierce Thermo Scientific). Proteins (100 µg) were reduced with dithiothreitol DTT, alkylated with iodoacetamide [98], and digested with either trypsin or LysC at a 1:50 protein:enzyme for 24 hours at 37°C or 18 hours at 30°C, respectively. LysC and trypsin digests were split into equal portions for low pH dimethylation [293] resulting in light [-$(CH_3)_2$] or heavy [-$(^{13}C^2H_3)_2$] labeled peptides that were individually subject to TMT[0] tagging according to manufacturer's protocol (Thermo Fisher). Pooled mixtures of light and heavy TMT[0] tagged peptides were separated using nanoflow reverse phase liquid chromatography (nRPLC) as previously described [98] with the following gradient (%A:%B): 90:10 for

5 minutes, 87:13 over 40 minutes, 80:20 over 50 minutes, 70:30 over 25 minutes, 40:60 over 15 minutes, 20:80 over 5 minutes, hold for 10 minutes, and re-equilibrate column for 30 minutes. Eluting peptides were nanosprayed into an LTQ Orbitrap Velos MS that was operated with data-dependent acquisition as follows: parent scan *m/z* range 300-1800, 60,000 resolution, top 7 ions were selected for CID-MS/MS (35% normalized collision energy, 2.0 isolation window, rejection of +4 or higher charge states) with HCD-MS^3 scans following each CID-MS/MS.   MS^3 spectra were acquired either from selection of the most intense ion in CID-MS/MS spectra [94] across the *m/z* range 300-800 or selection of the y$_1$ (*m/z* 371.2 ± 0.5 Da, within the top 50 most intense in MS/MS) fragment ion in CID-MS/MS spectra. RAW files were searched against the International Protein Index (IPI) for mouse proteome database (v3.87, 59534 sequences, 08/16/2012) using SEQUEST (Thermo Proteome Discoverer v1.3) with the following parameters: trypsin or lysC protease, two miscleavages, 15 ppm parent mass tolerance, 1 Da fragment mass tolerance, static modifications of light (28.031 Da) or heavy (36.076 Da) dimethylation on N-termini and carbamidomethyl (57.021 Da) on cysteine, dynamic modifications of oxidation (15.995 Da) on methionine and the TMT^0 tag (224.152 Da) on lysine. Raw data was searched against the database separately for static light and heavy dimethylation modifications (adding twice the search time). Both search results were manually combined for further data analysis processing. Decoy database searching was performed using a reverse protein database with FDRs set at 0.01 and 0.05 for high and medium confidence peptides, respectively. Two technical replicates for each pooled sample were acquired.

5.3. RESULTS AND DISCUSSION

For the presented global cPILOT workflow (Figure 5.1), different peptide samples (e.g., control and experimental, longitudinal, etc.) that arise from any source can be independently subject to low pH (~2.5) dimethylation, which selectively targets N-termini [293] in order to generate light or heavy labeled peptides. The mechanism for dimethylation involves the formation of an imine resulting from
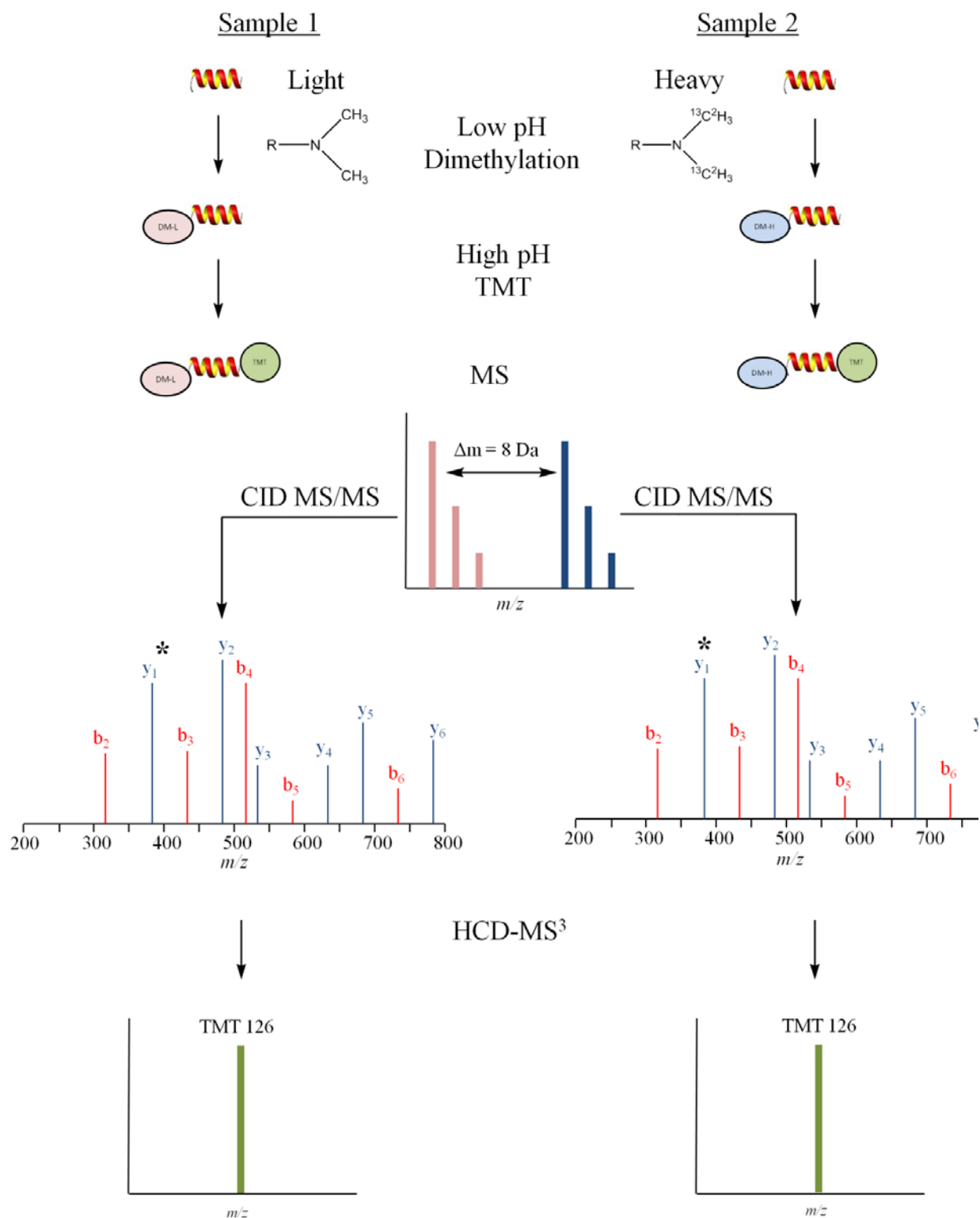
Figure 5.1. Schematic of the workflow for a global cPILOT approach applied to two samples that use TMT[0] reagents.

nucleophilic attack of primary amines to formaldehyde. The reaction is pH dependent to the reaction system pH and the amine pKa. Due to the pKa differences between amines of the lysine side chain (~10.5) and the peptide N-terminus (~7.5), the low pH (~2.5) conditions of 1% acetic acid solution are able to fully protonate lysines, while retaining reactivity of the N-terminus. Following dimethylation, samples can be further tagged with TMT reagents at high pH (~8.0), which will target lysine residues. After pooling, precursor spectra will show peak pairs separated in mass by 8 Da. Each peak is subject to CID and fragment ions are selected for HCD to generate MS^3 spectra based on two approaches described as top ion [94] and selective y_1 (Figure 5.1).

Figures 5.2a-c demonstrate the global cPILOT approach for tryptic mouse brain peptides. An example spectrum (Figure 5.2a) for the doubly-charged peptide D(dimethyl)SYVGDEAQSK(TMT^0) with precursor *m/z* values of 725.851 and 729.873 for the light and heavy peptides, respectively, shows a pair separated by an *m/z* shift of 4 (i.e., 8 Da). Figure 5.2b shows the CID fragmentation spectra for the light peptide (*heavy not shown*) and supports the sequence identified. The top ion-MS^3 method corresponds to selection of the y_2 fragment for both the light and heavy labeled peptides, resulting in detection of TMT^0 reporter ions (Figure 5.2c right panel). Using our selective y_1-MS^3 method (Figure 5.2c left panel), only the TMT^0 peaks are observed for the light and heavy labeled peptide peaks also demonstrating that this selection method gives similarly clean MS^3 spectra in the reporter ion region as the top ion method. Labeling efficiencies at both the low pH dimethylation and high pH TMT tagging steps were determined to be >98% and there was minimal cross labeling of reagents (*data not shown*). Overall, the combination of precursor low pH dimethylation with high pH TMT isobaric tagging provides a proteomics method that can be used for global quantitation of all peptides in a mixture, assuming the peptides contain free N-termini and C-terminal lysine residues. While the example shown in 5.2 represents the simplest case of two samples, through the use of additional TMT multiplex reagents an enhanced multiplexing experiment could be designed [98].

D(dimethyl)SYVGDEAQSK(TMT⁰)
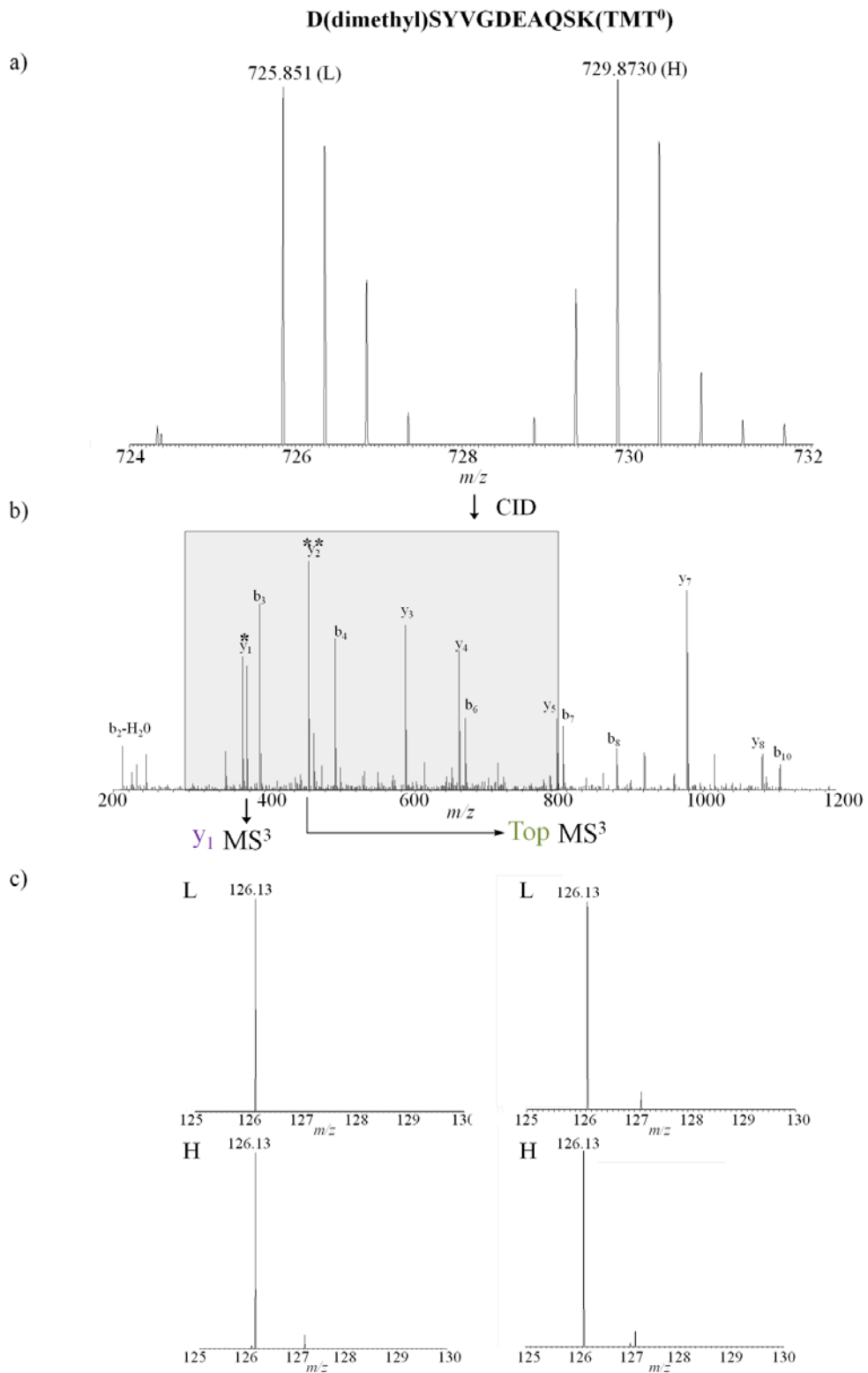
Figure 5.2. a) Precursor MS spectra for the peptide D(dimethyl)SYVGDEAQSK(TMT⁰) with b) corresponding CID-MS/MS for the light peptide. The shaded region corresponds to the *m/z* window for selection of the most intense ion for MS³, indicated by the (**). The (*) indicates the y_1 fragment selected. c) HCD-MS³ is shown for the top ion method (right) and the selective y_1 method (left) for light and heavy precursor peaks.

Selection of the top most intense ion for HCD-MS^3 data acquisition is limited by selection of CID-MS/MS fragments that do not contain a TMT tag. Examples include selection of a b-ion, miscleavage from enzymatic digestion, or selection of an unidentified background ion due to coisolation of another peak at the MS/MS level. Top ion-MS^3 selection is limited to the likelihood that a y-ion will be the most intense ion in the noted *m/z* range. One of the most frequent limitations occurs when a b-type ion is the most intense across the *m/z* range as opposed to a y-type ion (this occurs in ~20% of MS^3 spectra in these data). In this situation, the top ion-MS^3 method will fail to generate a reporter ion because the fragment will not contain any TMT-labeled amino acid. In order to increase the probability of selection of a TMT containing MS/MS fragment for HCD-MS^3, selective fragmentation of the y_1 ion corresponding to the C-terminal lysine-TMT fragment (*m/z* 371.2) can be applied. Figures 5.3a-c highlight an example for the doubly-charged D(dimethyl)FTPAAQAAFQK(TMT^0) light and heavy labeled peptides (Figure 5.3a) in which it is apparent that the b_3 fragment ion is the most intense in the shaded region of Figure 5.3b. Selection of this fragment ion with the top ion-MS^3 method does not generate reporter ion fragments (Figure 5.3c right panel). However, through use of the selective y_1 HCD-MS^3 method, reporter ions for the TMT^0 reagent are observed (Figure 5.3c left panel) demonstrating an advantage to this approach.

There are cases when both the top ion HCD-MS^3 and selective y_1 HCD-MS^3 methods will fail to generate reporter ions due to limitations of signal for low abundance ions and the need for high sensitivity to detect these ions at the MS^3 level. Despite these limitations, significantly more reporter ion spectra are observed with the selective y_1 MS^3 method (Table 5.1). For example, the total number of spectral counts (SC) for these methods is 4833 and 4960 for the top ion and selective y_1, respectively, when trypsin is used as the protease (Table 5.1). In addition, the number of SC containing reporter ions increased from 3023 to 3678 when the selective y_1 method was used instead of the top ion MS^3 method. In order to assess the reporter ion detection efficiency of each MS^3 method, we determined the total number of SC that should lead to generation of reporter ions based on sequence (from database search results). This

D(dimethyl)FTPAAQAAFQK(TMT⁰)

a)

773.922 (L)   777.944 (H)

773   775   777   779   781
m/z

CID ↓

b)

200   400   600   800   1000   1200
m/z

y₁ MS³ ⟶ Top MS³

c)
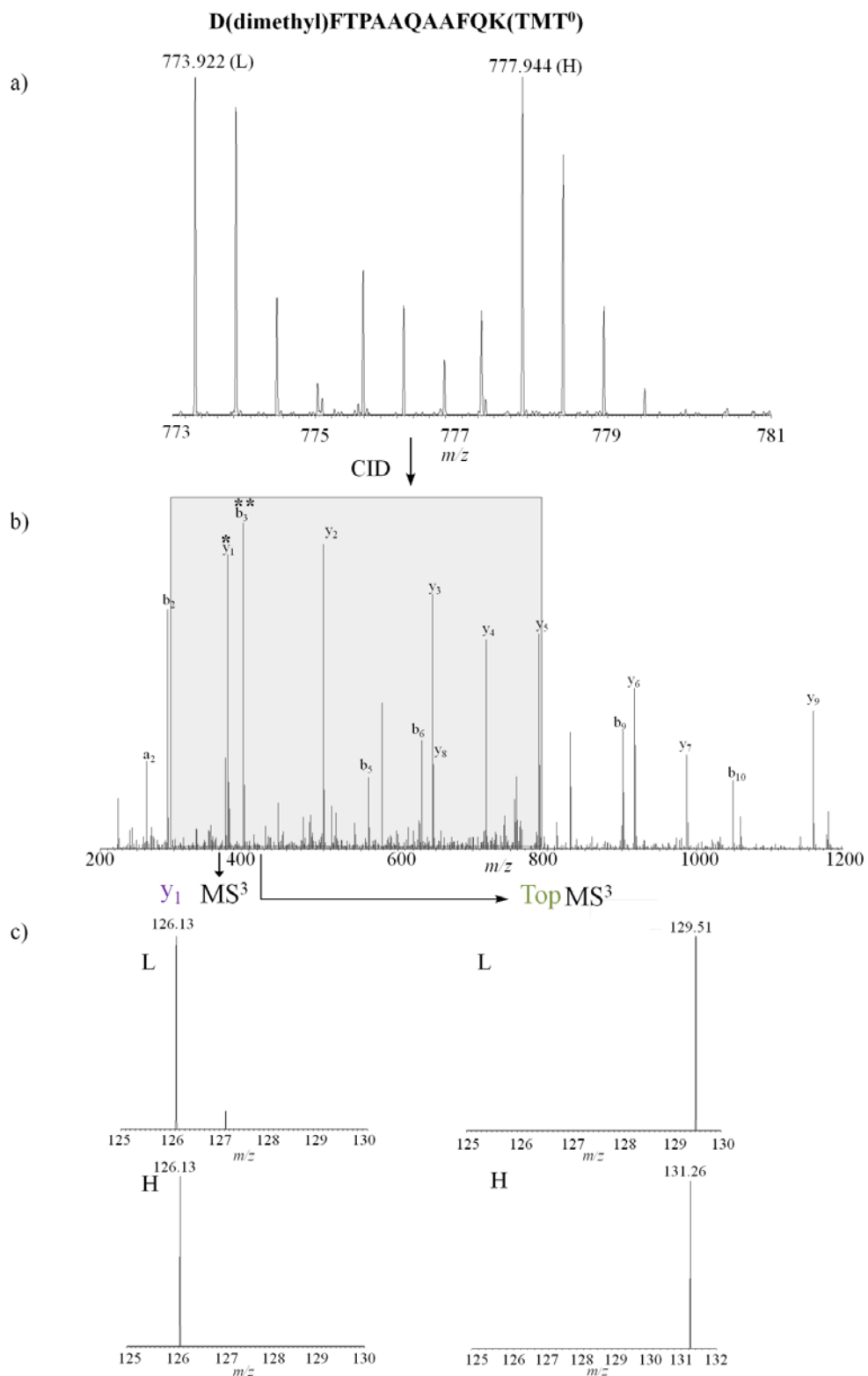
Figure 5.3. a) MS spectrum for the peptide D(dimethyl)FTPAAQAAFQK(TMT⁰) with b) CID-MS/MS for the light peptide. c) HCD-MS³ is shown for the top ion method (right) and the selective y₁ method (left) for light and heavy precursor peaks. The shaded region corresponds to the *m/z* window for selection of the most intense ion for MS³, indicated by the (**). The (*) indicates the y₁ fragment selected.

90

corresponds to 3844 and 3970 possible MS^3 reporter ion spectra using our cPILOT workflow with the top ion and selective y_1 HCD-MS^3 methods, respectively (Table 5.1). Based on the number of MS^3 spectra that contained reporter ions (minimum S/N $\geq$3), ~78% vs. ~93% efficiency was observed with the top ion vs. selective y_1 MS^3 methods, respectively.

In order to demonstrate the accuracy and reproducibility of the presented method, we prepared a 12-plex sample whereby a fixed amount (50 µg) of complex mouse liver digest was treated similarly for all reporter ion channels in light and heavy dimethylated steps. Triplicate MS analyses were performed using the selective y_1 HCD-MS^3 (m/z 376.3 Da) method. As shown in Figure 5.4a, reporter ion signal intensities are similar for m/z 126-131 for light and heavy dimethylated peaks of the example peptide Q(dimethyl)TALAELVK(TMT^6). Figure 5.4b shows the frequency distribution of protein ratios for each replicate considering all possible TMT reporter ions as the fixed channel. The average measured TMT ratios across all replicates were 1.02 (19% CV, N = 3254) and 1.00 (17% CV, N = 2723) for light and heavy modified proteins, respectively, providing support for suitable accuracy and reproducibility of this approach. Typical quantitative proteomic experiments using isobaric tags have a quantitative dynamic range of approximately two orders of magnitude [63, 67]. Although not assessed directly herein, we anticipate some limitations with dynamic range using our selective y_1-MS^3 approach. This is due to signal loss that occurs with each fragmentation step as is also a caveat to other methods that rely on MS^3 reporter ion signal for quantitation [94].

Finally, the use of LysC ensures that all MS^3 spectra contain a reporter ion regardless of b- or y-ion selection in MS/MS [94]. This advantage is lost during global cPILOT experiments because N-termini are modified with the dimethyl group. Additionally, trypsin digests have been shown to generate more quantifiable spectra with reporter ions when performing MS^3 data collection [294]. Our results are consistent with this as a lower number of SCs are observed when LysC is used (regardless of MS^3 method, Table 5.1). This could be attributed to the fact that LysC generates longer peptides, which typically contain higher charge state distributions that may decrease identifications [294, 295]. Higher

Table 5.1. Peptide and Spectra Evaluation

| Enzyme | Method | cPILOT Reporter Ion Spectral Counts (SC) | | | |
		SC	Predicted	Observed	Efficiency (%)
Trypsin	Top Ion	4833	3844	3023	78
LysC	Top Ion	2807	2751	2200	80
Trypsin	y_1 selection	4960	3970	3678	93
LysC	y_1 selection	2889	2853	2509	88
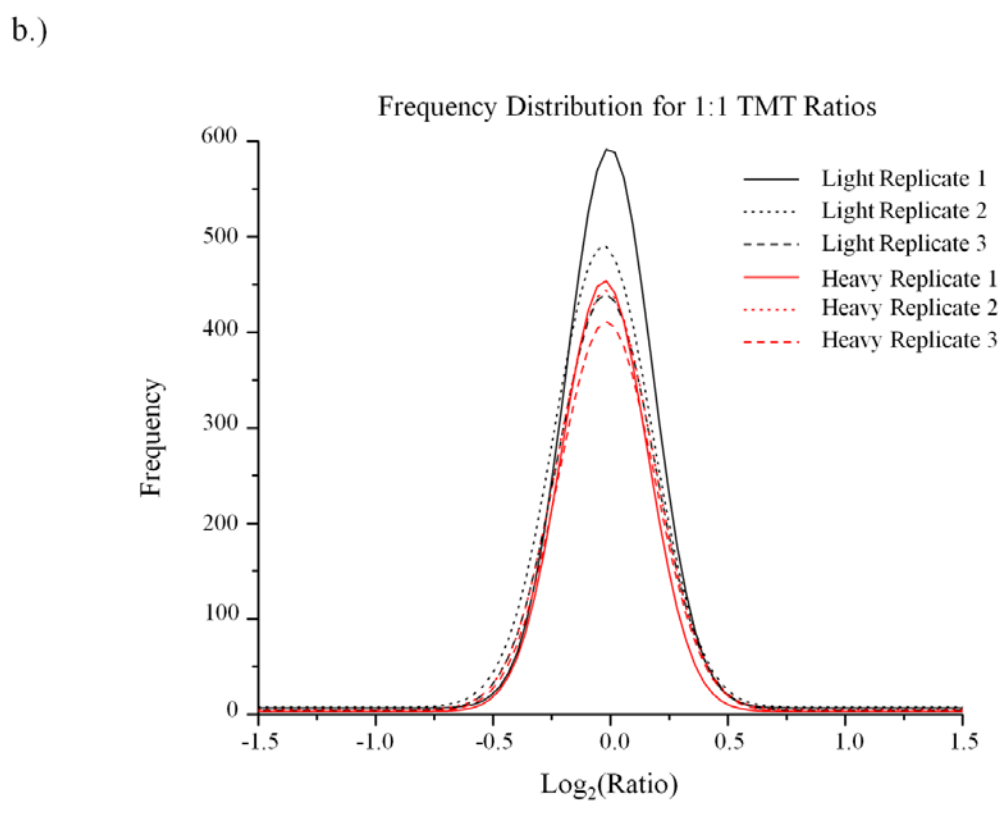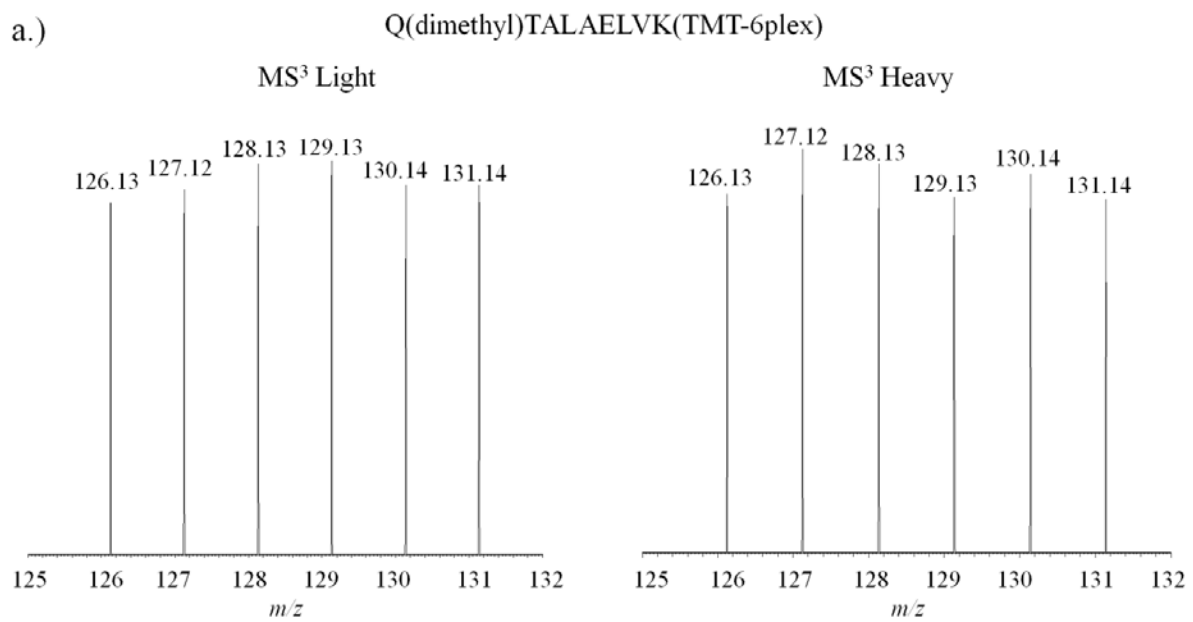
Figure 5.4. a) HCD-MS[3] fragmentation spectra (low m/z shown) for light (left) and heavy (right) petide Q(dimethyl)TALAELVK(TMT-6plex) showing equimolar twelve plex spectra. b) Log$_2$ plot of protein TMT ratios from three replicate experiments.

charge states ($\geq$4) are rejected in our workflow to minimize overlap between light and heavy precursor pairs.

5.4. CONCLUSIONS

Chapter 5 presents a novel global cPILOT method, which includes a selective y_1-MS^3 method for increased coverage of reporter ion spectra. Global cPILOT can be applied peptide mixtures (trypsin or LysC) from various sources (e.g., cell cultures, tissue, etc) and can be expanded to multiplex 12 and 16 samples for TMT and iTRAQ tags, respectively. Accurate and reproducible quantitation was demonstrated with < 20 % CV. **Chapter 6** expands global cPILOT to assess the dynamic range and applies the technique to biological tissues in a large scale discovery-based proteomics experiment.

6.0. GLOBAL cPILOT ANALYSIS OF THE APP/PS-1 MOUSE LIVER PROTEOME*

(*Information in this chapter is written based on a submitted manuscript, Evans, A.R.; Gu, L.; Guerrero Jr. R.; Robinson, R.A.S. *Proteomics Clinical Applications*.)

6.1. INTRODUCTION

Alzheimer's disease (AD) is a neurodegenerative disorder accounting for 60-80% of total dementia cases [296]. Symptoms include memory loss, confusion, decreased language skills and reduced motor function [297]. Senile plaques (SP), consisting of amyloid β (Aβ) peptides, are a major hallmark of AD, and are formed from the cleavage of amyloid precursor protein (APP) by α, β, and γ secretases [298, 299]. Presenilin-1 (PS-1) is a part of the γ-secretase complex and several mouse models of AD have been created which have APP and PS-1 mutations [300, 301]. Aβ peptides can be cleared from the brain by forming a complex with high density lipoprotein, which is facilitated by Apolipoprotein E (ApoE) [302]. Overexpression of ApoEε4 is a genetic risk factor for AD [303]. Disruption of cholesterol metabolism and homeostasis is linked to APP processing, β and γ-secretase activity, and Aβ peptide production [304, 305]. Other AD hallmarks include synapse loss, dystrophic neuritis, oxidative stress, mitochondrial dysfunction and neurofibrillary tangles composed of hyperphosphorylated tau protein [297]. AD is also a metabolic disorder as evidenced by alterations in glucose [306] and lipid metabolism [304], and insulin resistance [307]. Lower glucose metabolism in brains of AD subjects contributes to cognitive decline [308] and mitochondrial dysfunction [309].

Aside from the noted characteristics of AD present in the central nervous system there are also changes that take place in peripheral tissues, such as liver. Presenilin-2 (PS-2) is heritable in R1.40 human APP transgenic mouse liver [310]. Glucose intolerance and insulin resistance are observed in APP/PS-1

mouse liver and results in Aβ overproduction [311]. Docosahexaenoic acid (DHA), a neuroprotective fatty acid synthesized in the liver, decreases Aβ toxicity [312]. Impaired DHA biosynthesis correlates with cognitive impairment [313], while DHA administration decreases Aβ deposition [314]. The liver also plays a role in the clearance and degradation of Aβ peptides through liver low-density lipoprotein receptor-related protein (LRP) [315-317]. Higher LRP expression in liver increases Aβ peptide clearance and improves behavioral changes in APP/PS-1 and APPwIndJ20 mouse models of AD [318]. However, LRP is oxidized in AD which prevents Aβ peptide clearance ultimately contributing to elevated Aβ concentrations in the circulatory system [319]. It is clear that the liver plays a major role in AD however, the specific mechanisms and their relation to characteristic hallmarks in the central nervous system are not fully understood. The liver is responsible for system wide metabolic regulation, protein synthesis, and detoxification [320]. We believe that dyshomeostasis in the liver could contribute to AD pathogenesis. Here, we sought to measure changes in the liver proteome of an APP/PS-1 mouse model at advanced stages of disease [321] in comparison to heterozygous wild-type (WT) controls. Proteomic studies using this mouse model have been performed on the brain [322, 323], immune cells [324], astrocytes [325].

Enhanced multiplexing increases sample throughput and minimizes experimental variations, which result from multiple sample preparations and separate LC-MS injections. **Chapters 4 and 5** present cPILOT [98, 100], which increases sample multiplexing capabilities through multiple labeling steps. Global cPILOT enhances sample multiplexing and can be applied to protein digests from any sample origin (e.g., tissues, cell cultures, cell types, etc.) [100]. Here, we apply global cPILOT to the liver proteome of 14-month old APP/PS-1 and WT control mice. In a single proteomics workflow, six biological replicates are analyzed simultaneously. Independent verification of the changes in the liver proteome was performed using precursor dimethylation experiments of the six biological replicates independently. Merits of the cPILOT approach, results from the liver proteome analysis, and implications for AD are presented.

6.2. EXPERIMENTAL

6.2.1. Animal Housing and Tissue Harvesting

APP/PS-1 male mice [B6.Cg-Tg(APPswe, PSEN1dE9) 85Dbo/Mmjax, stock no. 005864, genetic background: C57BL/6J] and heterozygous controls were purchased from Jackson Laboratory and housed in the Division of Laboratory Animal Resources at the University of Pittsburgh. All animal protocols were approved by the Institutional Animal Care and Use Committee at the University of Pittsburgh. Mice were fed standard Purina rodent laboratory chow *ad libitum* and kept in a 12 hour light/dark cycle. Liver tissues were harvested from 14-month old APP/PS-1 (N=6) and WT (N=6) mice and stored at -80°C.

6.2.2. Protein Extraction and Digestion

Livers were individually homogenized in phosphate buffer saline (PBS) with 8 M urea using a Wheaton homogenizer. Homogenates were sonicated, centrifuged (13000 RPM, 4°C, 15 minutes), and supernatant collected. Protein concentrations were determined using BCA assay according to the manufacturer's protocol (Thermo Pierce, Rockford IL). Proteins (100 µg) were diluted to a concentration of 1.0 µg/µL in PBS with 8 M urea and spiked with bovine alpha-casein (Sigma, 1.0 µg) to serve as an internal quality control. Samples were digested with trypsin as previously described [98, 100]. Briefly, protein mixtures were treated with dithiothreitol (1:40 protein:reagent mol ratio, 2 hours, 37°C), iodoacetamide (1:80 protein:reagent mol ratio, 2 hours, 0°C, dark), and cysteine (1:40 protein:reagent mol ratio, 30 minutes, 25°C). Protein solutions were diluted using Tris buffer (0.2 M Tris, pH 8.0, 10 mM $CaCl_2$) and TPCK-treated trypsin was added (2.5% w/w enzyme/protein, 37°C, 24 hours). Digestions were quenched by flash freezing in liquid nitrogen, desalted using HLB C_{18} cartridges, and dried by speed-vac.

6.2.3. cPILOT Chemical Tagging

The global cPILOT [100] study design allows the simultaneous analysis of twelve biological samples in a single experiment (Figure 6.1). WT and APP/PS-1 mouse liver digests were paired using a random number generator and low pH (~2.5) dimethylation was performed to selectively modifies peptides with light [-(CH$_3$)$_2$] or heavy [-(^{13}C^{2}H$_3$)$_2$] dimethyl groups at the N-termini [100, 293]. Peptide digests were reconstituted in 1% acetic acid (0.25 µg/µL, pH = 2.5) and treated with either formaldehyde (60 mM)/sodium cyanoborohydride (24 mM) or ^{13}C,^{2}H$_2$-formaldehyde (60 mM)/sodium cyanoborodeuteride (24 mM) for light and heavy dimethylation, respectively. All samples were incubated (10 min, 25°C), quenched with 1% NH$_3$ (5 min, 25°C), acidified with 5% formic acid, and desalted using HLB C$_{18}$ cartridges. After sample cleanup, TMT^6 reagents are used to modify lysine residues at high pH (~8.5). Peptide solutions were reconstituted in 100 mM triethylammonium bicarbonate (TEAB) buffer (1 µg/µL) for TMT tagging (Thermo Scientific). Dimethylated WT and APP/PS-1 liver peptides were individually tagged with TMT reagents 126, 128, or 130 and TMT reagents 127, 129, or 131, respectively, according to the manufacturer's protocol. Samples were pooled to a single mixture, dried, and reconstituted in 25% acetonitrile (5 mM KH$_2$PO$_4$, pH 2.98).

6.2.4. Strong Cation Exchange

The pooled peptide sample (600 µg) was separated by offline strong cation exchange (SCX) on a Polysulfoethyl A column (Nest Group Inc., 2.1 mm i.d., 10.0 cm, 5U, 100Å) using a Waters 2695 LC with a Waters 996 PDA detector (210 nm – 400 nm). Buffer A was composed of 25% acetonitrile and 5 mM KH$_2$PO$_4$ (pH 3.0). Buffer B was composed of 25% acetonitrile, 5 mM KH$_2$PO$_4$, and 350 mM KCl (pH 3.0). Gradient elution was performed at 0.20 mL/min as follow (%A/%B): 100/0 for 5 minutes, 60/40 over 55 minutes, 40/60 over 25 minutes, 20/80 over 5 minutes, 0/100 over 10 minutes, hold 0/100 for 10 minutes, followed by column re-equilibration. Fractions were collected in a 96 well plate and

divided equally to create 13 equimolar fractions. Each fraction was cleaned using HLB C_{18} cartridges and dried by speed-vac.

6.2.5. RPLC-MS^3 Data Acquisition

SCX fractions were reconstituted in 0.1% formic acid solution and separated using nanoflow reversed phase liquid chromatography (nRPLC). Buffer A was composed of 3% acetonitrile (ACN) with 0.1% formic acid (FA) and buffer B was composed of 100% ACN with 0.1% FA. Samples were loaded onto a trap column (C_{18}, 200 Å, 2.0 cm, 5U, 3 μL/min), washed with buffer A for 3 minutes, and transferred onto an analytical column (C_{18}, 100 Å, 5U, 13.2 cm). Separation occurred at 300 nL/min with the following gradient: (%A/%B) 90/10 for 5 minutes, 85/15 over 20 minutes, 80/20 over 75 minutes, 70/30 in 20 minutes, 40/60 in 10 minutes, 20/80 in 5 minutes, hold 20/80 for 10 minutes, followed by column re-equilibration. Eluted peptides underwent nanospray ionization and were detected using an LTQ-Orbitrap Velos MS instrument. Parent MS scans (60,000 resolution, 400-1600 *m/z*, AGC $1x10^6$ ions, maximum injection time 500 ms) were performed followed by data-dependent acquisition (DDA). The top seven most intense ions were selected for CID MS/MS (500 minimum signal, 3 *m/z* isolation width, 35% NCE, 0.25 activation q, 10 ms activation time, $3x10^4$ AGC, 50 ms max injection time) followed by selection and fragmentation of the most intense ion from CID-MS/MS for HCD-MS^3 (Orbitrap detection, 200 minimum signal, 4 m/z isolation width, 60% NCE, 0.1 activation time, $3x10^5$ AGC, 250 ms IT, 300-1300 *m/z* MS/MS selection range, exclude unfragmented parent ion). Charge state screening was disabled, +4 or higher precursor mass charge states were rejected, and dynamic exclusion was disabled. To increase proteome coverage and the number of 12-plex peptides, second-tier experiments were performed for all samples using the same DDA conditions with the exception that the top 8 through 14th most intense ions were selected for CID-MS/MS. Triplicate injections were performed for all samples.

6.2.6. Database Searching and Processing

RAW files were searched with SEQUEST HT against the Uniprot mouse database (51178 sequences, 11/13/2013, bovine alpha-S1-casein P02662 added manually) and processed using Proteome Discoverer v1.4 (Thermo Scientific). Search parameters included: trypsin with two missed cleavages, peptide mass range 300-6000 Da, 15 ppm parent mass tolerance, 1 Da fragmentation tolerance, dynamic modifications of TMT-6plex (+229.163) on lysine residues, oxidation (+15.995) on methionine, static modifications of light (+28.031) or heavy (+36.076) dimethylation on the N-terminus, and carbamidomethyl (+57.021) on cysteine. Decoy database searching was performed using a reverse protein database with FDR settings at 0.01 and 0.05 for high and medium confidence peptides, respectively. Peptide reporter ion intensities were extracted using Proteome Discoverer v1.4 software (20 ppm mass tolerance, most confident peak, MS^3 scan event). The median value across an individual reporter ion channel was calculated from all peptides quantified. Next, the median of the medians for the twelve reporter ion channels was used to normalize reporter ion signals. Light or heavy peptide spectra containing at least one TMT tagged lysine and six reporter ions in HCD-MS^3 were used for quantification. Protein TMT ratios were calculated as the average of the summed reporter ion intensity ratio corresponding to assigned APP/PS-1 and WT pairs for each peptide (referred to hereafter as AD/WT). The following criteria were used to derive differentially-expressed proteins: one-way ANOVA ($p < 0.05$) with Bonferroni correction, protein score ≥ 10.0, spectral counts (SCs) ≥ 4, and biological replicate count ≥ 3. AD/WT ratios were considered differentially expressed if AD/WT values < 0.7 and > 1.4. Appropriate fold-change cutoff values were chosen based on the 95% confidence interval of average protein AD/WT ratios and previously described methods [100, 326, 327]. IPA pathway analysis, Panther [328], and Uniprot functional analysis was used to categorize differentially-expressed proteins by biological function.

Liver tissues were also subject to precursor dimethylation in six independent experiments [75]. WT (N=6) and APP/PS-1 (N=6) mouse homogenates (100 µg) were digested as described above, cleaned using HLB C_{18} cartridges, dried, and reconstituted in 100 mM TEAB buffer (0.25 µg/µL, pH = 8.5). WT and APP/PS-1 samples were treated with formaldehyde (60 mM)/sodium cyanoborohydride (24 mM) and $^{13}C,^2H_2$-formaldehyde (60 mM)/sodium cyanoborodeuteride (24 mM), respectively and incubated for 1 hour at 25°C. Samples were quenched with aqueous ammonia (0.1% final concentration), acidified with FA, and pooled pairwise to match the cPILOT experiment design (Supplemental Figure S3). Samples were cleaned using HLB C_{18} cartridges, dried, and reconstituted in 0.1% FA. Each sample was analyzed using nano-RPLC-MS/MS as described above with the following exceptions: 350-1700 *m/z* range for MS scans, selection of the top 15 most intense ions for CID-MS/MS, charge state screening enabled with rejection of +1 ions, and dynamic exclusion enabled (repeat count 2, 60 s duration). Database search parameters were performed with dynamic modifications of oxidation (+15.995) on methionine, light (+28.031) or heavy (+36.076) dimethylation on the N-terminus and lysine residues, and static modifications of carbamidomethyl (+57.021) on cysteine. Precursor signals were extracted using Proteome Discoverer v1.4 and peptide ratios (heavy/light for AD/WT) were calculated. Median peptide ratios across biological replicates were used for normalization.

6.3. RESULTS

6.3.1. *Global cPILOT Approach*

Global cPILOT [100] performed simultaneous analysis of twelve biological samples (Figure 6.1). To increase the number of peptide pairs resulting in 12-plex quantitation, we employed a two-tiered DDA method (Figure 6.2), which increased 12-plex peptides by approximately 50%. Tradeoffs to the multi-tier approach are additional instrument and data analysis times. We chose the top-ion-HCD-
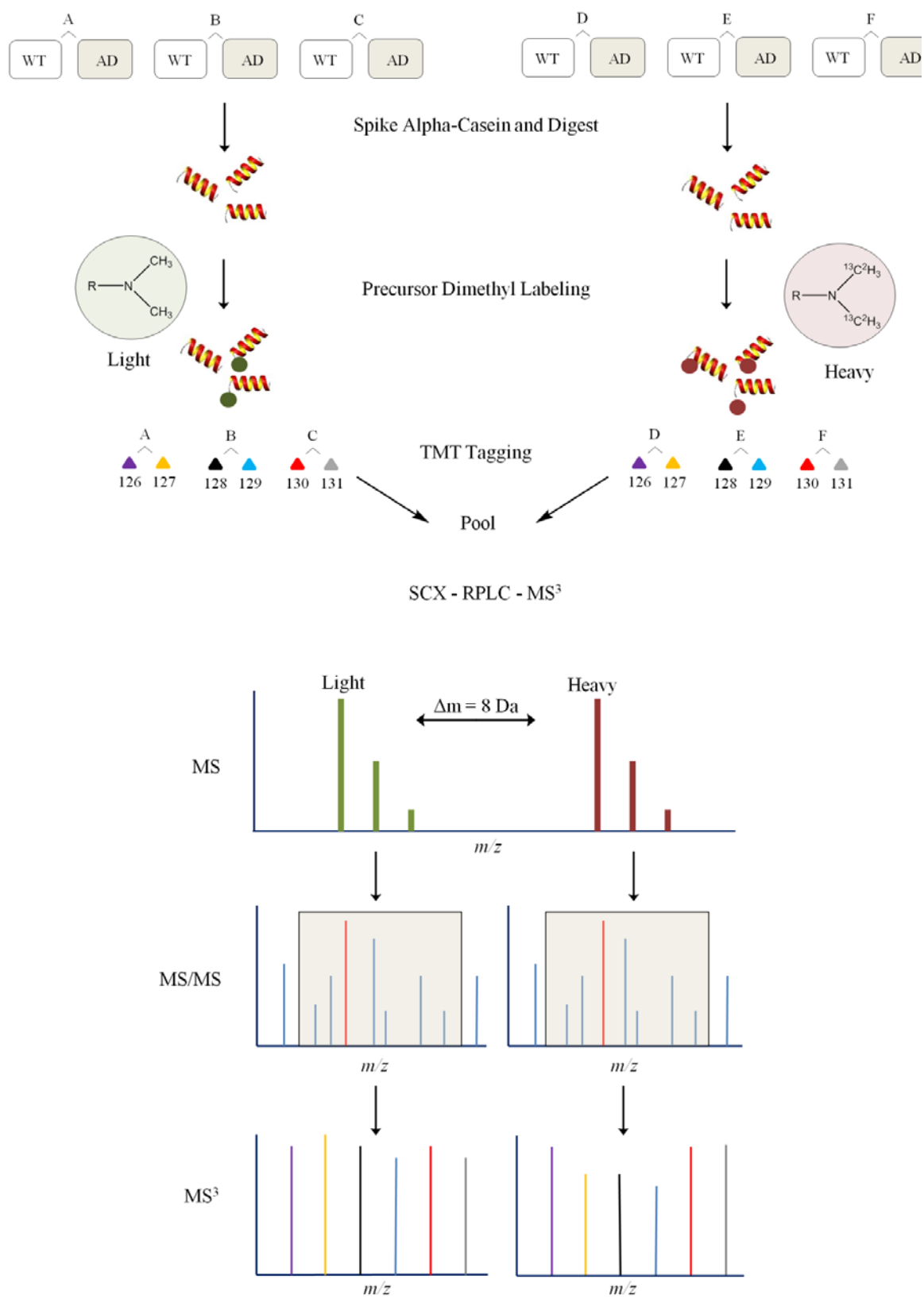
Figure 6.1. Schematic diagram of global cPILOT workflow. Details are described in text.
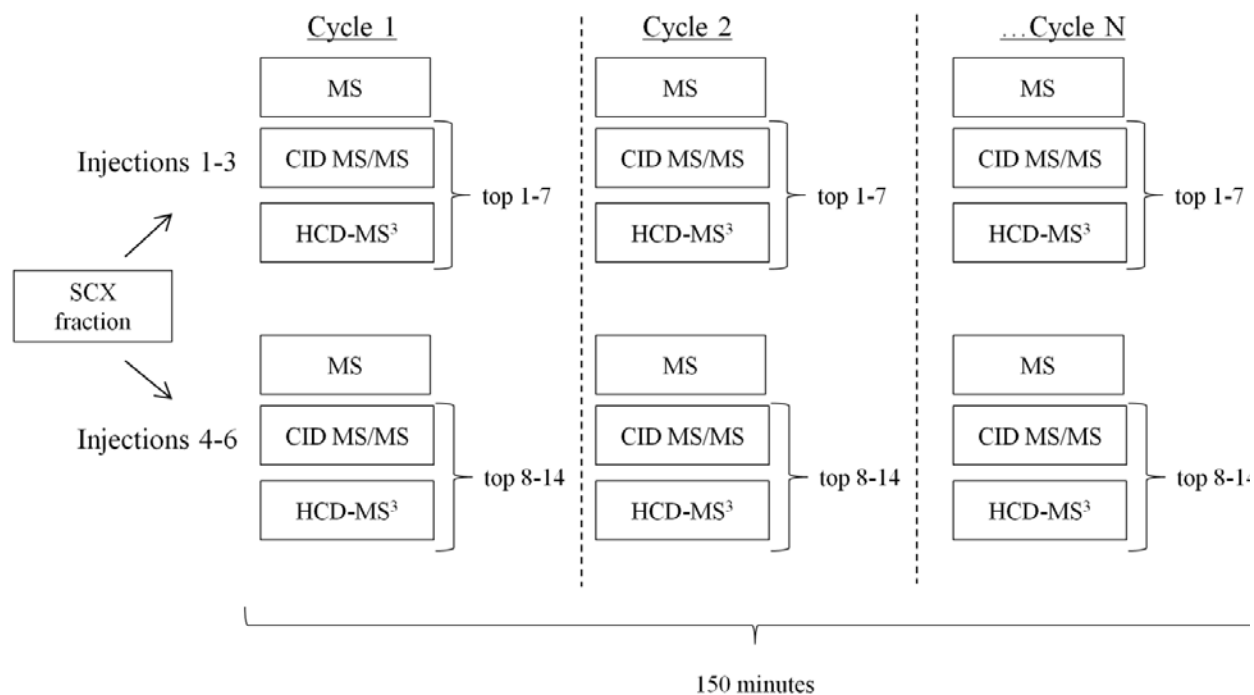
Figure 6.2. Data-dependent acquisition (DDA) method employed for AD mouse liver experiments. Offline SCX fractions were injected in triplicate and DDA parameters set to scan the top 1 through 7 most intense ions across 150 minutes of analysis time. Samples were re-injected three additional times and the top 8-14 most intense ions were selected and fragmented.

103

MS^3 [94] method since a 4-fold reduction in reporter ion signal was observed using the previously described selective y$_1$-MS^3 approach [100]. Reduced signal with selective y$_1$-MS^3 data acquisition can be attributed to the relatively lower signal (i.e., the y$_1$ fragment is ~35% of the base peak) of the selected MS/MS fragments and signal spread across six reporter ion channels and other MS^3 fragments.

6.3.2. Global cPILOT Accuracy and Dynamic Range

We assessed the accuracy of cPILOT across two orders of magnitude based on samples prepared as follows: 0.01:0.02:0.10:0.20:1.0:1.0 using TMT reagents that generate reporter ions at m/z = 126:127:128:129:130:131. Ratios were calculated with reporter ions at m/z = 130 or 131 as the numerator to measure fold-change values as follows: 1:1, 1:5, 1:10, 1:50, and 1:100. Box plots of experimental log$_2$ (TMT ratios) are shown in Figure 6.3. TMT ratios for light dimethylated precursors were 1.0:1.0 ± 0.1 (average ± standard deviation) (N=416 proteins), 1.0:6.0 ± 1.0 (N=784), 1.0:10.5 ± 2.1 (N=682), 1.0:46.4 ± 15.9 (N=316), and 1.0:72.4 ± 27.4 (N=132) while TMT ratios from heavy precursors were 1.0:1.0 ± 0.1 (N=218), 1.0:5.8 ± 0.8 (N=424), 1.0:10.7 ± 1.8 (N=390), 1.0:53.3 ± 11.5 (N=214), and 1.0:81.8 ± 20.5 (N=158) (average ± standard deviation). Linearity is observed across a 50-fold change range between reporter ion channels for light (r^2 = 0.9988) and heavy (r^2 = 0.9999) protein TMT ratios and across a 100-fold change range with r^2 = 0.9823 and 0.9791 for light and heavy protein TMT ratios, respectively. Based on these findings, cPILOT is accurate over a 50-fold change range.

6.3.3. cPILOT Analysis of the APP/PS-1 Liver Proteome

Global cPILOT was applied to the liver proteome of 14-month old male APP/PS-1 mice, mimicking advanced stages of AD. In total, 1734 unique proteins were identified from 5084 unique peptides (324517 SCs) and 545 proteins were quantified, which contain twelve reporter ion signals. In
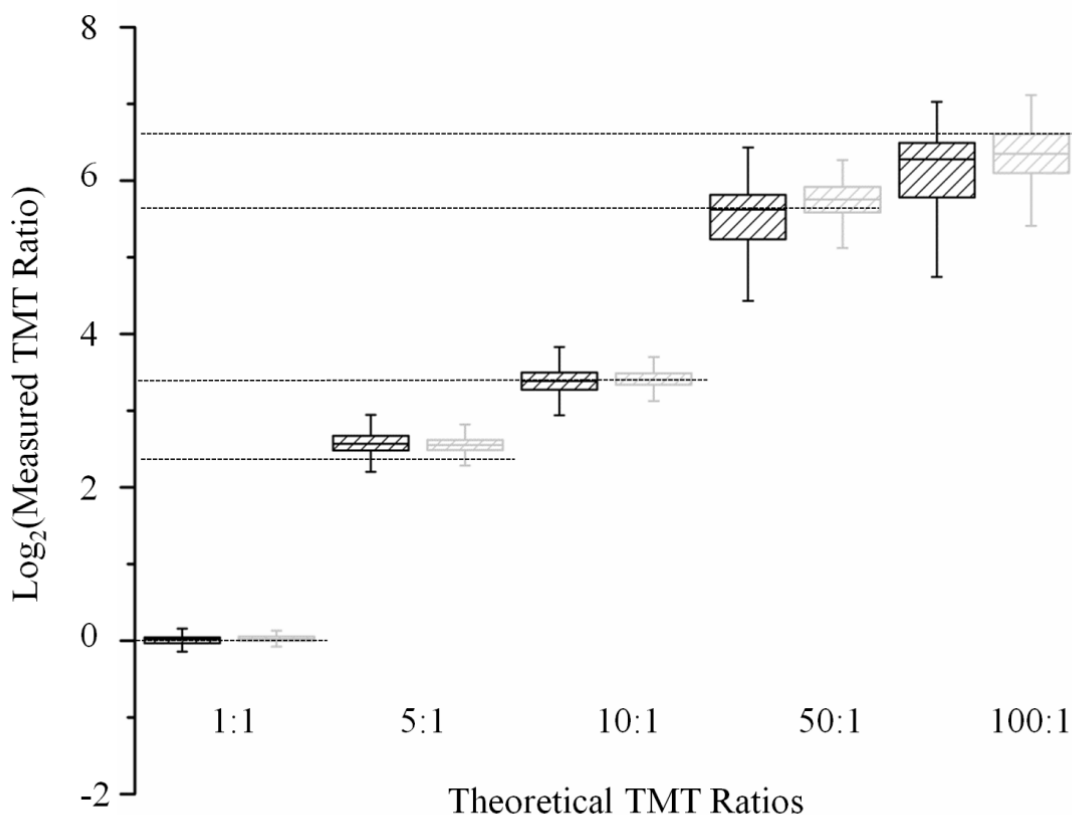
Figure 6.3. Box and whisker plot of experimental $\log_2$(TMT ratios) for light (black) and heavy (grey) precursor labeled proteins. Protein ratios (1:1) were calculated from reporter ions at m/z = 130:131, 5:1 from reporter ions at m/z = 130:129 and 131:129, 10:1 from reporter ions at m/z = 130:128 and 131:128, 50:1 from reporter ions at m/z = 130:127 and 131:127 and 100:1 from reporter ions at m/z = 130:126 and 131:126. Similar calculations were performed for light and heavy dimethylated protein ratios. Theoretical protein ratios are indicated by the dashed lines. Only LC-MS/MS was used to analyze this set of samples.

some cases, only a single dimethylated peak (i.e. light or heavy) was selected for MS/MS thus yielding results for less than six biological replicates. Figure 6.4a shows a sample 12-plex spectrum for the peptide [T(dimethyl)ITVSQDEGVRPSTTMQGLAK(TMT[6])+3H]$^{3+}$ which identifies to the protein 3-ketoacyl-CoA thiolase B, peroxisomal. HCD-MS^3 of light and heavy dimethylated peptides results in 12-plex quantitation (Figure 6.4b). Higher expression of this peptide is observed in AD tissue compared to WT (AD/WT = 1.4 ± 0.4, average ± standard deviation). Sixty-four proteins are differentially-expressed in AD liver (Figure 6.5) and have total reporter ion signals that span five orders of magnitude.

6.3.4. Precursor Dimethyl Labeling

Precursor isotopic dimethylation [75] was used as an independent means to verify cPILOT fold-change values (Figure 6.6). This approach included six duplex dimethylation experiments compared to the single 12-plex cPILOT analysis described above. Figure 6.4c displays the peptide [T(dimethyl)ITVSQDEGVRPSTTMQGLAK(dimethyl)+3H]$^{3+}$ observed in Figure 6.4a with light and heavy peaks. Similar to the cPILOT data, this peptide his higher abundance in the AD liver (1.4 ± 0.6). The six duplex dimethylation experiments resulted in 1415 proteins identified in which 712 proteins overlapped with the single 12-plex cPILOT experiment. Both approaches identified novel proteins that were not present in the other dataset. Overall, we have identified 2437 total liver proteins in these studies. Of the 64 differentially-expressed proteins from the cPILOT analysis, 22 protein ratios were verified using precursor dimethylation (Figure 6.7). Thirteen additional differentially-expressed proteins were detected using precursor dimethylation. Precursor dimethylation verified many of the cPILOT ratios.
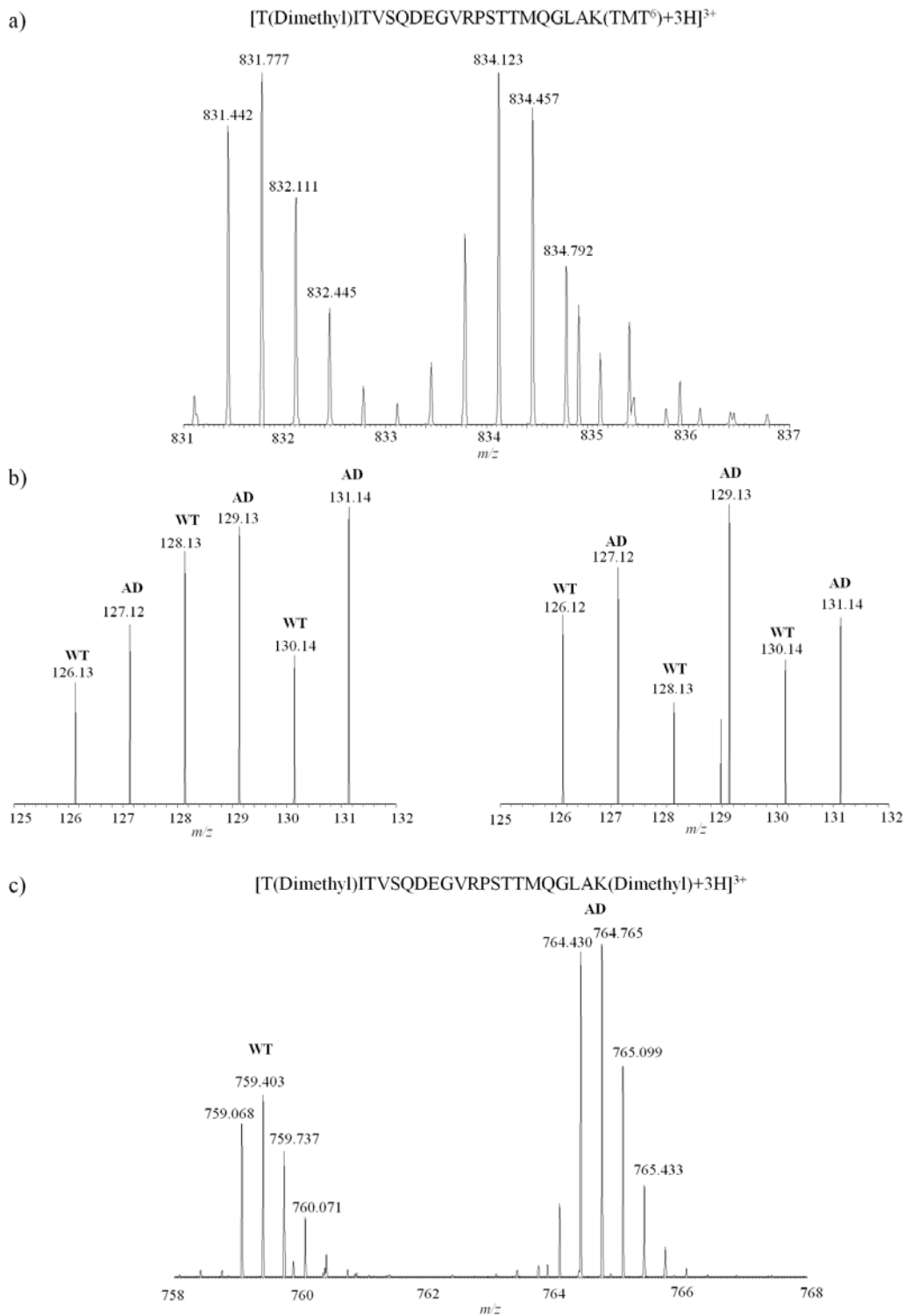
Figure 6.4. a) Precursor spectra for the peptide [T(dimethyl)ITVSQDEGVRPSTTMQGLAK(TMT[6])+3H][3+] which belongs to 3-Ketoacyl-CoA Thiolase B (Uniprot Acc. No. Q8VCH0) with b) left, HCD-MS[3] reporter ion spectra from light (m/z = 831.442) and right, heavy (m/z = 834.123) peptide peaks. Only the low m/z region is shown. c) Precursor specrum from the precursor dimethylation experiment of the same peptide from a). The light (m/z = 759.068) and heavy (m/z = 764.430) peptide peaks correspond to WT and AD samples, respectively.

107
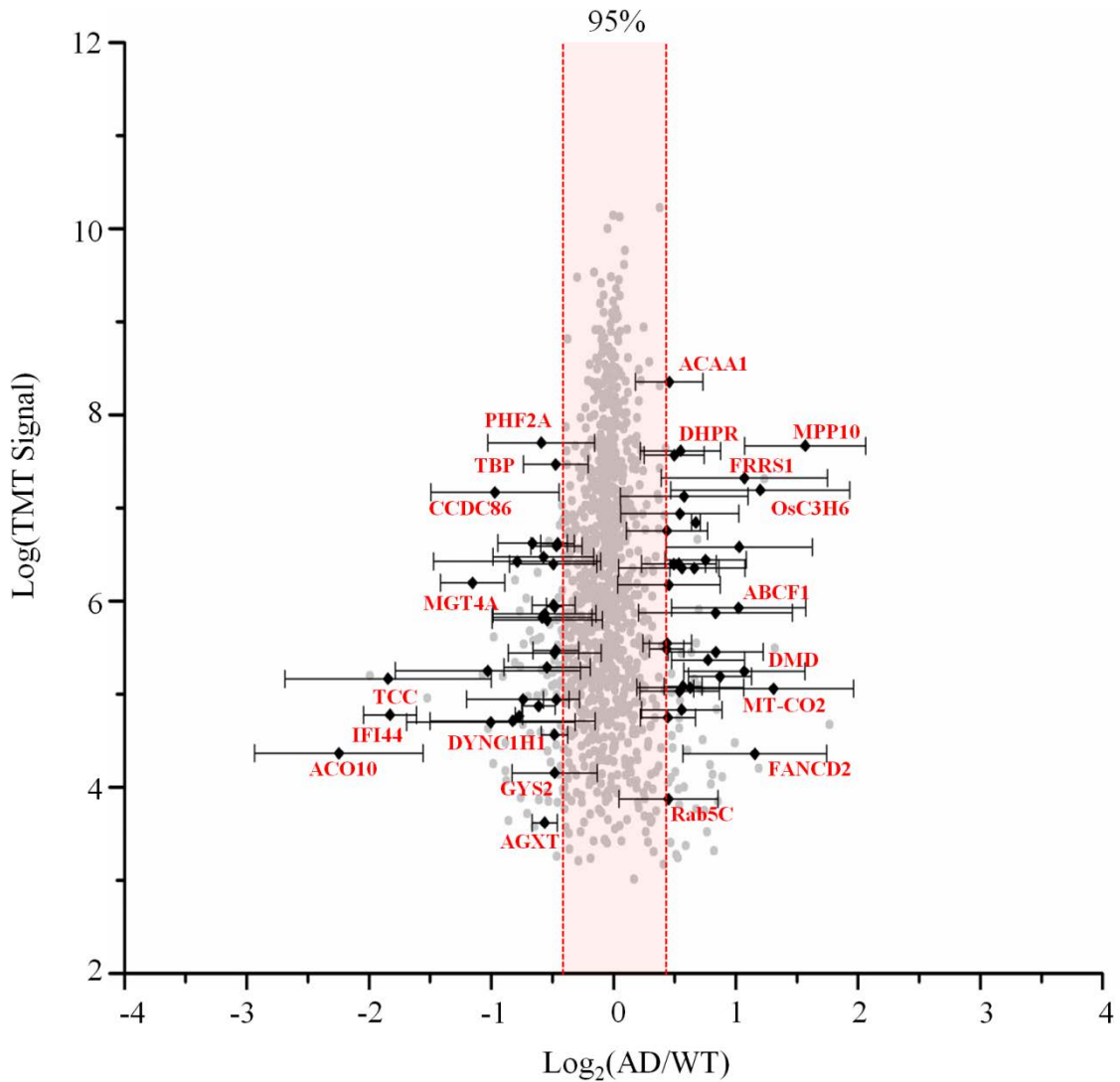
Figure 6.5. AD/WT protein ratios (log$_2$ scale) as a function of reporter ion signal (log scale). The highlighted area corresponds to a 95% confidence interval. Ratios for differentially-expressed proteins (◆) with error bars (coefficient of variation) are shown in the plot. The following proteins are labeled in the figure: 3-keto-CoA thiolase, peroxisomal (ACAA1), Dihydropteridine reductase (DHPR), U3 small nucleolar ribonucleoprotein (MPP10), Ferric-chelate reductase (FRRS1), Zinc finger CCCH domain-containing protein 6 (C3H6), ATP-binding cassette, sub-family F (ABCF1), Dystrophin (DMD), cytochrome c oxidase, subunit 2 (MT-CO2), Fanconi anemia group D2 (FANCD2), Ras-related protein Rab-5C (Rab5C), PHD finger protein 21A (PHF2A), TATA-box binding protein (TBP), Coiled-coil domain-containing protein 86 (CCDC86), Alpha-1,3-mannosyl-glycoprotein 4-beta-N-acetylglucosaminyltransferase A (MGT4A), tetratricopeptide repeat domain 6 (TCC), interferon-induced protein 44 (IFI44), cytoplasmic dynein 1 heavy chain 1 (DYNC1H1), Acyl-CoA thioesterase 10, mitochondrial (ACO10), Glycogen [starch] synthase, liver (GYS2), serine-pyruvate aminotransferase (AGXT).
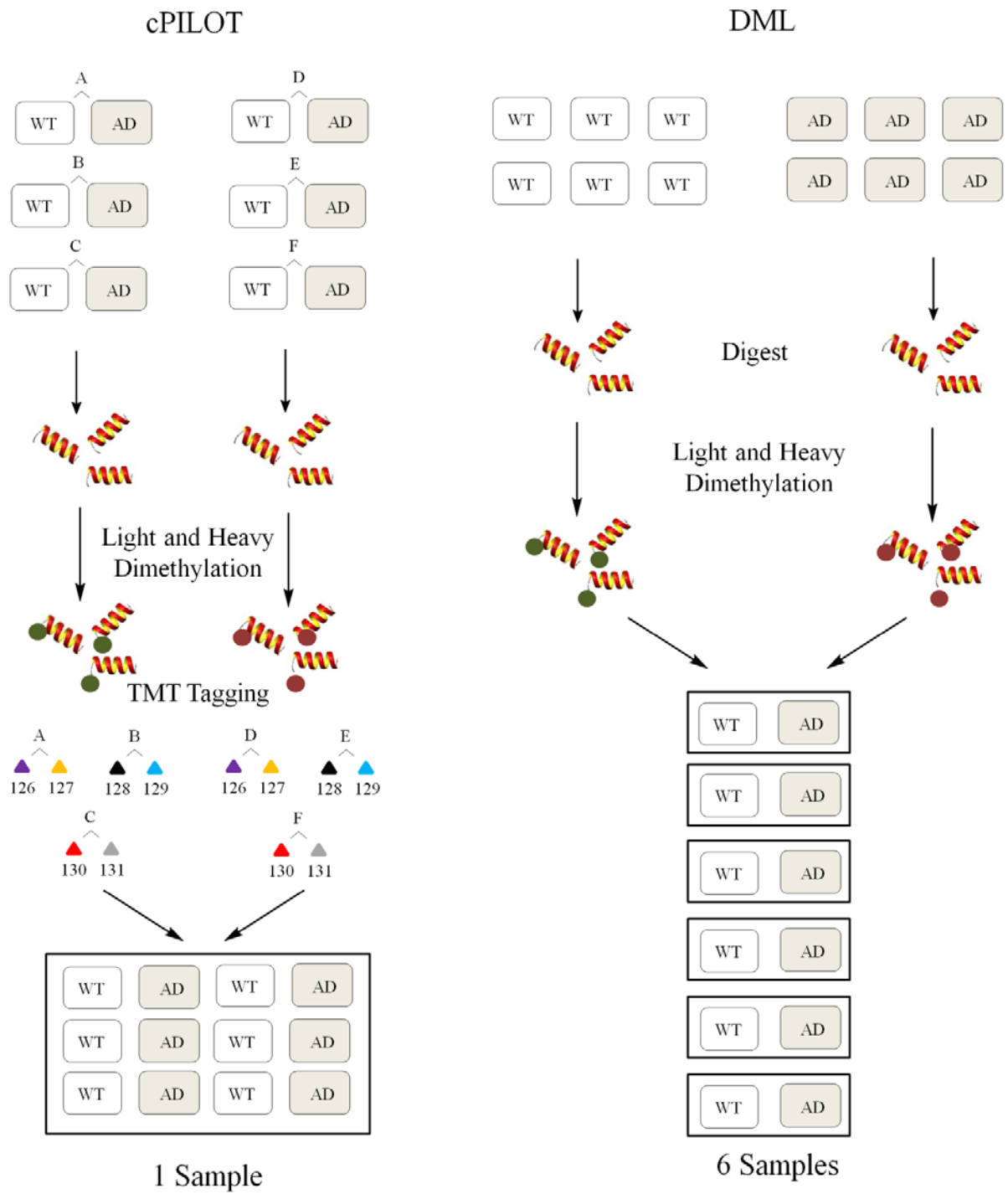
Figure 6.6. Schematic diagram of workflows used for cPILOT and precursor dimethylation experiments.
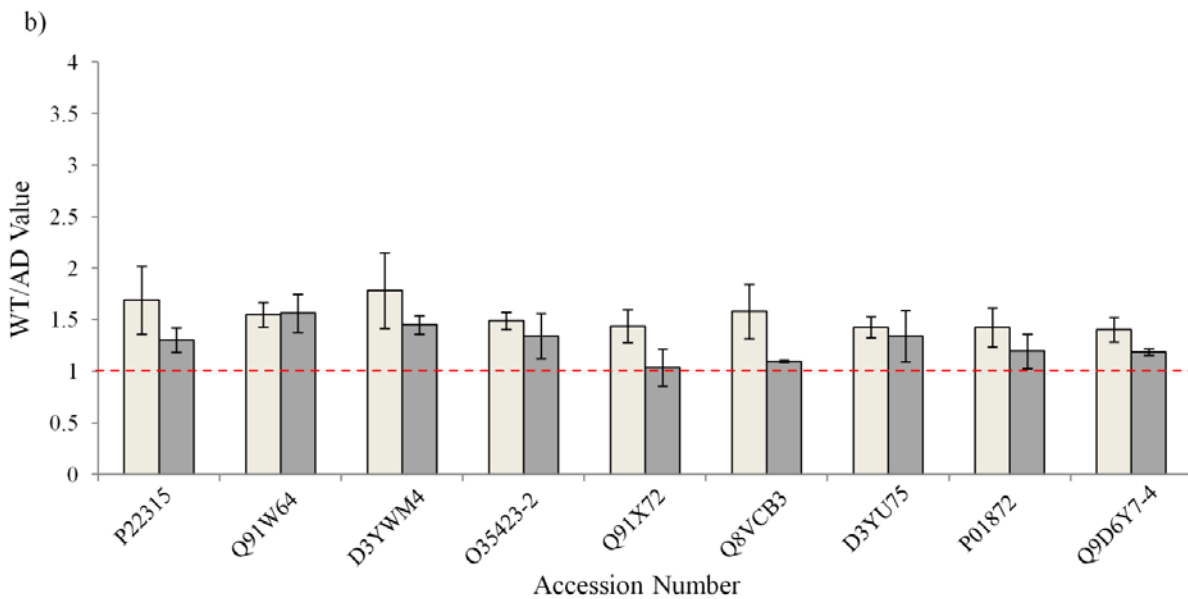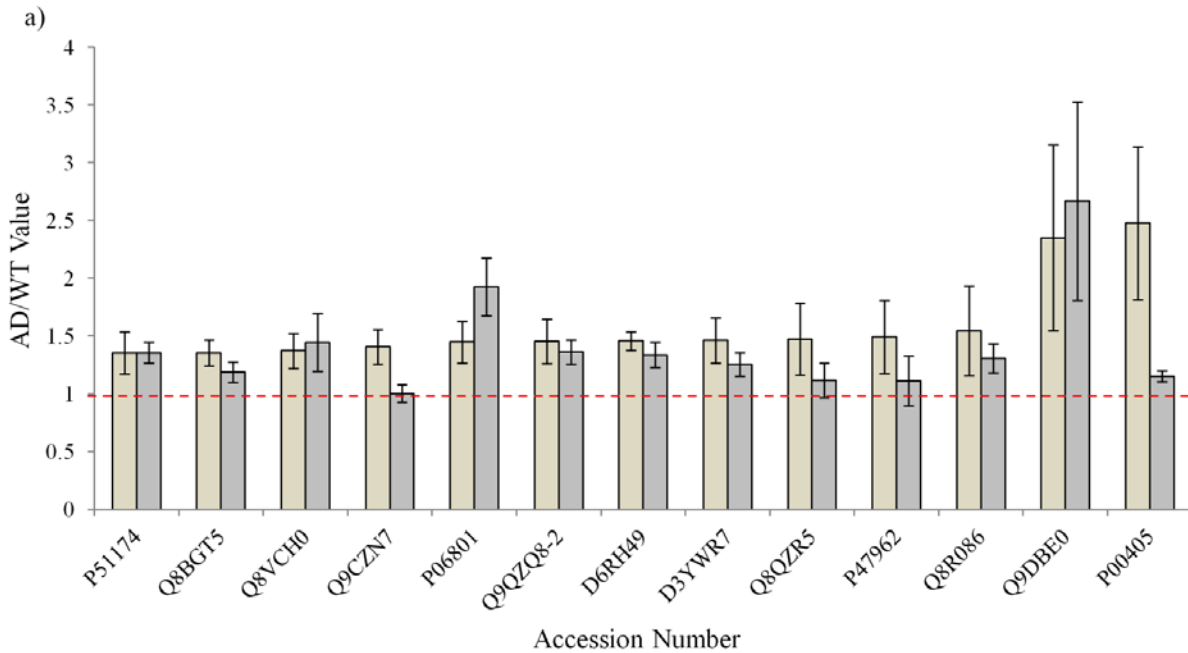
Figure 6.7. a) Bar graph comparing the AD/WT ratios (average ± standard deviation) calculated from cPILOT (light grey) and precursor dimethylation (dark grey) experiments. b) Bar graph comparing WT/AD ratios (average ± standard deviation) calculated from cPILOT (light grey) and precursor dimethylation (dark grey) experiments.

6.4. DISCUSSION

6.4.1. Global cPILOT Methodology

Previously, we presented global cPILOT, which performs precursor dimethylation at the N-termini followed by isobaric tagging of lysine residues [100]. Traditional analysis of twelve samples using stable isotopic labeling techniques requires six or two experiments using precursor dimethylation [75] or TMT tags [329], respectively. cPILOT provides the ability to perform simultaneous quantitation of twelve samples in a single experiment, which saves analysis time and isobaric tagging reagent. Fragmentation of both light and heavy dimethylated peptides is necessary to achieve 12-plex quantitation. This occurred for 59.3% of our quantified peptides, which is consistent with similar experiments previously presented [102]. Our two-tiered approach also resulted in detection of additional peptide pairs and increased overall peptide identification.

Significant overlap was observed between cPILOT and precursor dimethylation results in protein identifications, differentially expressed proteins, and similar protein fold change ratios (Figure 6.7), highlighting the complementary nature of these techniques. Interestingly, precursor dimethylation resulted in 703 additional unique proteins not detected using cPILOT, which we attribute to differences in data collection. cPILOT experiments required the selection of the top CID-MS/MS ion for MS^3 fragmentation to obtain maximum sensitivity due to enhanced reporter ion signal compared to selective y1-HCD-MS^3 [100]. We recommend disabling the dynamic exclusion parameter in cPILOT MS^3 experiments in order to maximize the number of peptides that contain full 12-plex information. We recognize that this impacts protein identification rates and compensated for the decrease by incorporating SCX fractionation and a two-tiered data collection method. These add-ons resulted in a total experimental time of ten days, compared to 2.5 days for the six duplex dimethylation experiments that lacked any fractionation. Similar fractionation experiments performed on six duplex dimethylation would have resulted in an experimental time of almost 30 days. New instrumentation, such as the Orbitrap

Fusion, performs multinotched MS^3 scan events [330], which may allow the dynamic exclusion setting with the enhanced MS^3 sensitivity, thus eliminating the need for a two-tiered data method. The faster scan rates of the Fusion significantly enhance proteome coverage coupled with highly sensitive MS^3 scans.

In future cPILOT experiments, it could be helpful to perform one analysis that focuses on identification of many features in the data similar to an accurate mass tag approach [331]. After this initial experiment, then inclusion or reject lists could be used to setup faster and more focused scanning methods based on HCD-MS^3 without CID-MS/MS. This would minimize the amount of time associated with these experiments. Compared to label-free analyses of the twelve samples, precursor labeling or multiple TMT samples that would incorporate multidimensional separations, we still believe that cPILOT drastically reduces experimental time and costs. Overall, cPILOT successfully performed high throughput protein identification and quantitation of relatively high abundant liver metabolism related proteins and is discussed below.

6.4.2. Differentially-Expressed Proteins in APP/PS-1 Liver

Decreased glucose metabolism, disruption of energy homeostasis, insulin resistance, and dysregulation of lipid metabolism are manifested in AD subjects and can greatly help our understanding of AD pathogenesis [308, 332]. Since the liver is responsible for metabolic regulation and detoxification of Aβ peptides, we sought to characterize the liver proteome in an AD mouse model (i.e., APP/PS-1) and assess if metabolic dysfunction is systemic in AD. It is noteworthy to highlight that there exists no mouse model which contains all characteristics and behaviors of AD. Sporadic AD accounts for a majority of cases, however autosomal dominant AD caused by genetic mutations contains similar characteristics and pathologies [333]. We refer the reader to extensive reviews on genetically modified AD mouse models as well as potential limitations of their use [300, 334]. The APP/PS-1 develops amyloid senile plaques at 6

months of age [335] and exhibits cognitive impairment by 12 months of age. The mice used in this study are 14 months of age, which is appropriate to study the effects of late stage AD on the liver proteome. Below is a brief discussion of major pathways identified across differentially-expressed proteins in AD liver.

6.4.3. Fatty Acid Metabolism

β-oxidation is the principle pathway for fatty acid metabolism that ends in the production of acetyl-CoA. β-oxidation can occur in mitochondria [336] or peroxisomes [337] that are present in the liver. Long chain specific acyl CoA dehydrogenase (1.4 ± 0.4), 3-keto-CoA thiolase (1.4 ± 0.4), and acyl–CoA thioesterase 10 (0.2 ± 0.1) are differentially-expressed in AD liver (Figure 6.8a), which suggests elevated fatty acid β-oxidation and increased acetyl-CoA production. This is consistent with acyl-CoA dehydrogenase in APP/PS-1 cerebral cortices [325] and enoyl-CoA hydratase in 3xTG-AD (APP/PS-1/Tau-p) cortices [338]. Our laboratory has simultaneously detected differential-expression of acyl-CoA oxidase in APP/PS-1 liver using a cysteine selective cPILOT approach [326]. Ketogenesis produces ketone bodies such as β-hydroxybutyrate, acetone, and acetoacetate from acetyl-CoA in liver, which supplies energy to other organs during starvation [339]. Increased ketone body-producing enzymes have been previously observed in AD mouse models [326, 338]. Ketogenic diets improve motor functions in APP/PS-1 mice and may be a potential therapeutic approach for neurological disorders [340, 341]. Since glucose metabolism is dysfunctional in AD brain [332], increased fatty acid metabolism in the AD mouse liver may increase ketone body formation. This would provide a compensatory energy source for AD brain (Figure 6.8b). We hypothesize there may be elevated ketone body synthesis in liver, transport of these ketone bodies to the brain, and ketone body metabolism in AD brain. However, further experiments are necessary in order to test this hypothesis.
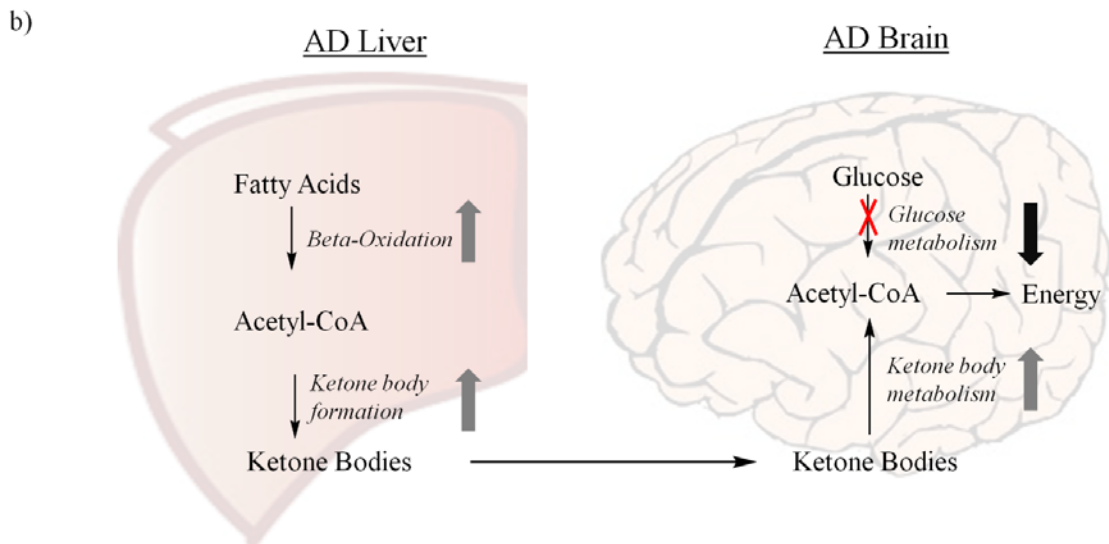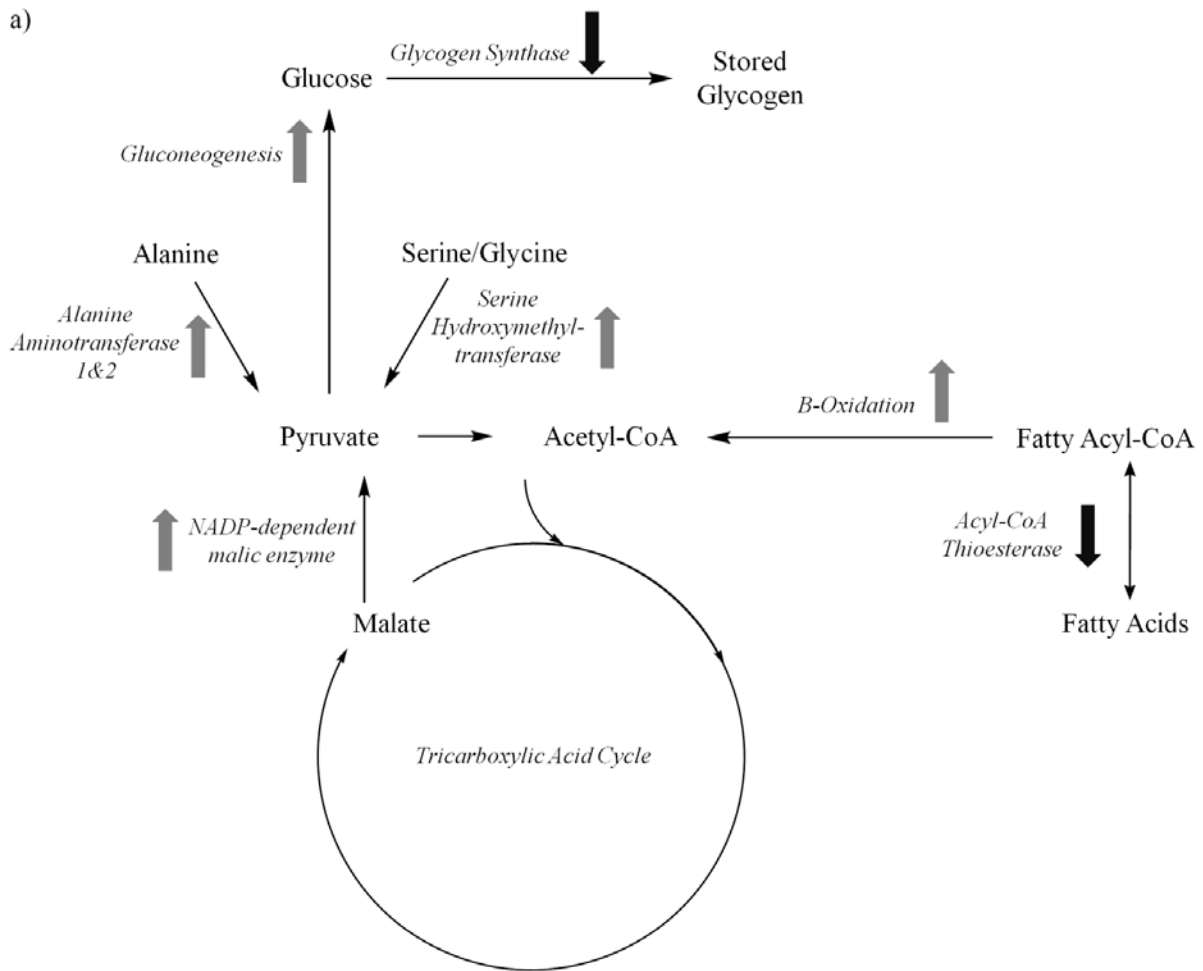
Figure 6.8. a) Metabolic pathways of selected differentially-expressed proteins in AD liver from cPILOT studies. Grey arrows represent elevated protein abundances and black arrows represent reduced protein abundances in AD liver. b) Proposed model of how metabolism changes in the AD liver are connected to AD brain.

6.4.4. Pyruvate Metabolism

Serine hydroxymethyltransferase (1.4 ± 0.4) and NADP-dependent malic enzyme (1.4 ± 0.4) are higher in AD liver, while serine-pyruvate aminotransferase (0.7 ± 0.1) was lower suggesting elevated pyruvate concentrations. Pyruvate is an essential metabolite that fuels the tricarboxylic acid cycle (TCA) and drives other biosynthetic pathways [342]. Alanine aminotransferase 1 (1.5 ± 0.8) and glutamic pyruvate transaminase 2 (1.4 ± 0.3) are enzymes involved in the alanine cycle that produce pyruvate in liver. The alanine cycle coupled with glutamate dehydrogenase creates α-ketogluterate and ammonia, which must be detoxified through the urea cycle [342]. The α-ketoglutarate dehydrogenase complex has decreased activity in AD brain [306] and is inhibited by elevated ammonia concentrations [343]. Our laboratory has measured differential expression in aspartate aminotransferase and glutamate synthetase in the APP/PS-1 mouse tissue elsewhere. Hyperammonemia can lead to hepatic encephalopathy, a neurological complication resulting from liver damage [344]. Clinically, elevated alanine aminotransferase activity is indicative of liver damage [345]. Impairment of ammonia detoxification may contribute to AD pathology and neurodegeneration [346].

6.4.5. Other Metabolic Processes

Gluconeogenesis is a process related to the alanine cycle in which glucose is synthesized from pyruvate and alanine. Phosphoenolpyruvate carboxykinase (3.9 ± 2.1) is involved in glucose synthesis. Differential-expression of glycogen synthase (0.7 ± 0.2) and glycogen break-down proteins [326] in AD liver suggests reduced glucose storage. The liver regulates glucose levels by balancing the synthesis and breakdown of glycogen. Diabetes, hyperglycemia, and insulin resistance may be metabolic mediators of AD [332]. Observed proteomic changes from cPILOT analysis point to dysregulation of blood-glucose levels in APP/PS-1 mouse liver. It is possible that this systemic dysregulation may correlate with altered glucose metabolism in AD brain.

Propionyl CoA carboxylase (0.7 ± 0.3) and methylmalonyl-CoA mutase (1.6 ± 1.3) are enzymes involved in catabolism of succinyl-CoA, an intermediate of the TCA cycle. Succinyl-CoA is a precursor for heme synthesis [347]. Ferrochelatase (0.6 ± 0.2) forms protoheme in heme biosynthesis and hemopexin (0.7 ± 0.1) is a heme scavenger [348]. Lower levels of these proteins in AD liver would result in low circulating heme levels. Mitochondrial dysfunction in AD can decrease TCA cycle activity, which depletes succinyl-CoA concentrations and reduces the cells' ability to synthesize heme [349]. Dihydropteridine reductase (1.5 ± 0.5) is involved in the formation of tetrahydrobiopterin, an important cofactor required in the biosynthesis of tyrosine in liver [350]. Higher dihydropteridine reductase levels in AD liver can cause more liver resident tyrosine. Tyrosine can be metabolized into fumarate for use in the TCA cycle or be converted into ketone bodies. Alterations in TCA cycle intermediates are likely due to mitochondrial dysfunction in AD liver.

6.4.6. Redox Signaling

Enzymes involved in the electron transport chain can generate reactive oxygen species by forming the superoxide anion from molecular oxygen [351]. We detected elevated levels of cytochrome C oxidase subunit 2 (2.5 ± 1.6) and sulfite oxidase (1.5 ± 0.7) in AD liver and hence potential elevation of oxidative phosphorylation. Changes in oxidative phosphorylation have been reported in triple transgenic AD mouse models [352]. Differentially-expressed redox enzymes which use NADPH as a cofactor are dihydropteridine reductase, NADP-dependent malic enzyme (1.4 ± 0.4), carbonyl reductase 1 (0.7 ± 0.1), ferric-chelate reductase 1 (2.1 ± 1.4), 25-hydroxycholesterol 7 alpha hydroxylase (0.6 ± 0.1), and protein-methionine sulfoxide oxidase (0.6 ± 0.3). Antioxidant regeneration relies on a continuous supply of NADH and NADPH, which may be altered in AD liver [353]. Oxidative stress is a key contributor to AD pathology [27] and may impact redox signaling activity of protein-methionine sulfoxide oxidase (0.6 ± 0.3) [354] and cytochrome p450 (0.7 ± 0.1) [27]. Ferric-chelate reductase 1 (2.1 ± 1.4) may also induce

metal-catalyzed oxidative damage. Imbalance of redox signaling enzymes and oxidative stress in liver tissue can result in cellular dysfunction and damage.

6.4.7. Transcription and Translation

We detected a number of differentially-expressed proteins involved in transcription and translation processes. 60S ribosomal protein L5 (1.5 ± 0.8), 39 ribosomal protein L22 (1.4 ± 0.2), 40S ribosomal protein S27 (1.4 ± 0.3), and zinc finger CCCH domain-containing protein 10 (2.3 ± 1.7), histone H2A (1.5 ± 0.5), and fanconi anemia group D2 (2.2 ± 1.4) are enzymes which play a role in RNA binding, protein synthesis or DNA transcription. RNA oxidation is increased in AD including 60S ribosomal fractions and can lead to dysregulation of protein synthesis [355]. Phosphorylated histone family proteins are indicative of DNA damage and lead to apoptosis [356]. Fanconi anemia group D2 actively eliminates damaged DNA during the cell replication [357] and higher levels in AD liver is likely in response to elevated damaged DNA. Alterations in transcription and protein synthesis in AD liver can be a result of damaged DNA and RNA, although additional studies are necessary to confirm this hypothesis.

6.5. CONCLUSIONS

We performed an enhanced multiplexed proteomic study of the APP/PS-1 liver proteome using the global cPILOT approach developed in our laboratory. Global cPILOT analysis allowed six biological replicates (twelve samples) of APP/PS-1 and WT mouse liver to be measured in a single proteomics experiment. Advantages of enhanced multiplexing include higher sample throughput, reduced variation across multiple samples, and lower cost of isobaric tagging reagents in comparison to the cost associated with repeated isobaric tagging experiments. However, we note that samples are not pooled in our

approach until after precursor labeling and isobaric tagging steps are complete. Precursor dimethylation was performed in parallel and verified differentially-expressed proteins from cPILOT. Necessary improvements to the approach are focused on increasing the duty cycle of the acquisition to increase selection of dimethylated pairs. For example, in some cases only the light or heavy dimethylated precursor ions were selected for MS/MS, which resulted in only half of the reporter ion channels being detected (although the other precursor in the pair was detected in parent scans). Also, we increased experimental time by incorporation of the two-tiered DDA approach to improve the likelihood of selecting dimethylated pairs. This could be reduced significantly by improvements to data acquisition or by using faster and more sensitive MS instruments such as the Orbitrap Fusion. In comparison to label-free or other isotopic labeling approaches, the overall experimental time was still significantly shorter. cPILOT provides the ability to perform high-throughput quantitative analysis of clinical laboratory samples using readily available chemical reagents. Multiplexing can be further increased by using iTRAQ 8-plex or TMT 10-plex reagents.

The cPILOT approach was used to successfully identify changes in the liver proteome of APP/PS-1 mice. Differentially-expressed proteins in the AD liver proteome are involved in fatty acid metabolism, pyruvate metabolism, redox signaling, transcription and translation processes, and gluconeogenesis. The changes observed in AD liver have considerable overlap with already reported metabolic changes in AD brain. Novel findings from this work highlight the potential use of ketone bodies produced in the liver as an alternative energy source for AD brain. Furthermore, hyperammonia production from the alanine cycle could lead to hepatic encephalopathy, which is linked with neurodegeneration. The changes observed in the liver proteome of APP/PS-1 mice provide further evidence that AD is a metabolic disorder and redox signaling and oxidative stress may be manifested in the periphery of AD subjects. Future studies that shed insight on the global or systemic changes that occur in AD are warranted. This work represents a promising step in that direction, which will lead to a more thorough and better understanding of AD.

7.0. EXPANDING VERSITILITY OF cPILOT USING N-N-DIMETHYL LEUCINE ISOBARIC TAGS

7.1. INTRODUCTION

Stable isotopic labeling in proteomics achieves relative quantitation of two or more samples in a single experiment using mass spectrometry (MS) [358]. Sample throughput and multiplexing is limited by the chemical tagging approach and the data collection method. **Chapter 1** highlights common techniques used in proteomics to perform relative quantitation. Precursor isotopic labeling employs a chemical tag, which creates a mass shift in MS and can multiplex up to five samples in an experiment using dimethylation [359]. Isobaric tags, such as tandem mass tags (TMT), achieves relative quantitation by comparing the signals from signature reporter ions, which are detected using tandem mass spectrometry (MS/MS) [88]. These tags offer multiplexing up to ten samples in a single shotgun proteomics experiment.

Enhanced multiplexing beyond the sample limitations mentioned above is achieved using combined precursor isotopic labeling and isobaric tagging (cPILOT) [100, 101]. The work presented in **Chapter 6** demonstrates protein quantitation of twelve samples in a single experiment by combining light and heavy dimethylation with TMT 6-plex reagents [101]. Multiplexing of 20 samples per experiment is possible using TMT 10-plex reagents with an Orbitrap resolution of R > 35,000 (m/z = 200) in higher energy collisional dissociation (HCD) MS/MS [85]. One disadvantage in current cPILOT methodology is the cost of the TMT reagents. Despite the sample throughput capabilities of isobaric tags, the cost to perform full multiplexed experiments is $516 and $933 per experiment for TMT 6-plex and 10-plex reagents, respectively (Thermo Scientific). cPILOT approaches can reduce the costs by half since TMT reagent vials can be split among light and heavy dimethylated peptides, however routine analysis is still approximately $250 per 12-plex experiment (**Chapter 6**). Deuterium isobaric amine reactive tags

(DiART) [82] and N-N-dimethyl leucine reagents (DiLeu) are alternative isobaric tagging reagents in quantitative proteomics. Specifically, DiLeu tags are chemically synthesized by performing dimethylation on the amine of L-leucine [83]. Additional heavy atoms are incorporated by performing ^{18}O exchange on the carbonyl group. Similar to other isobaric tags, DiLeu tags contain a reporter ion region (*m/z* 114-117), a mass balance region, and a peptide reactive group. Currently, these isobaric tags enhance reporter ion stability and are developed as 4-plex [83], 8-plex [360], and 12-plex reagents [361]. Herein, **Chapter 7** demonstrates the incorporation of DiLeu tags into the cPILOT method using bovine serum albumin. cPILOT using the DiLeu approach is benchmarked against the TMT^0 tag and a cost analysis is presented for multiplexed experiments. The implementation of DiLeu into the cPILOT approach demonstrates the versatility and accessibility of this high throughput quantitative proteomics method.

7.2. EXPERIMENTAL

7.2.1. BSA Digestion

Bovine serum albumin (BSA, Sigma) solution was prepared in PBS with 8M urea (1.0 µg/µL) and digested as previously described [107]. Briefly, 200 µg of BSA was treated with DTT (0.600 mM final concentration, 37°C, 2 hours), iodoacetamide (1.20 mM final concentration, 0°C, 2 hours), and L-cysteine (0.600 mM, 25 °C, 30 minutes). Tris buffer (0.2 M tris, 10 mM $CaCl_2$, pH 8.0) was added to the mixture resulting in a four time volume dilution. TPCK-treated trypsin (Sigma Aldrich) was added to each sample at 2% w:w enzyme:protein and incubated at 37°C for 24 hours. Samples were quenched by flash freezing in liquid nitrogen, cleaned using a Waters HLB C_{18} cartridge, and dried by speed vac.

7.2.2. Activation of Dimethyl Leucine Tag 118

N,N-dimethyl leucine tag 118 (DiLeu118) was synthesized as previously described [83]. To activate the tag, 11.1 mg of 4-(4,6-dimethoxy-1,3,5-triazin-2-yl)-4-methylmorpholinium tetrafluoroborate (DMTMM, Sigma) was dissolved in 350 µL 1% N-methylmorpholine in anhydrous dimethylformamide

and added (50 µL) to 1.0 mg of DiLeu118. The resulting mixture was stirred, incubated for 30 minutes (25 °C), and centrifuged (1000x g) to collect supernatant, which contains activated DiLeu118 reagent.

7.2.3. BSA Peptide Labeling

BSA digests were reconstituted in 1% acetic acid solution (0.25 µg/µL) for light and heavy dimethylation as previously described [100, 101]. Briefly, BSA digests were treated with either formaldehyde (60 mM)/sodium cyanoborohydride (24 mM) or $^{13}C,^{2}H_2$-formaldehyde (60 mM)/sodium cyanoborodeuteride (24 mM) for light and heavy dimethylation, respectively. All samples were incubated (10 min, 25°C), quenched with 1% NH_3 (5 min, 25°C), acidified with 5% formic acid, and desalted using HLB C_{18} cartridges. For DiLeu118 tagging, dimethylated peptides were reconstituted in 500 mM triethylammonium bicarbonate (TEAB) buffer (2.0 µg/µL). Anhydrous acetonitrile (1.6x volume) was added to the peptide solution followed by the activated DiLeu118 mixture (1:15 peptide:tag mol ratio). Peptides were incubated at 25°C for 3 hours followed by addition of hydroxylamine (50 mM) to quench the reaction. Samples were diluted two-fold with water, cleaned using SCX spin tips (Protea Biosciences) and desalted using C_{18} HLB solid phase extraction cartridges. For TMT^0 tagging, dimethylated BSA peptides were reconstituted in 100 mM TEAB buffer and modified with TMT^0 reagent according to manufacturer instructions (Thermo Scientific). Sample was desalted using C_{18} HLB solid phase extraction cartridges.

7.2.4. LC-MS/MS

Peptide samples were reconstituted in 0.1% formic acid solution and separated using nRPLC on a C_{18} column (1.7U, 130Å, 300nL/min) [98]. Buffer A was 5% DMSA and 0.1% formic acid (FA) in water and buffer B was 5% DMSO and 0.1% FA in acetonitrile. Gradient elution was performed as follow (%A/%B): 95/5 for 5 minutes, ramp to 65/35 over 55 minutes, ramp to 5/95 over 10 minutes followed by 15 minute column re-equilibration for a total run time of 85 minutes. DiLeu cPILOT peptides were detected using an LTQ-Orbitrap Elite mass spectrometer [49]. Parent MS scans were performed (1E6

AGC, 380-1600 *m/z*, R = 120,000) followed by data dependent acquisition selection of the top 10 most intense ions for HCD-MS/MS (2.0 Th isolation window, 29% NCE, 0.1 activation time, 5E4 AGC, R = 15,000) and detection using the Orbitrap (scans start at 110 *m/z*). Charge state screening was enabled and singly charged peptides were rejected for HCD-MS/MS scan events. The dynamic exclusion was enabled with a repeat count of one (five seconds, 500 max exclusion list). TMT^0 cPILOT BSA peptides were detected using an LTQ-Orbitrap Velos. Parent MS scans were performed (1E6 AGC, 300-1600 *m/z*) followed by data dependent acquisition selection of the top 10 most intense ions for HCD-MS/MS (2.0 Th isolation window, 29% NCE, 0.1 activation time, 3E5 AGC) and detection using the Orbitrap (scans start at 110 *m/z*). Charge state screening was enabled in which singly charged peptides were rejected for MS/MS scan events. The dynamic exclusion was enabled with a repeat count of one for a duration time of five seconds (500 max exclusion list). The small duration time for all dynamic exclusion parameters allows for the collection of more MS/MS events across a peptide extracted ion chromatogram. Since the samples are single protein digests, a more quantitative data collection method can be employed without the need for in-depth proteome coverage.

7.2.5. Database Searching

RAW files were searched using SEQUEST HT against the BSA sequence (Uniprot P02769) and processed using Proteome Discoverer v1.4 (Thermo Scientific). Search parameters included: trypsin with two missed cleavages, peptide mass range 300-5000 Da, 15 ppm parent mass tolerance, 1 Da fragmentation tolerance, dynamic modifications of DiLeu118 (+145.132) or TMT^0 (+224.152) on lysine residues, oxidation (+15.995) on methionine, static modifications of light (+28.031) or heavy (+36.076) dimethylation on the N-terminus, and carbamidomethyl (+57.021) on cysteine. Decoy database searching was performed using a reverse protein database with FDR settings at 0.01 and 0.05 for high and medium confidence peptides, respectively. Reporter ion intensities were extracted using Proteome Discoverer

software (30 ppm mass tolerance, most confident centroid) at m/z = 118.153 and 126.128 for DiLeu118 and TMT^0, respectively.

7.3. RESULTS AND DISCUSSION

7.3.1. cPILOT and N,N-Dimethyl Leucine Isobaric Tags

DiLeu tags are chemically synthesized isobaric tags, which can be employed in MS/MS quantitative proteomic experiments [83]. Figure 7.1a illustrates the chemical structure of the DiLeu118 reagent. Similar to other isobaric tags (i.e. iTRAQ, TMT), DiLeu118 contains a reporter ion region, a mass balance region, and a peptide reactive group. Four deuterium atoms are incorporated within the reporter ion region from dimethylation of L-leucine with ^{2}H-formaldehyde during tag synthesis. In order to modify peptides, the DiLeu tags must be activated with DMTMM to create a triazide-based reactive group towards peptide amines [83]. Global cPILOT was previously presented in **Chapters 5 and 6** using TMT^0 [100] or 6-plex tags [101]. Figure 7.1b illustrates the cPILOT method with incorporation of the DiLeu isobaric tags. BSA protein digests are modified with either light or heavy dimethyl groups at low pH to selectively modify peptide N-termini. After sample clean-up and a buffer exchange, activated DiLeu118 modifies the lysine residues. The method demonstrates the versatility of cPILOT by the incorporation of isobaric tagging reagents other than TMT.

7.3.2. BSA with DiLeu cPILOT

To benchmark the incorporation of the DiLeu118 isobaric tag into cPILOT, BSA samples were prepared using the TMT^0 reagent as previously described [100]. Figure 7.2a shows the sample peptide D(dimethyl)LGEEHFK(TMT^0) with light and heavy peaks at m/z 613.823 and 617.844, respectively. Isolation and HCD fragmentation of light and heavy peptides results in the MS/MS spectra shown in Figure 7.2b (only low m/z range shown). The presence of the reporter ion corresponding to the TMT^0 tag at m/z 126.13 is detected in the light (left) and heavy (right) HCD-MS/MS spectra similar to previously presented TMT cPILOT experiments [100]. DiLeu118 based cPILOT samples were prepared using BSA

a)

Reporter Ion   Balance   Reactive Group

b)

Sample 1   Sample 2

Light   Heavy

Low pH
Dimethylation

DiLeu Tagging

LC-MS/MS
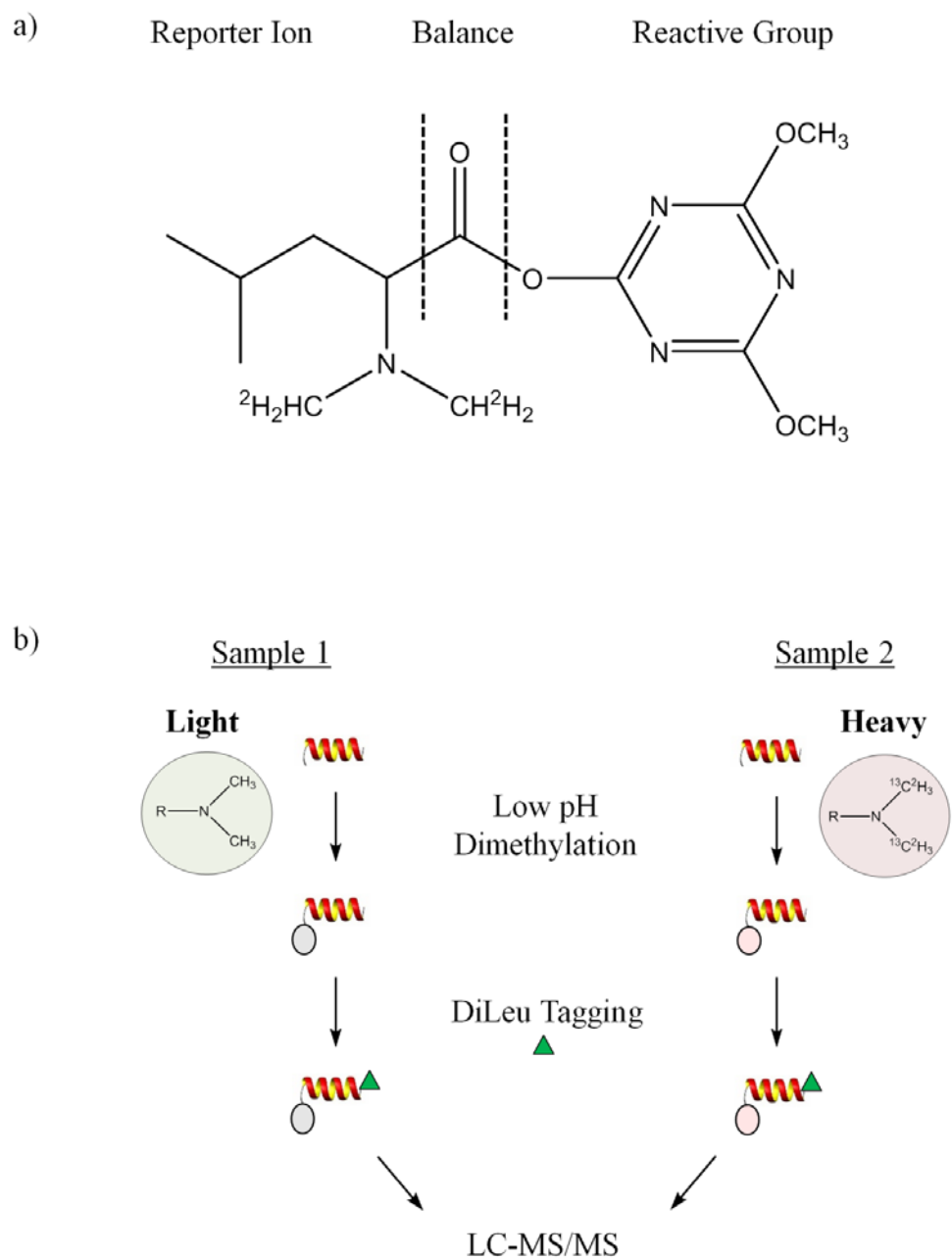
Figure 7.1. a) Chemical structure of the DiLeu118 isobaric tag. b) Incorporation of DiLeu tags into the cPILOT method.

a)

D(dimethyl)LGEEHFK(TMT^0)

617.844

613.823

614.324

618.346

614.826

618.847

| | | | | | | | | | | |
|612|613|614|615|616|617|618|619|620|621|622|

m/z

b)

HCD-MS/MS
m/z 613.82

HCD-MS/MS
m/z 617.84

126.13

TMT^0
Reporter
Ion

126.13

TMT^0
Reporter
Ion

| | | | | | | | |
|125|126|127|128|129|130|131|132|

m/z

| | | | | | | | |
|125|126|127|128|129|130|131|132|

m/z
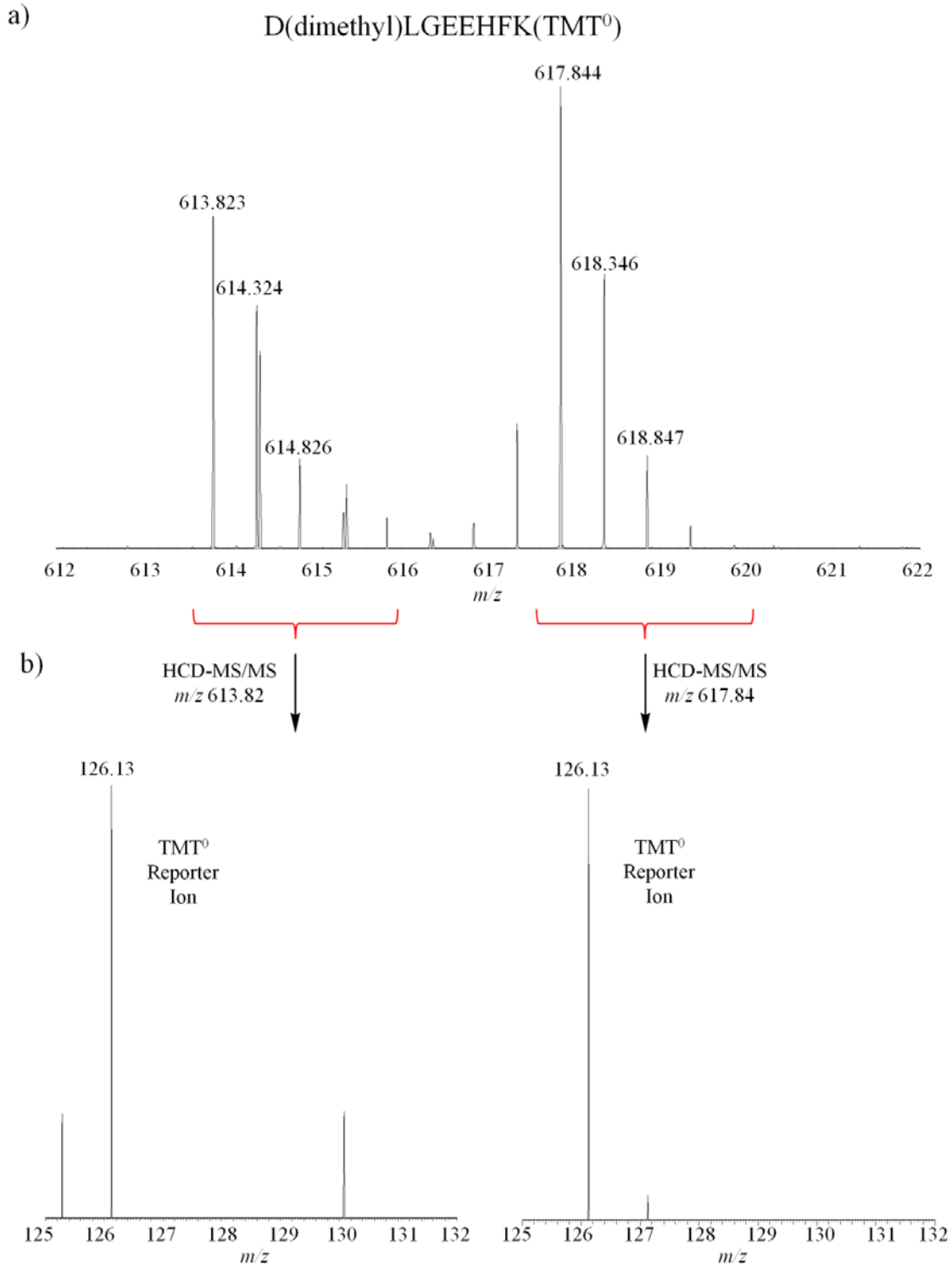
Figure 7.2. a) MS spectra for the peptide D(dimethyl)LGEEHFK(TMT^0) resulting in light (*m/z* = 613.823) and heavy peptide (*m/z* = 617.844) peaks. Isolation and fragmentation of b) light (left) and heavy (right) peptides results in the detection of the TMT^0 reporter ion at *m/z* = 126.13.

following the cPILOT procedure shown in Figure 7.1b. The MS spectra for the peptide D(dimethyl)LGEEHFK(DiLeu118) is shown in Figure 7.3a. Light and heavy dimethylated peptides are located at m/z 574.319 and 578.340, respectively, which corresponds to the mass shift of 8 Da per dimethyl modification [100]. DiLeu cPILOT peptides differ in m/z values compared to TMT^0 cPILOT peptides due to the mass differences between the isobaric tags, which are +145.132 Da and +224.152 Da for DiLeu118 and TMT^0, respectively. Figure 7.3b (left) shows the low m/z region of the HCD-MS/MS spectra resulting from fragmentation of the light peptide at m/z = 574.32, which results in the detection of the DiLeu118 reporter ion at m/z = 118.15. Isolation and fragmentation of the heavy peptide at m/z = 578.34 also results in the detection of the m/z 118.15 reporter ion peak. These spectra show that the DiLeu118 reporter ion is detected similarly for the same peptide sequences detected in TMT^0 cPILOT experiments.

We compared BSA proteome coverage and labeling efficiency between TMT-based cPILOT and DiLeu based cPILOT experiments. Overall, 62 unique peptides were detected in BSA samples tagged with DiLeu118, which corresponds to 81.6% protein sequence coverage Comparatively, TMT^0 cPILOT peptides produced an 88.3% protein sequence coverage resulting from the identification of 85 unique peptide sequences. Results show high protein sequence coverage from a large pool of peptides detected in both methods. To determine labeling efficiency in both methods, RAW files were searched with each isobaric tag as a dynamic modification, which allows mislabeled lysine residues to be reported in SEQUEST search results. Spectral count (SC) comparisons were performed between labeled and unlabeled lysine ending peptides only. Due to the cPILOT design, all Arg-ending peptides (from digestion with trypsin) will not be modified with an isobaric tag and are not considered in cPILOT data analysis. Labeling efficiency was 91% and 99% using DiLeu118 and TMT^0, respectively. DMTMM condensation reactions have been reported with 80-100% efficiency [362]. DiLeu activation and peptide labeling is highly sensitive to hydrolysis in aqueous solutions and can impact labeling efficiency compared to NHS reactions employed by TMT [83]. Drying agents such as $MgSO_4$ or adjusting the DMTMM/NMM ratio during DiLeu tag activation may improve labeling efficiency in future experiments.

126
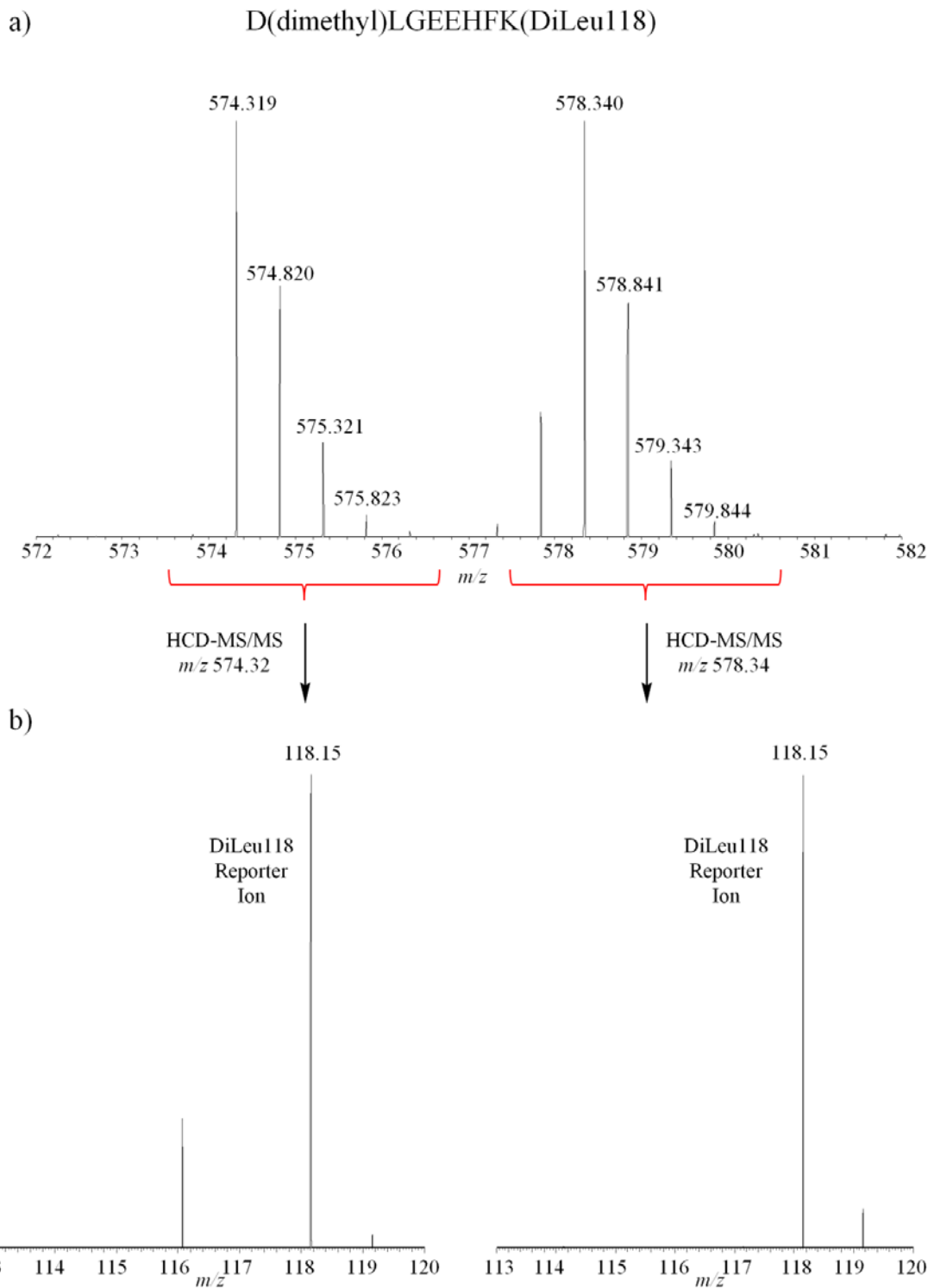
Figure 7.3. a) MS spectra for the peptide D(dimethyl)LGEEHFK(DiLeu118) resulting in light (*m/z* = 574.319) and heavy peptide (*m/z* = 578.340) peaks. Isolation and fragmentation of b) light (left) and heavy (right) peptides results in the detection of the DiLeu reporter ion at *m/z* = 118.15.

The experiments performed in **Chapter 7** employed data dependent acquisition selecting the top 10 most intense ions for HCD-MS/MS in order to collect more spectra containing the targeted reporter ion. HCD-MS/MS is more efficient at detecting reporter ion signal in MS/MS spectra compared to MS^3 spectra and was employed to verify successful DiLeu chemical labeling by the detection of the 118 reporter ion [294]. Peptides detected with both dimethyl and DiLeu tag modifications indicate a properly labeled peptide for cPILOT and should produce reporter ions at *m/z* 118.15 and 126.13 in the HCD-MS/MS spectra for DiLeu118 and TMT^0, respectively. Overall, 32 detected DiLeu cPILOT peptides overlapped with TMT^0 cPILOT peptides. These sample spectra and data demonstrate that DiLeu chemistry can be successfully incorporated into the cPILOT workflow after low pH dimethylation to modify lysine amines. Additionally 100% of cPILOT labeled peptides produced the reporter ion in HCD-MS/MS fragmentation spectra (S/N > 3) for both DiLeu118 and TMT^0. These results are consistent with previous reports of DiLeu tags, whereby a stable reporter ion is produced [83]. We note that in MS^3 quantitative multiplexed experiments, there is an expected increase in the number of spectra which contain missing reporter ions due to sensitivity limitations [100, 294]. Ongoing experiments include MS^3 data collection using DiLeu based cPILOT samples with multinotch data collection [330] and incorporation of DiLeu 12-plex reagents [361].

7.3.3. Cost Analysis

Substituting DiLeu tags in place of TMT tags for cPILOT provides a more cost-effective multiplexing approach. Table 7.1 compares the cost of TMT 6-plex tags, a 12-plex cPILOT or 20-plex cPILOT experiment, and a cPILOT experiment using the DiLeu 4-plex tags. Isobaric tags are approximately 100x the cost of precursor dimethylation reagents per experiment (Table 7.1) making these reagents the biggest contributor to experimental cost. Implementing less expensive isobaric tags in cPILOT is imperative to create a more cost-effective method. cPILOT experiments using commercially available isobaric tags were determined to be over $500 per experiment. Table 7.1 shows that DiLeu tags

128

Table 7.1. Multiplexing Cost

Multiplexed Experiment	TMT 6-plex	cPILOT 12-plex[a]	cPILOT 20-plex[a]	4-plex DiLeu	cPILOT 8-plex[b]
Isobaric Tag Cost per Kit	$2,563.00	$2,563.00	$2,800.00	$1,494.00	$1,494.00
Experiments per Kit[c]	5	5	3	100[d]	100[d]
Isobaric Tag Cost per Experiment	$512.60	$512.60	$933.33	$4.98	$14.94
Dimethylation Cost per Experiment	$0.00	$4.92	$7.52	$1.84	$3.68
Samples per experiment	6	12	20	4	20
Total Samples	30	60	60	400	800
Total Cost per Experiment	$512.60	$517.52	$940.85	$21.18	$18.62
Cost per Sample	$85.43	$43.13	$47.04	$5.30	$2.33

[a]TMT tags

[b]DiLeu tags

[c]Number of maximum multiplexing experiments

[d]Estimated based on average mass of synthesized DiLeu tags

129

offer multiplexing at roughly $15 per experiment which is significant savings compared to TMT reagents. This is attributed to the number of samples that can be labeled using DiLeu tags. Dimethyl leucine tags are synthesized in quantities that can label approximately 100 reactions per isobaric tag (estimated based on average product yields), compared to 30 total reactions using TMT tags (6-plex and 10-plex). cPILOT doubles the amount of samples analyzed per experiment resulting in a cost of $43.13 per 12-plex experiment. Substitution of the DiLeu 4-plex tags into cPILOT results in approximately a 25-fold reduction in cost per experiment. Cost can be reduced further using DiLeu 8-plex reagents [360] and 12-plex reagents [361]. It is also noteworthy that the cost of graduate student hours and synthesis tools were not factored into the calculation, however long term savings are expected due to the significantly higher sample throughput offered by DiLeu tags.

7.4. CONCLUSIONS

N,N-dimethyl leucine (DiLeu) isobaric tagging reagents can be synthesized in house and perform multiplexed experiments at a lower cost compared to TMT tags. DiLeu tags were implemented into the cPILOT workflow by substitution with TMT isobaric tags at high pH buffer conditions. DiLeu tags successfully bind to the lysine amines of light or heavy dimethylated peptides with labeling efficiencies > 90% as demonstrated using BSA. Fragmentation of DiLeu cPILOT peptide pairs results in the detection of the reporter ion at m/z 118.15 and is comparable to the TMT^0 reporter ion generated at m/z 126.13. Future work includes the optimization of tag activation, peptide labeling efficiency, multiplexing cPILOT with DiLeu tags, and implementation to study biological tissues. Overall, the incorporation of DiLeu tags into the cPILOT workflow enhances multiplexing, significantly reduces cost, and demonstrates the versatility and accessibility of this method.

8.0. CONCLUDING REMARKS AND FUTURE DIRECTIONS

8.1. SUMMARY

This dissertation presents novel multiplexing techniques in quantitative proteomics that increase sample throughput in a single experiment. **Chapter 2** presents a precursor quantitative technique called global internal standard technology (GIST), which adds light (-CH$_3$) or heavy (-C^{2}H$_3$) acetyl groups to peptide amines from two different samples. Relative quantitation is achieved by comparing the peak areas of light and heavy acetylated peptides. GIST was applied to study the spleen proteome of mice treated with Adriamycin, which revealed alterations to cell structural integrity and calcium binding proteins potentially leading to a weakened immune system in response to anti-cancer treatment. **Chapter 3** reviews the biological significance and proteomic techniques used to study 3-nitrotyrosine (3NT). Protein nitration is mediated by the presence of reactive oxygen species when cellular conditions are under oxidative stress. Neurodegenerative diseases, arthritis, and cardiovascular disease are associated with 3NT. Identification and quantitation of 3NT is analytically challenging due to the need for selective and sensitive approaches to isolate 3NT peptides. **Chapter 4** presents a novel approach termed "combined precursor isotopic labeling and isobaric tagging" (cPILOT), which selectively quantifies 3NT-modified peptides and enhances multiplexing in quantitative proteomics using TMT and iTRAQ tags. Acetylation (**Chapter 2**) blocks primary amines on 3NT peptides with light or heavy labels. Afterwards, 3NT is reduced to 3-aminotyrosine, which allows for selective addition of an isobaric tag directly on 3NT sites. Reporter ion detection in HCD-MS/MS confirms the location of 3NT modifications. In addition, relative quantitation of 12 and 16 nitrated samples is performed in a single experiment for TMT and iTRAQ tags, respectively. Due to the overlap of precursor acetylated peak pairs, it was determined that a mass shift of at least 5 Da is required to generate accurate and reproducible reporter ion quantitation in MS/MS using cPILOT.

Chapter 5 transforms cPILOT from a post-translation modification technique to a global approach (global cPILOT), which can be applied to protein samples of any origin. This is made possible by performing light ($-2CH_3$) or heavy ($-2^{13}C^2H_3$) dimethylation at low pH (~2.5) to selectively modify peptide N-termini. After sample cleanup and a buffer exchange, high pH conditions (~8.0) allow the modification of lysine residues with isobaric tags. Peptides exhibit a mass shift of 8 Da per precursor modification. Isolation and fragmentation of light and heavy dimethylated peaks results in the appearance of two sets of reporter ions for enhanced multiplexing and relative quantitation. Selective y_1-HCD-MS^3 targets TMT modified peptides for HCD fragmentation, which increases the number of MS^3 spectra containing reporter ions. Global cPILOT is accurate over a dynamic range of two orders of magnitude and is reproducible with < 25% CV.

Global cPILOT is applied to the liver proteome of APP/PS-1 mice to study the effects of metabolism in Alzheimer's disease (AD) liver in **Chapter 6**. Strong cation exchange and a multi-tiered data collection method resulted in 1734 proteins identified in AD liver. Six duplex precursor dimethylation experiments showed comparable results with 12-plex cPILOT analysis. Differentially-expressed proteins in AD liver were involved in fatty acid β-oxidation and pyruvate metabolic enzymes, which have significant overlap with the changes observed in AD brain. For example, increased fatty acid metabolism can result in the formation of ketone bodies in the liver, which can be a compensatory energy source in AD brain. While cPILOT successfully expands sample throughput in protein quantitation, the overall cost for routine cPILOT experiments is high (although less expensive compared to multiple isobaric tagging experiments). **Chapter 7** demonstrates the versatility of cPILOT by incorporating N,N-dimethyl leucine (DiLeu) isobaric tags into the method. The reporter ion corresponding to the DiLeu118 tags (m/z = 118.15) was detected in HCD-MS/MS spectra resulting from fragmentation of light and heavy dimethyated peptides. DiLeu tags have potential to provide a more cost-effective cPILOT workflow and multiplexing of 24 samples in a single experiment.

In summary, novel methods for increasing sample multiplexing in quantitative proteomics have been developed using stable isotopic labeling. The combination of precursor isotopic labeling with

isobaric tags enhances sample throughput. Currently, cPILOT can be adapted in any laboratory to simultaneously quantify 20 proteomic samples in a single experiment using TMT 10-plex reagents. cPILOT can be either selective to the PTM 3-nitrotyrosine or be used as a global approach to study disease conditions. cPILOT saves instrument time, reduces overall experimental cost, and is comparable to precursor techniques such as dimethylation in large scale experiments.

8.2. FUTURE DIRECTIONS

8.2.1. Improving cPILOT Sample Preparation Techniques

Currently cPILOT requires sample preparation using multiple reaction steps across twelve samples (using TMT 6-plex reagents) in approximately 3-4 days. While data normalization can account for errors associated with multiple pipetting steps and separate chemical reactions, emphasis should be placed on creating a lean workflow. Optimized sample preparation should focus on reduced clean-up steps and implementation of stable isotopes earlier in the procedure. One solution would be to perform all chemical reactions in a one pot system. Current cPILOT protocol employs dimethylation in a 1% acetic acid solution to obtain a reaction pH of 2.5. After dimethylation, the solution pH can be adjusted to 8.0 without sample clean up using base. This is only possible by ensuring a completely quenched dimethylation reaction prior to pH adjustment so the lysine amines are not modified with excess reagent. Additionally, the reagent that quenches the reaction should not be reactive with succinimide chemistry employed by most isobaric tags. This presents a chemical challenge as amines are the best quenching reagents for dimethylation, however secondary or tertiary amines may be possible since triethylammonium bicarbonate (TEAB) buffer currently used in TMT protocol does not interfere with the reaction. Another option is to perform peptide capture and chemical reactions on a resin. Thiol selective [363] and amine selective [364] peptide immobilization has been previously presented and may provide a starting point for resin-assisted cPILOT. Hydrophobic interaction-based capture methods may also be explored such as a high pore size C_{18} resin. This will provide the ability to perform multiple chemical reactions without the need for clean-up steps and provide optimal peptide recovery.

cPILOT requires manual preparation of twelve samples simultaneously, which introduces variation prior to instrumental analysis. Additionally as cPILOT continues to develop, it is possible that more samples will need to be prepared as multiplexing expands, which creates a need for high throughput sample preparation. This can be accomplished by using a 96 well plate with a liquid handling robotic arm as shown in Figure 8.1. Automation in sample preparation procedures reduces pipetting mixing errors and streamlines a continuous workflow for large scale studies. The use of a 96 well plate can also simultaneously perform multiple reactions (Figure 8.1). For example, the chemistries of multiple precursor labeling techniques (acetylation, dimethylation) and isobaric tags (TMT, iTRAQ, DiLeu) can be performed in one experiment. This could allow for cPILOT expansion, incorporation of more channels, and analysis of more samples prepared with minimal variation.

Reduced cPILOT variation can be achieved using alternative chemical labeling techniques. Metabolic labeling offers the lowest variation using stable isotopic chemical tags which incorporates heavy atoms at the earliest point in sample preparation. Metabolic labeling using SILAM (**Chapter 1**) adds stable isotopes in animal mouse models with sufficient labeling efficiency [365]. SILAM experiments are gradually increasing in popularity [365], which includes the newest generation of NeuCode tags [366]. While ideal, this technique is challenging to implement to new labs due to the high cost and need for multiple animal generations to obtain optimal labeling efficiency. Alternatively, protein chemical labeling techniques can provide reduced variation since the reactions occur before digestion. Samples can be labeled, digested, and chemically modified at the N-terminus with isobaric tags, which eliminates a post-digestion sample cleanup step. Protein labeling has been experimented in our laboratory and is shown in Figure 8.2. Here, dimethylation was performed on intact proteins to modify lysine residues. After digestion with chymotrypsin or Arg-C [367] proteases, the N-terminal is accessible for isobaric tagging. Figure 8.2a shows the sample peptide A(TMT[6])LK(Dimethyl)AWSVAR (Bovine serum albumin) showing light and heavy dimethylated peptides at m/z 629.897 and 633.919, respectively. Isolation and fragmentation spectra for both precursor peaks are shown in Figure 8.2b. Target reporter
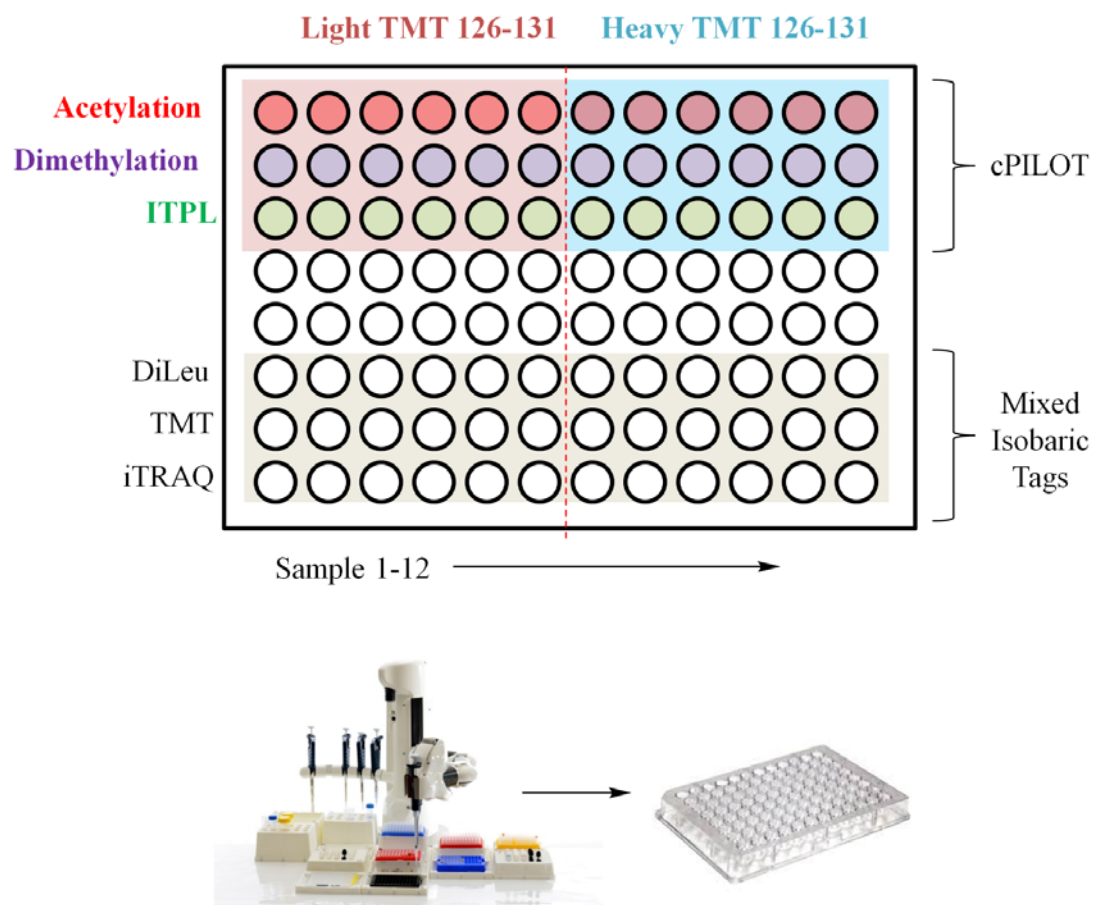
Figure 8.1. Sketch of cPILOT implementation on a 96-well plate with robotic arm attachment for high throughput sample preparation.
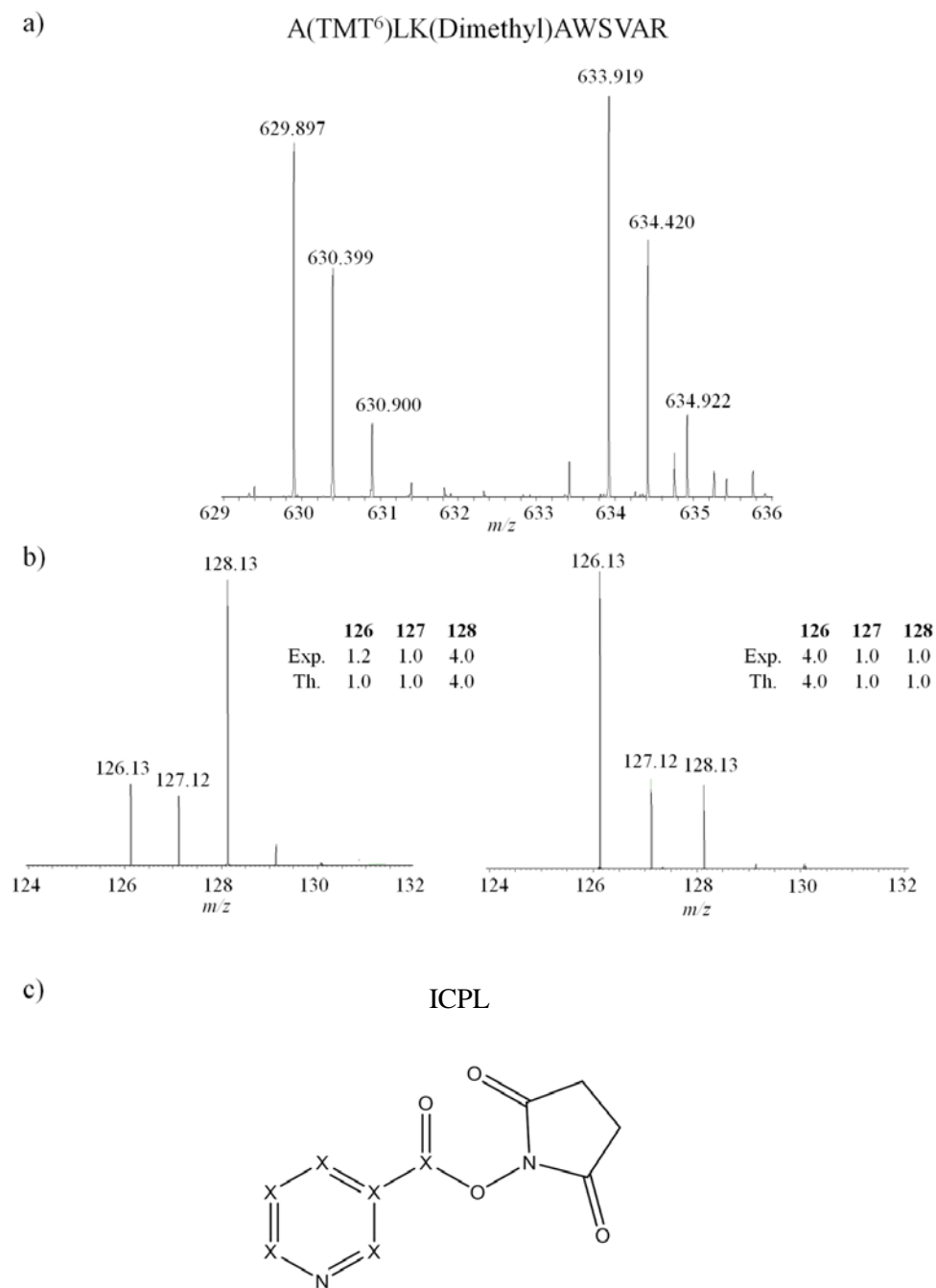
Figure 8.2. a) Precursor spectra for the protein labeled cPILOT peptide A(TMT⁶)LK(Dimethyl)AWSVAR showing light (*m/z* = 629.897) and heavy (*m/z* = 633.919) precursor peaks. b) HCD-spectra showing isolation and fragmentation light (left) and heavy (right) peptides. c) Alternative protein tagging using isotope coded protein labels. "X" indicates the atoms ^{12}C and ^{13}C for light and heavy ICPL tags, respectively.

ion ratios are 1:1:4 (TMT 126:127:128) and 4:1:1 (TMT 126:127:128) for light and heavy dimethylated proteins, respectively. As seen in Figure 8.2b, accurate reporter ion ratios were detected. These preliminary results are promising, however optimization is required since labeling efficiency was determined to be approximately 85%. Precursor labeling using isotope coded protein labels (ICPL, Figure 8.2c) provides labeling efficiency greater than 95% and modifies peptide lysine residues prior to digestion creating accurate and reproducible quantitation [368, 369]. Future protein labeling based cPILOT experiments should explore ICPL reagents.

8.2.2. Enhanced Multiplexing

cPILOT expansion can occur by creating additional precursor and isobaric channels to further enhance the multiplexing shown in Figure 8.3. Currently, cPILOT employs two precursor dimethylated channels, which can easily be expanded to add a third "middle" channel resulting in a +4 Da mass shift (Figure 8.3a). Challenges with this approach are ensuring precursor peaks do not overlap so that clean MS/MS spectra are obtained. To accomplish this, the isolation window during data collection should be narrowed to 1.5-2.0 Th. It is also likely that peptides with charge states of three or higher may not be used for analysis due to closely spaced precursors. A different approach to enhanced multiplexing combines TMT and iTRAQ tags in a single experiment [106]. Peptides modified with different isobaric tags will not co-elute, which prevents quantitation across different isobaric tags, however enhanced multiplexing and sample throughput is still achieved. TMT tags produce reporter ions at m/z 126-131, while iTRAQ tags produce reporter ions at m/z 113-121 (exclude m/z 120). Methods which employ both sets of tags will perform quantitation of 14 samples in a single MS/MS spectrum (m/z range 113-131) as illustrated in Figure 8.3b. Multiple precursor labeling techniques could also be applied to one cPILOT sample, such as acetylation and dimethylation seen in Figure 8.1. These approaches rely on the ability to perform selective N-terminal modification using succinimide based chemical tags, which should work since the reaction mechanism begins with nucleophilic attack of the primary amine rather than the
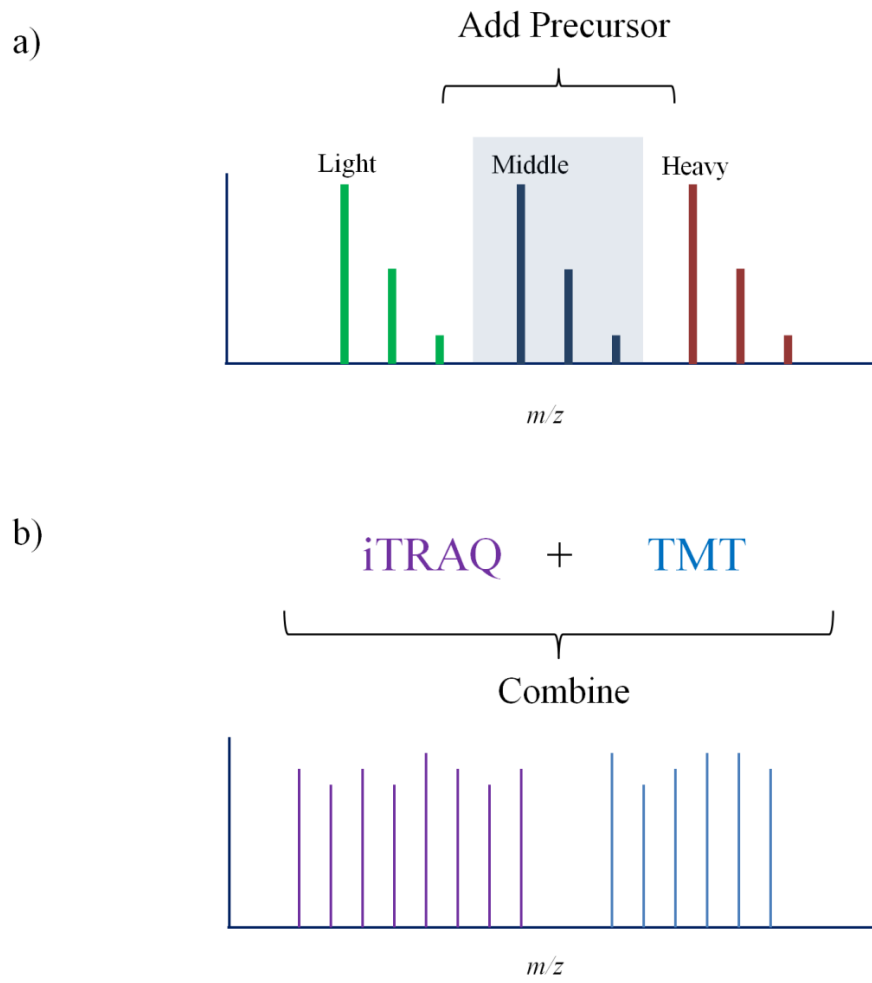
Figure 8.3. Increases in sample throughput using cPILOT can be done by a) the addition of more precursor channels or b) combining iTRAQ and TMT isobaric tags in a single experiment.

chemical nature of the electrophile. However, increasing multiplexing in quantitative proteomics creates a paradox. Large scale proteomic experiments typically perform protein identification simultaneously with relative quantitation. To identify as many unique proteins as possible in a single experiment, data collection methods employ as many fragmentation scan events as possible, which requires efficient separations, fast scanning mass spectrometers, careful exclusion parameters, and a high scan count per instrument cycle. Quantitation requires the collection of multiple points across a single peptide extracted ion chromatogram. As a result, there is a tradeoff between qualitative and quantitative based experiments. Increasing multiplexing channels in quantitative proteomics using cPILOT also has a similar tradeoff. As more precursor channels are added, unique peptide identifications will decrease because MS/MS scan events are performed on the same peptide sequence to obtain complete quantitative information. cPILOT can be developed to further enhance multiplexing beyond the current maximum of 20 samples, however a sample limit will eventually be reached due to the impact in unique protein identification rates. Figure 8.4a shows the scan cycle for a typical cPILOT experiment performed in **Chapters 5 and 6**. After precursor MS scans in the Orbitrap, the top seven most intense ions are selected for CID-MS/MS and HCD-MS^3 for each instrument cycle. The LTQ Orbitrap Velos instrument performs approximately 48,000 total scans, which includes 22,400 CID-MS/MS scans during cPILOT experiments (Table 8.1). As more precursor peaks are added to increase cPILOT multiplexing, MS/MS and MS^3 scan events must be performed on the same peptide sequence in order to obtain complete reporter ion coverage under all peaks. As seen in Table 8.1, the number of predicted MS/MS scan events on unique precursor ions decreases proportionally by the number of precursor channels added, which will impact identification. This can be circumvented by implementing multi-dimensional separations or longer LC gradients (i.e. 7+ hours) because more MS/MS spectra will be acquired. Additionally, this calculation is assuming uniform selection of all precursor channels (i.e. light, middle, heavy, etc) across the entire experiment, which does not happen under data dependent acquisition (DDA) conditions since precursor 1:1 ratios have approximately 20% CV. This leads to the most important future direction in cPILOT method development, which is changing data collection strategies discussed below.

a)

| Orbitrap | MS | MS^3 | MS^3 | MS^3 | MS^3 | MS^3 | MS^3 | MS^3 |
| Ion Trap | MS/MS | MS/MS | MS/MS | MS/MS | MS/MS | MS/MS | MS/MS | |

~3 sec

b)

m/z
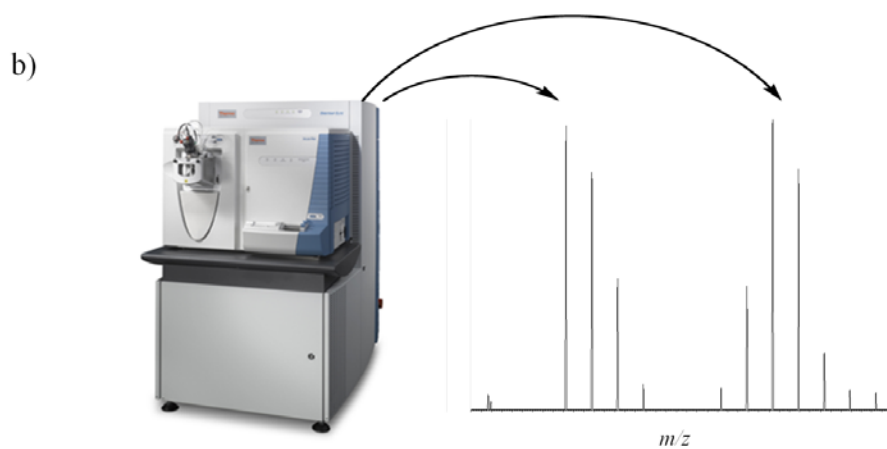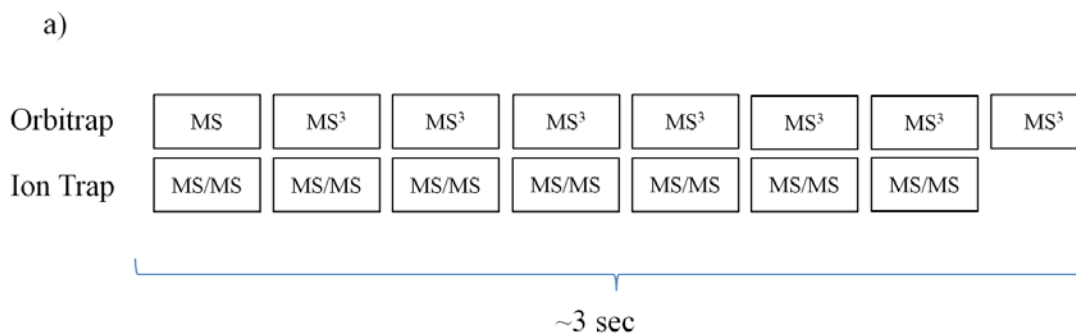
Figure 8.4. a) Scan event process and timing for cPILOT experiments presented in **Chapters 5 and 6.** b) cPILOT data collection would be improved by performing DDA acquisition according to the most intense precursor pairs as opposed to most intense ions.

Table 8.1. Predicted Number of MS/MS Scans with Increasing Precursor peaks for cPILOT Expansion.

	TMT only	Current cPILOT	Triplex cPILOT	Four Precursors
Number of precursor peaks per peptide[a]	1	2	3	4
Number of samples (TMT 6-plex reagent)	6	12	18	24
Total MS/MS scans available[b]	22400	22400	22400	22400
MS/MS scans required to cover all precursor[c]	1	2	3	4
MS/MS scans of unique peptides	22400	11200	7467	5600

[a]Number of precursors for added multiplex in cPILOT.

[b]Estimated based on 3 hour LC gradient and top 7 CID-MS/MS and HCD-MS^3.

[c]Added Precursor channels requires a separate fragmentation scan for each peak.

8.2.3. cPILOT Data Collection and Processing

DDA determines which fragmentation events to perform in real time based on the previous MS scan. The Orbitrap scans with high resolution and high mass accuracy, which can be exploited to search for dimethylated peak pairs in real time. After MS scans, isolation and fragmentation should occur on peaks which are separated by the mass corresponding to dimethylated peptides (Figure 8.4b). This would create a targeted data collection method specific to cPILOT peptide pairs and eliminate the random nature of DDA. Selection for MS/MS by peak pairing would also result in additional 12-plex peptide pairs in current cPILOT experiments since MS/MS events for each peptide pair would be back-to-back scans in the instrument cycle.

cPILOT presented in **Chapters 5 and 6** utilized MS^3 to obtain accurate reporter ion quantitation. While this is powerful in quantitative proteomics, the tradeoff is the need to perform slow HCD-MS^3 scan events (300-400 ms) using the Orbitrap Velos, which reduces the number of proteins identified. Additionally, reporter ion sensitivity decreases in MS^3 scan events compared to MS/MS, which increases the likelihood of missing reporter ions. The most recent hybrid mass spectrometer, the Orbitrap Fusion (Thermo Scientific, 2013), can circumvent these limitations by performing ~20 fragmentation scans/second and synchronous MS^3 to enhance sensitivity [52, 330]. The Orbitrap Fusion is an ideal instrument for MS^3 experiments, and increases reporter ion signal in MS^3 scan events by 10-fold [330]. Additionally, the enhanced Fourier Transform algorithm recently reported doubles the resolving power of the Orbitrap under the similar transient lengths currently used [52, 370]. Performing faster high resolution scan events, synchronous MS^3 scans, and collection of more total MS/MS spectra provide the ability to enhance protein identification in cPILOT experiments.

Ion mobility in quantitative proteomics would also add an additional dimension of separation for enhanced protein identification, while simultaneously cleaning precursor windows for accurate quantitation. Global cPILOT currently employs multiple SCX fractions and a two tiered experiment in cPILOT. Ion mobility has the advantage of both enhancing proteome coverage and reducing co-fragmentation of neighboring peptides, which eliminates the need to perform MS^3 scan events [91, 92].

Ion mobility appears to be growing in popularity in proteomic experiments [35, 36] and would provide an additional separation technique.

Finally, new data processing strategies are required for any enhanced multiplexing. Currently, commercially available software, such as Proteome Discoverer, cannot process cPILOT data or other multiplexed strategies properly. For example, Proteome Discoverer combines reporter ion signals collected by fragmentation of light and heavy peptide ions, which much remain separate to perform accurate quantitation across all channels. New software technology and processing tools should be developed to streamline data analysis of cPILOT experiments. Variables to control in cPILOT data processing include normalization, determination of fold-change cutoffs, statistical analysis and protein filtering criteria.

8.2.4. Alzheimer's Disease and the Liver

Chapter 6 revealed alteration in enzymes involved in fatty acid and pyruvate metabolic proteins in APP/PS-1 mouse liver. To summarize, elevated fatty acid oxidation can lead to the production of ketone bodies, which travel to other organs as an alternative energy source when glucose metabolism is low. Reduced glucose metabolism and mitochondrial dysfunction is observed in Alzheimer's disease (AD) brain [306]. When glucose levels are low, the brain relies on ketone body and glucose production through gluconeogenesis as fuel sources, which are processes that occur in the liver [371]. Proteomic data from **Chapter 6** reveals elevations in the alanine cycle, which suggests elevated pyruvate, the precursor required for gluconeogenesis [101]. The alanine cycle also results in ammonia as a downstream byproduct, which must be detoxified [342, 372]. Ammonia is elevated in both the blood and brain of AD patients, which suggest a correlation between ammonia concentrations and cognitive impairment [346]. In order to metabolize and detoxify ammonia from cells, it must be converted to urea and eliminated by the kidneys. Therefore, a proteomic study on the kidneys of APP/PS-1 mice may reveal alterations in nitrogen metabolism and the urea cycle. Additionally, alanine aminotransferase (ALT) was elevated in APP/PS-1 mouse liver and is clinically measured in serum to determine liver failure. Acute liver failure

results in altered cognitive function and often results in acute kidney injury [373]. Due to the reported elevated levels of ammonia coupled with an altered pyruvate/alanine cycle, the kidney is the next logical peripheral organ to study in APP/PS-1 mice due to its involvement in the urea cycle and ammonia detoxification. Combining studies of multiple peripheral organs provides the ability to fully trace metabolism changes throughout AD and would present an in-depth understanding of AD metabolism.

Ketone bodies are an alternative energy source to the brain in states of glucose shortage. These small molecules are formed when fatty acid metabolism (β-oxidation) is elevated [374]. Experiments should be performed to evaluate key metabolites in β-oxidation. During fatty acid metabolism, long chain fatty acids are esterfied with coenzyme A (CoA), then modified with L-carnitine to form acylcarnitines, which shuttle into the mitochondria matrix for metabolism [375]. Measurements of acylcarnitine concentrations using mass spectrometry can verify altered fatty acid metabolism in AD liver (**Chapter 6**). Derivatization using butanol and HCl adds a butyl group to the carboxylic acid group of acylcarnitines for MS analysis (Figure 8.5a). It is noteworthy to point out that Figure 8.5 depicts L-carnitine, however the derivatization is similar for acylcarntines [376, 377]. Butyl derivatization creates hydrophobic metabolites that allows for optimal reversed phase separation conditions [376]. Additionally, stable isotopic labeling is performed for differential analysis between WT and AD samples by using $^2H_{10}$-butanol. Preliminary targeted experiments are shown in Figure 8.5b. Butyl carnitine exhibits a mass of 218.1726 (singly charged, experiments at R = 100,000), which is detected in MS (Figure 8.5a). Isolation and fragmentation of this ion results in a signature buytl-acylcarnitine ion at *m/z* 159.04 in MS/MS (Figure 8.5b). By selectively scanning for this MS/MS fragment, targeted quantitation of fatty acid metabolites can be achieved within a complex mixture. Heavy $^2H_9$-acylcarnitine would present a total mass of approximately 227.2 Da with a signature fragment nine Da higher in mass at *m/z* 168.2. While the data shown is collected using the ion trap, the Orbitrap is capable of performing parallel reaction monitoring (PRM) at high resolution if multiple peaks co-elute during targeted MS/MS analysis [378]. Additionally, the benchtop Q-Exactive would be the optimal instrument of choice due to the quadrupole filtering prior to Orbitrap analysis for multiplexed selected ion monitoring and PRM data collection [50].
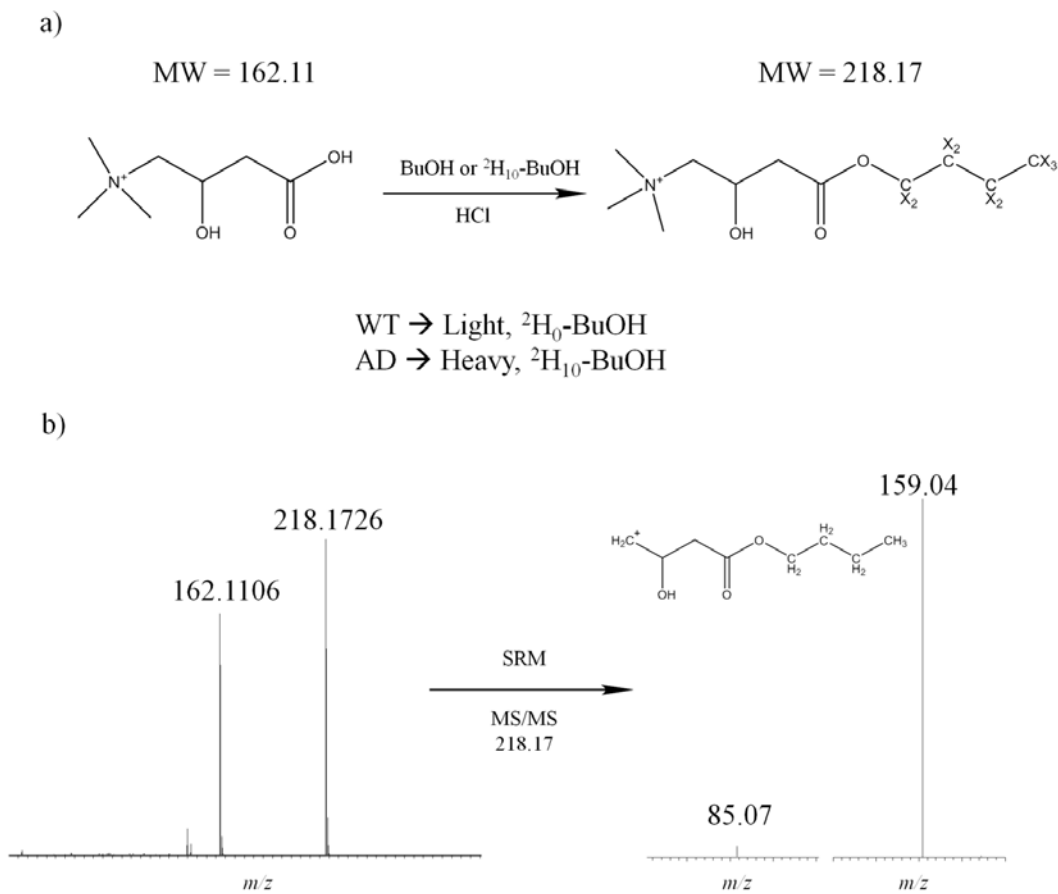
Figure 8.5. a) Chemical derivatization of l-carnitine using light or heavy isotopic butanol in HCl. Targeted MS/MS data collection is shown in b) by scanning for the signature butyl carnitine peak at *m/z* 159.04. The peak at *m/z* 85.07 is present in both derivatized and underivatized carnitines and can be used to verify the presence of the analyte.

Future work should focus on development and optimization of the assay in order to quantify acylcarnitines in liver and serum from APP/PS-1 mice.

APPENDIX A Table 2.3. Peptides Detected in Spleen Proteome of ADR-Treated Mice.

APPENDIX A Table 2.4. Peptides Used for Quantitation in Spleen Proteome of ADR-Treated Mice.

APPENDIX B

APPENDIX B Table 5.2. Protein Identification in Mouse Brain Tissue .

APPENDIX B Table 5.3. Peptide Identification in Mouse Brain Tissue.

Appendix C Table 6.1. Peptide Identification Using Multi-Tier Data Dependent Acquisition.

Identification Category	DDA Top 1 to 7	DDA Top 8 to 14	Combined
Total PSMs	211453	113064	324517
6-plex PSMs[a]	144357	72895	217252
Unique Peptides	3258	4289	5084
Quantified Peptides[b]	2090	2606	3068
12-plex Peptide Pairs[d]	1206	1246	1821

[a] Identified Peptide Spectra with 6 TMT channels

[b] Peptides used for protein quantification

[d] Peptides identified with both precursor dimethyl labels
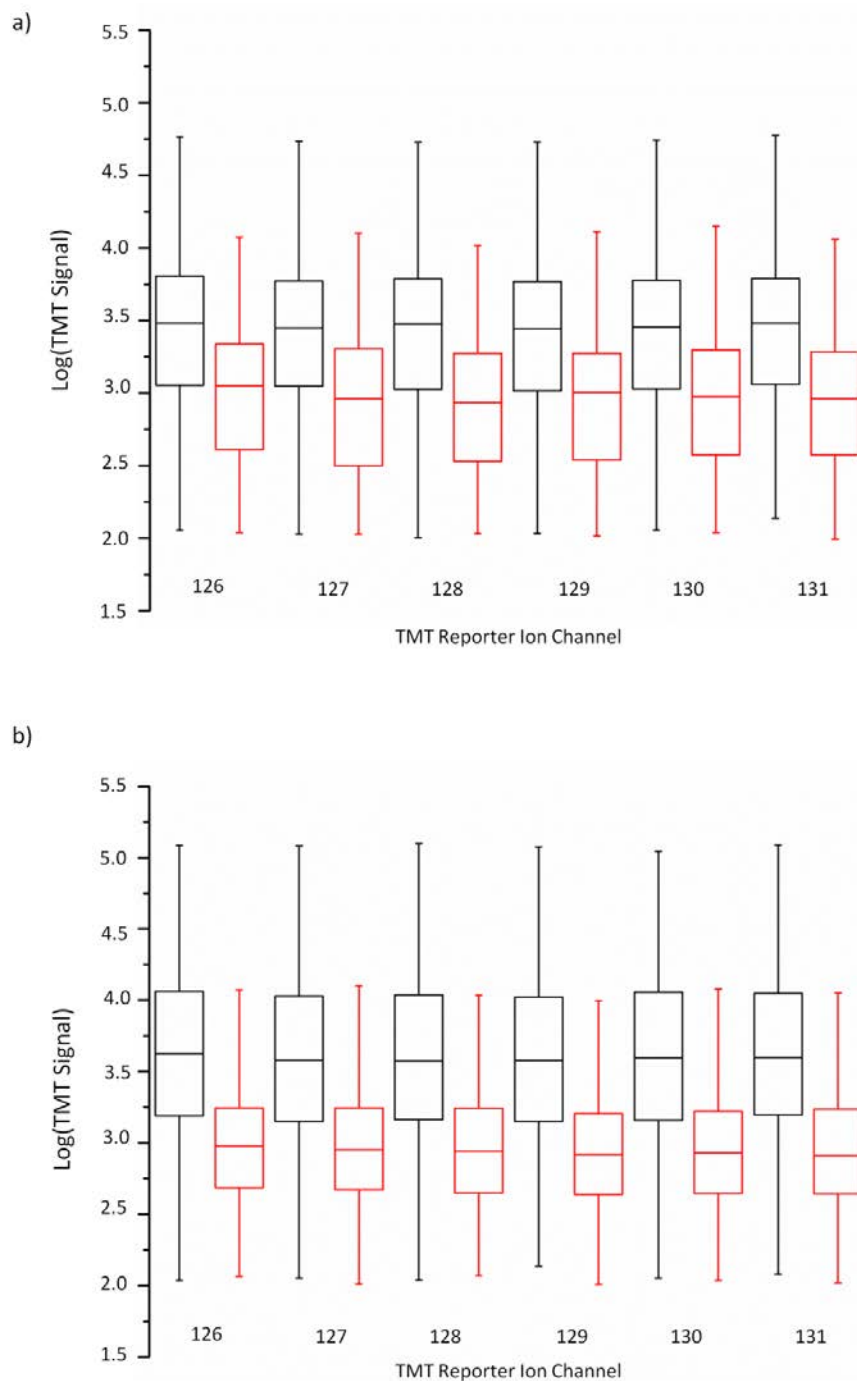
Appendix C Figure 6.9. Box plot of reporter ion signal (log scale) for top-ion-HCD-MS^3 (black) and selective-y_1-HCD-MS^3 (red) using an equim olar 12-plex liver digest. Reporter ion signals for each TMT channel correspond to a) light and b) heavy dimethylated peptides. The number of peptides, N, shown in a) are as f ollows [top-ion-HCD-MS^3 (selective-y_1-HCD-MS^3)]: 1637 (510), 1622 (522), 1667 (600), 1597 (524), 1618 (533), 1522 (519), for reporter ions at *m/z* = 126, 127, 128, 12 9, 130, and 131, respectively. The number of peptides, N, shown in b) are as follows [top-ion-HCD-MS^3 (selective-y_1-HCD-MS^3)]: 1612 (776), 1604 (775), 1637 (827), 1586 (763), 1586 (793), 1574 (763), for reporter ions at *m/z* = 126, 127, 128, 129, 130, and 131, respectively. Only LC-MS/MS was applied to this set of samples.

151

a) **Unique Peptides**

cPILOT 3390 | 1694 | 3251 DML

b) **Unique Proteins**

cPILOT 1022 | 712 | 703 DML

c) **Quantified Proteins**

cPILOT 556 | 554 | 261 DML
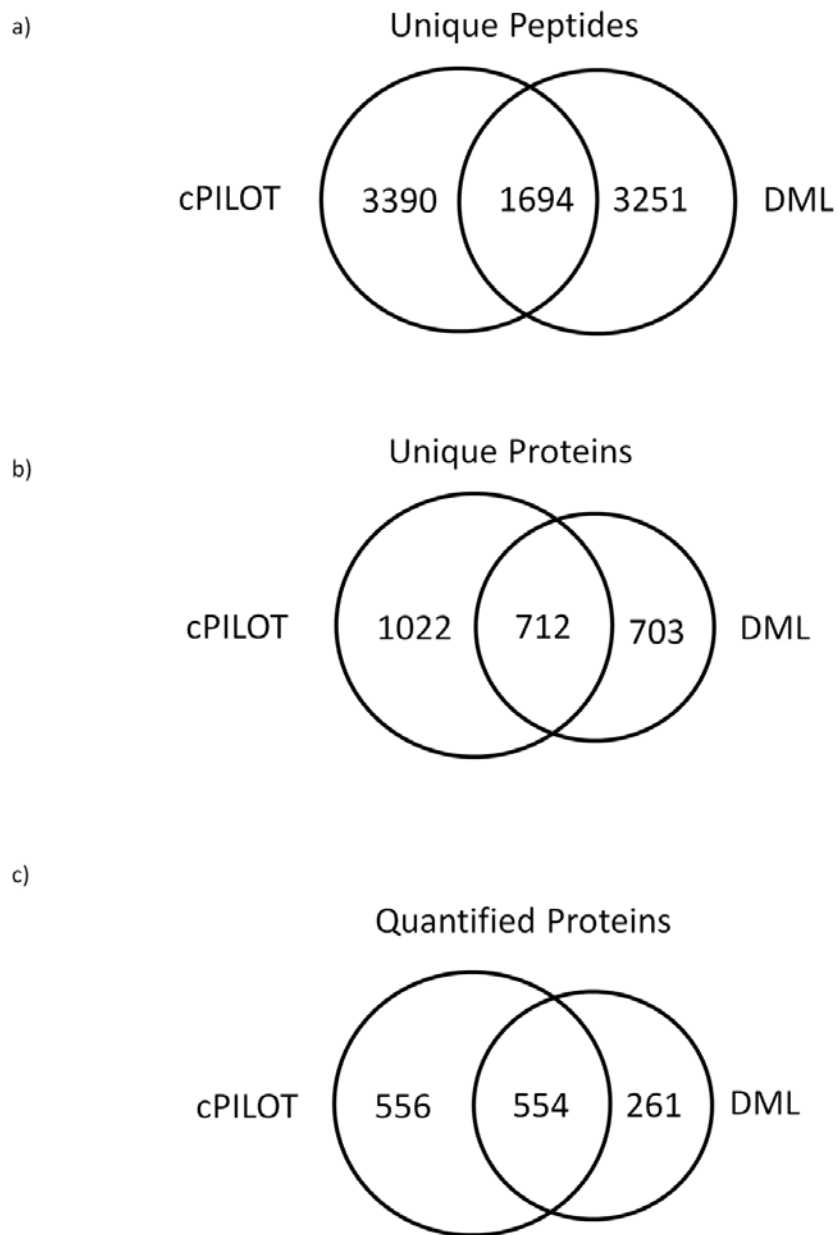
Appendix C Figure 6.10. Venn Diagrams illustrating overl ap between cPILOT and precursor dimethylation experiments regarding the number of uniquely identified a) peptides and b) proteins and c) the number of quantified proteins.

REFERENCES

[1] Aebersold, R., Mann, M., Mass spectrometry-based proteomics. *Nature* 2003, *422*, 198-207.

[2] Yates, J. R., 3rd, The revolution and evolution of shotgun proteomics for large-scale proteome analysis. *J Am Chem Soc* 2013, *135*, 1629-1640.

[3] Hernandez-Fernaud, J. R., Reid, S. E., Neilson, L. J., Zanivan, S., Quantitative mass spectrometry-based proteomics in angiogenesis. *Proteomics Clin Appl* 2013, *7*, 464-476.

[4] Cox, J., Mann, M., Quantitative, high-resolution proteomics for data-driven systems biology. *Annu Rev Biochem* 2011, *80*, 273-299.

[5] Lehmann, S., Hoofnagle, A., Hochstrasser, D., Brede, C.*, et al.*, Quantitative Clinical Chemistry Proteomics (qCCP) using mass spectrometry: general characteristics and application. *Clin Chem Lab Med* 2013, *51*, 919-935.

[6] Rabilloud, T., Chevallet, M., Luche, S., Lelong, C., Two-dimensional gel electrophoresis in proteomics: Past, present and future. *J Proteomics* 2010, *73*, 2064-2077.

[7] Van den Bergh, G., Arckens, L., Fluorescent two-dimensional difference gel electrophoresis unveils the potential of gel-based proteomics. *Curr Opin Biotechnol* 2004, *15*, 38-43.

[8] Tao, Q., Wang, Z., Zhao, H., Baeyens, W. R.*, et al.*, Direct chemiluminescent imaging detection of human serum proteins in two-dimensional polyacrylamide gel electrophoresis. *Proteomics* 2007, *7*, 3481-3490.

[9] Patton, W. F., Detection technologies in proteome analysis. *J Chromatogr B Analyt Technol Biomed Life Sci* 2002, *771*, 3-31.

[10] Han, X., Aslanian, A., Yates, J. R., 3rd, Mass spectrometry for proteomics. *Curr Opin Chem Biol* 2008, *12*, 483-490.

[11] Lopez, J. L., Two-dimensional electrophoresis in proteome expression analysis. *J Chromatogr B Analyt Technol Biomed Life Sci* 2007, *849*, 190-202.

[12] Zhang, Y., Fonslow, B. R., Shan, B., Baek, M. C., Yates, J. R., 3rd, Protein analysis by shotgun/bottom-up proteomics. *Chem Rev* 2013, *113*, 2343-2394.

[13] Preisler, J., Hu, P., Rejtar, T., Karger, B. L., Capillary electrophoresis--matrix-assisted laser desorption/ionization time-of-flight mass spectrometry using a vacuum deposition interface. *Anal Chem* 2000, *72*, 4785-4795.

[14] Faserl, K., Sarg, B., Kremser, L., Lindner, H., Optimization and evaluation of a sheathless capillary electrophoresis-electrospray ionization mass spectrometry platform for peptide analysis: comparison to liquid chromatography-electrospray ionization mass spectrometry. *Anal Chem* 2011, *83*, 7297-7305.

[15] Hebert, A. S., Richards, A. L., Bailey, D. J., Ulbrich, A.*, et al.*, The one hour yeast proteome. *Mol Cell Proteomics* 2014, *13*, 339-347.

[16] Schrimpf, S. P., Weiss, M., Reiter, L., Ahrens, C. H.*, et al.*, Comparative functional analysis of the Caenorhabditis elegans and Drosophila melanogaster proteomes. *PLoS Biol* 2009, *7*, e48.

[17] Witze, E. S., Old, W. M., Resing, K. A., Ahn, N. G., Mapping protein post-translational modifications with mass spectrometry. *Nat Methods* 2007, *4*, 798-806.

[18] Junger, M. A., Aebersold, R., Mass spectrometry-driven phosphoproteomics: patterning the systems biology mosaic. *Wiley Interdiscip Rev Dev Biol* 2014, *3*, 83-112.

[19] Paulsen, C. E., Carroll, K. S., Cysteine-mediated redox signaling: chemistry, biology, and tools for discovery. *Chem Rev* 2013, *113*, 4633-4679.

[20] Gould, N., Doulias, P. T., Tenopoulou, M., Raju, K., Ischiropoulos, H., Regulation of protein function and signaling by reversible cysteine S-nitrosylation. *J Biol Chem* 2013, *288*, 26473-26479.

[21] Choudhary, C., Weinert, B. T., Nishida, Y., Verdin, E., Mann, M., The growing landscape of lysine acetylation links metabolism and cell signalling. *Nat Rev Mol Cell Biol* 2014, *15*, 536-550.

[22] Ma, J., Hart, G. W., O-GlcNAc profiling: from proteins to proteomes. *Clin Proteomics* 2014, *11*, 8.

[23] Finley, D., Ciechanover, A., Varshavsky, A., Ubiquitin as a central cellular regulator. *Cell* 2004, *116*, S29-32, 22 p following S32.

[24] Maes, E., Tirez, K., Baggerman, G., Valkenborg, D.*, et al.*, The use of elemental mass spectrometry in phosphoproteomic applications. *Mass Spectrom Rev* 2014.

[25] Gault, J., Malosse, C., Machata, S., Millien, C.*, et al.*, Complete posttranslational modification mapping of pathogenic Neisseria meningitidis pilins requires top-down mass spectrometry. *Proteomics* 2014, *14*, 1141-1151.

[26] Butterfield, D. A., Dalle-Donne, I., Redox proteomics. *Antioxid Redox Signal* 2012, *17*, 1487-1489.

[27] Butterfield, D. A., Dalle-Donne, I., Redox proteomics: from protein modifications to cellular dysfunction and disease. *Mass Spectrom Rev* 2014, *33*, 1-6.

[28] Butterfield, D. A., Gu, L., Di Domenico, F., Robinson, R. A., Mass spectrometry and redox proteomics: applications in disease. *Mass Spectrom Rev* 2014, *33*, 277-301.

[29] Sultana, R., Perluigi, M., Newman, S. F., Pierce, W. M.*, et al.*, Redox proteomic analysis of carbonylated brain proteins in mild cognitive impairment and early Alzheimer's disease. *Antioxid Redox Signal* 2010, *12*, 327-336.

[30] Baraibar, M. A., Ladouce, R., Friguet, B., Proteomic quantification and identification of carbonylated proteins upon oxidative stress and during cellular aging. *J Proteomics* 2013, *92*, 63-70.

[31] Yeo, W. S., Kim, Y. J., Kabir, M. H., Kang, J. W., Kim, K. P., Mass spectrometric analysis of protein tyrosine nitration in aging and neurodegenerative diseases. *Mass Spectrom Rev* 2014.

[32] Feeney, M. B., Schoneich, C., Proteomic approaches to analyze protein tyrosine nitration. *Antioxid Redox Signal* 2013, *19*, 1247-1256.

[33] Butterfield, D. A., Perluigi, M., Reed, T., Muharib, T.*, et al.*, Redox proteomics in selected neurodegenerative disorders: from its infancy to future applications. *Antioxid Redox Signal* 2012, *17*, 1610-1655.

[34] Zhou, H., Ning, Z., Starr, A. E., Abu-Farha, M., Figeys, D., Advancements in top-down proteomics. *Anal Chem* 2012, *84*, 720-734.

[35] Helm, D. V., J.; Hughes, C. J.; Hahne, H.; Ruprecht, B.; Pachl, F.; Grzyb, A.; Richardson, K.; Wildgoose, J.; Maier, S. K.; Marx, H.; Wilhelm, M.; Becher, I.; Lemeer, S.; Bantscheff, M.; Langridge, J.

I.; Kuster, B., Ion Mobility Tandem Mass Spectrometry Enhances Performance of Bottom-up Proteomics. *mol Cell Proteomics* 2014, Article in Press.

[36] Brown, L. M., in: Woods, A. G. D., C. C. (Ed.), *Advancements of Mass Spectrometry in Biomedical Research*, Springer International Puiblishing, Springer International Publishing Switzerland 2014, pp. 79-91.

[37] Simpson, D. C., Smith, R. D., Combining capillary electrophoresis with mass spectrometry for applications in proteomics. *Electrophoresis* 2005, *26*, 1291-1305.

[38] Righetti, P. G., Sebastiano, R., Citterio, A., Capillary electrophoresis and isoelectric focusing in peptide and protein analysis. *Proteomics* 2013, *13*, 325-340.

[39] Eng, J. K., McCormack, A. L., Yates, J. R., An approach to correlate tandem mass spectral data of peptides with amino acid sequences in a protein database. *J Am Soc Mass Spectrom* 1994, *5*, 976-989.

[40] Fenn, J. B., Mann, M., Meng, C. K., Wong, S. F., Whitehouse, C. M., Electrospray ionization for mass spectrometry of large biomolecules. *Science* 1989, *246*, 64-71.

[41] Karas, M., Hillenkamp, F., Laser desorption ionization of proteins with molecular masses exceeding 10,000 daltons. *Anal Chem* 1988, *60*, 2299-2301.

[42] Takats, Z., Wiseman, J. M., Ifa, D. R., Cooks, R. G., Desorption Electrospray Ionization (DESI) Analysis of Tryptic Digests/Peptides. *CSH Protoc* 2008, *2008*, pdb prot4993.

[43] Trimpin, S., Inutan, E. D., Herath, T. N., McEwen, C. N., Laserspray ionization, a new atmospheric pressure MALDI method for producing highly charged gas-phase ions of peptides and proteins directly from solid solutions. *Mol Cell Proteomics* 2010, *9*, 362-367.

[44] Pagnotti, V. S., Chubatyi, N. D., McEwen, C. N., Solvent assisted inlet ionization: an ultrasensitive new liquid introduction ionization method for mass spectrometry. *Anal Chem* 2011, *83*, 3981-3985.

[45] Xian, F., Hendrickson, C. L., Marshall, A. G., High resolution mass spectrometry. *Anal Chem* 2012, *84*, 708-719.

[46] Perry, R. H., Cooks, R. G., Noll, R. J., Orbitrap mass spectrometry: instrumentation, ion motion and applications. *Mass Spectrom Rev* 2008, *27*, 661-699.

[47] Page, J. S., Masselon, C. D., Smith, R. D., FTICR mass spectrometry for qualitative and quantitative bioanalyses. *Curr Opin Biotechnol* 2004, *15*, 3-11.

[48] Olsen, J. V., Schwartz, J. C., Griep-Raming, J., Nielsen, M. L.*, et al.*, A dual pressure linear ion trap Orbitrap instrument with very high sequencing speed. *Mol Cell Proteomics* 2009, *8*, 2759-2769.

[49] Michalski, A., Damoc, E., Lange, O., Denisov, E.*, et al.*, Ultra high resolution linear ion trap Orbitrap mass spectrometer (Orbitrap Elite) facilitates top down LC MS/MS and versatile peptide fragmentation modes. *Mol Cell Proteomics* 2012, *11*, O111 013698.

[50] Michalski, A., Damoc, E., Hauschild, J. P., Lange, O.*, et al.*, Mass spectrometry-based proteomics using Q Exactive, a high-performance benchtop quadrupole Orbitrap mass spectrometer. *Mol Cell Proteomics* 2011, *10*, M111 011015.

[51] Denisov, E. D., E.; Lange, O.; Makarov, A., Orbitrap Mass Spectrometry with Resolving Powers above 1,000,000. *International Journal of Mass Spectrometry* 2012, *325-327*, 80-85.

[52] Senko, M. W., Remes, P. M., Canterbury, J. D., Mathur, R.*, et al.*, Novel parallelized quadrupole/linear ion trap/Orbitrap tribrid mass spectrometer improving proteome coverage and peptide identification rates. *Anal Chem* 2013, *85*, 11710-11714.

[53] Michalski, A., Cox, J., Mann, M., More than 100,000 detectable peptide species elute in single shotgun proteomics runs but the majority is inaccessible to data-dependent LC-MS/MS. *J Proteome Res* 2011, *10*, 1785-1793.

[54] Shen, Y., Tolic, N., Xie, F., Zhao, R.*, et al.*, Effectiveness of CID, HCD, and ETD with FT MS/MS for degradomic-peptidomic analysis: comparison of peptide identification methods. *J Proteome Res* 2011, *10*, 3929-3943.

[55] Kocher, T., Pichler, P., Schutzbier, M., Stingl, C.*, et al.*, High precision quantitative proteomics using iTRAQ on an LTQ Orbitrap: a new mass spectrometric method combining the benefits of all. *J Proteome Res* 2009, *8*, 4743-4752.

[56] Olsen, J. V., Macek, B., Lange, O., Makarov, A.*, et al.*, Higher-energy C-trap dissociation for peptide modification analysis. *Nat Methods* 2007, *4*, 709-712.

[57] Dayon, L., Pasquarello, C., Hoogland, C., Sanchez, J. C., Scherl, A., Combining low- and high-energy tandem mass spectra for optimized peptide quantification with isobaric tags. *J Proteomics* 2010, *73*, 769-777.

[58] MacCoss, M. J., Wu, C. C., Yates, J. R., 3rd, Probability-based validation of protein identifications using a modified SEQUEST algorithm. *Anal Chem* 2002, *74*, 5593-5599.

[59] Bairoch, A., Apweiler, R., Wu, C. H., Barker, W. C., *et al.*, The Universal Protein Resource (UniProt). *Nucleic Acids Res* 2005, *33*, D154-159.

[60] Qian, W. J., Liu, T., Monroe, M. E., Strittmatter, E. F., *et al.*, Probability-based evaluation of peptide and protein identifications from tandem mass spectrometry and SEQUEST analysis: the human proteome. *J Proteome Res* 2005, *4*, 53-62.

[61] Eng, J. K., Fischer, B., Grossmann, J., Maccoss, M. J., A fast SEQUEST cross correlation algorithm. *J Proteome Res* 2008, *7*, 4598-4602.

[62] Kall, L., Storey, J. D., MacCoss, M. J., Noble, W. S., Assigning significance to peptides identified by tandem mass spectrometry using decoy databases. *J Proteome Res* 2008, *7*, 29-34.

[63] Bantscheff, M., Lemeer, S., Savitski, M. M., Kuster, B., Quantitative mass spectrometry in proteomics: critical review update from 2007 to the present. *Anal Bioanal Chem* 2012, *404*, 939-965.

[64] Wasinger, V. C., Zeng, M., Yau, Y., Current status and advances in quantitative proteomic mass spectrometry. *Int J Proteomics* 2013, *2013*, 180605.

[65] Bantscheff, M., Schirle, M., Sweetman, G., Rick, J., Kuster, B., Quantitative mass spectrometry in proteomics: a critical review. *Anal Bioanal Chem* 2007, *389*, 1017-1031.

[66] Schulze, W. X., Usadel, B., Quantitation in mass-spectrometry-based proteomics. *Annu Rev Plant Biol* 2010, *61*, 491-516.

[67] Xie, F., Liu, T., Qian, W. J., Petyuk, V. A., Smith, R. D., Liquid chromatography-mass spectrometry-based quantitative proteomics. *J Biol Chem* 2011, *286*, 25443-25449.

[68] Zhu, W., Smith, J. W., Huang, C. M., Mass spectrometry-based label-free quantitative proteomics. *J Biomed Biotechnol* 2010, *2010*, 840518.

[69] Wang, M., You, J., Bemis, K. G., Tegeler, T. J., Brown, D. P., Label-free mass spectrometry-based protein quantification technologies in proteomic analysis. *Brief Funct Genomic Proteomic* 2008, *7*, 329-339.

[70] Ong, S. E., Blagoev, B., Kratchmarova, I., Kristensen, D. B.*, et al.*, Stable isotope labeling by amino acids in cell culture, SILAC, as a simple and accurate approach to expression proteomics. *Mol Cell Proteomics* 2002, *1*, 376-386.

[71] Rauniyar, N., McClatchy, D. B., Yates, J. R., 3rd, Stable isotope labeling of mammals (SILAM) for in vivo quantitative proteomic analysis. *Methods* 2013, *61*, 260-268.

[72] Wu, C. C., MacCoss, M. J., Howell, K. E., Matthews, D. E., Yates, J. R., 3rd, Metabolic labeling of mammalian organisms with stable isotopes for quantitative proteomic analysis. *Anal Chem* 2004, *76*, 4951-4959.

[73] Chakraborty, A., Regnier, F. E., Global internal standard technology for comparative proteomics. *J Chromatogr A* 2002, *949*, 173-184.

[74] Boersema, P. J., Aye, T. T., van Veen, T. A., Heck, A. J., Mohammed, S., Triplex protein quantification based on stable isotope labeling by peptide dimethylation applied to cell and tissue lysates. *Proteomics* 2008, *8*, 4624-4632.

[75] Boersema, P. J., Raijmakers, R., Lemeer, S., Mohammed, S., Heck, A. J., Multiplex peptide stable isotope dimethyl labeling for quantitative proteomics. *Nat Protoc* 2009, *4*, 484-494.

[76] Gygi, S. P., Rist, B., Gerber, S. A., Turecek, F.*, et al.*, Quantitative analysis of complex protein mixtures using isotope-coded affinity tags. *Nat Biotechnol* 1999, *17*, 994-999.

[77] Schmidt, A., Kellermann, J., Lottspeich, F., A novel strategy for quantitative proteomics using isotope-coded protein labels. *Proteomics* 2005, *5*, 4-15.

[78] Patton, G. C., Sanci, L. A., Sawyer, S. M., Adolescent medicine. *Med J Aust* 2002, *176*, 3.

[79] Bantscheff, M., Kuster, B., Quantitative mass spectrometry in proteomics. *Anal Bioanal Chem* 2012, *404*, 937-938.

[80] Becker, G. W., Stable isotopic labeling of proteins for quantitative proteomic applications. *Brief Funct Genomic Proteomic* 2008, *7*, 371-382.

[81] Nasef, A., Fouillard, L., El-Taguri, A., Lopez, M., Human bone marrow-derived mesenchymal stem cells. *Libyan J Med* 2007, *2*, 190-201.

[82] Zhang, J., Wang, Y., Li, S., Deuterium isobaric amine-reactive tags for quantitative proteomics. *Anal Chem* 2010, *82*, 7588-7595.

[83] Xiang, F., Ye, H., Chen, R., Fu, Q., Li, L., N,N-dimethyl leucines as novel isobaric tandem mass tags for quantitative proteomics and peptidomics. *Anal Chem* 2010, *82*, 2817-2825.

[84] McAlister, G. C., Huttlin, E. L., Haas, W., Ting, L.*, et al.*, Increasing the multiplexing capacity of TMTs using reporter ion isotopologues with isobaric masses. *Anal Chem* 2012, *84*, 7469-7478.

[85] Viner, R. B., R.; Blank, M.; Rogers, J., Increasing the Multiplexing of Protein Quantitation from 6- to 10-plex with Reporter Ion Isotopologues. *Thermo Fisher Scientific Technical Note* 2013.

[86] Bantscheff, M., Boesche, M., Eberhard, D., Matthieson, T.*, et al.*, Robust and sensitive iTRAQ quantification on an LTQ Orbitrap mass spectrometer. *Mol Cell Proteomics* 2008, *7*, 1702-1713.

[87] Karp, N. A., Huber, W., Sadowski, P. G., Charles, P. D.*, et al.*, Addressing accuracy and precision issues in iTRAQ quantitation. *Mol Cell Proteomics* 2010, *9*, 1885-1897.

[88] Christoforou, A. L., Lilley, K. S., Isobaric tagging approaches in quantitative proteomics: the ups and downs. *Anal Bioanal Chem* 2012, *404*, 1029-1037.

[89] Wenger, C. D., Lee, M. V., Hebert, A. S., McAlister, G. C.*, et al.*, Gas-phase purification enables accurate, multiplexed proteome quantification with isobaric tagging. *Nat Methods* 2011, *8*, 933-935.

[90] Wuhr, M., Haas, W., McAlister, G. C., Peshkin, L.*, et al.*, Accurate multiplexed proteomics at the MS2 level using the complement reporter ion cluster. *Anal Chem* 2012, *84*, 9214-9221.

[91] Shliaha, P. V., Jukes-Jones, R., Christoforou, A., Fox, J.*, et al.*, Additional precursor purification in isobaric mass tagging experiments by traveling wave ion mobility separation (TWIMS). *J Proteome Res* 2014, *13*, 3360-3369.

[92] Sturm, R. M., Lietz, C. B., Li, L., Improved isobaric tandem mass tag quantification by ion mobility mass spectrometry. *Rapid Commun Mass Spectrom* 2014, *28*, 1051-1060.

[93] Savitski, M. M., Sweetman, G., Askenazi, M., Marto, J. A.*, et al.*, Delayed fragmentation and optimized isolation width settings for improvement of protein identification and accuracy of isobaric mass tag quantification on Orbitrap-type mass spectrometers. *Anal Chem* 2011, *83*, 8959-8967.

[94] Ting, L., Rad, R., Gygi, S. P., Haas, W., MS3 eliminates ratio distortion in isobaric multiplexed quantitative proteomics. *Nat Methods* 2011, *8*, 937-940.

[95] Cihoric, N., Tapia, C., Kruger, K., Aebersold, D. M.*, et al.*, IMRT with (1)(8)FDG-PET\CT based simultaneous integrated boost for treatment of nodal positive cervical cancer. *Radiat Oncol* 2014, *9*, 83.

[96] Qu, J., Young, R., Page, B. J., Shen, X.*, et al.*, Reproducible ion-current-based approach for 24-plex comparison of the tissue proteomes of hibernating versus normal myocardium in swine models. *J Proteome Res* 2014, *13*, 2571-2584.

[97] Nouri-Nigjeh, E., Sukumaran, S., Tu, C., Li, J.*, et al.*, Highly multiplexed and reproducible ion-current-based strategy for large-scale quantitative proteomics and the application to protein expression dynamics induced by methylprednisolone in 60 rats. *Anal Chem* 2014, *86*, 8149-8157.

[98] Robinson, R. A., Evans, A. R., Enhanced sample multiplexing for nitrotyrosine-modified proteins using combined precursor isotopic labeling and isobaric tagging. *Anal Chem* 2012, *84*, 4677-4686.

[99] Evans, A. R. R., R. A. S., Proteomics Quantification of Protein Nitration. *Reviews in Analytical Chemistry* 2013, *32*, 173-187.

[100] Evans, A. R., Robinson, R. A., Global combined precursor isotopic labeling and isobaric tagging (cPILOT) approach with selective MS(3) acquisition. *Proteomics* 2013, *13*, 3267-3272.

[101] Evans, A. R. G., L.; Guerrero Jr., R.; Robinson, R. A. S., Global cPILOT Analysis of the APP/PS-1 Liver Proteome. *Manuscript Submitted* 2014.

[102] Dephoure, N., Gygi, S. P., Hyperplexing: a method for higher-order multiplexed quantitative proteomics provides a map of the dynamic response to rapamycin in yeast. *Sci Signal* 2012, *5*, rs2.

161

[103] Everley, R. A., Kunz, R. C., McAllister, F. E., Gygi, S. P., Increasing Throughput in Targeted Proteomics Assays: 54-plex Quantitation in a Single Mass Spectrometry Run. *Anal Chem* 2013.

[104] Werner, T., Becher, I., Sweetman, G., Doce, C.*, et al.*, High-resolution enabled TMT 8-plexing. *Anal Chem* 2012, *84*, 7188-7194.

[105] Merrill, A. E., Hebert, A. S., MacGilvray, M. E., Rose, C. M.*, et al.*, NeuCode Labels for Relative Protein Quantification. *Mol Cell Proteomics* 2014, *13*, 2503-2512.

[106] Parker, J. B., K.; Zhu, F.; Zhu, N.; Chen, S., cysTMTRAQ - An Integrative Method for Unbiased Thiol-based Redox Proteomics. *Mol Cell Proteomics* 2014, Article in Press.

[107] Evans, A. R., Miriyala, S., St Clair, D. K., Butterfield, D. A., Robinson, R. A., Global effects of adriamycin treatment on mouse splenic protein levels. *J Proteome Res* 2012, *11*, 1054-1064.

[108] Bonadonna, G., Evolving concepts in the systemic adjuvant treatment of breast cancer. *Cancer Res* 1992, *52*, 2127-2137.

[109] Di Marco, A., Gaetani, M., Scarpinato, B., Adriamycin (NSC-123,127): a new antibiotic with antitumor activity. *Cancer Chemother Rep* 1969, *53*, 33-37.

[110] Chuang, R. Y., Chuang, L. F., Inhibition of chicken myeloblastosis RNA polymerase II activity by adriamycin. *Biochemistry* 1979, *18*, 2069-2073.

[111] Cummings, J., Anderson, L., Willmott, N., Smyth, J. F., The molecular pharmacology of doxorubicin in vivo. *Eur J Cancer* 1991, *27*, 532-535.

[112] Buzdar, A. U., Marcus, C., Smith, T. L., Blumenschein, G. R., Early and delayed clinical cardiotoxicity of doxorubicin. *Cancer* 1985, *55*, 2761-2765.

[113] Aluise, C. D., Sultana, R., Tangpong, J., Vore, M.*, et al.*, Chemo brain (chemo fog) as a potential side effect of doxorubicin administration: role of cytokine-induced, oxidative/nitrosative stress in cognitive dysfunction. *Adv Exp Med Biol* 2010, *678*, 147-156.

[114] Schagen, S. B., Hamburger, H. L., Muller, M. J., Boogerd, W., van Dam, F. S., Neurophysiological evaluation of late effects of adjuvant high-dose chemotherapy on cognitive function. *J Neurooncol* 2001, *51*, 159-165.

[115] Multani, P., White, C. A., Grillo-Lopez, A., Non-Hodgkin's lymphoma: review of conventional treatments. *Curr Pharm Biotechnol* 2001, *2*, 279-291.

[116] Handa, K., Sato, S., Generation of free radicals of quinone group-containing anti-cancer chemicals in NADPH-microsome system as evidenced by initiation of sulfite oxidation. *Gan* 1975, *66*, 43-47.

[117] Chen, Y., Jungsuwadee, P., Vore, M., Butterfield, D. A., St Clair, D. K., Collateral damage in cancer chemotherapy: oxidative stress in nontargeted tissues. *Mol Interv* 2007, *7*, 147-156.

[118] Aluise, C. D., St Clair, D., Vore, M., Butterfield, D. A., In vivo amelioration of adriamycin induced oxidative stress in plasma by gamma-glutamylcysteine ethyl ester (GCEE). *Cancer Lett* 2009, *282*, 25-29.

[119] Joshi, G., Sultana, R., Tangpong, J., Cole, M. P.*, et al.*, Free radical mediated oxidative stress and toxic side effects in brain induced by the anti cancer drug adriamycin: insight into chemobrain. *Free Radic Res* 2005, *39*, 1147-1154.

[120] Llesuy, S. F., Milei, J., Gonzalez Flecha, B. S., Boveris, A., Myocardial damage induced by doxorubicins: hydroperoxide-initiated chemiluminescence and morphology. *Free Radic Biol Med* 1990, *8*, 259-264.

[121] DeAtley, S. M., Aksenov, M. Y., Aksenova, M. V., Carney, J. M., Butterfield, D. A., Adriamycin induces protein oxidation in erythrocyte membranes. *Pharmacol Toxicol* 1998, *83*, 62-68.

[122] Qin, X. J., He, W., Hai, C. X., Liang, X., Liu, R., Protection of multiple antioxidants Chinese herbal medicine on the oxidative stress induced by adriamycin chemotherapy. *J Appl Toxicol* 2008, *28*, 271-282.

[123] Prahalathan, C., Selvakumar, E., Varalakshmi, P., Remedial effect of DL-alpha-lipoic acid against adriamycin induced testicular lipid peroxidation. *Mol Cell Biochem* 2004, *267*, 209-214.

[124] Kalaiselvi, P., Pragasam, V., Chinnikrishnan, S., Veena, C. K.*, et al.*, Counteracting adriamycin-induced oxidative stress by administration of N-acetyl cysteine and vitamin E. *Clin Chem Lab Med* 2005, *43*, 834-840.

[125] Siegfried, J. A., Kennedy, K. A., Sartorelli, A. C., Tritton, T. R., The role of membranes in the mechanism of action of the antineoplastic agent adriamycin. Spin-labeling studies with chronically hypoxic and drug-resistant tumor cells. *J Biol Chem* 1983, *258*, 339-343.

[126] Kusuoka, H., Futaki, S., Koretsune, Y., Kitabatake, A.*, et al.*, Alterations of intracellular calcium homeostasis and myocardial energetics in acute adriamycin-induced heart failure. *J Cardiovasc Pharmacol* 1991, *18*, 437-444.

[127] Singh, V., Singh, S. M., Effect of high cell density on the growth properties of tumor cells: a role in tumor cytotoxicity of chemotherapeutic drugs. *Anticancer Drugs* 2007, *18*, 1123-1132.

[128] Joshi, G., Aluise, C. D., Cole, M. P., Sultana, R.*, et al.*, Alterations in brain antioxidant enzymes and redox proteomic identification of oxidized brain proteins induced by the anti-cancer drug adriamycin: implications for oxidative stress-mediated chemobrain. *Neuroscience* 2010, *166*, 796-807.

[129] Joshi, G., Hardas, S., Sultana, R., St Clair, D. K.*, et al.*, Glutathione elevation by gamma-glutamyl cysteine ethyl ester as a potential therapeutic strategy for preventing oxidative stress in brain mediated by in vivo administration of adriamycin: Implication for chemobrain. *J Neurosci Res* 2007, *85*, 497-503.

[130] Aluise, C. D., Miriyala, S., Noel, T., Sultana, R.*, et al.*, 2-Mercaptoethane sulfonate prevents doxorubicin-induced plasma protein oxidation and TNF-alpha release: implications for the reactive oxygen species-mediated mechanisms of chemobrain. *Free Radic Biol Med* 2011, *50*, 1630-1638.

[131] Chen, Y., Daosukho, C., Opii, W. O., Turner, D. M.*, et al.*, Redox proteomic identification of oxidized cardiac proteins in adriamycin-treated mice. *Free Radic Biol Med* 2006, *41*, 1470-1477.

[132] Chen, S. T., Pan, T. L., Tsai, Y. C., Huang, C. M., Proteomics reveals protein profile changes in doxorubicin--treated MCF-7 human breast cancer cells. *Cancer Lett* 2002, *181*, 95-107.

[133] Hammer, E., Bien, S., Salazar, M. G., Steil, L.*, et al.*, Proteomic analysis of doxorubicin-induced changes in the proteome of HepG2cells combining 2-D DIGE and LC-MS/MS approaches. *Proteomics* 2010, *10*, 99-114.

[134] Dong, X., Xiong, L., Jiang, X., Wang, Y., Quantitative proteomic analysis reveals the perturbation of multiple cellular pathways in jurkat-T cells induced by doxorubicin. *J Proteome Res* 2010, *9*, 5943-5951.

[135] Jiang, Y. J., Sun, Q., Fang, X. S., Wang, X., Comparative mitochondrial proteomic analysis of Rji cells exposed to adriamycin. *Mol Med* 2009, *15*, 173-182.

[136] Sultana, R., Di Domenico, F., Tseng, M., Cai, J., *et al.*, Doxorubicin-induced thymus senescence. *J Proteome Res* 2010, *9*, 6232-6241.

[137] Zhang, J. T., Liu, Y., Use of comparative proteomics to identify potential resistance mechanisms in cancer treatment. *Cancer Treat Rev* 2007, *33*, 741-756.

[138] Peng, X., Gong, F., Xie, G., Zhao, Y., *et al.*, A proteomic investigation into adriamycin chemo-resistance of human leukemia K562 cells. *Mol Cell Biochem* 2011, *351*, 233-241.

[139] Shen, S. H., Gu, L. J., Liu, P. Q., Ye, X., *et al.*, Comparative proteomic analysis of differentially expressed proteins between K562 and K562/ADM cells. *Chin Med J (Engl)* 2008, *121*, 463-468.

[140] Zhu, F., Wang, Y., Zeng, S., Fu, X., *et al.*, Involvement of annexin A1 in multidrug resistance of K562/ADR cells identified by the proteomic study. *OMICS* 2009, *13*, 467-476.

[141] Keenan, J., Murphy, L., Henry, M., Meleady, P., Clynes, M., Proteomic analysis of multidrug-resistance mechanisms in adriamycin-resistant variants of DLKP, a squamous lung cancer cell line. *Proteomics* 2009, *9*, 1556-1566.

[142] Brown, K. J., Fenselau, C., Investigation of doxorubicin resistance in MCF-7 breast cancer cells using shot-gun comparative proteomics with proteolytic 18O labeling. *J Proteome Res* 2004, *3*, 455-462.

[143] Gehrmann, M. L., Fenselau, C., Hathout, Y., Highly altered protein expression profile in the adriamycin resistant MCF-7 cell line. *J Proteome Res* 2004, *3*, 403-409.

[144] Strong, R., Nakanishi, T., Ross, D., Fenselau, C., Alterations in the mitochondrial proteome of adriamycin resistant MCF-7 breast cancer cells. *J Proteome Res* 2006, *5*, 2389-2395.

[145] Orsini, F., Pavelic, Z., Mihich, E., Increased primary cell-mediated immunity in culture subsequent to adriamycin or daunorubicin treatment of spleen donor mice. *Cancer Res* 1977, *37*, 1719-1726.

[146] Ji, J., Chakraborty, A., Geng, M., Zhang, X., *et al.*, Strategy for qualitative and quantitative analysis in proteomics based on signature peptides. *J Chromatogr B Biomed Sci Appl* 2000, *745*, 197-210.

[147] Mebius, R. E., Kraal, G., Structure and function of the spleen. *Nat Rev Immunol* 2005, *5*, 606-616.

[148] Lee, J. W., Sung, N. Y., Kim, J. K., Kim, J. H., *et al.*, Effect of gamma irradiation on spleen cell function and cytotoxicity of doxorubicin. *Chem Biol Interact* 2008, *173*, 205-214.

[149] Miranda, C. J., Makui, H., Soares, R. J., Bilodeau, M.*, et al.*, Hfe deficiency increases susceptibility to cardiotoxicity and exacerbates changes in iron metabolism induced by doxorubicin. *Blood* 2003, *102*, 2574-2580.

[150] Wu, W. R., Zheng, J. W., Li, N., Bai, H. Q.*, et al.*, Immunosuppressive effects of dihydroetorphine, a potent narcotic analgesic, in dihydroetorphine-dependent mice. *Eur J Pharmacol* 1999, *366*, 261-269.

[151] Zhang, X. Y., Li, W. G., Wu, Y. J., Zheng, T. Z.*, et al.*, Proanthocyanidin from grape seeds potentiates anti-tumor activity of doxorubicin via immunomodulatory mechanism. *Int Immunopharmacol* 2005, *5*, 1247-1257.

[152] Cesta, M. F., Normal structure, function, and histology of the spleen. *Toxicol Pathol* 2006, *34*, 455-465.

[153] Gerke, V., Moss, S. E., Annexins: from structure to function. *Physiol Rev* 2002, *82*, 331-371.

[154] Zhang, F., Zhang, L., Zhang, B., Wei, X.*, et al.*, Anxa2 plays a critical role in enhanced invasiveness of the multidrug resistant human breast cancer cells. *J Proteome Res* 2009, *8*, 5041-5047.

[155] Munoz, L. E., Frey, B., Pausch, F., Baum, W.*, et al.*, The role of annexin A5 in the modulation of the immune response against dying and dead cells. *Curr Med Chem* 2007, *14*, 271-277.

[156] Gehrmann, M. L., Hathout, Y., Fenselau, C., Evaluation of metabolic labeling for comparative proteomics in breast cancer cells. *J Proteome Res* 2004, *3*, 1063-1068.

[157] Gelebart, P., Opas, M., Michalak, M., Calreticulin, a Ca2+-binding chaperone of the endoplasmic reticulum. *Int J Biochem Cell Biol* 2005, *37*, 260-266.

[158] Gold, L. I., Eggleton, P., Sweetwyne, M. T., Van Duyn, L. B.*, et al.*, Calreticulin: non-endoplasmic reticulum functions in physiology and disease. *FASEB J* 2010, *24*, 665-683.

[159] Tufi, R., Panaretakis, T., Bianchi, K., Criollo, A.*, et al.*, Reduction of endoplasmic reticulum Ca2+ levels favors plasma membrane surface exposure of calreticulin. *Cell Death Differ* 2008, *15*, 274-282.

[160] Mayur, Y. C., Jagadeesh, S., Thimmaiah, K. N., Targeting calmodulin in reversing multi drug resistance in cancer cells. *Mini Rev Med Chem* 2006, *6*, 1383-1389.

[161] Nicotera, P., Bellomo, G., Orrenius, S., Calcium-mediated mechanisms in chemically induced cell death. *Annu Rev Pharmacol Toxicol* 1992, *32*, 449-470.

[162] Storck, S., Shukla, M., Dimitrov, S., Bouvet, P., Functions of the histone chaperone nucleolin in diseases. *Subcell Biochem* 2007, *41*, 125-144.

[163] Bonello, T. T., Stehn, J. R., Gunning, P. W., New approaches to targeting the actin cytoskeleton for chemotherapy. *Future Med Chem* 2009, *1*, 1311-1331.

[164] Oikonomou, K. G., Zachou, K., Dalekos, G. N., Alpha-actinin: a multidisciplinary protein with important role in B-cell driven autoimmunity. *Autoimmun Rev* 2011, *10*, 389-396.

[165] Yang, Y. X., Sun, X. F., Cheng, A. L., Zhang, G. Y.*, et al.*, Increased expression of HSP27 linked to vincristine resistance in human gastric cancer cell line. *J Cancer Res Clin Oncol* 2009, *135*, 181-189.

[166] Zhang, L. H., Zhang, X., Roles of GRP78 in physiology and cancer. *J Cell Biochem* 2010, *110*, 1299-1305.

[167] Kubota, H., Hynes, G., Willison, K., The chaperonin containing t-complex polypeptide 1 (TCP-1). Multisubunit machinery assisting in protein folding and assembly in the eukaryotic cytosol. *Eur J Biochem* 1995, *230*, 3-16.

[168] Kazerounian, S., Yee, K. O., Lawler, J., Thrombospondins in cancer. *Cell Mol Life Sci* 2008, *65*, 700-712.

[169] Piccard, H., Van den Steen, P. E., Opdenakker, G., Hemopexin domains as multifunctional liganding modules in matrix metalloproteinases and other proteins. *J Leukoc Biol* 2007, *81*, 870-892.

[170] Hempel, N., Carrico, P. M., Melendez, J. A., Manganese superoxide dismutase (Sod2) and redox-control of signaling events that drive metastasis. *Anticancer Agents Med Chem* 2011, *11*, 191-201.

[171] Yen, H. C., Oberley, T. D., Vichitbandha, S., Ho, Y. S., St Clair, D. K., The protective role of manganese superoxide dismutase against adriamycin-induced acute cardiac toxicity in transgenic mice. *J Clin Invest* 1996, *98*, 1253-1260.

[172] Tokarska-Schlattner, M., Wallimann, T., Schlattner, U., Alterations in myocardial energy metabolism induced by the anti-cancer drug doxorubicin. *C R Biol* 2006, *329*, 657-668.

[173] Lee, J. R., Lee, S. J., Kim, T. W., Kim, J. K.*, et al.*, Chemical approach for specific enrichment and mass analysis of nitrated peptides. *Anal Chem* 2009, *81*, 6620-6626.

[174] Yamakura, F., Taka, H., Fujimura, T., Murayama, K., Inactivation of human manganese-superoxide dismutase by peroxynitrite is caused by exclusive nitration of tyrosine 34 to 3-nitrotyrosine. *J Biol Chem* 1998, *273*, 14085-14089.

[175] Ferrante, R. J., Shinobu, L. A., Schulz, J. B., Matthews, R. T.*, et al.*, Increased 3-nitrotyrosine and oxidative damage in mice with a human copper/zinc superoxide dismutase mutation. *Ann Neurol* 1997, *42*, 326-334.

[176] Kong, S. K., Yim, M. B., Stadtman, E. R., Chock, P. B., Peroxynitrite disables the tyrosine phosphorylation regulatory mechanism: Lymphocyte-specific tyrosine kinase fails to phosphorylate nitrated cdc2(6-20)NH2 peptide. *Proc Natl Acad Sci U S A* 1996, *93*, 3377-3382.

[177] Squier, T. C., Oxidative stress and protein aggregation during biological aging. *Exp Gerontol* 2001, *36*, 1539-1550.

[178] Peluffo, G., Radi, R., Biochemistry of protein tyrosine nitration in cardiovascular pathology. *Cardiovasc Res* 2007, *75*, 291-302.

[179] Nemirovskiy, O. V., Radabaugh, M. R., Aggarwal, P., Funckes-Shippy, C. L.*, et al.*, Plasma 3-nitrotyrosine is a biomarker in animal models of arthritis: Pharmacological dissection of iNOS' role in disease. *Nitric Oxide* 2009, *20*, 150-156.

[180] Butterfield, D. A., Reed, T., Sultana, R., Roles of 3-nitrotyrosine- and 4-hydroxynonenal-modified brain proteins in the progression and pathogenesis of Alzheimer's disease. *Free Radic Res* 2011, *45*, 59-72.

[181] Reynolds, M. R., Berry, R. W., Binder, L. I., Nitration in neurodegeneration: deciphering the "Hows" "nYs". *Biochemistry* 2007, *46*, 7325-7336.

[182] Good, P. F., Hsu, A., Werner, P., Perl, D. P., Olanow, C. W., Protein nitration in Parkinson's disease. *J Neuropathol Exp Neurol* 1998, *57*, 338-342.

[183] Butterfield, D. A., Reed, T., Newman, S. F., Sultana, R., Roles of amyloid beta-peptide-associated oxidative stress and brain protein modifications in the pathogenesis of Alzheimer's disease and mild cognitive impairment. *Free Radic Biol Med* 2007, *43*, 658-677.

[184] Sowell, R. A. B., D.A., in: Landow, M. L. (Ed.), *Cognitive Impairment: Causes, Diagnosis and Treatment*, Nova Science Publishers Inc, Hauppauge, NY 2010.

[185] Sultana, R., Reed, T., Perluigi, M., Coccia, R.*, et al.*, Proteomic identification of nitrated brain proteins in amnestic mild cognitive impairment: a regional study. *J Cell Mol Med* 2007, *11*, 839-851.

[186] Reed, T. T., Pierce, W. M., Jr., Turner, D. M., Markesbery, W. R., Butterfield, D. A., Proteomic identification of nitrated brain proteins in early Alzheimer's disease inferior parietal lobule. *J Cell Mol Med* 2009, *13*, 2019-2029.

[187] Castegna, A., Thongboonkerd, V., Klein, J. B., Lynn, B.*, et al.*, Proteomic identification of nitrated proteins in Alzheimer's disease brain. *J Neurochem* 2003, *85*, 1394-1401.

[188] Mazzola, J. L., Sirover, M. A., Reduction of glyceraldehyde-3-phosphate dehydrogenase activity in Alzheimer's disease and in Huntington's disease fibroblasts. *J Neurochem* 2001, *76*, 442-449.

[189] Aksenova, M., Butterfield, D. A., Zhang, S. X., Underwood, M., Geddes, J. W., Increased protein oxidation and decreased creatine kinase BB expression and activity after spinal cord contusion injury. *J Neurotrauma* 2002, *19*, 491-502.

[190] Sultana, R. S., R.A.; Butterfield, D.A., in: Veasey, S. C. (Ed.), *Oxidative Neural Injury*, Humana Press Inc., New York, NY 2009, pp. 137-157.

[191] Coleman, P. D., Flood, D. G., Neuron numbers and dendritic extent in normal aging and Alzheimer's disease. *Neurobiol Aging* 1987, *8*, 521-545.

[192] Sly, W. S., Hu, P. Y., Human carbonic anhydrases and carbonic anhydrase deficiencies. *Annu Rev Biochem* 1995, *64*, 375-401.

[193] Bubber, P., Haroutunian, V., Fisch, G., Blass, J. P., Gibson, G. E., Mitochondrial abnormalities in Alzheimer brain: mechanistic implications. *Ann Neurol* 2005, *57*, 695-703.

[194] Castegna, A., Lauderback, C. M., Mohmmad-Abdul, H., Butterfield, D. A., Modulation of phospholipid asymmetry in synaptosomal membranes by the lipid peroxidation products, 4-hydroxynonenal and acrolein: implications for Alzheimer's disease. *Brain Res* 2004, *1004*, 193-197.

[195] Danielson, S. R., Held, J. M., Schilling, B., Oo, M.*, et al.*, Preferentially increased nitration of alpha-synuclein at tyrosine-39 in a cellular oxidative model of Parkinson's disease. *Anal Chem* 2009, *81*, 7823-7828.

[196] Jovanovic, S. V., Clements, D., MacLeod, K., Biomarkers of oxidative stress are significantly elevated in Down syndrome. *Free Radic Biol Med* 1998, *25*, 1044-1048.

[197] Browne, S. E., Ferrante, R. J., Beal, M. F., Oxidative stress in Huntington's disease. *Brain Pathol* 1999, *9*, 147-163.

[198] Cookson, M. R., Shaw, P. J., Oxidative stress and motor neurone disease. *Brain Pathol* 1999, *9*, 165-186.

[199] Abe, K., Pan, L. H., Watanabe, M., Kato, T., Itoyama, Y., Induction of nitrotyrosine-like immunoreactivity in the lower motor neuron of amyotrophic lateral sclerosis. *Neurosci Lett* 1995, *199*, 152-154.

[200] Horiguchi, T., Uryu, K., Giasson, B. I., Ischiropoulos, H.*, et al.*, Nitration of tau protein is linked to neurodegeneration in tauopathies. *Am J Pathol* 2003, *163*, 1021-1031.

[201] Turko, I. V., Murad, F., Protein nitration in cardiovascular diseases. *Pharmacol Rev* 2002, *54*, 619-634.

[202] Lee, J. R., Kim, J. K., Lee, S. J., Kim, K. P., Role of protein tyrosine nitration in neurodegenerative diseases and atherosclerosis. *Arch Pharm Res* 2009, *32*, 1109-1118.

[203] Upmacis, R. K., Atherosclerosis: A Link Between Lipid Intake and Protein Tyrosine Nitration. *Lipid Insights* 2008, *2*, 75-88.

[204] Surmeli, N. B., Litterman, N. K., Miller, A. F., Groves, J. T., Peroxynitrite Mediates Active Site Tyrosine Nitration in Manganese Superoxide Dismutase. Evidence of a Role for the Carbonate Radical Anion. *J Am Chem Soc* 2010.

[205] Leeuwenburgh, C., Hardy, M. M., Hazen, S. L., Wagner, P*., et al.*, Reactive nitrogen intermediates promote low density lipoprotein oxidation in human atherosclerotic intima. *J Biol Chem* 1997, *272*, 1433-1436.

[206] Sandhu, J. K., Robertson, S., Birnboim, H. C., Goldstein, R., Distribution of protein nitrotyrosine in synovial tissues of patients with rheumatoid arthritis and osteoarthritis. *J Rheumatol* 2003, *30*, 1173-1181.

[207] Turko, I. V., Li, L., Aulak, K. S., Stuehr, D. J*., et al.*, Protein tyrosine nitration in the mitochondria from diabetic mouse heart. Implications to dysfunctional mitochondria in diabetes. *J Biol Chem* 2003, *278*, 33972-33977.

[208] Azad, N., Rojanasakul, Y., Vallyathan, V., Inflammation and lung cancer: roles of reactive oxygen/nitrogen species. *J Toxicol Environ Health B Crit Rev* 2008, *11*, 1-15.

[209] Pacher, P., Beckman, J. S., Liaudet, L., Nitric oxide and peroxynitrite in health and disease. *Physiol Rev* 2007, *87*, 315-424.

[210] Marshall, A., Lutfeaili, R., Raval, A., Chakravarti, D. N., Chakravarti, B., Differential hepatic protein tyrosine nitration of mouse due to aging - Effect on mitochondrial energy metabolism, quality control machinery of the endoplasmic reticulum and metabolism of drugs. *Biochem Biophys Res Commun* 2012.

[211] Zingarelli, B., Szabo, C., Salzman, A. L., Reduced oxidative and nitrosative damage in murine experimental colitis in the absence of inducible nitric oxide synthase. *Gut* 1999, *45*, 199-209.

[212] Thangaswamy, S., Bridenbaugh, E. A., Gashev, A. A., Evidence of increased oxidative stress in aged mesenteric lymphatic vessels. *Lymphat Res Biol* 2012, *10*, 53-62.

[213] Bronte, V., Kasic, T., Gri, G., Gallana, K*., et al.*, Boosting antitumor responses of T lymphocytes infiltrating human prostate cancers. *J Exp Med* 2005, *201*, 1257-1268.

[214] Birnboim, H. C., Lemay, A. M., Lam, D. K., Goldstein, R., Webb, J. R., Cutting edge: MHC class II-restricted peptides containing the inflammation-associated marker 3-nitrotyrosine evade central tolerance and elicit a robust cell-mediated immune response. *J Immunol* 2003, *171*, 528-532.

[215] Bayden, A. S., Yakovlev, V. A., Graves, P. R., Mikkelsen, R. B., Kellogg, G. E., Factors influencing protein tyrosine nitration--structure-based predictive models. *Free Radic Biol Med* 2011, *50*, 749-762.

[216] Kissner, R., Nauser, T., Bugnon, P., Lye, P. G., Koppenol, W. H., Formation and properties of peroxynitrite as studied by laser flash photolysis, high-pressure stopped-flow technique, and pulse radiolysis. *Chem Res Toxicol* 1997, *10*, 1285-1292.

[217] Radi, R., Nitric oxide, oxidants, and protein tyrosine nitration. *Proc Natl Acad Sci U S A* 2004, *101*, 4003-4008.

[218] Abello, N., Kerstjens, H. A., Postma, D. S., Bischoff, R., Protein tyrosine nitration: selectivity, physicochemical and biological consequences, denitration, and proteomics methods for the identification of tyrosine-nitrated proteins. *J Proteome Res* 2009, *8*, 3222-3238.

[219] Alvarez, B., Radi, R., Peroxynitrite reactivity with amino acids and proteins. *Amino Acids* 2003, *25*, 295-311.

[220] Radi, R., Protein tyrosine nitration: biochemical mechanisms and structural basis of functional effects. *Acc Chem Res* 2013, *46*, 550-559.

[221] Monteiro, H. P., Arai, R. J., Travassos, L. R., Protein tyrosine phosphorylation and protein tyrosine nitration in redox signaling. *Antioxid Redox Signal* 2008, *10*, 843-889.

[222] Guo, W., Adachi, T., Matsui, R., Xu, S.*, et al.*, Quantitative assessment of tyrosine nitration of manganese superoxide dismutase in angiotensin II-infused rat kidney. *Am J Physiol Heart Circ Physiol* 2003, *285*, H1396-1403.

[223] Rubbo, H., Radi, R., Protein and lipid nitration: role in redox signaling and injury. *Biochim Biophys Acta* 2008, *1780*, 1318-1324.

[224] Spickett, C. M., Pitt, A. R., Protein oxidation: role in signalling and detection by mass spectrometry. *Amino Acids* 2012, *42*, 5-21.

[225] Sokolovsky, M., Riordan, J. F., Vallee, B. L., Conversion of 3-nitrotyrosine to 3-aminotyrosine in peptides and proteins. *Biochem Biophys Res Commun* 1967, *27*, 20-25.

[226] Souza, J. M., Peluffo, G., Radi, R., Protein tyrosine nitration--functional alteration or just a biomarker? *Free Radic Biol Med* 2008, *45*, 357-366.

[227] Casagrande, S., Bonetto, V., Fratelli, M., Gianazza, E.*, et al.*, Glutathionylation of human thioredoxin: a possible crosstalk between the glutathione and thioredoxin systems. *Proc Natl Acad Sci U S A* 2002, *99*, 9745-9749.

[228] Uchida, K., Stadtman, E. R., Covalent attachment of 4-hydroxynonenal to glyceraldehyde-3-phosphate dehydrogenase. A possible involvement of intra- and intermolecular cross-linking reaction. *J Biol Chem* 1993, *268*, 6388-6393.

[229] Adibhatla, R. M., Hatcher, J. F., Lipid oxidation and peroxidation in CNS health and disease: from molecular mechanisms to therapeutic opportunities. *Antioxid Redox Signal* 2010, *12*, 125-169.

[230] Yates, J. R., Ruse, C. I., Nakorchevsky, A., Proteomics by mass spectrometry: approaches, advances, and applications. *Annu Rev Biomed Eng* 2009, *11*, 49-79.

[231] Li, B., Held, J. M., Schilling, B., Danielson, S. R., Gibson, B. W., Confident identification of 3-nitrotyrosine modifications in mass spectral data across multiple mass spectrometry platforms. *J Proteomics* 2011, *74*, 2510-2521.

[232] Dekker, F., Abello, N., Wisastra, R., Bischoff, R., Enrichment and detection of tyrosine-nitrated proteins. *Curr Protoc Protein Sci* 2012, *Chapter 14*, Unit 14 13.

[233] Helman, M., Givol, D., Isolation of nitrotyrosine-containing peptides by using an insoluble-antibody column. *Biochem J* 1971, *125*, 971-974.

[234] Zhan, X., Desiderio, D. M., Nitroproteins from a human pituitary adenoma tissue discovered with a nitrotyrosine affinity column and tandem mass spectrometry. *Anal Biochem* 2006, *354*, 279-289.

[235] Nuriel, T., Deeb, R. S., Hajjar, D. P., Gross, S. S., Protein 3-nitrotyrosine in complex biological samples: quantification by high-pressure liquid chromatography/electrochemical detection and emergence of proteomic approaches for unbiased identification of modification sites. *Methods Enzymol* 2008, *441*, 1-17.

[236] Nikov, G., Bhat, V., Wishnok, J. S., Tannenbaum, S. R., Analysis of nitrated proteins by nitrotyrosine-specific affinity probes and mass spectrometry. *Anal Biochem* 2003, *320*, 214-222.

[237] Abello, N., Barroso, B., Kerstjens, H. A., Postma, D. S., Bischoff, R., Chemical labeling and enrichment of nitrotyrosine-containing peptides. *Talanta* 2010, *80*, 1503-1512.

[238] Zhang, Q., Qian, W. J., Knyushko, T. V., Clauss, T. R.*, et al.*, A method for selective enrichment and analysis of nitrotyrosine-containing peptides in complex proteome samples. *J Proteome Res* 2007, *6*, 2257-2268.

[239] Kim, J. K., Lee, J. R., Kang, J. W., Lee, S. J.*, et al.*, Selective enrichment and mass spectrometric identification of nitrated peptides using fluorinated carbon tags. *Anal Chem* 2011, *83*, 157-163.

[240] Amoresano, A., Chiappetta, G., Pucci, P., D'Ischia, M., Marino, G., Bidimensional tandem mass spectrometry for selective identification of nitration sites in proteins. *Anal Chem* 2007, *79*, 2109-2117.

[241] Dremina, E. S., Li, X., Galeva, N. A., Sharov, V. S.*, et al.*, A methodology for simultaneous fluorogenic derivatization and boronate affinity enrichment of 3-nitrotyrosine-containing peptides. *Anal Biochem* 2011, *418*, 184-196.

[242] Ghesquiere, B., Colaert, N., Helsens, K., Dejager, L.*, et al.*, In vitro and in vivo protein-bound tyrosine nitration characterized by diagonal chromatography. *Mol Cell Proteomics* 2009, *8*, 2642-2652.

[243] Brown, J. R., Hartley, B. S., Location of disulphide bridges by diagonal paper electrophoresis. The disulphide bridges of bovine chymotrypsinogen A. *Biochem J* 1966, *101*, 214-228.

[244] Oldreive, C., Bradley, N., Bruckdorfer, R., Rice-Evans, C., Lack of influence of dietary nitrate/nitrite on plasma nitrotyrosine levels measured using a competitive inhibition of binding ELISA assay. *Free Radic Res* 2001, *35*, 377-386.

[245] Khan, J., Brennand, D. M., Bradley, N., Gao, B.*, et al.*, 3-Nitrotyrosine in the proteins of human plasma determined by an ELISA method. *Biochem J* 1998, *330 (Pt 2)*, 795-801.

[246] Wayenberg, J. L., Ransy, V., Vermeylen, D., Damis, E., Bottari, S. P., Nitrated plasma albumin as a marker of nitrative stress and neonatal encephalopathy in perinatal asphyxia. *Free Radic Biol Med* 2009, *47*, 975-982.

[247] Bayir, H., Kagan, V. E., Clark, R. S., Janesko-Feldman, K.*, et al.*, Neuronal NOS-mediated nitration and inactivation of manganese superoxide dismutase in brain after experimental and human brain injury. *J Neurochem* 2007, *101*, 168-181.

[248] Ceriello, A., Mercuri, F., Quagliaro, L., Assaloni, R.*, et al.*, Detection of nitrotyrosine in the diabetic plasma: evidence of oxidative stress. *Diabetologia* 2001, *44*, 834-838.

[249] Jin, H., Webb-Robertson, B. J., Peterson, E. S., Tan, R.*, et al.*, Smoking, COPD, and 3-nitrotyrosine levels of plasma proteins. *Environ Health Perspect* 2011, *119*, 1314-1320.

[250] Weber, D., Kneschke, N., Grimm, S., Bergheim, I.*, et al.*, Rapid and sensitive determination of protein-nitrotyrosine by ELISA: Application to human plasma. *Free Radic Res* 2012, *46*, 276-285.

[251] Qu, L. N., Yang, T. B., Yuan, Y. H., Zhong, P.*, et al.*, A novel competitive ELISA for both free and protein-bound nitrotyrosine. *Hybrid Hybridomics* 2003, *22*, 401-406.

[252] Pan, S., Aebersold, R., Chen, R., Rush, J.*, et al.*, Mass spectrometry based targeted protein quantification: methods and applications. *J Proteome Res* 2009, *8*, 787-797.

[253] Duncan, M. W., A review of approaches to the analysis of 3-nitrotyrosine. *Amino Acids* 2003, *25*, 351-361.

[254] Righetti, P. G. A., P.; Simo, C.; Citterio, A., in: Agrawal, G. K. R., R. (Ed.), *Plant Proteomics: Technologies, Strategies, and Applications* 2008, pp. 9-31.

[255] Liu, F., Xiong, J., Huang, G. Y., Wang, W., [Study on the underlying mechanism of acupuncture in regulating neuroendocrine activity in dysmenorrhea rats]. *Zhen Ci Yan Jiu* 2009, *34*, 3-8.

[256] Viera, L., Ye, Y. Z., Estevez, A. G., Beckman, J. S., Immunohistochemical methods to detect nitrotyrosine. *Methods Enzymol* 1999, *301*, 373-381.

[257] Franco Mdo, C., Fortes, Z. B., Akamine, E. H., Kawamoto, E. M.*, et al.*, Tetrahydrobiopterin improves endothelial dysfunction and vascular oxidative stress in microvessels of intrauterine undernourished rats. *J Physiol* 2004, *558*, 239-248.

[258] Morrissey, B. M., Schilling, K., Weil, J. V., Silkoff, P. E., Rodman, D. M., Nitric oxide and protein nitration in the cystic fibrosis airway. *Arch Biochem Biophys* 2002, *406*, 33-39.

[259] Soderling, A. S., Hultman, L., Delbro, D., Hojrup, P., Caidahl, K., Reduction of the nitro group during sample preparation may cause underestimation of the nitration level in 3-nitrotyrosine immunoblotting. *J Chromatogr B Analyt Technol Biomed Life Sci* 2007, *851*, 277-286.

[260] Bigelow, D. J., Qian, W. J., Quantitative proteome mapping of nitrotyrosines. *Methods Enzymol* 2008, *440*, 191-205.

[261] Wisastra, R., Poelstra, K., Bischoff, R., Maarsingh, H.*, et al.*, Antibody-free detection of protein tyrosine nitration in tissue sections. *Chembiochem* 2011, *12*, 2016-2020.

[262] Liu, H., Sadygov, R. G., Yates, J. R., 3rd, A model for random sampling and estimation of relative protein abundance in shotgun proteomics. *Anal Chem* 2004, *76*, 4193-4201.

[263] Smith, R. D., Anderson, G. A., Lipton, M. S., Pasa-Tolic, L.*, et al.*, An accurate mass tag strategy for quantitative and high-throughput proteome measurements. *Proteomics* 2002, *2*, 513-523.

[264] Willard, B. B., Ruse, C. I., Keightley, J. A., Bond, M., Kinter, M., Site-specific quantitation of protein nitration using liquid chromatography/tandem mass spectrometry. *Anal Chem* 2003, *75*, 2370-2376.

[265] Ruse, C. I., Willard, B., Jin, J. P., Haas, T.*, et al.*, Quantitative dynamics of site-specific protein phosphorylation determined using liquid chromatography electrospray ionization mass spectrometry. *Anal Chem* 2002, *74*, 1658-1664.

[266] Chen, H. J., Chiu, W. L., Simultaneous detection and quantification of 3-nitrotyrosine and 3-bromotyrosine in human urine by stable isotope dilution liquid chromatography tandem mass spectrometry. *Toxicol Lett* 2008, *181*, 31-39.

[267] Chen, H. J., Chen, Y. C., Reactive nitrogen oxide species-induced post-translational modifications in human hemoglobin and the association with cigarette smoking. *Anal Chem* 2012, *84*, 7881-7890.

[268] Riggs, L., Seeley, E. H., Regnier, F. E., Quantification of phosphoproteins with global internal standard technology. *J Chromatogr B Analyt Technol Biomed Life Sci* 2005, *817*, 89-96.

[269] Tsumoto, H., Taguchi, R., Kohda, K., Efficient identification and quantification of peptides containing nitrotyrosine by matrix-assisted laser desorption/ionization time-of-flight mass spectrometry after derivatization. *Chem Pharm Bull (Tokyo)* 2010, *58*, 488-494.

[270] Feeney, M. B., Schoneich, C., Proteomic Approaches to Analyze Protein Tyrosine Nitration. *Antioxid Redox Signal* 2012.

[271] Haandel, L. V. K., J.; Li, X.; Schoneich, C.; Stobaugh, J.F., Phenylisothiocyanate as a Multiple Chemical Dimension Reagent for the Relative Quantitation of Protein Nitrotyrosine. *Chromatographia* 008, *68*, 507-516.

[272] Zhang, R., Regnier, F. E., Minimizing resolution of isotopically coded peptides in comparative proteomics. *J Proteome Res* 2002, *1*, 139-147.

[273] Thompson, A., Schafer, J., Kuhn, K., Kienle, S.*, et al.*, Tandem mass tags: a novel quantification strategy for comparative analysis of complex protein mixtures by MS/MS. *Anal Chem* 2003, *75*, 1895-1904.

[274] Ross, P. L., Huang, Y. N., Marchese, J. N., Williamson, B.*, et al.*, Multiplexed protein quantitation in Saccharomyces cerevisiae using amine-reactive isobaric tagging reagents. *Mol Cell Proteomics* 2004, *3*, 1154-1169.

[275] Chiappetta, G., Corbo, C., Palmese, A., Galli, F.*, et al.*, Quantitative identification of protein nitration sites. *Proteomics* 2009, *9*, 1524-1537.

[276] Petersson, A. S., Steen, H., Kalume, D. E., Caidahl, K., Roepstorff, P., Investigation of tyrosine nitration in proteins by mass spectrometry. *J Mass Spectrom* 2001, *36*, 616-625.

[277] Sarver, A., Scheffler, N. K., Shetlar, M. D., Gibson, B. W., Analysis of peptides and proteins containing nitrotyrosine by matrix-assisted laser desorption/ionization mass spectrometry. *J Am Soc Mass Spectrom* 2001, *12*, 439-448.

[278] Gokulrangan, G., Zaidi, A., Michaelis, M. L., Schoneich, C., Proteomic analysis of protein nitration in rat cerebellum: effect of biological aging. *J Neurochem* 2007, *100*, 1494-1504.

[279] Kanski, J., Hong, S. J., Schoneich, C., Proteomic analysis of protein nitration in aging skeletal muscle and identification of nitrotyrosine-containing sequences in vivo by nanoelectrospray ionization tandem mass spectrometry. *J Biol Chem* 2005, *280*, 24261-24266.

[280] Jiao, K., Mandapati, S., Skipper, P. L., Tannenbaum, S. R., Wishnok, J. S., Site-selective nitration of tyrosine in human serum albumin by peroxynitrite. *Anal Biochem* 2001, *293*, 43-52.

[281] Sacksteder, C. A., Qian, W. J., Knyushko, T. V., Wang, H.*, et al.*, Endogenously nitrated proteins in mouse brain: links to neurodegenerative disease. *Biochemistry* 2006, *45*, 8009-8022.

[282] van Haandel, L. K., J.; Li, X.; Schoneich, C.; Stobaugh, J. F., Phenylisothiocyanate as a Multiple Chemical Dimension Reagent for the Relative Quantitation of Protein Nitrotyrosine. *Chromatographia* 2008, *68*, 507-516.

[283] Stevens, S. M., Jr., Prokai-Tatrai, K., Prokai, L., Factors that contribute to the misidentification of tyrosine nitration by shotgun proteomics. *Mol Cell Proteomics* 2008, *7*, 2442-2451.

[284] Ghesquiere, B., Goethals, M., Van Damme, J., Staes, A.*, et al.*, Improved tandem mass spectrometric characterization of 3-nitrotyrosine sites in peptides. *Rapid Commun Mass Spectrom* 2006, *20*, 2885-2893.

[285] Ghesquiere, B., Helsens, K., Vandekerckhove, J., Gevaert, K., A stringent approach to improve the quality of nitrotyrosine peptide identifications. *Proteomics* 2011, *11*, 1094-1098.

[286] Zhang, Y., Yang, H., Poschl, U., Analysis of nitrated proteins and tryptic peptides by HPLC-chip-MS/MS: site-specific quantification, nitration degree, and reactivity of tyrosine residues. *Anal Bioanal Chem* 2011, *399*, 459-471.

[287] Kim, J. Y., Kim, K. W., Kwon, H. J., Lee, D. W., Yoo, J. S., Probing lysine acetylation with a modification-specific marker ion using high-performance liquid chromatography/electrospray-mass spectrometry with collision-induced dissociation. *Anal Chem* 2002, *74*, 5443-5449.

[288] Kuzyk, M. A., Ohlund, L. B., Elliott, M. H., Smith, D.*, et al.*, A comparison of MS/MS-based, stable-isotope-labeled, quantitation performance on ESI-quadrupole TOF and MALDI-TOF/TOF mass spectrometers. *Proteomics* 2009, *9*, 3328-3340.

[289] Ow, S. Y., Salim, M., Noirel, J., Evans, C.*, et al.*, iTRAQ underestimation in simple and complex mixtures: "the good, the bad and the ugly". *J Proteome Res* 2009, *8*, 5347-5355.

[290] Vincent, C. E. L., A. R.; Westphall, M. S.; Coon, J. J., *59th ASMS Conference on Mass Spectrometry and Allied Topics*, American Society of Mass Spectrometry, Denver, CO 2011.

[291] Pichler, P., Kocher, T., Holzmann, J., Mazanek, M.*, et al.*, Peptide labeling with isobaric tags yields higher identification rates using iTRAQ 4-plex compared to TMT 6-plex and iTRAQ 8-plex on LTQ Orbitrap. *Anal Chem* 2010, *82*, 6549-6558.

[292] Pierce, A., Unwin, R. D., Evans, C. A., Griffiths, S.*, et al.*, Eight-channel iTRAQ enables comparison of the activity of six leukemogenic tyrosine kinases. *Mol Cell Proteomics* 2008, *7*, 853-863.

[293] Koehler, C. J., Arntzen, M. O., de Souza, G. A., Thiede, B., An approach for triplex-isobaric peptide termini labeling (triplex-IPTL). *Anal Chem* 2013, *85*, 2478-2485.

[294] Dayon, L., Sonderegger, B., Kussmann, M., Combination of gas-phase fractionation and MS(3) acquisition modes for relative protein quantification with isobaric tagging. *J Proteome Res* 2012, *11*, 5081-5089.

[295] Thingholm, T. E., Palmisano, G., Kjeldsen, F., Larsen, M. R., Undesirable charge-enhancement of isobaric tagged phosphopeptides leads to reduced identification efficiency. *J Proteome Res* 2010, *9*, 4045-4052.

[296] Association, A. s., 2013 Alzheimer's Disease Facts and Figures. *Alzheimer's Dementia* 2013, *9*.

[297] Duyckaerts, C., Delatour, B., Potier, M. C., Classification and basic pathology of Alzheimer disease. *Acta Neuropathol* 2009, *118*, 5-36.

[298] Wolfe, M. S., The gamma-secretase complex: membrane-embedded proteolytic ensemble. *Biochemistry* 2006, *45*, 7931-7939.

[299] Papassotiropoulos, A., Fountoulakis, M., Dunckley, T., Stephan, D. A., Reiman, E. M., Genetics, transcriptomics, and proteomics of Alzheimer's disease. *J Clin Psychiatry* 2006, *67*, 652-670.

[300] Hall, A. M., Roberson, E. D., Mouse models of Alzheimer's disease. *Brain Res Bull* 2012, *88*, 3-12.

[301] Saito, T., Matsuba, Y., Mihira, N., Takano, J*., et al.*, Single App knock-in mouse models of Alzheimer's disease. *Nat Neurosci* 2014, *17*, 661-663.

[302] Jiang, Q., Lee, C. Y., Mandrekar, S., Wilkinson, B*., et al.*, ApoE promotes the proteolytic degradation of Abeta. *Neuron* 2008, *58*, 681-693.

[303] Hooijmans, C. R., Kiliaan, A. J., Fatty acids, lipid metabolism and Alzheimer pathology. *Eur J Pharmacol* 2008, *585*, 176-196.

[304] Grimm, M. O., Rothhaar, T. L., Hartmann, T., The role of APP proteolytic processing in lipid metabolism. *Exp Brain Res* 2012, *217*, 365-375.

[305] Xiong, H., Callaghan, D., Jones, A., Walker, D. G*., et al.*, Cholesterol retention in Alzheimer's brain is responsible for high beta- and gamma-secretase activities and Abeta production. *Neurobiol Dis* 2008, *29*, 422-437.

[306] Chen, Z., Zhong, C., Decoding Alzheimer's disease from perturbed cerebral glucose metabolism: implications for diagnostic and therapeutic strategies. *Prog Neurobiol* 2013, *108*, 21-43.

[307] Steculorum, S. M., Solas, M., Bruning, J. C., The paradox of neuronal insulin action and resistance in the development of aging-associated diseases. *Alzheimers Dement* 2014, *10*, S3-11.

[308] Cunnane, S., Nugent, S., Roy, M., Courchesne-Loyer, A*., et al.*, Brain fuel metabolism, aging, and Alzheimer's disease. *Nutrition* 2011, *27*, 3-20.

[309] Lin, M. T., Beal, M. F., Mitochondrial dysfunction and oxidative stress in neurodegenerative diseases. *Nature* 2006, *443*, 787-795.

[310] Sutcliffe, J. G., Hedlund, P. B., Thomas, E. A., Bloom, F. E., Hilbush, B. S., Peripheral reduction of beta-amyloid is sufficient to reduce brain beta-amyloid: implications for Alzheimer's disease. *J Neurosci Res* 2011, *89*, 808-814.

[311] Zhang, Y., Zhou, B., Zhang, F., Wu, J*., et al.*, Amyloid-beta induces hepatic insulin resistance by activating JAK2/STAT3/SOCS-1 signaling pathway. *Diabetes* 2012, *61*, 1434-1443.

[312] Veszelka, S., Toth, A. E., Walter, F. R., Datki, Z*., et al.*, Docosahexaenoic acid reduces amyloid-beta induced toxicity in cells of the neurovascular unit. *J Alzheimers Dis* 2013, *36*, 487-501.

[313] Astarita, G., Jung, K. M., Berchtold, N. C., Nguyen, V. Q.*, et al.*, Deficient liver biosynthesis of docosahexaenoic acid correlates with cognitive impairment in Alzheimer's disease. *PLoS One* 2010, *5*, e12538.

[314] Hooijmans, C. R., Rutters, F., Dederen, P. J., Gambarota, G.*, et al.*, Changes in cerebral blood volume and amyloid pathology in aged Alzheimer APP/PS1 mice on a docosahexaenoic acid (DHA) diet or cholesterol enriched Typical Western Diet (TWD). *Neurobiol Dis* 2007, *28*, 16-29.

[315] Ghiso, J., Shayo, M., Calero, M., Ng, D.*, et al.*, Systemic catabolism of Alzheimer's Abeta40 and Abeta42. *J Biol Chem* 2004, *279*, 45897-45908.

[316] Sagare, A., Deane, R., Bell, R. D., Johnson, B.*, et al.*, Clearance of amyloid-beta by circulating lipoprotein receptors. *Nat Med* 2007, *13*, 1029-1031.

[317] Tamaki, C., Ohtsuki, S., Iwatsubo, T., Hashimoto, T.*, et al.*, Major involvement of low-density lipoprotein receptor-related protein 1 in the clearance of plasma free amyloid beta-peptide by the liver. *Pharm Res* 2006, *23*, 1407-1416.

[318] Sehgal, N., Gupta, A., Valli, R. K., Joshi, S. D.*, et al.*, Withania somnifera reverses Alzheimer's disease pathology by enhancing low-density lipoprotein receptor-related protein in liver. *Proc Natl Acad Sci U S A* 2012, *109*, 3510-3515.

[319] Sagare, A. P., Deane, R., Zetterberg, H., Wallin, A.*, et al.*, Impaired lipoprotein receptor-mediated peripheral binding of plasma amyloid-beta is an early biomarker for mild cognitive impairment preceding Alzheimer's disease. *J Alzheimers Dis* 2011, *24*, 25-34.

[320] Reddy, J. K., Rao, M. S., Lipid metabolism and liver inflammation. II. Fatty liver disease and fatty acid oxidation. *Am J Physiol Gastrointest Liver Physiol* 2006, *290*, G852-858.

[321] Garcia-Alloza, M., Robbins, E. M., Zhang-Nunes, S. X., Purcell, S. M.*, et al.*, Characterization of amyloid deposition in the APPswe/PS1dE9 mouse model of Alzheimer disease. *Neurobiol Dis* 2006, *24*, 516-524.

[322] Robinson, R. A., Joshi, G., Huang, Q., Sultana, R.*, et al.*, Proteomic analysis of brain proteins in APP/PS-1 human double mutant knock-in mice with increasing amyloid beta-peptide deposition: insights

into the effects of in vivo treatment with N-acetylcysteine as a potential therapeutic intervention in mild cognitive impairment and Alzheimer's disease. *Proteomics* 2011, *11*, 4243-4256.

[323] Sultana, R., Robinson, R. A., Di Domenico, F., Abdul, H. M.*, et al.*, Proteomic identification of specifically carbonylated brain proteins in APP(NLh)/APP(NLh) x PS-1(P264L)/PS-1(P264L) human double mutant knock-in mice model of Alzheimer disease as a function of age. *J Proteomics* 2011, *74*, 2430-2440.

[324] Cao, Z., Robinson, R. A., Proteome characterization of splenocytes from an Abetapp/ps-1 Alzheimer's disease model. *Proteomics* 2013.

[325] Lv, J., Ma, S., Zhang, X., Zheng, L.*, et al.*, Quantitative proteomics reveals that PEA15 regulates astroglial Abeta phagocytosis in an Alzheimer's disease mouse model. *J Proteomics* 2014, *110C*, 45-58.

[326] Gu, L., Evans, A.; Robinson, R.A.S, Sample Multiplexing with Cysteine-selective Approaches: cysDML and cPILOT. *J. Amer. Soc. Mass Spec.*, Manuscript Submitted.

[327] Cao, Z., Yende, S., Kellum, J. A., Robinson, R. A., Additions to the Human Plasma Proteome via a Tandem MARS Depletion iTRAQ-Based Workflow. *Int J Proteomics* 2013, *2013*, 654356.

[328] Mi, H., Muruganujan, A., Thomas, P. D., PANTHER in 2013: modeling the evolution of gene function, and other gene attributes, in the context of phylogenetic trees. *Nucleic Acids Res* 2013, *41*, D377-386.

[329] Dayon, L., Hainard, A., Licker, V., Turck, N.*, et al.*, Relative quantification of proteins in human cerebrospinal fluids by MS/MS using 6-plex isobaric tags. *Anal Chem* 2008, *80*, 2921-2931.

[330] McAlister, G. C., Nusinow, D. P., Jedrychowski, M. P., Wuhr, M.*, et al.*, MultiNotch MS3 enables accurate, sensitive, and multiplexed detection of differential expression across cancer cell line proteomes. *Anal Chem* 2014, *86*, 7150-7158.

[331] Fang, R., Elias, D. A., Monroe, M. E., Shen, Y.*, et al.*, Differential label-free quantitative proteomic analysis of Shewanella oneidensis cultured under aerobic and suboxic conditions by accurate mass and time tag approach. *Mol Cell Proteomics* 2006, *5*, 714-725.

[332] de la Monte, S. M., Tong, M., Brain metabolic dysfunction at the core of Alzheimer's disease. *Biochem Pharmacol* 2014, *88*, 548-559.

[333] Wong, B. X., Hung, Y. H., Bush, A. I., Duce, J. A., Metals and cholesterol: two sides of the same coin in Alzheimer's disease pathology. *Front Aging Neurosci* 2014, *6*, 91.

[334] Sowell, R. A., Owen, J. B., Butterfield, D. A., Proteomics in animal models of Alzheimer's and Parkinson's diseases. *Ageing Res Rev* 2009, *8*, 1-17.

[335] Jankowsky, J. L., Fadale, D. J., Anderson, J., Xu, G. M*., et al.*, Mutant presenilins specifically elevate the levels of the 42 residue beta-amyloid peptide in vivo: evidence for augmentation of a 42-specific gamma secretase. *Hum Mol Genet* 2004, *13*, 159-170.

[336] Bartlett, K., Eaton, S., Mitochondrial beta-oxidation. *Eur J Biochem* 2004, *271*, 462-469.

[337] Reddy, J. K., Hashimoto, T., Peroxisomal beta-oxidation and peroxisome proliferator-activated receptor alpha: an adaptive metabolic system. *Annu Rev Nutr* 2001, *21*, 193-230.

[338] Chou, J. L., Shenoy, D. V., Thomas, N., Choudhary, P. K*., et al.*, Early dysregulation of the mitochondrial proteome in a mouse model of Alzheimer's disease. *J Proteomics* 2011, *74*, 466-479.

[339] Owen, O. E., Ketone Bodies as a fuel for the Brain during Starvation. *Biochemistry and Molecular Biology Education* 2005, *33*, 246-251.

[340] Henderson, S. T., Ketone bodies as a therapeutic for Alzheimer's disease. *Neurotherapeutics* 2008, *5*, 470-480.

[341] Beckett, T. L., Studzinski, C. M., Keller, J. N., Paul Murphy, M., Niedowicz, D. M., A ketogenic diet improves motor performance but does not affect beta-amyloid levels in a mouse model of Alzheimer's disease. *Brain Res* 2013, *1505*, 61-67.

[342] Gray, L. R., Tompkins, S. C., Taylor, E. B., Regulation of pyruvate metabolism and human disease. *Cell Mol Life Sci* 2014, *71*, 2577-2604.

[343] Lai, J. C., Cooper, A. J., Brain alpha-ketoglutarate dehydrogenase complex: kinetic properties, regional distribution, and effects of inhibitors. *J Neurochem* 1986, *47*, 1376-1386.

[344] Ott, P., Vilstrup, H., Cerebral effects of ammonia in liver disease: current hypotheses. *Metab Brain Dis* 2014.

[345] Senior, J. R., Alanine aminotransferase: a clinical and regulatory tool for detecting liver injury-past, present, and future. *Clin Pharmacol Ther* 2012, *92*, 332-339.

[346] Seiler, N., Ammonia and Alzheimer's disease. *Neurochem Int* 2002, *41*, 189-207.

[347] Ponka, P., Cell biology of heme. *Am J Med Sci* 1999, *318*, 241-256.

[348] Jomova, K., Vondrakova, D., Lawson, M., Valko, M., Metals, oxidative stress and neurodegenerative disorders. *Mol Cell Biochem* 2010, *345*, 91-104.

[349] Atamna, H., Frey, W. H., 2nd, Mechanisms of mitochondrial dysfunction and energy deficiency in Alzheimer's disease. *Mitochondrion* 2007, *7*, 297-310.

[350] Foxton, R. H., Land, J. M., Heales, S. J., Tetrahydrobiopterin availability in Parkinson's and Alzheimer's disease; potential pathogenic mechanisms. *Neurochem Res* 2007, *32*, 751-756.

[351] Dumont, M., Beal, M. F., Neuroprotective strategies involving ROS in Alzheimer disease. *Free Radic Biol Med* 2011, *51*, 1014-1026.

[352] Rhein, V., Song, X., Wiesner, A., Ittner, L. M*., et al.*, Amyloid-beta and tau synergistically impair the oxidative phosphorylation system in triple transgenic Alzheimer's disease mice. *Proc Natl Acad Sci U S A* 2009, *106*, 20057-20062.

[353] Dringen, R., Pawlowski, P. G., Hirrlinger, J., Peroxide detoxification by brain cells. *J Neurosci Res* 2005, *79*, 157-165.

[354] Erickson, J. R., Joiner, M. L., Guan, X., Kutschke, W*., et al.*, A dynamic pathway for calcium-independent activation of CaMKII by methionine oxidation. *Cell* 2008, *133*, 462-474.

[355] Ding, Q., Markesbery, W. R., Cecarini, V., Keller, J. N., Decreased RNA, and increased RNA oxidation, in ribosomes from early Alzheimer's disease. *Neurochem Res* 2006, *31*, 705-710.

[356] Myung, N. H., Zhu, X., Kruman, II, Castellani, R. J*., et al.*, Evidence of DNA damage in Alzheimer disease: phosphorylation of histone H2AX in astrocytes. *Age (Dordr)* 2008, *30*, 209-215.

[357] McKinnon, P. J., DNA repair deficiency and neurological disease. *Nat Rev Neurosci* 2009, *10*, 100-112.

[358] Altelaar, A. F., Frese, C. K., Preisinger, C., Hennrich, M. L*., et al.*, Benchmarking stable isotope labeling based quantitative proteomics. *J Proteomics* 2013, *88*, 14-26.

[359] Wu, Y., Wang, F., Liu, Z., Qin, H*., et al.*, Five-plex isotope dimethyl labeling for quantitative proteomics. *Chem Commun (Camb)* 2014, *50*, 1708-1710.

[360] Li, L. X., F.; Greer, T.; Frost, D.; Liang, Z., United States 2013.

[361] Frost, D. C., Greer, T., Li, L., High-resolution Enabled 12-Plex DiLeu Isobaric Tags for Quantitative Proteomics. *Anal Chem* 2014.

[362] Kaminski, Z. J., Kolesinska, B., Kolesinska, J., Sabatino, G*., et al.*, N-triazinylammonium tetrafluoroborates. A new generation of efficient coupling reagents useful for peptide synthesis. *J Am Chem Soc* 2005, *127*, 16912-16920.

[363] Hu, W., Tedesco, S., Faedda, R., Petrone, G*., et al.*, Covalent selection of the thiol proteome on activated thiol sepharose: a robust tool for redox proteomics. *Talanta* 2010, *80*, 1569-1575.

[364] Weston, L. A., Bauer, K. M., Skube, S. B., Hummon, A. B., Selective, bead-based global peptide capture using a bifunctional cross-linker. *Anal Chem* 2013, *85*, 10675-10679.

[365] McClatchy, D. B. Y., J. R., in: Martins-de-Souza, D. (Ed.), *Shotgun Proteomics: Methods in Molecular Biology*, Springer, New York 2014, pp. 133-146.

[366] Hebert, A. S. M., A. E.; Richards, A. L.; MacGilvray, M. E.; Kwiecien, N. W.; Rose, C. M.; Bailey, D. J.; Coon, J., NeuCode Mouse and One Hour Proteomics. *Mol Cell Proteomics* 2014, *13*, S31-S32.

[367] Saveliev, S. E., L.; Strauss, E.; Jones, R.; Rosenblatt, M., in: Note, P. T. (Ed.) 2012.

[368] Kellermann, J., ICPL--isotope-coded protein label. *Methods Mol Biol* 2008, *424*, 113-123.

[369] Com, E., Clavreul, A., Lagarrigue, M., Michalak, S*., et al.*, Quantitative proteomic Isotope-Coded Protein Label (ICPL) analysis reveals alteration of several functional processes in the glioblastoma. *J Proteomics* 2012, *75*, 3898-3913.

[370] Lange, O. D., E.; Wieghaus, A.; Makarov, A., ENhanced Fourier Transform for Orbitrap Mass Spectrometry. *International Journal of Mass Spectrometry* 2014, *369*, 16-22.

[371] Cherrington, A. D. E., D.; Sindelar, D. K., The Direct and Indirect Effects of Insulin on Hepatic Glucose Production in Vivo. *Diabetologia* 1998, *41*, 987-996.

[372] Brosnan, J. T., Glutamate, at the interface between amino acid and carbohydrate metabolism. *J Nutr* 2000, *130*, 988S-990S.

[373] Moore, J. K., Love, E., Craig, D. G., Hayes, P. C., Simpson, K. J., Acute kidney injury in acute liver failure: a review. *Expert Rev Gastroenterol Hepatol* 2013, *7*, 701-712.

[374] Wang, X. L., Suzuki, R., Lee, K., Tran, T.*, et al.*, Ablation of ARNT/HIF1beta in liver alters gluconeogenesis, lipogenic gene expression, and serum ketones. *Cell Metab* 2009, *9*, 428-439.

[375] Schooneman, M. G., Vaz, F. M., Houten, S. M., Soeters, M. R., Acylcarnitines: reflecting or inflicting insulin resistance? *Diabetes* 2013, *62*, 1-8.

[376] Mansour, F. R., Wei, W., Danielson, N. D., Separation of carnitine and acylcarnitines in biological samples: a review. *Biomed Chromatogr* 2013, *27*, 1339-1353.

[377] Santa, T., Derivatization reagents in liquid chromatography/electrospray ionization tandem mass spectrometry. *Biomed Chromatogr* 2011, *25*, 1-10.

[378] Peterson, A. C., Russell, J. D., Bailey, D. J., Westphall, M. S., Coon, J. J., Parallel reaction monitoring for high resolution and high mass accuracy quantitative, targeted proteomics. *Mol Cell Proteomics* 2012, *11*, 1475-1488.